Biophysical factors governing the structure, function, and dynamics of the NF-B essential modulator protein (NEMO)

Catici, Anca Maria Dragana

Award date:
2019

Awarding institution:
University of Bath

Biophysical factors governing the structure, function, and dynamics of the NF-κB essential modulator protein (NEMO)

ANCA MARIA DRAGANA CATICI
139374469

A thesis submitted for the degree of Doctor of Philosophy
University of Bath
Department of Biology and Biochemistry
January 2019

“It is surprising that people do not believe that there is imagination in science. It is a very interesting kind of imagination, unlike that of the artist. The great difficulty is in trying to imagine something that you have never seen, that is consistent in every detail with what has already been seen, and that is different from what has been thought of; furthermore, it must be definite and not a vague proposition. That is indeed difficult”— Richard P. Feynman, The Meaning of It All: Thoughts of a Citizen-Scientist

Acknowledgments

I would like to take this opportunity to thank my supervisor, Dr Chris Pudney, who offered me a chance to carry out this project and develop as a scientist. Your willingness to teach me new skills and concepts and patience in answering questions was invaluable throughout my PhD. Thank you for always encouraging me to not be scared of hard tasks or tackling hard scientific questions.

I would also like to thank my parents, family and friends for their constant support and for never giving up on me, even at times when I did. Thank you to my colleagues in labs 1.38, 1.28, and 0.39 for making me feel welcome and ensuring every day in the lab was fun. Thank you especially to Hannah Jones, Maria Vittoria Ortenzi, Elena Corujo Simon, Holly Stock, and Veronika Sabolova for being the best friends and for looking after me. Thank you to Christina Gulacsy and Rory Crean for their help in teaching me new techniques. Thank you to Saiyada Faizal and Nadya Freyther for their support and help.

Thank you to Timothy Hoffmann for always being there, your constant support, encouragement, and caring were invaluable and much needed throughout this. Thank you for helping me figure things out.

I would also like to dedicate this to my late aunt and uncle who sadly passed away during my PhD and did not get to see this to completion and be part of the celebrations.

Priznanje

Velika hvala mojoj obitelji, mami i neni, majkam i dedam, i Petru, za njinu pomoc i podržaj uz moj Dokorat. I majki babi i dedi tati, koji nažalost nesu stigli da me vide ce sam svršila. Hvala svem če ste bili uz mene.

TABLE OF CONTENTS

ABBREVIATIONS & SYMBOLS

$\frac{dQ}{dt}$: fluctuation in thermal power

$\frac{dP}{dt}$: product formation with respect to time

$\boldsymbol{v}$: enzyme velocity

$\boldsymbol{K_m}$: Michaelis-Menten constant

Ala: Alanine

ANS: 1-Anilino-8-naphthalenesulfonic acid

ATP: adenosine triphosphate

CBP: CREB binding domain

CC: coiled-coil

E,S,P: enzyme, substrate, product

EPR: electron paramagnetic resonance

F: phenyl-alanine

FEL: free energy landscape

FRET: fluorescence resonance energy transfer

IDP: intrinsically disordered protein

IKK: inhibitor kinase of IκB

iNUB: inhibitor of NEMO-ubiquitin binding

ITC: isothermal titration calorimetry

IκB : inhibitor of κB

$\boldsymbol{k_{cat}}$: rate of turnover

LC-MS: liquid chromatography couples with mass spectrometry

LZ: leucine zipper

mM: milimolar

nM: nanomolar

NADH: Nicotinamide adenine dinucleotide

NBD: NEMO binding domain

NEMO: NF-κB essential modulator

NES: nuclear export signal

NF-κB: nuclear factor interacting with the enhancer element of the immunoglobulin κ-light chain of activated human B cells

NIK: NF-κB inducing kinase

NLS: nuclear localisation signal

NMR: nuclear magnetic resonance

NOA: NEMO-optineurin-ABIN

REES: red edge excitation shift

RHD: Rel-homology domain

S,T: electron singlet, triplet state

SEC-SAXS: size exclusion chromatography coupled with small-angle X-ray scattering

Ser: Serine

TAD: transactivation domain

TAK1: TGFβ-activated kinase 1

Tyr: tyrosine

UV: ultra violet

µM: micromolar

vFLIP: viral FLICE-like inhibitory protein

W: tryptophan

Y: tyrosine

ZF: Zinc finger

ΔG: change in Gibbs free energy

$\Delta G^{\ddagger}$: change in activation energy of transition state

ΔH: change in enthalpy

ΔS: change in entropy

ΔT: change in temperature

ΔV: change in specific volume

$\Delta \alpha$: change in compressibility

$\Delta \beta$: change in expansivity

φ : fluorescence quantum yield

hϑ: photon

LIST OF TABLES

LIST OF FIGURES

LIST OF EQUATIONS

ABSTRACT

The NF-κB essential modulator (NEMO) is an important human protein, in charge of ensuring the activation the NF-κB signalling pathway in response to canonical stimuli. Very little consensus exists about the structure, dynamics, and the role of the protein. Here we offer evidence to support the dynamic nature of NEMO, with binding to ligands inducing a ligand-dependent conformational change in the protein. We propose the use of an optical phenomenon known as Red edge excitation shift (REES) as a new tool to study and quantify protein dynamics. We also emphasise the importance of taking into consideration the effect of the intracellular environment on modulating the structure and dynamics of NEMO. Furthermore, we shed light onto the cytoplasmic role of NEMO in mediating an important enzyme:susbstrate interaction as part of NF-κB activation. These findings underline the dynamic nature of NEMO and its sensitivity to the environment and may also explain the diversity of data published of NEMO so far. Moreover, we also offer evidence to support the importance of NEMO presence for the interaction between IKKβ:IκBα during NF-κB canonical activation. These are potentially crucial aspects to be considered when developing therapeutic targets that aim to modulate the abnormal NF-κB response in many human medical conditions.

Chapter 1: Introduction to NF-κB signalling pathway and its key elements

1. NF-κB signalling pathway – role and species distribution

Cell signalling is a strictly regulated process, with many key molecules ensuring the proper transfer of information both inside and between cells. These signalling pathways are crucial for regulating vital cellular processes such as cell development and differentiation (Dumstrei *et al.*, 2004), autophagy (He and Klionsky, 2009), apoptosis (Muñoz-Pinedo, 2012), inflammation (Lawrence, 2009), and others.

The NF-κB signalling pathway is an important human regulatory network, predominantly acting on the immune and nervous systems, involved in inflammation (Brambilla *et al.*, 2005), neurogenesis (Koo *et al.*, 2010), neuroprotection (Fridmacher *et al.*, 2003), neuronal development (Correa *et al.*, 2004), and neuronal inflammation (Shih *et al.*, 2015).

The pathway was first described in 1986 through the discovery of one NF-κB protein acting as a nuclear factor interacting with the enhancer element of the immunoglobulin κ-light chain of activated human B cells, hence the name NF-κB and its role in activating the immune system (Sen and Baltimore, 1986). With developments in genetic tools, the presence of NF-κB proteins has been shown to also be found in zebrafish (Correa *et al.*, 2004), insects (Hetru and Hoffmann, 2009), invertebrates such as sponges (Gauthier and Degnan, 2008), cnidarians (eg. sea anemones, hydra, coral) (Wolenski *et al.*, 2011; Sullivan *et al.*, 2007; Meyer *et al.*, 2009), and even the protist *Capsaspora owczarzaki* (Sebé-Pedrós *et al.*, 2011). Refer to Figure 1 for detailed species distribution of NF-κB proteins. Recently, the presence of NF-κB has been reported in the horseshoe crab (*Carcinoscorpius rotundicauda*) (Wang *et al.*, 2006), also known as one of the most ancient arthropods (Størmer, 1952). In addition to motif homology shared with their vertebrate equivalent, the horseshoe crab NF-κB proteins may even be able to respond and interact with mammalian κB proteins (Wang *et al.*, 2006). In contrast, NF-κB-like transcription factors appear to be missing in yeast and nematodes (Irazoqui *et al.*, 2010; Pujol *et al.*, 2001), where it is thought that other signalling pathways contribute to mediating immune responses to pathogens.

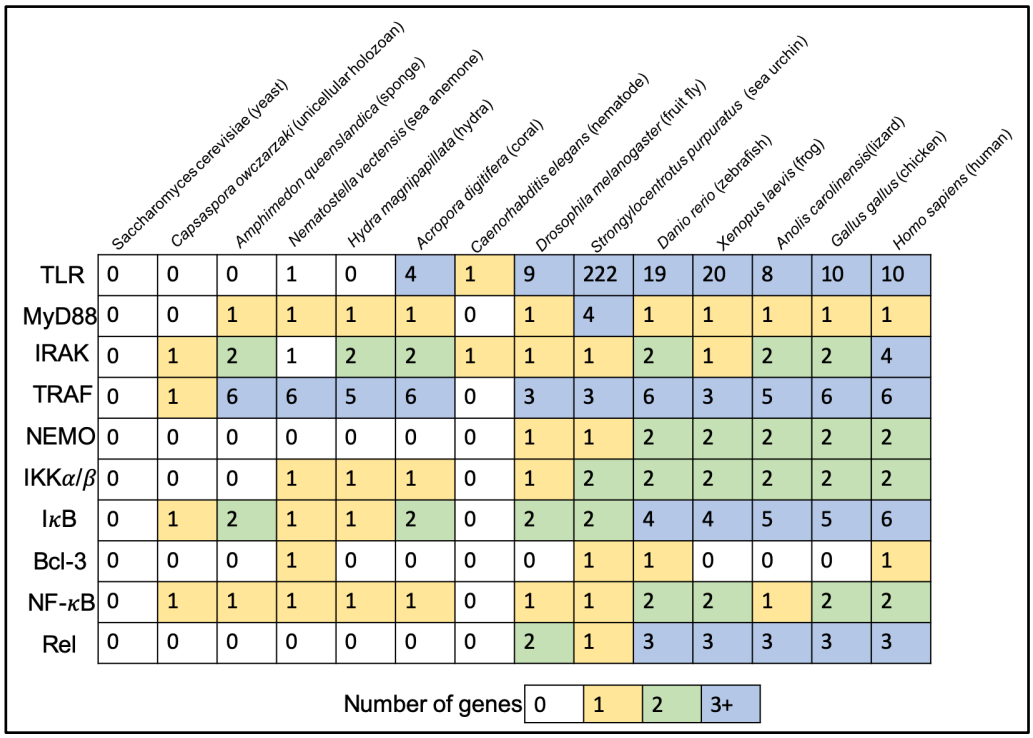

Figure 1. NF-κB proteins and receptors species distribution (adapted from (Gilmore and Wolenski, 2012). **The family members for each NF-κB protein and receptor protein found in various model organisms, listed from morphologically simple organisms (left) to more complex organisms (right). TLR, Toll-like receptor; MyDD88, MyD88 adapter protein myeloid differentiation primary response protein 88; IRAK, IL-1R-associated kinases; TRAF, TNF-receptor associated factor protein.**

A comprehensive phylogenetic analysis of the origin of the NF-κB proteins and receptors has been reported previously, with specific focus on the distribution of the Rel Homology domain-containing proteins (Gilmore and Wolenski, 2012). Here the authors trace the origin of NF-κB to 1,000 million years ago, with subsequent species distribution coinciding with development of higher order organisms. This offers answers for the conserved function in mediating the immune response in response to inflammatory stimuli and controlling cell survival and apoptosis of NF-κB in complex organisms (Gilmore and Wolenski, 2012).

1.1 NF-κB: stimuli, target genes, and its role in health & disease

A variety of stimuli are known to activate the NF-κB signalling pathway (Gilmore and Wolenski, 2012). These include, but are not limited to: pathogens infections including viruses (Santoro *et al.*, 2003; Harhaj and Sun, 1999) and bacteria (Rahman and McFadden, 2011), cytokines (eg. TNFα) (Middleton *et al.*, 2000),

radiation (UV) (O'Dea *et al.*, 2008) and physiological conditions (e.g. ischemia) (Duckworth *et al.*, 2006). So far, more than 150 target genes were linked to NF-κB activation (Yang *et al.*, 2016), but as some of these regulate the expression of other transcription factors, the NF-κB regulatory gene pool may in fact include far more. Amongst the NF-κB target genes are also the genes encoding for various NF-κB proteins, evidencing the self-regulatory nature of this pathway (Ten *et al.*, 1992).

NF-κB has also been linked to a variety of diseases and medical conditions, resulting from aberrant NF-κB activity or various mutations/deletions in in the NF-κB genes themselves (Smahi *et al.*, 2002). Many studies also suggest conflicting NF-κB involvement in many cancers and its potential as a target for therapeutics or (Gamble *et al.*, 2012; Hoesel and Schmid, 2013).

1.2 NF-κB proteins

The NF-κB signalling pathway is composed of three protein families: the NF-κB transcription factor proteins, the inhibitors IκBs, and, the IKK proteins. In unstimulated cells, inhibitor IκBs bind to various NF-κB proteins and sequester them in the cytoplasm in the absence of a stimulus (Baeuerle and Baltimore, 1988). Upon stimulation, the IκB:NF-κB protein complex is targeted by IKK proteins, which phosphorylate the IκBs on specific serine residues (depending on the type of IκB protein and type of stimulus), thus targeting them for degradation and freeing the NF-κB proteins (Gilmore, 2006). Following release from inhibitors, NF-κB proteins are able to translocate to the nucleus and regulate gene expression in response to specific stimuli. See Figures 1-2 for NF-κB proteins, receptors and species distribution.

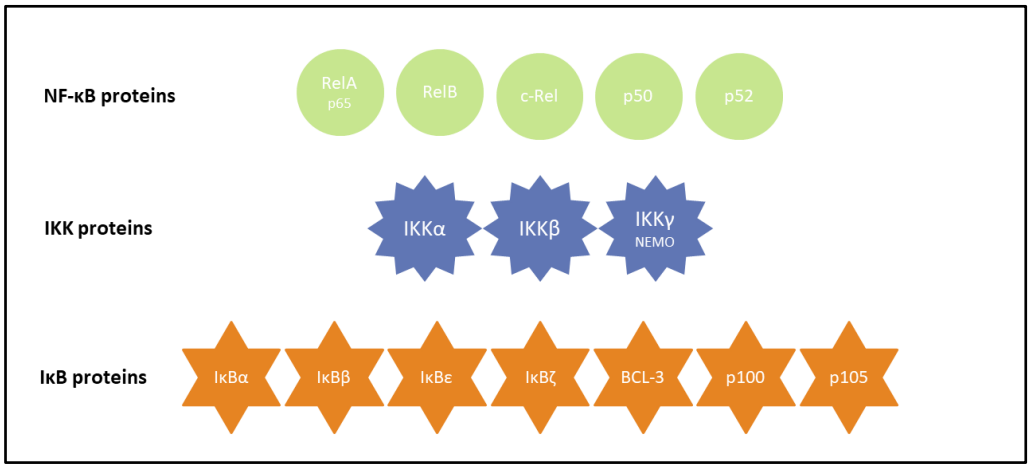

Figure 2. NF-κB protein families, including NF-κB, IKK, and IκB proteins. Shown in green are the five members of the NF-κB transcription factors (RelA/p65, RelB, c-Rel, p50, p52), blue are the IKK proteins (IKKα, IKKβ, IKKγ/NEMO), and in orange are the IκB inhibitors (IκBα, IκBβ, IκBε, IκBζ, BCL-3, p100, p105).

1.2.1 NF-κB transcription factors

In most vertebrates including humans, there are five NF-κB transcription factors: RelA (or p65), RelB, c-Rel, p50 (formed by cleaving of its precursor p105), and p52 (formed from cleaving its precursor p100)(O'Dea and Hoffmann, 2009; Gilmore, 2006). Their main function as transcription factors is to bind to nucleic acids and regulate gene expression upon binding of a stimulus.

A common feature of these five proteins is the presence of a 300-amino acid sequence at the N-terminus, called the Rel homology domain or RHD (Ghosh *et al.*, 1998). All but two NF-κB transcription factors also have a transactivation domain or TAD, located at the C-terminus (Ishikawa *et al.*, 1993; Ryseck *et al.*, 1992). Both the RHD and TAD carry functional roles. The RHD domain is required for dimerization and DNA binding (Rothwarf and Karin, 1999). The nuclear localisation signal required for translocation of the transcription factors into the nucleus is also located within the RHD region (Verma *et al.*, 1995). The TAD region of RelA, RelB, and c-Rel is required to initiate transcription (Ghosh *et al.*, 1998; Schmitz *et al.*, 1995). For p50 and p52 proteins lacking the TAD domain, transcription is achieved though binding to TAD-containing proteins either part of NF-κB or various non-Rel proteins able to induce transactivation (Lernbecher *et al.*, 1993).

In contrast p50 and p52 contain instead ankyrin repeats (Betts and Nabel, 1996; Xiao

et al., 2001). The ankyrin repeats are found in many different proteins, including the inhibitors IκBs, thought to be important for mediating protein interactions (Mosavi *et al.*, 2004). In the case of p50 and p52, the ankyrin repeats may also control their cytoplasmic localisation (Wan and Lenardo, 2009).

NF-κB transcription factors form homo- or heterodimers, with a total of 15 theoretical dimerisation possibilities out of which 12 have been demonstrated so far to be able to bind to nucleic acid (Huxford and Ghosh, 2009). The targets of these transcription factors consist of DNA sequences between 9-11 base pairs long (known as κB binding sites) which are either part of enhancer or promoter domains of genes (DiDonato *et al.*, 1996).

Dimer combinations appear to be influenced by the type of stimulus present and the genetic promoter (Wang *et al.*, 2012). Dimer exchange upon binding to promoters has also been reported and appears to be stimulus specific (Saccani *et al.*, 2003). Various explanations have been given for this, one relating to dimer exchange being linked to controlling the timing of transcription (to potentially coincide with other cellular events) (Saccani *et al.*, 2003). Studies have shown that although p50 and p52 dimers cannot initiate transcription as they lack the TAD domain, they have been found to bind to DNA and prevent other NF-κB dimers from binding (Ten *et al.*, 1992).

1.2.2 IκB proteins

The IκB family of proteins consists of seven members, including: IκBα, IκBβ, IκBε, IκBζ, BCL-3 (B-cell lymphoma 3), p100, and p105 (Hayden and Ghosh, 2012). An additional IκB protein was reported in mice, IκBγ, resulting from an different processing of the p105 (Grumont and Gerondakis, 1994). All IκB proteins share a 5-7 repeat of a 33-amino acid domain known as the ankyrin domain at their C-terminus (Verma *et al.*, 1995), essential for binding to NF-κBs and cytoplasmic anchoring (Blank *et al.*, 1991).

IκBs function as inhibitors of NF-κB transcription factors and different IκBs will bind to different NF-κB dimers with different affinities, depending on the stimulus and the type of cell they are found in. This interaction occurs between the RHD domain of

NF-κB dimers and the IκB ankyrin repeats (Malek *et al.*, 2003). Structural studies have shown that these complexes are able to stay in the cytoplasm due to the nuclear localisation sequence (NLS) of the transcription factors being masked by the interaction with the IκBs (Beg *et al.*, 1992). This was thought to be the main mechanism by which the NF-κB response was regulated, as the anchoring of the NF-κB proteins in the cytoplasm by IκBs prevented them from binding to DNA and initiating transcription (Baeuerle and Baltimore, 1988). However, this was later challenged by the presence of some NF-κB:IκB complexes in the nucleus (Wessells *et al.*, 2004). X-ray crystal structures show some NF-κB:IκB complexes only manage to conceal one NLS of the transcription factors, thus allowing the complex to still translocate to the nucleus (Huxford *et al.*, 1998). Moreover, the presence of IκBs in the nucleus may function to competitively bind NF-κBs over DNA, thus regulating transcription (Sue *et al.*, 2011). An active shuttling between cytoplasm and nucleus and *vice versa* is also facilitated by the presence of two leucine-rich regions in the C- and N- termini of most IκBs, known as the nuclear export signal (NES) (Arenzana-Seisdedos *et al.*, 1997), also present in some NF-κBs (Harhaj and Sun, 1999; Huang and Miyamoto, 2001).

1.2.3 The IKK complex

Whilst inhibition of NF-κB is achieved through binding to IκBs, activation is dependent on the activation of the inhibitor kinase of IκB complex, IKK. This is comprised of three proteins: the kinases IKKα (IKK1) and IKKβ (IKK2), and a non-catalytic member known as IKKγ or NEMO (NF-κB essential modulator). The kinases share three structural characteristics: a kinase domain located at the N-terminus, a leucine zipper (required for dimer formation and activation), and a helix-loop-helix domain at the C-terminus (also important for activation and protein interactions) (Zandi *et al.*, 1998). The two kinases also show a high degree of sequence similarity within their catalytic regions, with a 50 % sequence identity (Cheng *et al.*, 2012) and 65 % similarity in their catalytic domain (Rothwarf and Karin, 1999). IKKα and IKKβ may form homo- or heterodimers, with the latter preferentially found in cells due to their increased catalytic ability (Mercurio *et al.*, 1997; Huynh *et al.*, 2000) . The X-ray crystal structures of human IKKβ (Liu *et al.*, 2013) and IKKα (Polley *et al.*, 2016) are in Fig.3**.**

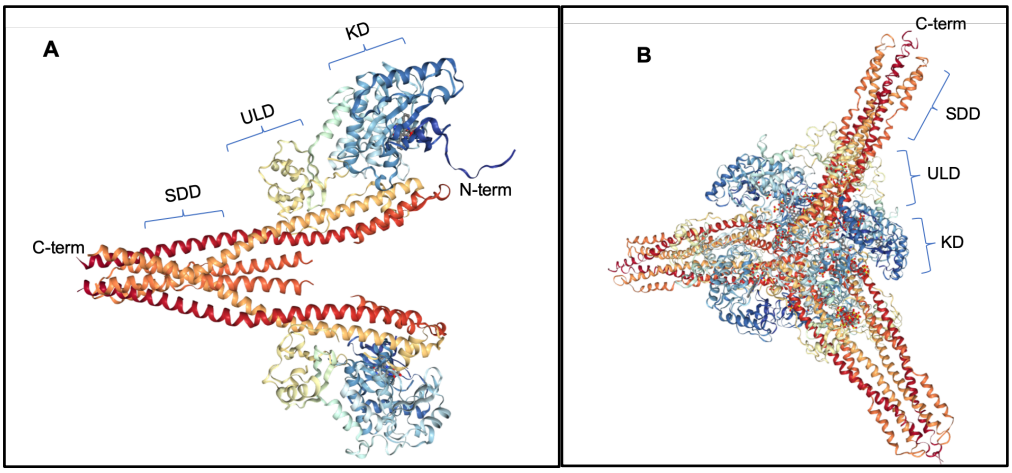

Figure 3. X-ray crystal structure of human IKKβ (A) and IKKα (B) kinase (Figures adapted from Liu *et al.*, 2013 and Polley *et al.*, 2016). **A, IKKβ structure at 2.8 Å resolution seen as a dimer of dimers (PDB ID: 4KIK). B, IKKα structure at 4.5 Å resolution seen as trimer of dimers (PDB ID: 5EBZ). Both structure consist of an N-terminal kinase domain (KD), a central ubiquitin-like domain (ULD), and a C-terminal scaffold/dimerization domain (SDD).**

A specific region within the C-terminus of both IKK enzymes, known as the NEMO binding domain (NBD) and containing the LDWSWL sequence was shown to play a crucial role in facilitating binding to NEMO (May *et al.*, 2000). The two kinases display different affinities for binding to NEMO (Rushe *et al.*, 2008), with IKKβ having a higher affinity, K_D= 2.2 ±0.8 nM (Cote *et al.*, 2013). Experimental studies have also demonstrated an additional function for the C-terminus of both IKKα and IKKβ in control of enzyme dimerisation (McKenzie *et al.*, 2000; Kwak *et al.*, 2000). In addition to dimerisation and binding to NEMO, IKK activation also requires phosphorylation of specific serine residues on the two kinases (Makris *et al.*, 2002; Mercurio *et al.*, 1999), specifically S176 and S180 for IKKα (Régnier *et al.*, 1997; Ling *et al.*, 1998) and S177 and S181 for IKKβ (Zandi *et al.*, 1998; Mercurio *et al.*, 1997).

Structural analyses offer insight into the conformational changes that follow phosphorylation and activation of IKKα and IKKβ. Activated dimers assume an *apo* conformation that allows for efficient substrate access (Liu *et al.*, 2013; Polley *et al.*, 2013), whilst inactive/non-phosphorylated dimers show different, more compact conformations (Xu *et al.*, 2011; Larabi *et al.*, 2013). IKK phosphorylation can be achieved through two main routes. It is thought that IKK kinase dimerisation facilitates

conformational reorganisation whereby *trans*-autophosphorylation can occur (Polley *et al.*, 2013; Xu *et al.*, 2011). Additionally, it has also been shown that other kinases my also induce phosphorylation of IKKα and IKKβ (Malinin *et al.*, 1997; Zhao and Lee, 1999), due to NF-κB crosstalk with other signalling pathways. Activation of NF-κB will not proceed in the absence of phosphorylated IKK kinases, as demonstrated by mutation studies (Rogers *et al.*, 1986). The many ways of IKK phosphorylation offer a guarantee that activation of the signalling pathway can proceed in response to a plethora of stimuli.

Activated kinases function to target IκBs for proteoasomal degradation. This is a two-step process: firstly, IKK kinases will phosphorylate specific IκB serine residues (DiDonato *et al.*, 1996; Traenckner *et al.*, 1994). This acts as a signal for the recruitment of an E3 ubiquitin ligase (β-TrCp) (Christian *et al.*, 2016), which further modifies the IκBs through the addition of a lysine48-ubiquitin at particular lysine residues (Amir *et al.*, 2004). This is the final step in ensuring IκBs proteoasomal degradation and the freeing of NF-κB dimers, thus achieving the activation of the signalling pathway.

The substrates of IKKα and IKKβ extend beyond the IκBs, with the two kinases having been associated with phosphorylation of other proteins including the H3 chromatin histone protein (Anest *et al.*, 2003), and other signalling molecules (Lee *et al.*, 2007). It is clear that not only is the IKK complex vital for NF-κB functioning, but it also enhances the ability of NF-κB to interact with other regulatory pathways and affect various cellular functions, such as with Toll-like receptor signalling pathway during activation of specific immune responses following viral infection (Kawai and Akira, 2007).

1.3 NF-κB activation: canonical vs non-canonical

Activation of NF-κB is dependent on the activation of the IKK complex and the subsequent release of NF-κB proteins from their cytoplasmic inhibitors. However, depending on the type of stimulus, presence of NF-κB proteins, and type of response

required, two different activation mechanisms can be described for this pathway: the canonical (classic) and non-canonical (alternative) pathways (Gilmore, 2006). Refer to Figure 3 for detailed diagram on NF-κB activation. Generally, the canonical pathway relies on the activation of the IKKβ enzyme, the targets of which are IκBα, IκBβ and IκBε (Hoffmann *et al.*, 2006). IKKα activation and its subsequent targeting of p100 for phosphorylation are characteristic of the non-canonical pathway (Xiao *et al.*, 2001). Some evidence also exists for IKKα involvement in the processing and degradation of IκBα during canonical activation (Adli *et al.*, 2010). As such, the main difference between the two activation pathways in the dependence on NEMO of the canonical pathway, a characteristic distinctly not shared with the alternative pathway.

A comprehensive list of all NF-κB canonical stimuli and target genes has been published by Matsuda *et al.* (Matsuda *et al.*, 2003); these include:

- Bacterial products (Lipoteichoic acid) (Kao *et al.*, 2005), fungal products (Glycosylphosphatidylinositols) (Zhu *et al.*, 2005), and viral products (Ebola viral matrix & glycoprotein) (Martinez *et al.*, 2007);
- Physiological stress conditions: appendicitis (Pennington *et al.*, 2000), , hypothermia (Fairchild *et al.*, 2005);
- Physical stress: sleep deprivation (Brandt *et al.*, 2004), simulated microgravity environment (Sharma *et al.*, 2008);
- Inflammatory cytokines: IL1 (Kida *et al.*, 2005); human septic serum (Kumar *et al.*, 2005); thrombopoietin (Romanelli *et al.*, 2006);
- Environmental hazards: cigarette smoke (Preciado *et al.*, 2008);
- Therapeutics: diclofenac (Cho *et al.*, 2005), proteasome inhibitors (Dolcet *et al.*, 2006), epinephrine (Lymperopoulos *et al.*, 2006)
- Hormones: insulin (Madonna *et al.*, 2007); prostratin (Williams *et al.*, 2004), relaxin (Ho *et al.*, 2007);
- Chemical agents: cadmium (Hyun *et al.*, 2007); fluoride (Zhang *et al.*, 2008), MDMA (Tiangco *et al.*, 2005);

The molecular basis of NF-κB signalling pathway is a complex network of a variety of different stimuli and specialised receptors that ensure the signal transmission and appropriate cellular response. For the canonical activation, these receptors include tumour necrosis factor receptor (TNFR) and Toll-like receptor/interleukin-1 receptor (TLR/IL-1R) superfamilies. A characteristic shared by all these receptors is that activation does not rely on the enzymatic action of the receptor bur rather requires ligand binding and subsequent conversion of the signal by specialised adaptor proteins to ensure stimulation of kinases (Hayden and Ghosh, 2014). It has been proposed that ligand binding acts as a signal to initiate the formation of specific oligomeric receptor/ligand assemblies (Hayden and Ghosh, 2014).

- Activation *via* TNFR

In response to cytokine stimuli (eg. TNF-α) TNFR receptors allow activation of NF-κB activation to occur through ligand-induced trimerisation of the TNFR and the subsequent recruitment of TNFR-associated factors (TRAFs) to the receptors (Napetschnig and Wu, 2013). This interaction is often mediated through interactions with adaptor proteins (Ye *et al.*, 2002; Xie, 2013): for example, binding of TNF-α induces association of the adapter protein TRADD with the TNFR1 receptor (interaction mediated through death domain) which consequently also results in the binding of TRAF2/RIP1 to the complex (Pobezinskaya and Liu, 2012). In addition to the death domain, the RIP (Receptor Interacting Protein) homotypic interaction motifs (RHIM) and TRAF (TNF Receptor Associated Factor) domains have also been involved in mediating signal transduction during TNFR activation of NF-κB (Li *et al.*, 2013). TRAF2 acts as a target for cIAP1/2 (Mahoney *et al.*, 2008) , which in turn binds the LUBAC complex (consisting of HOIP, HOIL and SHARPIN) (Ikeda *et al.*, 2011), while RIP1 interacts with NEMO to mediate the interaction between TAK1 and the IKK complex through NEMO (Yang *et al.*, 2011), thus ensuring the activation of NF-κB .

- Activation via TLR/IL-1R

The TLR/IL-1R receptors specifically recognise pathogen-associated molecular patterns (PAMPs) which for the activation of NF-κB include: lipopolysaccharides of gram-negative bacteria, peptidoglycan and lipoteichoic acid of gram-positive bacteria, viral RNAs, and a number of externa stress signals (Napetschnig and Wu, 2013). Following ligand-induced activation, TLRs and IL-1Rs form dimers or undergo conformation

change (Latz *et al.*, 2007; Tsukamoto *et al.*, 2010) or may undergo conformation change (Liu *et al.*, 2008; Kang *et al.*, 2009). Similarly, to activation through TNFR, these conformational changes promote complex molecular assemblies. In the case of TLR/IL-1R receptors, these include protein assemblies which consists of three protein complexes and they rely on interactions with various K48- and K63-polyubiquitin chains. These protein complexes are formed in a stepwise manner by interaction of various IRAK and TRAF proteins, which start with association at the membrane of Complex I (MyD88, Tollip, IRAK-1, IRAK-4 and TRAF6) and II (TRAF6-TAK1-TAB1-TAB2/TAB3). Here, IRAK1 undergoes ubiquitination and the remaining IRAK/TRAF protein complex translocate to the cytoplasm where interactions with E2 ubiquitin-conjugating enzyme (Ubc13/Uev1A) and K63-polyubiquitin chains promote association with TAB2, ultimately leading to the activation of TAK1. TAK1 subsequently phosphorylates and thus activates IKKβ, resulting in the activation of the NF-κB canonical pathway (Verstrepen *et al.*, 2008; Napetschnig and Wu, 2013).

- Activation *via* T- and B-cell receptors

Activation of the non-canonical NF-κB pathway requires T- and B-cell receptors, and is initiated when stimulated by B-cell activating factor belonging to the TNF family (BAFF) (Morrison *et al.*, 2005), lymphotoxin b (LTb) (Madge *et al.*, 2008) and CD40L (Seigner *et al.*, 2018). It has been proposed that the T-cell receptor (TCR) uses the LAT-SLP76 and/or the GLK complex to activate PKCθ (Smith-Garvin *et al.*, 2009; Chuang *et al.*, 2011), while CD28 stimuli activate PKCθ through PI3K and PDK1 (Garçon *et al.*, 2008; Kang *et al.*, 2017). Once activated PKCθ promotes the formation of the CBM complex (CARMA1, BCL10, MALT1) (Schulze-Luehrmann and Ghosh, 2006). The CBM complex interacts with the ubiquitin ligases TRAF6, TRAF2 and/or MIB2 to allow for signal transmission to the IKK complex (Paul and Schaefer, 2013), resulting the activation of the pathway.

IKKα may also play a role during canonical activation, however, attempts to understand this have so far yielded inconsistent results. IKKα is thought to function similarly to IKKβ and target IκBα for degradation (Kim *et al.*, 2010) or associate with NF-κB inhibitors (Shembade *et al.*, 2011). Studies in mice show that IKKβ and NEMO deficiency result in embryonic death (Li *et al.*, 1999; Rudolph *et al.*, 2000), whilst mice lacking IKKα show developmental and morphological issues (Hu *et al.*, 1999). These

findings suggest the evolutionary and cooperative importance of the two activating pathways, with the canonical pathway responsible for controlling much of the immune response, whilst the alternative pathway could be seen to function as an extension or even as an additional regulator of NF-κB signalling. More NF-κB activating pathways undoubtedly exist; for example tyrosine phosphorylation of IκBα instead of serine is able to activate NF-κB in response to oxidative stress and does not depend on degradation of IκBα (Takada *et al.*, 2003; Imbert *et al.*, 1996).

Figure 4 illustrates a simplistic diagram of the canonical and alternative NF-κB, with the corresponding receptors and focus only on the events after IKK activation and omitting the cascade of interactions described above.

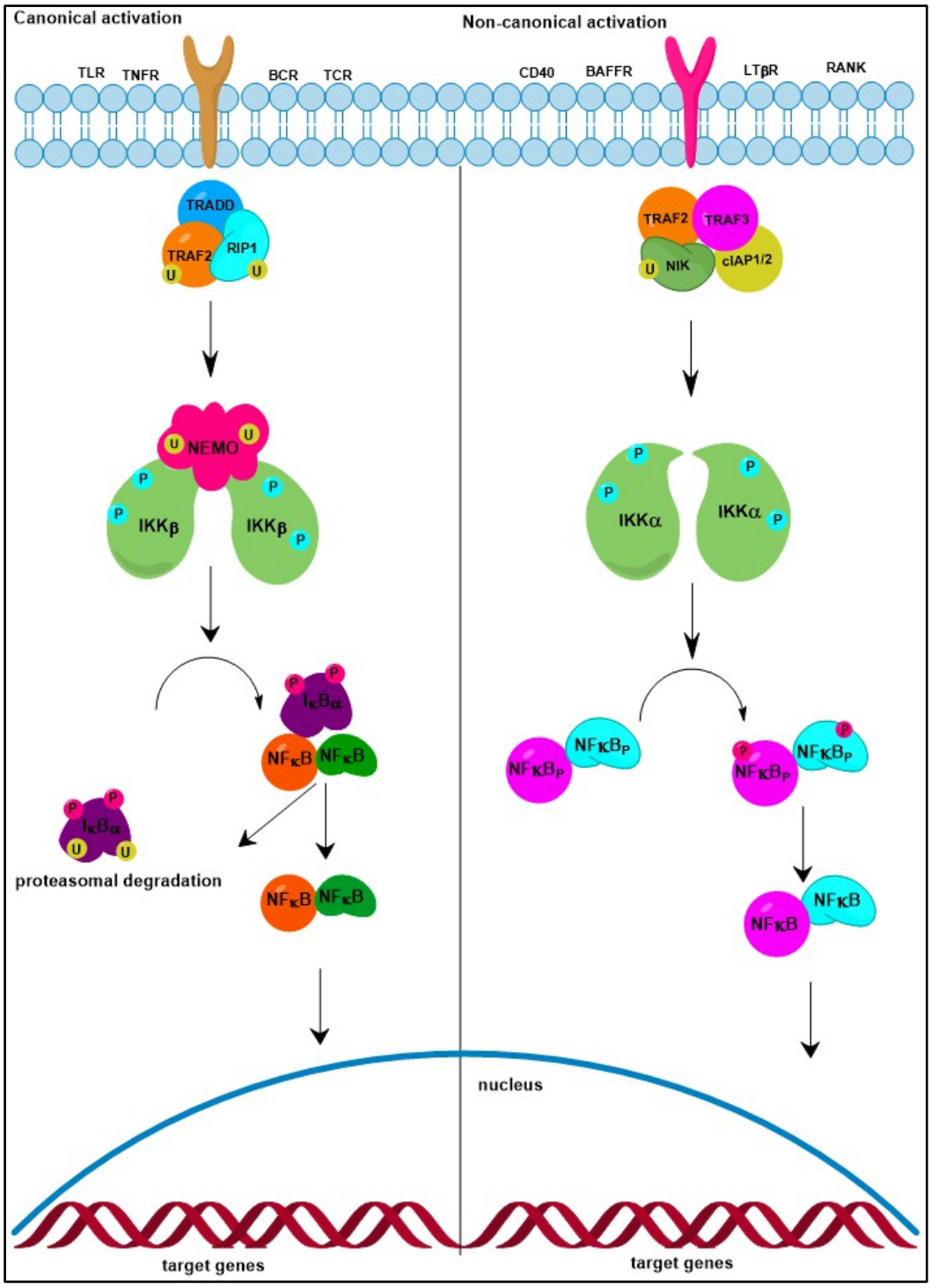

Figure 4. Canonical and alternative NF-κB activating pathways and their specific proteins. **Schematic showing the activation of NF-κB in response to canonical and non-canonical stimuli. P, phosphorylation; U, ubiquitination; NF-κB$_p$, NF-κB precursors. Activation of the IKK kinases complex during canonical activation is carried out by various kinases (depending on the nature of the stimulus) which promote association with NEMO (canonical) or IKKα (alternative), thus activating the IKK complex and ensuring targeting of IκBs for proteasomal degradation. TLR, TNFR, BCR, TCR are the receptors for canonical stimuli; CD40, BAFFR, LTβR, RANK are the receptors for alternative pathway stimuli.**

The NF-κB alternative pathway is activated by a select few types of stimuli and its activation is essential for more specialised cellular functions such as development of the lymphatic system (Sun, 2011), as well as neuronal and bone functioning (Dejardin, 2006). NEMO is not required for this pathway and activation of IKKα is credited to its interaction with the NF-κB-inducing kinase (NIK) (Xiao *et al.*, 2001). Additionally, the alternative pathway has a much slower rate and a long-lasting activity compared to the canonical activation (Hoffmann and Baltimore, 2006; Shih *et al.*, 2011; Sun, 2011). As is the case for NF-κB, the activation of IKKα by NIK leads to targeting of NF-κB inhibitors (in this case p100), as well as the subsequent proteoasomal degradation of NIK, thus acting as a self-regulatory unit (Razani *et al.*, 2010).

1.4 NF-κB essential modulator (NEMO): structure, function, and importance

NEMO forms the non-catalytic subunit of the IKK complex together with the two kinases, IKKα and IKKβ. It is a 48-kDa protein, and as the name suggests it function as the main regulator of the NF-κB canonical activation (Rothwarf *et al.*, 1998; Yamaoka *et* al.,1998). NEMO ensures the activation of the canonical pathway by associating with the IKKβ kinase, which induces activation of the kinase either through autophosphorylation or phosphorylation by RIP or TAK enzymes (Wu *et al.*, 2010; Wang *et al.*, 2001). Following this IKKβ can bind to specific inhibitors such as IκBα and thus free the sequestered NF-κB proteins, which can now enter the nucleus and regulate transcription. Even though NEMO is the main activator of the canonical pathway, it is often assigned a passive role in achieving this. Most published reports suggest NEMO acts a 'scaffold' protein, ensuring IKKβ and its substrates are in close proximity to each other for their interactions to occur (Schröfelbauer *et al.*, 2012).

The exact mechanism of action of NEMO within the NF-κB signalling pathway is still a debatable topic. Embryonic lethality is observed in mice lacking NEMO, and in cells lacking NEMO, the canonical activation of NF-κB is also not observed (Rothwarf *et al.*, 1998; Rudolph *et al.*, 2000).

1.4.1 NEMO structure

Many studies have attempted to elucidate the structure of NEMO. The only available X-ray structures are of truncated versions of the protein and/or bound to an interacting partner, most of them showing regions that display helical structures (Lo *et al.*, 2009; Rahighi *et al.*, 2009; Ivins *et al.*, 2009; Tokunaga *et al.*, 2009). The 419-amino acid protein is thought to have two coiled-coiled domain CC1 and CC2 at the N- and C-terminus, respectively, and an alpha-helical domain at the n-terminus. The C-terminus also includes the NOA domain, a leucine zipper and zinc finger, as depicted in the Figure 5.

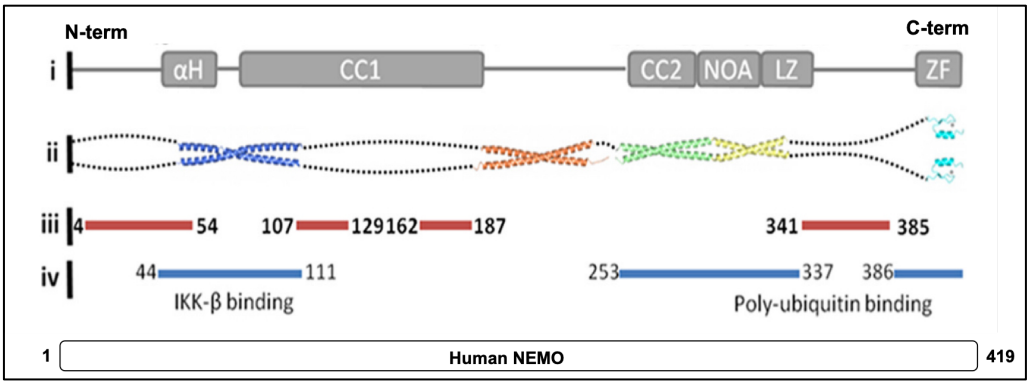

Figure 5. NEMO known structural details and predicted disordered regions (Figure adapted from Catici *et al.*, 2015). **i, NEMO regions, including: α-helical domain, coiled coil region 1 (CC1), coiled coil region 2 (CC2), NEMO Optineurin Abin (NOA or UBAN or ABIN), leucine zipper (LZ), and zinc finger (ZF); ii, X-ray crystallography solved NEMO structures (PDB ID: 3BRV, 3CL3, 2ZVN, 2JVX); iii, part of NEMO predicted to be disordered as determined using PONDR-FIT, ANCHOR, IUPred, and SPINE-D; iv, specific NEMO regions for interaction with IKKβ (amino acids 44-111) and poly-ubiquitin (amino acids 253-337 & 386-409).**

At the N-terminus, the CC1 domain facilitates interactions with the C-terminus of IKK enzymes (Rushe *et al.*, 2008), while the CC2 –LZ domain ensures interactions with various poly-ubiquitin partners (Rahighi *et al.*, 2009; Ivins *et al.*, 2009; Tokunaga *et al.*, 2012). Interactions with poly-ubiquitin are essential for NEMO and NF-κB activation, the details of which will be addressed later.

1.4.2 NEMO ZINC FINGER

The zinc finer (ZF) is a shared protein motif found in both prokaryotes and eukaryotes, required for interactions with nucleic acids, proteins, and lipids (Gozani *et al.*, 2003; Hall, 2005; Gamsjaeger *et al.*, 2007; Eom *et al.*, 2016), with possible links to many human diseases (Cassandri *et al.*, 2017). The name is derived from the structural arrangements of amino acid residues present in different numbers (most commonly cysteine and histidine) around a Zinc ion. The structure of the NEMO ZF, determined using nuclear magnetic resonance, shows the regions adopt a ββα conformation (Cordier *et al.*, 2008; Cordier *et al.*, 2009), similar to other ZF proteins (Malgieri *et al.*, 2015). The structure can be seen in Fig.6.

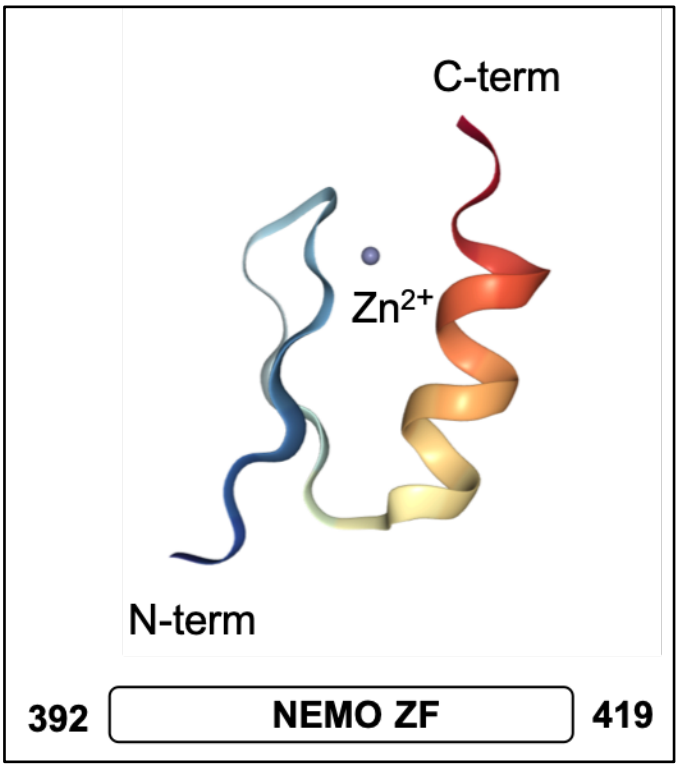

Figure 6. Structure of human NEMO ZF region (Figure adapted from Cordier *et al.*, 2008)**. The structure was determined using nuclear magnetic resonance and is shown here bound to a Zn^{2+} (PDB ID: 2JVX). Gradient from blue to red shows the 394–419 residues of human NEMO.**

The function of the NEMO ZF is to facilitate ubiquitin binding and ensure NF-κB activation (Cordier *et al.*, 2009; Ngadjeua *et al.*, 2013). Mutations within the NEMO ZF

can results in mice embryo lethality (Smahi *et al.*, 2000), are associated with impairment of NF-κB signalling (Fusco *et al.*, 2008; Ngadjeua *et al.*, 2013) and are observed in many clinical conditions, such as ectodermal dysplasia with immunodeficiency (Döffinger *et al.*, 2001). Complete activation of IKK requires the presence of NEMO ZF, whilst mutations allow only for partial activation, being responsive to some but not all activating signals (Makris *et al.*, 2002).

1.4.3 NEMO LEUCINE ZIPPER

The leucine zipper (LZ) is common pattern observed in many protein structures, consisting of regions of leucine repeats every seven residues (Hakoshima, 2005). LZs typically display helical arrangements, as a result of the structural organisation of the leucine residues within the LZ regions. The non-Leucine residues also contribute to the overall stability of the regions by ensuring burying of hydrophobic amino acids and through the presence of stabilising non-covalent interaction (Lee *et al.*, 2003). Consequently, due to their structure and stability, LZs have been assigned roles in promoting protein dimerisation. Within NEMO, the CC2-LZ region is thought to play a role in promoting NEMO dimer formation and to facilitate binding to poly-ubiquitin chains (Grubisha *et al.*, 2010) and consequently NEMO activation (Bloor *et al.*, 2008).

1.4.4 NEMO NOA DOMAIN

In addition to LZ, the NEMO Optineurin Abin (NOA or UBAN or ABIN), is also known to facilitate ubiquitin interactions. Mutations in the NOA domain have been found in a number of diseases associated with NEMO (Rahighi *et al.*, 2009; Filipe-Santos *et al.*, 2006). The X-ray crystal structures of mouse CC2-LZ regions (including NOA domain) showing a coiled-coil structure are shown in Fig.7.

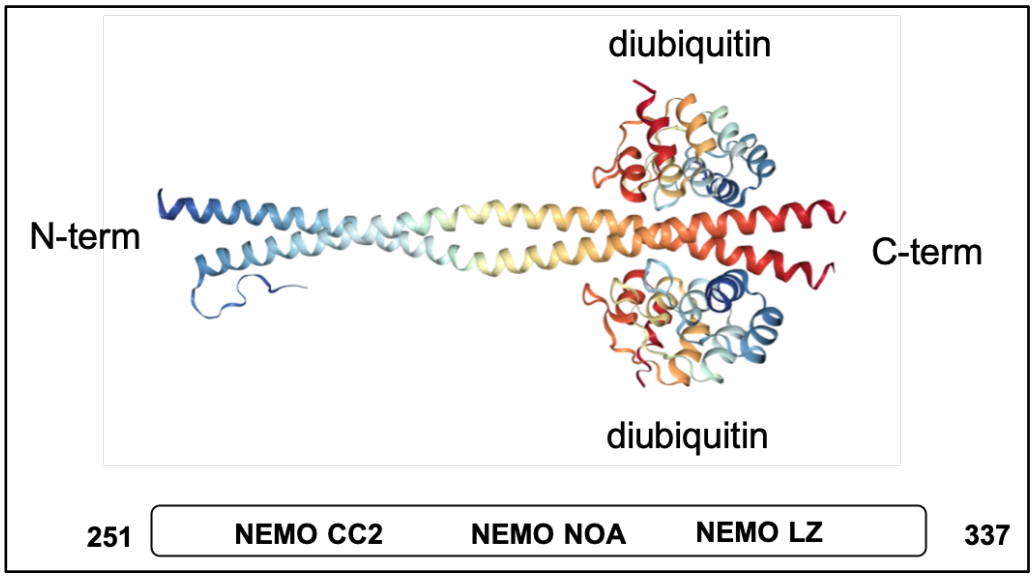

Figure 7. X-ray crystal structures of mouse NEMO CC2-LZ including the NOA domain bound to ubiquitin (Figure adapted from Chiaravalli *et al.*, 2011)**. NEMO structure solved at 2.9 Å, showing the CC2, NOA, and LZ domains, shown here bound to two molecules of diubiquitin (PDB ID: 2V4H).**

1.5 NEMO:UBIQUITIN INTERACTIONS

Ubiquitin is a small protein abundant in all eukaryotic cells with a plethora of functions, including tagging of molecules to undergo proteoasomal degradation (Pickart, 2004), cell signalling (Haglund and Dikic, 2005), DNA repair (Uckelmann and Sixma, 2017), and others. Ubiquitin owns its many functions to its ability to form complex ensembles with other ubiquitin proteins, linking at specific lysine residues (K6, K11, K27, K29, K33, K48, K63) and resulting in poly-ubiquitin chains (Komander and Rape, 2012). It can also exist as linear or Met 1-linked polyubiquitin chains, whereby the C-terminus of one ubiquitin can bind the N-terminal methionine residues of another ubiquitin (Komander and Rape, 2012; Rittinger and Ikeda, 2017).

Within NF-κB signalling, ubiquitin has been demonstrated to play important roles in initiation of activation of the pathway, mainly through non-covalent interactions with NEMO (Hadian *et al.*, 2011; Gautheron and Courtois, 2010), through the LZ and NOA domains.

NEMO binds to a variety of ubiquitin chains, including linear (Met1 (Rahighi *et al.*, 2009)), K11 (Hadian *et al.*, 2011), K48 (Yuan *et al.*, 2014), K63 (Laplantine *et al.*, 2009). NEMO activation upon binding to ubiquitin is not yet fully understood, and a few

mechanistic models have been proposed to explain this functional interaction. Potentially binding of ubiquitin functionalises NEMO by ensuring the protein assumes a conformation that promotes recruitment of IκBα, to facilitate the interaction between IKKβ: IκBα (Schröfelbauer *et al.*, 2012). This is thought to be achieved through ubiquitin allosteric control, as the binding sites for ubiquitin and IKKβ do not overlap (Catici *et al.*, 2015). Other studies suggest that activation of IKKβ is achieved through *trans*-autophosphorylation following conformational changes within the IKK complex (Polley *et al.*, 2013), upon binding of ubiquitin to NEMO (Rahighi *et al.*, 2009). A similar model suggests that NEMO ubiquitination acts as a tag for the recruitment of kinases that can phosphorylate IKKβ and thus activate it. This is supported by localisation of NEMO to the cell membrane (Nakamori *et al.*, 2006; Konig *et al.*, 2012), where the enzyme TAK1, an activator of IKK (Wang *et al.*, 2001) is activated in response to NF-κB stimuli (Jiang *et al.*, 2002). TAK1 phosphorylates IKKβ at the Ser 177, which induces the autophosphorylation of the Ser 181, thus leading to the activation of IKKβ (Zhang *et al.*, 2014). Activated IKK enzymatic complexes have also been reported in various membrane compartments of axons *in vitro* (König *et al.*, 2018). Similar mechanisms were reported in a study where binding of ubiquitin to the enzyme RIP1 promoted the interaction and ubiquitination of NEMO and subsequently allowed for the recruitment of TAK1 and activation of IKK complex resulting in NF-κB activation (Ea *et al.*, 2006). Refer to Fig.8 for detailed activation models.

The CC2-NOA-LZ (known as NEMO CoZi) binds linear ubiquitin chains with an affinity of 1.6 μM, approximately 100 times higher than K63 ubiquitin, due to each NEMO monomers binding in a two-way fashion to neighbouring ubiquitin chains (Lo *et al.*, 2009). NEMO ZF contributes a second ubiquitin binding site, with no notable preference for Met1 or K63-linked ubiquitin (Laplantine *et al.*, 2009). Structural studies report that NEMO CoZi domain assumes a dimeric conformation and binds linear ubiquitin resulting forming a heterotetrametric complex of NEMO dimers with two linear ubiquitins. Specifically, hydrophobic patches of one NEMO monomer interact with the Leu8-Ile44-Val70 triad of the distal ubiquitin, while the polar regions of the other NEMO monomer bind to a surface adjacent to the proximal ubiquitins hydrophobic patch (Rahighi *et al.*, 2009). Binding to K63-linked chains is mediated

through one binding side, with only the hydrophobic NEMO residues being involved in this interaction (Yoshikawa *et al.*, 2009). Binding to linear ubiquitin functions to activate NEMO and promote interactions with the IKK complex (Fujita *et al.*, 2014; Tokunaga *et al.*, 2012), thus initiating activation of NF-κB.

NEMO has also been reported to bind Met1/K63-ubiquitin hybrid chains (Emmerich *et al.*, 2013). While Met1 chains activate NEMO and promote IKK association, the presence of K63 chains is thought to facilitate the translocation of the NEMO:IKKβ complex to the membrane to allow IKKβ activation through interactions with TAK1 enzyme (Emmerich *et al.*, 2013). As activation of TAK1 requires K63-ubiquitin chains (Xia *et al.*, 2009), potentially the role of NEMO binding to K63-ubiquitin hybrid chains is to ensure both the IKK complex and their activating kinases (such as TAK1) are colocalised to the same polyubiquitin chain, thus facilitating the activation of the NF-κB canonical pathway.

The multitude of polyubiquitin binding possibilities for NEMO accounts for the variety of models for NEMO-dependent IKK and NF-κB activation, where different activating mechanisms function to ensure that transmission of a plethora of stimuli for NF-κB successfully results in the activation of the pathway.

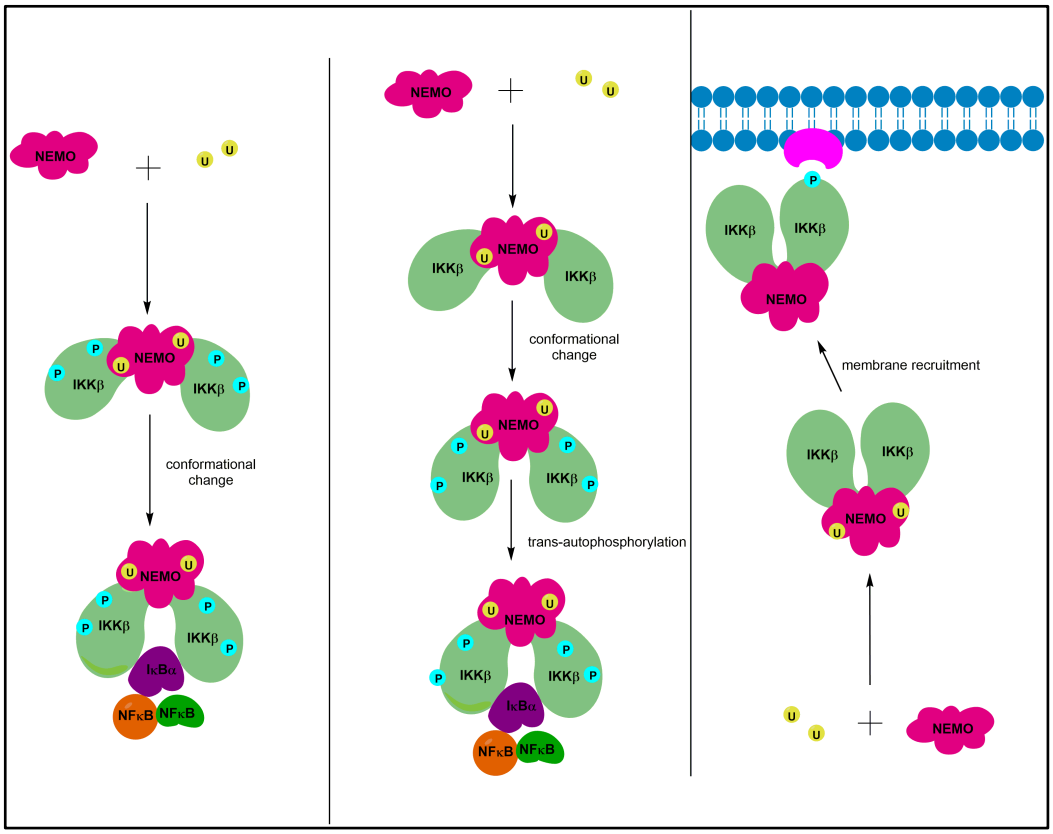

Figure 8. Proposed mechanisms for ubiquitin mediated NEMO and NF-κB activation.
Models for the activation of NEMO upon binding to ubiquitin and subsequent activation of NF-κB in response to canonical stimuli. P, phosphorylation; U, ubiquitination.

A generalised ubiquitin activation model of NEMO and NF-κB is proving difficult to predict due to the variety of NF-κB activating stimuli and the diversity of cells containing the signalling pathway. It is possible that the NEMO:ubiquitin interaction is stimulus dependent. Reports show stimulation of NF-κB through TNF and IL-1 involve different ubiquitin proteins, illustrating another layer of specificity within the pathway (Tarantino *et al.*, 2014). Consequently, the above-mentioned models should not be considered mutually exclusive, but rather a synergistic representation of the complexity of NF-κB signalling.

As polyubiquitin chains play crucial role in activating NF-κB, a number of deubiquitinates have been found to negatively regulate the pathway (Harhaj and Dixit, 2011). A20 deubiquitinase controls inhibition of NF-κB by associating with the C-terminal domain of NEMO and ensuring deubiquitination of K63-linked ubiquitin chains (Zilberman-Rudenko *et al.*, 2016). Similar results have been reported for

deubiquitination of K63-linked ubiquitin chains from TRAF6, resulting in termination of NF-κB (Lin *et al.*, 2008). Cezanne or Cellular zinc finger anti-NF-κB deubiquitinase inhibits NF-κB by targeting K11-ubiquitn chains on substrates present in the TNFR complex (Bremm *et al.*, 2010). Another deubiquitinase, cylindromatosis (CYLD) targets both NEMO and TAK1 K11-lysince chains and acts as a tumour suppressor (Kovalenko *et al.*, 2003).

1.6 NEMO OLIGOMERIC STATE

A consensus has yet to be reached about NEMO oligomerisation state. Experiments using only the C-terminal coiled coil region show the oligomerisation state of NEMO is concentration dependent, with the CC2 region existing as monomer, dimer, and trimer, at various protein concentration (Agou *et al.*, 2004). Full-length recombinant NEMO was reported to also exist as dimers (Huang *et al.*, 2002) and trimer (Rothwarf *et al.*, 1998) under *in vitro* cross-linking conditions . In contrast, purified NEMO from HeLa cells appears to form tetramers (Tegethoff *et al.*, 2003), whilst other studies report HeLa cells purified NEMO to exist in its dimeric and trimeric forms (Agou *et al.*, 2002). NEMO pentamers were also identified in cross-linking experiments of recombinantly produced protein (Fontan *et al.*, 2007) and from truncated NEMO N-termini (Lo *et al.*, 2008).

Many of these discrepancies arise due to different cross-linking and purification conditions, specific NEMO regions studied, as well as differences in cell type and protein concentration. These findings also reveal the plethora of conformations available for NEMO to access and illustrate the dynamic nature of the protein. The majority of these studies agree that the presence of a binding partner contributes towards the type of NEMO oligomeric state observed. Taking into account the range of NEMO roles both within and outside NF-κB and its increased number of interacting partners in the cell (~100) (Fenner *et al.*, 2010) suggests that the many theories about NEMO oligomeric state will be challenging to unite. Instead, the oligomeric state of the protein should be viewed in lieu of the functional significance of NEMO conformation(s).

1.7 NEMO - lack of consensus on structure and a case for disorder

The degree of disorder or molecular flexibility for NEMO is predicted to be between 41-49 % (Catici *et al.*, 2015). These findings suggested the existence of intrinsically unstructured regions at both the N- and C-termini, and have been corroborated with far UV-circular dichorism measurements (Catici *et al.*, 2015). The predicted disordered NEMO regions also appear to overlap with the regions proving challenging to structurally characterise using standard structural techniques such as X-ray crystallography or nuclear magnetic resonance. The findings suggest that NEMO adopts a molten globule state, with the protein capable of undergoing functional conformational change when bound to different ligands.

Very little consensus exists within literature about the nature of these unstructured regions, and of NEMO overall. One study reports a 'native' coiled-coil conformation at the C-terminus of NEMO upon the addition of a disulphide bond at two specific cysteine residues (Zhou *et al.*, 2014). Indeed, the two cysteine residues located at positions 54 and 347 do form disulphide bonds *in vivo* and in response to treatment with H_2O_2 (Herscovitch *et al.*, 2008). However, such findings must be considered with caution, as the study predicts the overall protein structure based on a truncated construct.

An alternative approach examines the use of NEMO binding partners (or mimics of such) in structural studies to elucidate protein functional structural changes, such as binding to IKKβ (Guo *et al.*, 2014). The structure of truncated human NEMO bound to a viral protein (vFLIP) was solved using X-ray crystallography and shows the protein sequence corresponding to amino acids 150-272 is a helical conformation and adopts a coiled-coiled arrangement (Bagnéris *et al.*, 2008). Structure can be seen in Fig.9.

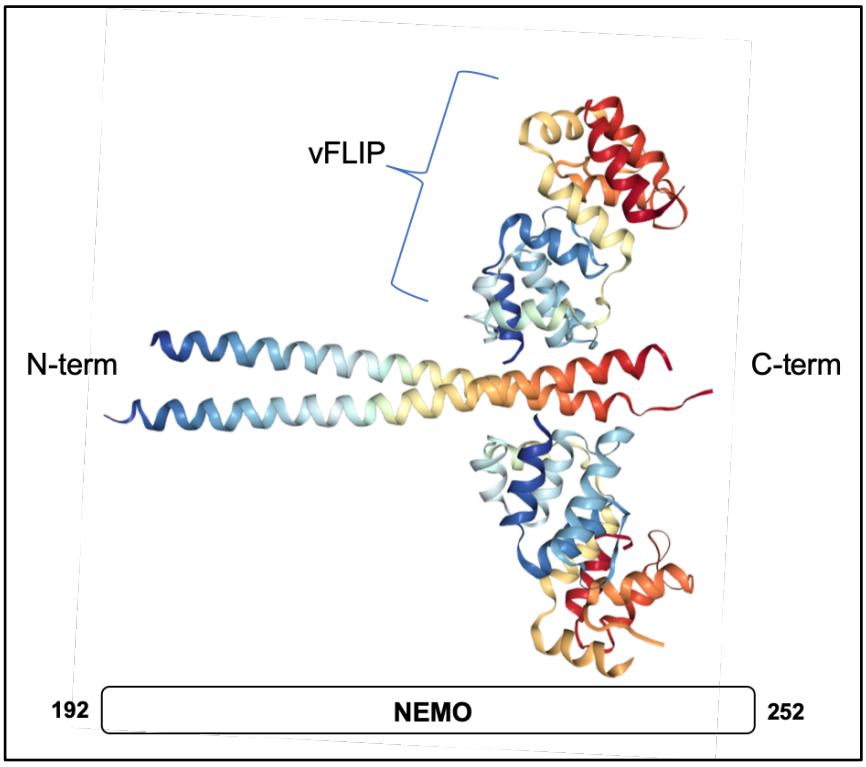

Figure 9. X-ray structure of human NEMO bound to viral protein vFLIP (Figure adapted from Bagnéris *et al.*, 2008)**. Human NEMO amino acid region 192-252 solved at 3.2 Å resolution (PDB ID: 3CL3), bound to vFLIP amino acids 1-178.**

The vFLIP protein is an important NEMO binding partner as it is used to control activation of NF-κB following viral infections. vFLIP, also known as viral flice-interacting protein, is a viral protein associated with Kaposi sarcoma-associated herpes virus (KSHV) (Jenner *et al.*, 2001). The protein is able to bind to NEMO and activate the IKK complex (Matta *et al.*, 2003), as well as protect against apoptosis of infected cells (Tolani *et al.*, 2014).

The NEMO:vFLIP complex was subjected to further structural characterisation using electron paramagnetic resonance (EPR) spectroscopy (Bagnéris *et al.*, 2015). In this study a truncated human NEMO protein (with missing parts of the C- and N-termini) was reported to adopt helical conformations across the entirety of the protein, with no evidence for unstructured regions. The study also used IKKβ fragment (644-756) and diubiquitin to determine the NEMO conformation in response to binding these ligands (Fig. 10).

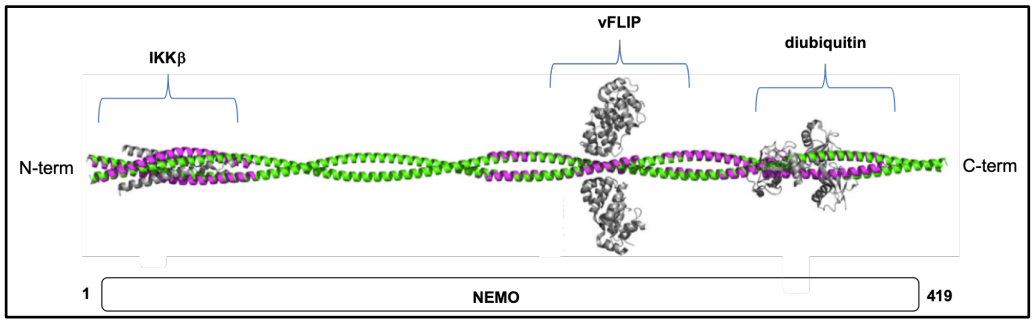

Figure 10. Model of full-length NEMO incorporating X-ray crystal structures of solved NEMO domains (Adapted from Bagnéris *et al.*, 2015)**. The figure includes solved structures of NEMO (shown in magenta) bound to IKKβ ,vFLIP, and diubiquitin (shown in grey), and a theoretical model for regions missing crystallographic data (shown in green). This This research was originally published in the Journal of Biological Chemistry, Bagnéris, C., *et* al. (2015) Probing the solution structure of IκB kinase (IKK) subunit γ and its interaction with Kaposi sarcoma-associated herpes virus flice-interacting protein and IKK subunit β by EPR spectroscopy. Journal of Biological Chemistry, 290(27), pp.16539–16549.**

Recently, new evidence has emerged that challenges the model of NEMO as a rigid molecule. Using size exclusion chromatography coupled with small-angle X-ray scattering (SEC–SAXS), it was shown that NEMO is not one long coiled-coil but rather is capable of undergoing conformational change when interacting with vFLIP (fused to a MBP tag), as well as in response to interacting with ubiquitin (Hauenstein *et al.*, 2017). The SAXS structure of full-length structure of full-length human NEMO can be seen in Fig.11.

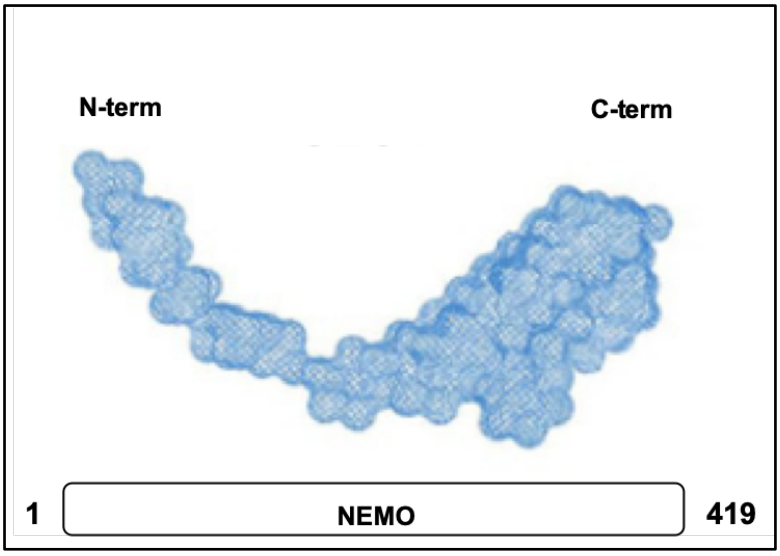

Figure 11. Structure of NEMO bound to vFLIP (not shown here) as determined by small-angle X-ray scattering (Figure adapted from Hauenstein *et al.*, 2017). **Full-length human NEMO as determined by SAXS following *ab initio* modelling showing the refined protein envelope upon binding to vFLIP (ligand omitted in this model).**

The structure shows NEMO adopt a 'comma' shaped conformation, ~ 320 Å in size, smaller than the predicted extended coil-coil structure. The authors report a compact conformation for unstimulated NEMO, proposing a model where both the N- and C-termini are capable of undergoing conformational change; both in the MBP-vFLIP bound state (due to allosteric regulation), as well as for unbound NEMO (a movement thought to control activation of NEMO in absence of stimuli). Based on these findings, a new model for NEMO structure has been proposed, where the protein exists mostly as a coiled-coil, with parts of the protein capable of undergoing conformational change upon binding to a ligand, a conformation similar to molten globule (Hauenstein *et al.*, 2017).

1.7.1 WHAT IS PROTEIN DISORDER?

As mentioned, much debate exists about the structure of NEMO and its potential dynamic nature. Protein disorder is now accepted as a more common feature in nature, with proteins from all kingdoms of life (including viruses) exhibiting varying degrees of disorder (Xue *et al.*, 2012; Ward *et al.*, 2004; Dunker *et al.*, 2008). The concept was first met with much scepticism, as it challenged the central dogma of protein biochemistry where proteins fold to assume a stable native conformation in order to be considered functional inside the cell. Intrinsically disordered proteins (IDPs) are protein that lack an obvious native conformation, but appear to be functional (Uversky, 2011). Crucially, many IDPs have been shown to carry out important roles, including in: cell signalling and regulatory networks (Tantos *et al.*, 2012; Haynes *et al.*, 2006), cell division (Galea *et al.*, 2008), acting as chaperones (Treweek *et al.*, 2010; Reichmann *et al.*, 2012; Ivanyi-Nagy *et al.*, 2005), scaffold proteins (Cortese *et al.*, 2008; Xue *et al.*, 2013), forming complex molecular assemblies (eg. in the ribosomal complex contain disorder regions (Peng *et al.*, 2014)).

Although present in all phyla of life, the abundance of protein disorder is now seen as a potential evolutionary development in response to the complexity of multicellular life (Pancsa and Tompa, 2012; Schad *et al.*, 2011). The disorder regions within proteins are also rich in post-translational modification sites, thus allowing for another layer of structural and potentially functional heterogeneity in disordered

proteins (Collins *et al.*, 2008; Gao and Xu, 2012).

The free energy landscape (FEL) model of protein folding accounts for the existence of disordered proteins and their subsequent folding following molecular interactions or changes in the environment. FELs encompass a series of energetic 'hills' and 'valleys', each corresponding to a particular folding intermediate, with the protein native state usually residing at the bottom of the funnel-like energy landscape. Unlike proteins with a well-defined native structure, disordered proteins or proteins that contain disordered regions are described as having a more 'rugged' FEL, accounting for the high degree of structural flexibility (Shown in Fig.12). The conformations on a disordered protein FEL will exhibit different degrees of thermodynamic stability, even in the absence of a well-defined folded structure.

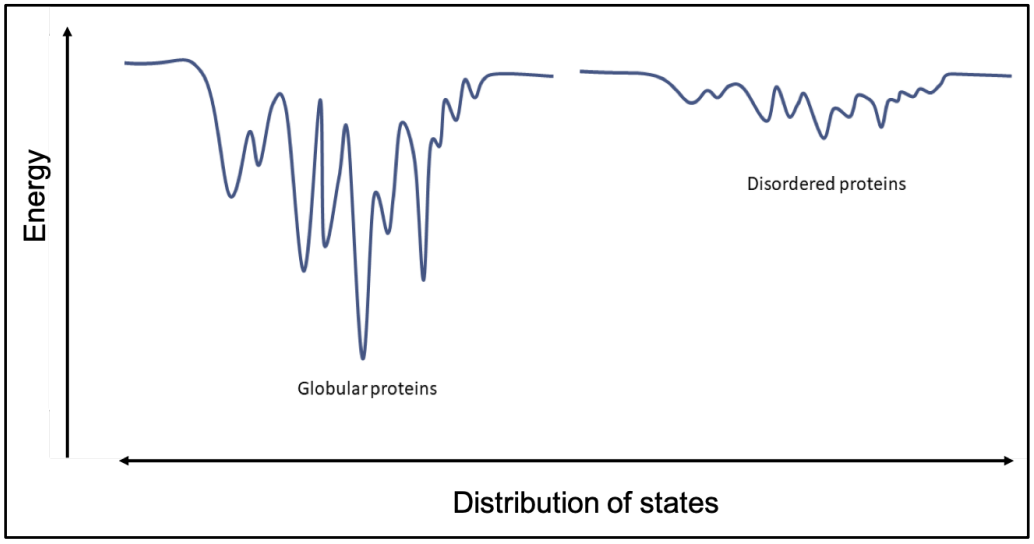

Figure 12. Cartoon representation of a hypothetical free-energy landscape (FEL) of globular proteins *vs* disordered. Disordered protein FELs are typically described as more 'rugged' compared to non-disordered (or globular) proteins, the FELs of which are much more 'funnel-like' .

There are a number of advantages to protein disorder. These include: ligand binding promiscuity (Tompa *et al.*, 2005), control through allostery (Ferreon *et al.*, 2012), accommodation of many PTM sites (Xie *et al.*, 2007). Due to their many advantages, disordered proteins also have industrial applications, including in biomineralisation (Boskey and Villarreal-Ramirez, 2016), cryo-protection of biological

agents (Matsuo *et al.*, 2018), and potentially assist in the design of novel drug targets (Cheng *et al.*, 2006; Metallo, 2010). However, disordered protein have also been linked to a number of pathological conditions, including neurodegenerative diseases (such as Parkinson's disease and Alzheimer's diseases), and various cancers (Uversky *et al.*, 2014).

1.7.2 NEMO flexibility and ligand induced conformational change

NEMO as a molten globule exhibits many of the characteristic features of IDPs, including: presence of amino acid sequence specific for disordered regions (Radivojac *et al.*, 2007; Dunker *et al.*, 2008), the ability to accommodate an array of PTMs (Sebban *et al.*, 2006; Wuerzberger-Davis *et al.*, 2007; Mabb *et al.*, 2006). Conformational flexibility is present in other NF-κB proteins as well. For instance, the X-ray crystal structure of inhibitor IκBα bound to p50 and p65 shows very little evidence of flexibility (Jacobs and Harrison, 1998). However, experiments using 8-Anilinonaphthalene-1-sulfonic acid (ANS) and amide exchange report that IκBα undergoes conformational change upon binding to NF-κB proteins, showing molten globule-like behaviour with specific regions within the ankyrin repeats displaying varying degrees of flexibility (even upon binding to p50 or p65) (Truhlar *et al.*, 2006). Similar conformational changes in IκBα have also been reported using other structural techniques (Croy *et al.*, 2004; Sue *et al.*, 2008; Trelle *et al.*, 2016).

More recently, studies using super-resolution microscopy have observed for the first time the organisation of NEMO oligomers determined in two cell types which appear to be missing in patients suffering from a NEMO-associated condition known as *Incontinentia pigmenti* (Scholefield *et al.*, 2016). The formation of the NEMO 'lattice' was also highly dependent on ubiquitin binding, suggesting that ubiquitin guides the NEMO oligomerisation. The authors also report that the catalytic subunit of IKK contribute towards lattice formation. These complex protein assemblies are thought to be important for activation of the IKK complex, and offer more information for understanding the role of NEMO in the activation of NF-κB signalling (Scholefield *et al.*, 2016). Evidence for NEMO:IKK protein cellular assemblies has also been provided in a

previous study where canonical and non-canonical NF-κB stimuli promoted complex protein assemblies at the cell membrane in U20S cells (Tarantino *et al.*, 2014). As a result, a new model of NEMO oligomerisation and activation has been proposed, whereby the complex NEMO lattices are formed by N-termini of one protein interacting with one of more N-termini of another NEMO molecule, with similar interactions happening at the C-termini (Scholefield *et al.*, 2016). As such, multimers can be observed, which have already been proposed as a potential mechanism for IKK and NF-κB activation. See Fig.13 for proposed NEMO oligomerisation model based on the structure of the NEMO lattice.

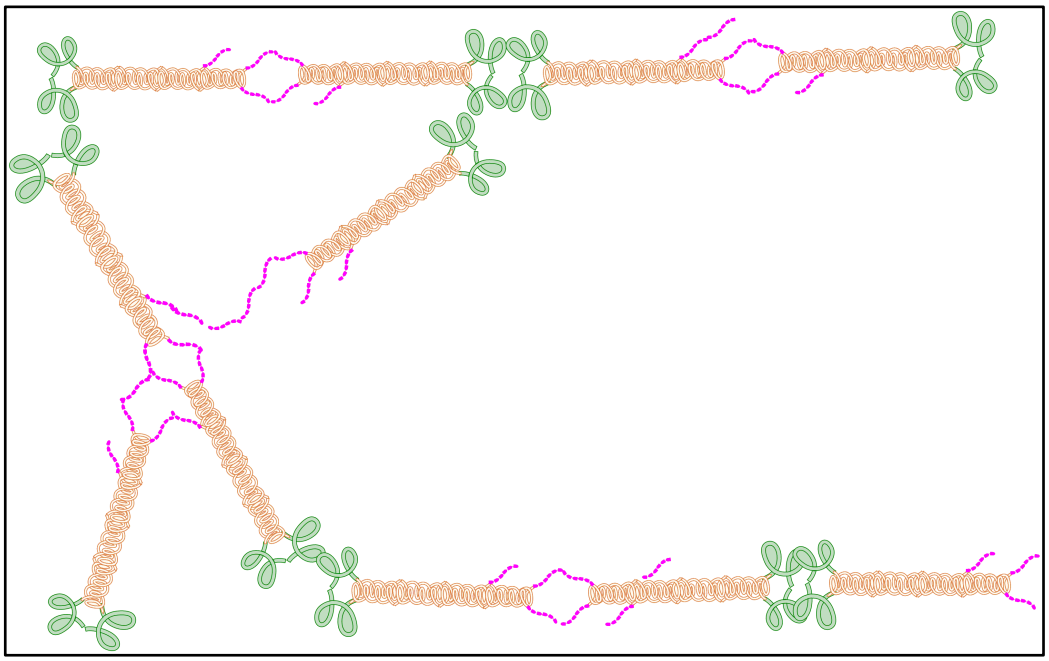

Figure 13. Proposed mechanism for NEMO oligomerisation. Shown in green are IKKβ dimers, in pink are chains of ubiquitin, light orange are NEMO dimers (Based on model proposed by Scholefield *et al.*, 2016). The model shows the proposed mechanism by which NEMO oligomerisation is driven by interaction with IKKβ and ubiquitin chains. These lead to the formation of NEMO lattice structures, whereby the N-terminus of one NEMO monomer interact with the N-terminus of another NEMO monomer, with similar interactions proposed for NEMO C-termini.

1.8 NEMO in health & disease

A number of pathological conditions have been associated with NEMO. These include conditions arising due to genetic modifications of the NEMO gene, such as immunodeficiency (Fusco *et al.*, 2008), anhidrotic ectodermal dysplasia with

immunodeficiency (Smahi *et al.*, 2000), and *Incontinentia pigmenti* (Hanson *et al.*, 2008). The latter is considered one of the more severe conditions as it often results in male embryonic lethality (Scheuerle and Ursini, 1993). The IKBKG gene (the gene for NEMO) is located on the long arm of the X-chromosome (Xq28) (Fusco *et al.*, 2008), and transmission of a mutated version to a male embryo is not compatible with life (Wettke-Schäfer and Kantner, 1983). Improper NEMO and NF-κB functioning have also been linked to play crucial roles in a number of inflammatory diseases (Maubach and Naumann, 2017) and some cancers (Park and Hong, 2016). Many studies have focussed on identifying targets capable of modulating the activation of NEMO and NF-κB in human disease (Zilberman-Rudenko *et al.*, 2016; Luedde *et al.*, 2007). These have raised concerns about the complex effects and safety of suppressing NEMO or NF-κB activation, as they control important physiological processes in cells. Pharmacological development is further complicated by the crosstalk between NF-κB and other regulatory networks, as the effects of modulating NEMO and NF-κB activation could extend beyond the canonical activation of NF-κB.

One of the most studied targets for inhibition of NF-κB activation through inhibition of the formation of the NEMO: IKKβ complex is a short peptide mimicking the NEMO-binding domain of IKK enzymes, known as the NBD peptide (May *et al.*, 2000). The 11 amino acid peptide has been shown to reduce inflammation in murine models of inflammatory diseases *in vitro* (May *et al.*, 2000). More recently, the peptide was part of a phase I clinical trial for the treatment of canine B-cell lymphoma, successfully reducing the growth of malignant B-cell, with no toxicity effects reported (Habineza Ndikuyeze *et al.*, 2014). Other promising therapeutic effects were also observed upon treatment with NBD in mice models of acute lung injury (Huang *et al.*, 2016), as well as mouse (Reay *et al.*, 2011; Peterson *et al.*, 2011) and dog (Kornegay *et al.*, 2014) models of muscular dystrophy. Although many animal studies report positive results, the cost associated with the production of the inhibitory peptide and its reduced half-life suggest further exploring of other therapeutic routes (Zhao *et al.*, 2018; Rhodes *et al.*, 2018).

Studies looking at inhibiting NEMO-mediated activation of NF-κB have also focussed on developing therapeutic peptides that bind to the NEMO NOA domain, to inhibit activation through ubiquitination of NEMO, rather than target the IKK complex (Chiaravalli *et al.*, 2011). More recently, an inhibitory peptide (iNUB) targeting the NEMO NOA domain was reported to modulate canonical activation of NF-κB signalling in response to some stimuli (Vincendeau *et al.*, 2016). The peptide impairs NEMO binding to ubiquitin and is hypothesised to be used to treat some NF-κB conditions while still allowing activation through other stimuli.

Despite considerable scientific advancement in understanding NEMO and NF-κB signalling, it is clear that further analysis of the structure, function, and their links to protein dynamics holds the key to answering many of the questions about the role of the NF-κB master regulator NEMO and develop better therapeutics for the treatment of NF-κB associated disorders.

1.9 AIM & OBJECTIVES

The aim of this PhD study is to understand the biophysical factors governing the structure, function, and dynamics of NEMO. To achieve this a combination of biophysical & biochemical techniques will be applied, such as pressure and temperature perturbations, red edge excitation shift spectroscopy, and isothermal titration calorimetry-based enzyme assays. Previous studies address the dynamic nature of the NEMO and emphasize the importance to taking into account its interactions with NF-κB ligands when considering its structure and dynamics. As such, the first objective of this study was to validate the use of an optical phenomenon known as Red edge excitation shift (REES) in studying protein dynamics. Whilst many structural techniques are available to use in elucidating protein structures, this study focused not on one particular NEMO conformation, but rather on understanding the breadth of conformational states available to the protein under specific conditions (ie. macromolecular crowding or ligand binding). REES spectroscopy is a technique that reports on the relationship between fluorophores and their surrounding environments. In the case of NEMO, a single tryptophan amino acid located at the N-

terminus of the protein in a region of the protein involved in interacting with the IKKβ enzyme will be used as an intrinsic fluorophore. Peptide mimics of all NEMO interacting partners will be used so as to avoid any fluorescence signal arising from the complex proteins and ensure that the REES signal observed is attributed to NEMO conformational change.

Secondly, information about the thermodynamics of NEMO conformational change can best be probed using hydrostatic pressure and temperature perturbations. In this instance, 8-Anilinonaphthalene-1-sulfonic acid (ANS) will be used an extrinsic fluorophore now allowing for monitoring of protein global conformational changes. These findings will complement the results from the local NEMO REES probe and help understand any differences in the dynamic nature of the protein and determine whether different parts of the protein exhibit different degrees of dynamics. Similarly, the effects of NEMO ligand binding on the thermodynamics of the protein will also be evaluated using *p*/*T* perturbations to further characterise the NEMO functional conformational change. In addition to testing the NEMO conformational changes in simple buffered conditions, thus study also aims to mimic the intracellular milieu, focussing on understanding the effect of the physical parameters of the intracellular milieu on the structure and dynamics of NEMO.

Understanding the role of NEMO inactivating the NF-κB signalling is of great interest, especially seen as a high number of clinical conditions are linked to improper functioning of NEMO/NF-κB. In order to elucidate the role of NEMO in mediating the interaction between the enzyme IKKβ and its substrate, the inhibitor IκBα during canonical activation of the pathway. The kinetics of the IKKβ enzyme will be monitored using isothermal titration calorimetry (ITC), both in the presence and absence of NEMO. Using ITC allows for monitoring the enzyme reaction under continuous conditions, and whilst a number of studies have tackled this question previously, but this is the first time the full length-NEMO and IKKβ are used. The results of these measurements will help better understand the scaffold role of NEMO and the

Taken together, these objectives will offer a comprehensive understanding of NEMO conformational change in response to ligand binding and changes in the environment, as well as help in understanding the scaffold role of NEMO and the complex activation of the NF-κB signalling. The different experimental set-ups described above ensure a detailed and complementary analysis of the biophysical factors affecting the structure, dynamics, and function of NEMO.

Chapter 2: Introduction to methodologies

2.1 Spectroscopic methods to study protein conformational change

The central dogma of biochemistry states that there is an intrinsic relationship between protein structure and function. Proteins carry out important cellular functions, based on their native structures and cellular localisation (Uhlen *et al.*, 2010). Intrinsically disordered proteins or conformationally dynamic proteins challenge the structure-function relationship, as they have been proven to have specific cellular functions even in the absence of a defined native structure (Uversky, 2011; Forman-Kay and Mittag, 2013). Many available techniques aimed at determining molecular structure pose obstacles to being used on such flexible systems, due to a number of factors, including: size restriction and signal-to-noise ratio. Fluorescence spectroscopy is a commonly used technique for studying protein conformations, including disordered or flexible proteins (Gong *et al.*, 2008; Ferreon *et al.*, 2012). The techniques relies on protein intrinsic fluorescence (Gorinstein *et al.*, 2000) or in the absence of intrinsic fluorophores, extrinsic probes are commonly used to monitor protein structures and conformational change (Hawe *et al.*, 2008). NEMO contains one intrinsic fluorophore, allowing for its intrinsic fluorescence to be easily measured using fluorescence spectroscopy to better understand the structure and conformational change of the protein.

2.2 Fluorescence – Principles and Applications

Fluorescence is a type of photoluminescence and together with phosphorescence has long been used as a technique in chemical and biological research (Sanders *et al.*, 1994). The basic principle of fluorescence depends on the ability of a compound or molecule to absorb and subsequently emit light (Lakowicz, 2006). In order to do so, molecules rely on electrons from the outermost electronic shell to move to a higher energy level upon absorption of extra energy applied to the system, normally in the form of a photon of a specific wavelength (Valeur, 2001).

The phenomenon was first studied in the 16th century (Valeur and Berberan-Santos, 2011; Acuña *et al.*, 2009) and nowadays fluorescence underpins many research fields, including: forensics research (Denny *et al.*, 2018), medical diagnosis (Lombardi *et al.*,

2015; Wang *et al.*, 2016), DNA sequencing (Lewis *et al.*, 2005), microscopy and cellular imaging (Sanderson *et al.*, 2014), and many more.

Briefly, fluorescence can be generally described as a three-step process: fluorophore excitation and photon absorption, fluorescence lifetime, and, emission of absorbed photon (Lakowicz, 2006). The classic way to illustrate the processes of photon absorption and emission that occur when a molecule is excited is through the use of a Jablonski diagram (Berezin and Achilefu, 2010). This energy-level diagram depicts the main electronic levels of ground and excited state electrons, and the main stages of fluorescence. Refer to Fig. 14 for Jablonski diagram.

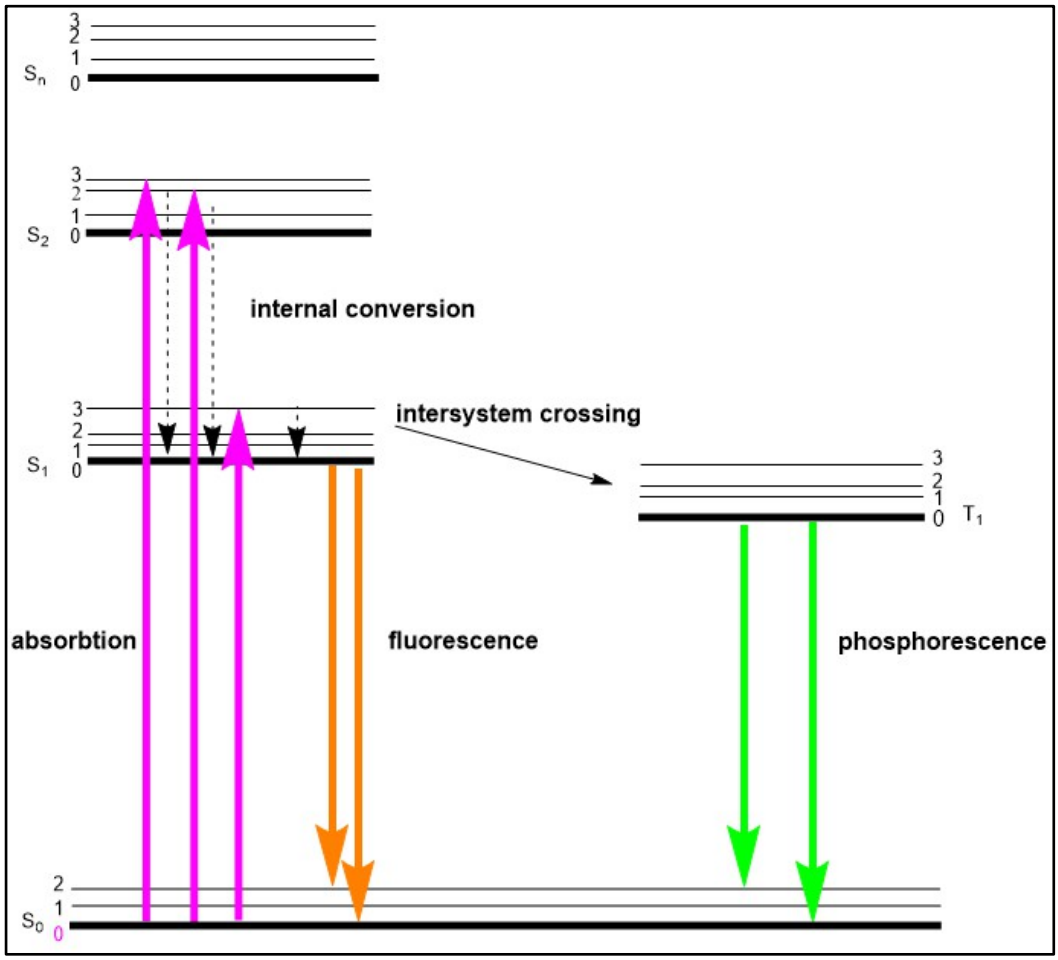

Figure 14. Jablosnki diagram illustrating the basic principle of fluorescence spectroscopy and phosphorescence (Figure adapted from Lakowicz, 2006)**. S,T, singlet and triplet electron states, respectively. The magenta, orange, and green arrows illustrate energy absorption, emission through fluorescence, and emission through phosphorescence, respectively. Molecules in the ground state (S_0) transition to higher energetic levels or excited states (S_1 or S_2) following absorption of energy. Due to processes such as internal conversion, some of the initial energy is lost before the electrons return to the ground state from the lowest energetic state of the excited state (S_1^0). Intersystem crossing may also occur, whereby electrons undergo spin conversion and transition to the triplet electronic state (T_1), and in this case phosphorescence is observed upon return to the S_0.**

2.2.1 Excitation

An external source is employed to generate a photon of energy ($h\vartheta_{ex}$), which gets absorbed by a fluorophore allowing it to transition from a ground electronic state (S_0) to a higher vibrational state of either S_1 or S_2, known as the excited state (Lakowicz, 2006; Berezin and Achilefu, 2010). See Figure 14 for details of various electronic states. Electronic levels of molecules are comprised of vibrational and rotational levels, denoted with 0,1,2 in Fig. 14. The ability of molecules to absorb and emit light and populate electronic excited states relies on the source of external energy emitting a photon with an energy that matches the energy difference between the different electronic states (S_0,S_1,S_2) in order for electronic transition to occur (Lakowicz, 2006).

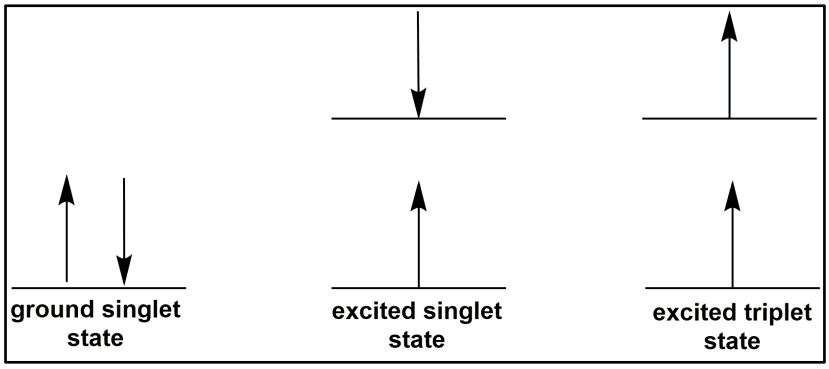

Figure 15. Electronic ground and excited states and corresponding electron spins. The arrows illustrate the electron spins for different energetic states, in accordance to Pauli's exclusion principle (Pauli, 1946). When an external energy force is applied, the electron spins change and will end up either parallel or antiparallel to the direction of the force ((Galitski and Spielman, 2013; Kleinpoppen and Becker, 1999). The antiparallel state is also known as the singlet (S) state, as the total spin number is zero. The ground state of the majority of organic molecules will be a singlet state, from which excitation will usually occur(Lakowicz, 2006; Chen *et al.*, 2017).

2.2.2 Fluorescence Lifetime

The fluorescence lifetime is the ability of fluorophores to stay in the excited state before losing the excess energy and emitting the absorbed photon, subsequently returning to the ground state (Lakowicz, 2006). The fluorescence lifetime is highly dependent on the quantum yield (φ) of the fluorophore, that is the proportion of photons emitted *vs* photons absorbed (Laverdant *et al.*, 2011; Lakowicz, 2006). Different fluorophores will have different fluorescence lifetimes due to: intrinsic

properties of the fluorophores (Szabó *et al.*, 2018), temperature (Vyšniauskas *et al.*, 2015), viscosity and polarity variations (Pant *et al.*, 1995), type of solvent (Magde *et al.*, 1999), as well as presence of other molecules in the environment, known as quenchers, which can act to decrease fluorescence lifetime (Lakowicz and Weber, 1973). Additionally, the fluorophore concentration may also lead to a reduction in the fluorescence lifetime. This is due to the inner filter effect, a process where the emitted photon is re-absorbed by fluorophore molecules instead of being emitted, or the concentration of fluorophore is so high that it hinders the detection of the emitted photon (Van De Weert and Stella, 2011).

Following excitation and transition to higher electronic levels, in the majority of cases due to events such as internal conversion, excited molecules will rapidly relax to the lowest vibrational level of S_1. This process is usually on the scale of 10^{-12} seconds, whilst fluorescence lifetime typically requires ~10^{-8} seconds (Shanker and Bane, 2008). As a consequence, emission will occur from the lowest energy level of S_1 (Lakowicz, 2006). Another possible transition from the S_1 state is towards the excited triplet state (T_1), in a process called inter-system crossing (Lakowicz, 2006). This is a complex transition and requires the electrons to undergo spin conversion (due to the differences in electron spin state between the S and T states) (Chan *et al.*, 2017). The emission of a photon from this state is called phosphorescence, and is not often observed in organic compound (Lakowicz, 2006). In addition to inter-system crossing and internal conversion, S states may also be subjected to other processes by which energy loss can occur. In some instances, energy transfer between molecules in close proximity can be observed (Shanker and Bane, 2008). It this case it is possible for the energy from one excited state molecule (known as donor molecule) to be transferred to the neighbouring molecule (known as acceptor molecule), thus causing the latter to transition to an excited state (Ma *et al.*, 2014). This process is called Fluorescence resonance energy transfer (FRET) or Förster resonance energy transfer, and in this instance, no emission or absorption occurs; instead, the energy transfer is achieved through coupling of donor and acceptor dipole moments (Förster, 1948). This is observed in nature in photosynthesis, a process where light is captured by specialised cells and subsequently transferred to chlorophylls, in an important process of plant

metabolism (Johnson, 2016). FRET can also be applied to studying molecular interactions (Ma *et al.*, 2014), to the design of chemical or biochemical sensors and is often used in combination with other techniques (Chen *et al.*, 2013; Sekar and Periasamy, 2003).

2.2.3 Emission

The last stage of fluorescence is the emission of a photon ($h\vartheta_{EM}$) and return of fluorophore electrons to the ground state. Due to the energy loss during fluorescence lifetime, $h\vartheta_{EM}$ photons will have a lower energy than $h\vartheta_{EX}$ photons and therefore be at a longer wavelength (Lakowicz, 2006). This phenomenon is called Stokes shift or Stokes law, named after Sir. G. G. Stokes who was the first to report this phenomenon in 1852 using quinine fluorescence (Stokes, 1852). This is often observed due the emission and excitation spectra of different fluorophores not overlapping, but rather being mirror images of each other (Voet and Voet, 2011). This is due to the similar distance between the electronic levels of the ground and excited states, compared to the reduced distances between the excited levels themselves, i.e., S_1 and S_2 (Lakowicz, 2006).

2.3 Fluorescence fundamental principles

Fluorescence is governed by two fundamental rules, which include Stokes shift and Kasha's rule. The first rule, Stokes law (or Stokes shift) shows that emission of a photon will always occur at longer wavelengths compared to the excitation wavelength (Stokes, 1852), as a result of a combination of processes whereby some of the initial photon energy is lost (Lakowicz, 2006). Various fluorophores and chromophores display different Stokes shift, depending on: their rigidity (Piatkevich *et al.*, 2013; Abbyad *et al.*, 2007), their dipole moments (the overall electronic displacement of the molecule following excitation) (Stopel *et al.*, 2014), the polarity of the environment the fluorophore is in (Haidekker *et al.*, 2005), temperature (Sasaki *et al.*, 2003; Watanabe *et al.*, 2017) and pH (Abbyad *et al.*, 2007; Baruah *et al.*, 2006). The Stokes shift phenomenon is seen in many fluorophores as well as in proteins, with Stokes shift spectroscopy having many applications, including in cellular imaging (Gao

et al., 2017) and potentially even for biomedical research in cancer fingerprinting and detection (Pu *et al.*, 2013).

A second characteristic of fluorescence is the fact that emission spectra do not depend on the excitation wavelength, a phenomenon known as Kasha's rule (Kasha, 1950). Due to the Stokes shift, emission will always occur from the lowest level of the S_1 state, and thus is independent of the excitation wavelength, as described previously. This is sometimes also referred to as the Kasha-Vavilov rule, as Vavilov showed that fluorescence quantum yields are also not influenced by the excitation wavelength (Birks, 1971; Lakowicz, 2006).

2.3.1 Exceptions: Inhomogenous Broadening of Spectra

Inhomogenous broadening of spectra is an optical phenomenon whereby as the excitation energy shift to higher wavelengths, the same can be observed for the emission spectra (Azumi *et al.*, 1976; Itoh and Azumi, 1973; Itoh and Azumi, 1975). This is known as the red edge excitation shift (REES) phenomenon and has been reported to occur in fluorophores located in polar or viscous environments (Azumi *et al.*, 1976; Itoh and Azumi, 1973; Itoh and Azumi, 1975). REES can be explained photophysically by the presence of different relaxation rates for the fluorophore and the environment upon excitation. If the time required for the newly excited fluorophore to undergo dipole reorganisation and relaxation is slower than that of the environment in which it is, emission is observed from a higher energy excited fluorophore instead of the relaxed state (Demchenko, 2002). See Figure 16 for Jablonski diagram showing the detailed REES effect.

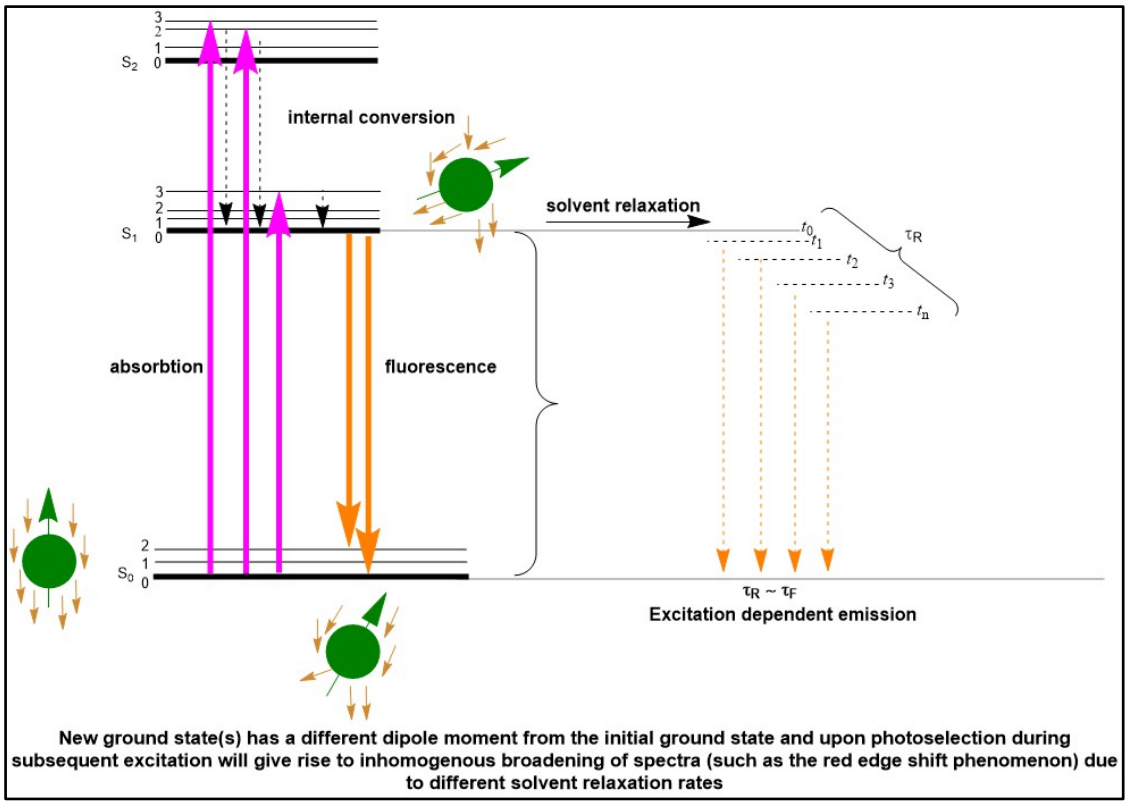

Figure 16. Jablosnki diagram showing the red edge excitation shift (REES) phenomenon. τ_R, τ_F, relaxation time and fluorescence time, respectively. The magenta, orange, and green arrows illustrate energy absorption, emission through fluorescence, and emission through phosphorescence, respectively. Green and brown arrows show the dipole moment of the fluorophore and environment, respectively.

Essentially, the REES effect reports on the interactions between the fluorophore and its environment. If the relation rates of the environment are slower than that of the fluorophore, when the fluorophore returns to the ground state upon emission, the environment will be different to that of the initial ground state. This is because the environment relaxation rates are slower compared to the fluorophore, and the new ground state when photoselected during further excitation will give rise to Inhomogenous broadening of spectra as a result of different relaxation rates and dipole-moments reorganisation following excitation.

The REES effect is strongly dependent on the interaction between solvent and fluorophore and can be used to photoselect for various fluorophore: environment conformations which possess different energetic requirements (Demchenko, 2002; Itoh and Azumi, 1975). Although initially reported in 1973 (Itoh and Azumi, 1973),

REES has only more recently become a useful tool in studying protein dynamics and conformational change (Haldar *et al.*, 2011; Chakraborty and Chattopadhyay, 2017).

2.4 Fluorescence in proteins

There are two categories of fluorophores: intrinsic (naturally occurring fluorophores) and extrinsic, a class of compounds that need to be added to desired samples to aid fluorescence (Lakowicz, 2006). The major contributor to protein fluorescence is the indole group (Teale and Weber, 1957). See Figure 16 for indole structure.

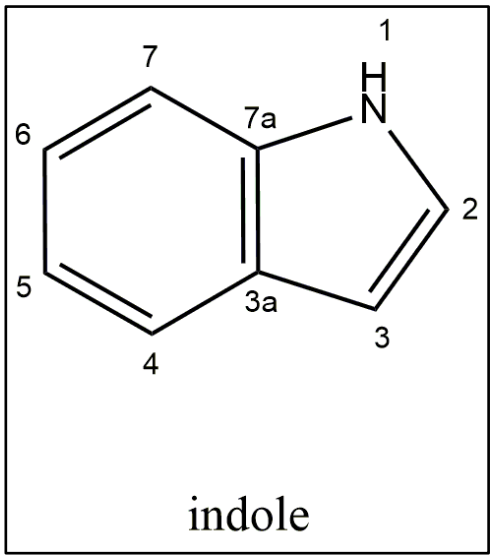

Figure 17. Structure of indole group.

This molecule is excited by light at 280 nm wavelength and will emit in the 340 nm wavelength region (Lakowicz, 2006). Due to its sensitivity to the environment, fluorescence of the indole group is often used as a probe for protein research (Ghisaidoobe and Chung, 2014). The emission of the indole group has been reported at higher energies (or lower wavelengths) in the compact structures of folded proteins (known as a blue-shifted emission), whereas the solvent exposed backbone of denatured proteins contributes to a lower energy emission (or higher wavelengths), a process known as red-shifted emission (Lakowicz, 2006).

In proteins, three naturally occurring fluorophores exist: tryptophan, tyrosine and phenylalanine (refer to Figure 18 for amino acid structures). However, only tryptophan

possesses the indole ring, and as such is the most commonly used in fluorescent studies, also due to its sensitivity to the environment solvation and polarity (Lakowicz, 2006). Phenylalanine and tyrosine are not often used as intrinsic fluorophores due to their low quantum yield and quenched emission, respectively (Munishkina and Fink, 2007). This is mainly attributable to the different photophysical properties of the three amino acids, with the asymmetric indole ring of tryptophan allowing for a greater electronic redistribution upon excitation, a phenomenon not observed for tyrosine and phenyl-alanine fluorescence (Teale and Weber, 1957).

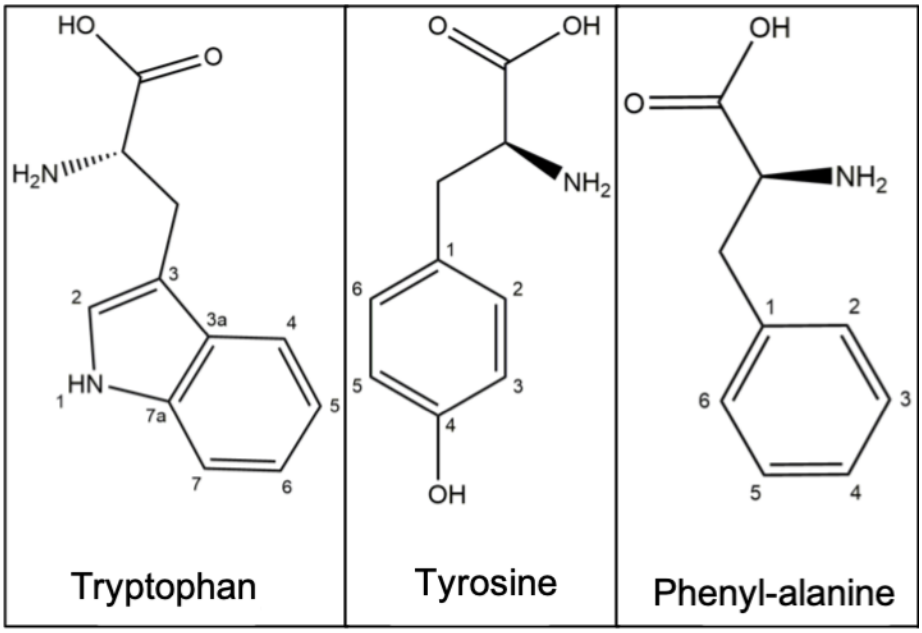

Figure 18. Structures of aromatic amino acids.

In addition to amino acids, other cellular components also contribute to the intrinsic biological fluorescence, and these include: elastin (Deyl *et al.*, 1980), collagen (Menter, 2006), nicotinamide dinucleotide (NADH) (Aubin, 1979) and flavins (Benson *et al.*, 1979).

Changes in spectroscopic characteristics of fluorophores such as intensity of the fluorescence emission, modulation of the fluorescence spectra, fluorescence lifetime, fluorophore quenching and others are quantifiable variables that allow fluorescence to be combined with a number of other techniques to offer detailed descriptions of protein behaviours. Some of these techniques include: fluorescence anisotropy (allows

for detection of changes in fluorophore between during excitation and emission) (Gijsbers *et al.*, 2016), fluorescence quenching (monitoring of protein binding and conformational change) (Mátyus *et al.*, 2006), FRET (analysis of protein complexes and protein dynamics) (Ma *et al.*, 2014). Fluorescence is a very versatile and information rich technique and thus used frequently in characterisation studies of proteins.

3. Hydrostatic pressure and temperature perturbations to study protein conformational change

Pressure and temperature have traditionally been used to study protein denaturation, the first ever such studies dating back to 1914 (Bridgman, 1914). Over the last 30 years, pressure perturbations have become commonly used in association with other techniques, such as nuclear magnetic resonance spectroscopy (Roche *et al.*, 2015), infrared spectroscopy (Liu *et al.*, 2014), stopped flow (Luong and Winter, 2015), fluorescence spectroscopy (Dang *et al.*, 2012), molecular dynamics simulations (Golub *et al.*, 2017), to obtain information beyond the denaturing role of pressure and thus answer questions about protein structure, function, and dynamics.

Proteins respond to the presence of a perturbant in the environment following Le Chatelier's principle. Thus, with increasing pressure, the equilibrium of a system will shift in such a way as to minimise the effect of the perturbant. For proteins, this means that an increase in pressure will promote a conformational shift to more compact protein conformations (Akasaka, 2006). These changes can be described using the following equation [Eq.1]:

$$\Delta G = -RTlnK = \Delta E + P\Delta V - \mathrm{T}\Delta S \qquad [eq.1]$$

where, ΔG, ΔE, ΔV, ΔS, are changes: in Gibbs free energy, internal energy, volume, and entropy, respectively, and R, T, K, P represent the gas constant, temperature, equilibrium constant, and pressure, respectively.

Similarly, an increase in temperature for proteins results in the system reacting in such a way as to minimise this effect. This can be explained by the van't Hoff equation [Eq.2]:

$$lnK = -\frac{\Delta H}{RT} + \frac{\Delta S}{R} \qquad [eq.2]$$

where, ΔH, ΔS, R, T, K are enthalpy change, entropy change, universal gas constant, and equilibrium constant, respectively.

Here, the effect of temperature on the system in accordance with Le Chatelier's is observed on the equilibrium constant of the reaction. In the case of protein structure, the equilibrium between native and unfolded states is affected by changes in temperature (Campbell, 1985).

3.1 Thermodynamic effects of pressure and temperature

The primary structures of most proteins will not be affected by pressures lower than 10kbar, as they are mainly stabilised by covalent bonds (Mozhaev *et al.*, 1996); higher order oligomers are sensitive to pressures over 3 kbar (Royer, 2005). Similarly, protein secondary structures are often insensitive to pressures of up to 3 kbar (Iwadate *et al.*, 2001; Lerch *et al.*, 2015), with most proteins denaturing at pressures between 4-10 kbar (Mozhaev *et al.*, 1996; Oliveira *et al.*, 1994; Ruan *et al.*, 2001; Herberhold *et al.*, 2003; Kamatari *et al.*, 2004) . Non-covalent interactions are most sensitive to pressure changes, as they are major contributors to protein stability (Nick Pace *et al.*, 2014; Černý and Hobza, 2007).

Under the effect of pressure, proteins will adopt more compact conformations, in accordance with Le Chatelier's principle. This is governed by a variety of the thermodynamics parameters including changes in: enthalpy (ΔH), entropy (ΔS), compressibility ($\Delta \beta$), expansivity ($\Delta \alpha$), heat capacity (ΔC_p), and specific volume (ΔV).

Specific volume or partial molar volume refers to the space occupied by the protein, internal cavities and solvation envelope included (V=$V_{protein}$+V_{void}+$V_{solvent}$) (Akasaka, 2006); this will be different for each different protein conformation, especially varying between the native state and unfolded state. The differences in the specific volume arise mostly due to hydration changes and packaging of protein cavities (Cioni and

Gabellieri, 2011). These changes in hydration state and overall volume give an explanation to the existence of various protein states, which populate the FEL and can be easily accessed using hydrostatic pressure. The major difference between native and unfolded protein state is in the hydration state, as unfolded proteins have an increased surface area compared to native structures, thus showing an increased hydration (Royer 2005).

The magnitude and sign of Δ*V* are sensitive to pressure and temperature changes, as both affect the structure and solvation of proteins. Generally, under denaturing pressures, proteins exhibit a positive Δ*V* at lower pressure and a negative value is seen at higher-pressure ranges (Kauzmann, 1987). Similarly, temperature denaturation leads to an increase and positive value in Δ*V* compared to native state (Chen and Makhatadze, 2017). Although pressure is largely seen to induce compaction (Akasaka, 2006), the seemingly contrasting values and sign of Δ*V* arise due to differences in internal voids (Dellarole *et al.*, 2013) and degree of hydration (Royer, 2005).

Thermal expansion coefficient (α) represents the fluctuation in volume of the system (solvent included) with respect to temperature (Vasilchuk *et al.*, 2014). The sign and value of the expansion coefficient of proteins are sensitive to temperature and pressure perturbations. Individual α values for different amino acids have been determined experimentally (Lin *et al.*, 2002; Mitra *et al.*, 2006); the general trends suggest that at low temperatures, polar residues show positive and increased α values, (possibly due to solvent electrostriction). On the other hand, non-polar residues show increased and negative values for α at low temperatures; this is thought to arise as a result of reorganisation of water molecules (Lin *et al.*, 2002; Mitra *et al.*, 2006).

Thermal compressibility coefficient (β) reports on the changes in the volume of the system in response to pressure (Heremans and Smeller, 1998).
Thermal compressibility can also be used as a probe of the free energy landscape of proteins, as it is sensitive to conformational heterogeneity (Frauenfelder *et al.*, 1990). Studies show that generally, amino acids possess negative compressibility (Millero *et al.*, 1976), due to the differences in compressibility between them and solvent

(Kharakoz and Sarvazyan, 1993). However, the presence of protein internal cavities negates this, with the overall protein compressibility carrying a positive sign (Kharakoz, 2000). Cavities are an important contributor to the compressibility of macromolecular structures, and protein compressibility is not often uniform. Computer simulations shows that this arises due bigger cavities being more compressible than smaller cavities (Paci and Marchi, 1996). The presence of different secondary structures also contribute to uneven compressibility, as helices appear to be less sensitive to pressure perturbations compared to non-helical regions (Iwadate *et al.*, 2001)

Thermodynamics defines **enthalpy** (*H*) as: $H = E + PV$, where E represents the total energy of the system, and PV is the product of the volume of the system and the pressure.

Entropy (*S*) is usually defined as a measure of the level of randomness or disorder in a system. For proteins, entropy refers to conformational entropy, reporting on the distribution of states available for the protein to access.

$$\Delta S = -\frac{\Delta \mathrm{H}}{T} \qquad [eq.3]$$

In thermodynamics, the **Gibbs free energy** represents the energy available for the system to carry out work. For proteins, the Gibbs free energy is a thermodynamic measure of how energetically favourable conformational changes are. Energetically favourable conformations are not a measure of probability of conformational changes occurring.

$$\Delta G = \Delta H - T\Delta S \qquad [eq.4]$$

Heat capacity (*C*p) :The heat capacity is a measure of changes in the entropy and enthalpy of the system in response to changes in temperature (Prabhu and Sharp,

2005). Heat capacity is perhaps the most information rich parameter, but also the most challenging to describe. In protein, the heat capacity is related to changes in solvation (Prabhu and Sharp, 2005); covalent and non-covalent interactions are also major contributors towards protein C_p (Gómez *et al.*, 1995). As pressure induces solvation changes in protein structures, pressure perturbations offer access to understanding and measuring the changes in heat capacity that follow the effect of pressure. This is important for understanding the nature of the conformational observed and the unique behaviour of proteins under pressure and temperature perturbations.

3.2 Protein structure and the role of water

Unlike temperature, which changes the internal energy of the system, pressure perturbations will only affect the activation volume of the system. This can be expressed with the following (Eq.5):

$$\left(\frac{\Delta lnK}{\Delta P}\right)T = -\left(\frac{\Delta V}{RT}\right) \qquad [eq.5]$$

As protein structures cannot be considered independent of their solvation envelope and their internal cavities, the fluctuations in the activation volume of the proteins when under pressure can be explained to arise because of changes in these two features (Levy and Onuchic, 2004). See Figure 19 for schematic.

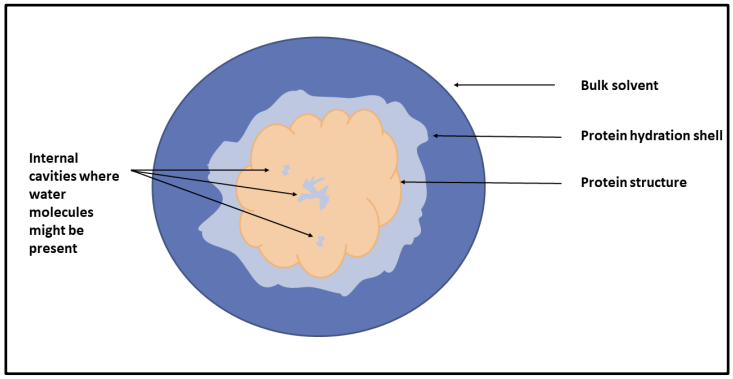

Figure 19. Representation of protein solvation envelope and internal cavities. The cartoon shows a representation of a globular protein (sand colour) with small internal cavities where water might be present, the protein hydration shell, as well as the bulk solvent around the protein.

Water is found both outside the protein, as well as inside protein cores, and it has also been shown to aid with protein folding and stabilisation (Huggins, 2016). The main role of the solvation envelope is to ensure stability of the protein by promoting hydrogen bonding (Shiraga *et al.*, 2016; Levy and Onuchic, 2004). On the other hand, water molecules found inside protein cavities assume more ordered configurations, with some having been reported to interact with the protein backbone and side chains (Martini *et al.*, 2013). Internal cavities are the results of side chain and residues packaging during protein folding and are important contributors to stabilising proteins (Roche *et al.*, 2012). The molecules in the protein solvation envelope show a different behaviour compared to the bulk solvent, having a more dynamic nature, particularly important for conformationally dynamic proteins (and their functions) (Fenimore *et al.*, 2002).

Water from the protein core may be replaced with bulk water, as some amino acids can function as a two-way valve, allowing for water exchange between solvent and protein, as well as protein core and solvent (Masson *et al.*, 1999). This has been reported in the case of human butyrylcholinesterase, where two residues, aspartate-70 and glutamate-197, were found to contribute to the stabilisation of the protein (Masson *et al.*, 1999), by allowing water exchange between solvent ⇔ protein. Mutations within the two residues resulted in changes to this, allowing water to move in one direction only, from the protein core to the solvent, thus safeguarding access to internal cavities (Masson *et al.*, 1999). The diversity of protein primary structure offers many explanations for the different pressure effects observed on some proteins.

3.3 Hydrostatic pressure and protein denaturation

Hydration state changes are the main contributors to protein structure changes under pressure. It was initially thought that protein unfolding under the effect of pressure resulted as a consequence of water molecules penetrating the protein cores (Silva *et al.*, 2014) and inducing denaturation in a similar manner to chemical denaturants. Theoretical and experimental data corroborated these findings, suggesting that the main contributor to protein denaturation under pressure is the relocation of water from the bulk solvent to the protein core, instead of an increase in

solvation envelope (Hummer *et al.*, 1998). Increased hydration of the protein core may be seen as a contradiction to Le Chatelier's principle, whereby proteins generally become more compact under high pressure. To further investigate this, high-resolution NMR studies on ubiquitin at pressures of up to 2.5kbar reported no transfer of water molecules into protein cavities (Fu *et al.*, 2012). As ubiquitin denatures at pressure above 5kbar, it is possible that the protein is initially unaffected by water penetration at non-denaturing pressures, with the possibility of it becoming more prone to water penetration at higher/denaturing pressures (Day and García, 2008). On the other hand, high-pressure crystallography studies of a T4 lysozyme variant mutated to contain a substantial hydrophobic cavity reported the presence of water molecules inside the cavity at 2kbar pressures (Collins *et al.*, 2005). Pressure denaturation of proteins is a complex process, and these studies show the difficulty in generalising the effects of pressure in the absence of a full pressure range examination.

3.4 Effect of hydrostatic pressure and temperature on protein structures

The pressure ranges at which proteins unfold and the degree of compaction and hydration state change will all be protein specific. That proteins undergo compaction under the effect of pressure is clearly the result of many contributing factors.

- **Electrostatic interactions**

An increase in pressure promotes disruptions of electrostatic interactions in protein molecules (Mozhaev *et al.*, 1996). This is due to breaking of ionic bonds leading to a decrease in the overall volume as a result of electrostriction (Heremans and Heremans, 1989). Disruption of important electrostatic interaction in the active site of chymotrypsin under pressure results in the inactivation of the enzyme, with its function being restored upon decompression (Heremans and Heremans, 1989). However, in the case of glutamate dehydrogenase it was found that electrostatic interactions were important contributors towards protein stabilisation during pressure perturbations (Sun *et al.*, 2001). In this case, the stabilisation was due to the newly

adopted protein conformations not allowing for protein aggregation to occur (Sun *et al.*, 2001).

Electrostatic interactions have been found to contribute positively to protein stabilisation in response to thermal increase generally (Okazaki *et al.*, 2012), as evidenced by their abundance in thermophilic proteins compared to the mesophillic homologues (Xia *et al.*, 2018). However, this stabilisation appears to be sequence specific (Ma and Cui, 2006), and is not the sole contributor to protein thermal stabilisation (Ji and Liu, 2011).

- **Hydrogen bonds**

In contrast to ionic bonds, pressure has been shows to have stabilising effects on hydrogen bonds (Nisius and Grzesiek, 2012). This is thought to arise due to compression of protein resulting in reduction of some H-bond lengths (Hua Li *et al.*, 1998). However, some H-bonds are still sensitive to pressure, as is the case for longer-range interactions, observed in the structure of pressure-treated ubiquitin (Nisius and Grzesiek, 2012). These findings show that the contribution of H-bonds to protein stability under pressure is not homogenous, with some being sensitive to pressure perturbations. An increase in temperature has the opposite effect on H-bonds; these tend to be destabilised by a thermal increase due to the distances between the atoms increasing with an increase in temperature (Nisius and Grzesiek, 2012). Due to these differences, some protein H-bonds are more sensitive to temperature than other, eg. residues H-bonded with water will be more sensitive to temperature compared to H-bonds from the protein core (Baxter and Williamson, 1997).

- **Disulphide bonds**

The presence of disulphide bonds in protein structures may help stabilise native conformations (Pace *et al.*, 1988). Lysozyme, which has a total of four disulphide bonds, is structurally insensitive to increased pressure, with the subsequent conformation however showing structural similarity to the native state and being stable enough to be observed using NMR measurements (Akasaka, 2003). In contrast, the effect of increased pressure on apomyopglobin, a protein with no disulphide bonds (but similar in size to lysozyme), leads to a conformational change resulting in a unstable protein structure (Kitahara *et al.*, 2002; McCarthy and Grigera, 2006).

Disulphide bonds are less sensitive to temperature changes, and as such are often used in the thermostabilisation of various protein (Liu *et al.*, 2016; Siddiqui *et al.*, 2005).

- **Oligomers**

Protein oligomers have been found to be sensitive to pressure between 0.3-3 kbar, readily dissociating from their supramolecular structures at such pressures (Payens and Heremans, 1969; Nieuwenhuysen *et al.*, 1980). Evidence also exists for some oligomeric proteins from thermophilic and hyperthemophilic organisms being stabilised by pressure (Sun *et al.*, 1999; Michels and Clark, 1997). Factors such as increased hydrophobicity and more efficient amino acid packing appear to be responsible for stabilisation of these oligomeric proteins (Hei and Clark, 1994). Temperature increase leads to an increase of the internal energy of the system, and for proteins this means that new conformational states situated higher up on the energy landscape can be populated now. As such, oligomerisation and higher order fibril formation are observed. In the case of heat shock protein 90 (Hsp90), it was found that the rate of oligomerisation increased with an increase in temperature (Giese and Vierling, 2002). This is thought to help with the chaperone function of the protein (Chadli *et al.*, 2000).

An increase in α-synuclein oligomerisation and subsequent fibril formation is also observed upon an increase in temperature (Bhak *et al.*, 2014).

3.5 Pressure & temperature- more useful tools than just for protein denaturation

The applications of pressure & temperature perturbations to research extend beyond using it as a tool to study protein folding/unfolding. Pressure studies can also be applied to understanding protein aggregation and misfolding. In the case of chemically induced aggregation of rhodanese by urea, dissociation of protein aggregates at pressure 2kbar was reported (Gorovits and Horowitz, 1998). In contrast, the homodimeric interferon-γ protein forms aggregates following cycles of compression and decompression using pressure, an effect that is abrogated by the addition of sucrose (an osmolyte) (Webb *et al.*, 2001). Similarly, application of pressure

leads to fibril formation in the tumour suppressor protein p53 (Ishimaru *et al.*, 2003). p53 in an important target for cancer research, and its interactions NF-κB activator have been shown to be required for NF-κB activation under certain stimuli (Schneider *et al.*, 2010). Sucrose shows similar protecting effects against pressure denaturation in proteins, promoting more compact conformation and a reduction in ΔV (Ruan *et al.*, 2003).

High pressure has been successfully used in viral research to support therapeutic formulations of inactivated viruses (Tian *et al.*, 2000; Pontes *et al.*, 2001) , as the use of live viruses still poses immunogenicity and attenuation issues (Minor, 2015; Bull, 2015). Pressure has also been applied in the food industry for the prevention of food-transmitted diseases (Da Poian *et al.*, 1996; Considine *et al.*, 2008). Pressure is an attractive option, as it does not introduce any exogenous substances or additives to foods, thus also preserving flavours (Considine *et al.*, 2008; Da Poian *et al.*, 1996).

The application of pressure to study macromolecules offers a plethora of information about their structure and dynamics. Traditional structural biology methods pose their own limitations to using them to study conformationally heterogeneous proteins. Consequently, non-denaturing pressure and temperature perturbation can be considered as an attractive alternative. They offer comprehensive information on the free energy of landscape of proteins, which can be used in the design of better therapeutics and answering fundamental biological questions.

4. Using isothermal calorimetry to study the enzyme kinetics

The canonical NF-κB signalling pathway requires the activation of IKKβ enzyme to target NF-κB inhibitors for proteoasomal degradation and thus free the NF-κB transcription factors to allow them to initiate DNA regulation (Gilmore, 2006). Understanding the initial phosphorylation step has been the topic of much research. In particular, understanding the role of NEMO during the IKKβ: IκBα interaction, as the

canonical activation is NEMO-dependent. Although NEMO is often assumed to play a scaffold, more passive role within the signalling pathway, it is important to determine whether its role extends beyond this and its ability to potentially assist in the phosphorylation of IκBα.

4.1 What are enzyme and enzyme catalysed reactions?

Enzymes are an important class of proteins that function to speed up the rate of chemical reactions and are thus also called biocatalysts. They are found across all kingdoms of life (including viruses) and many important cellular processed require the presence of enzymes. Enzymes also play roles in a number of diseases, with many being used either as markers or therapeutic targets for various medical conditions (Du *et al.*, 2015), and may even be used to help with biofuel production (Noraini *et al.*, 2014).

Enzyme-catalysed reactions consist of three main stages: the formation of the enzyme-substrate complex, product formation, and release [Eq.6];

$$\boldsymbol{E + S \leftrightarrows ES \leftrightarrows EP \longrightarrow E + P} \quad \boldsymbol{[eq.6]}$$

where E,S,P stand for enzyme, substrate, and product, respectively.

The first step relies on molecular recognition between enzymes and their various substrates. Although high substrate specificity appears to be an essential step in ensuring the formation of the correct enzyme-substrate complex, studies have shown that enzymes also display promiscuity, both for the nature of the substrate and type of enzymatic reaction catalysed (Pandya *et al.*, 2014; Pabis and Kamerlin, 2016).

4.2 How do enzymes work?

How enzymes catalyse chemical reactions is still an active topic in biochemistry research. Enzyme works to speed up the rate of chemical reactions by lower the energy barrier of a reaction, more specifically, lowering the $\Delta G^{\ddagger}$ (activation energy) of the transition state (Voet and Voet, 2011). The mechanisms whereby $\Delta G^{\ddagger}$ can be

lowered include: solvation changes (Warshel *et al.*, 1989), steric reorganisation, electrostatic and dipole (re)organisation (Kamerlin *et al.*, 2010; Ariafard and Yates, 2009). Other catalytic mechanisms of lowering $\Delta G^{\ddagger}$ also include: acid-base catalysis, covalent bond catalysis, and metal-ion mediated (Voet and Voet, 2011). Combinations of experimental and computational methods all demonstrate that the successful role of biocatalysts results most probably from a combination of the mentioned stabilisation methods (Devi-Kesavan and Gao, 2003; Garcia-Viloca *et al.*, 2004; Náray-Szabó *et al.*, 2013), rather than one contributing factor.

4.2.1 Michaelis-Menten kinetics

Michaelis-Menten kinetics is often used to best describe the efficiency of enzyme-catalysed reactions. As substrate concentration increases, so does the rate until a point is reached- *Vmax* or the maximum velocity - where all enzyme active sites are fully occupied by substrates, and increasing the substrate concentration will no longer affect the rate (Voet and Voet, 2011). This can be defined using the Michaelis-Menten equation [Eq.7] as follows:

$$v = \frac{v_{max}[S]}{[S] + K_m} \qquad [eq.7]$$

where, V is the enzyme velocity, V_{max} is the maximum enzyme velocity, and K_m is the Michaelis-Menten constant, given by the following [Eq.8,9]:

$$E + S \underset{k-1}{\overset{k1}{\leftrightarrow}} ES \overset{k_2}{\rightarrow} E + P \qquad [eq.8]$$

$$K_m = \frac{k_{-1} + k_2}{k_1} \qquad [eq.9]$$

where, k_1, k_{-1} are the rate for the forward and the reverse reaction, respectively, and k2 is the rate of product formation.

From the Michaelis-Menten plot, K_m is also the point at which half the enzyme active sites are occupied by substrate. If the concentration of the enzyme is known and the V_{max} for the reaction has been determined, the rate of turnover (k_{cat}) can be calculated using [eq.10]:

$$k_{cat} = \frac{V_{max}}{[E]} \qquad [eq.10]$$

The turnover rate is expressed in time^{-1} and is a measure of how many substrate molecules each enzyme molecule has converted per unit time. A variety of information about the catalytic efficacy of enzymatic reactions can be extracted from the values of K_m and k_{cat}. A high value for the K_m suggests the enzyme has a low affinity for the substrate (as the time it takes to reach V_{max} will be longer), whereas a small value for K_m would indicate a high affinity for the substrate (which would decrease the time needed for the enzyme to reach V_{max}). This is crucial information for the development of pharmaceuticals that target enzymatic reaction.

4.3 Methods to study enzyme kinetics

Traditionally, the way to study enzymes reactions is through the use of colorimetric assays and spectroscopy. These methods rely on the ability of a substrate to absorb and/or emit light that can be detected using a spectrometer or fluorimeter. This technique provides an easy, simple, and cost-effective way of measuring initial enzyme kinetics. However, not all enzymes will have a chromophoric or flurophoric substrate associated with their reaction. To tackle this, such substrates have been coupled to a secondary molecule (usually another enzyme) which will have a colourimetric assay associated with its catalytic activity. This technique was first proposed by McClure (McClure, 1969) and Easterby (Easterby, 1973) and is now commonly used in commercially available enzyme kits, which can easily be added to desired enzymes and substrates. These offer quick and cheap ways to analyse enzyme kinetics and only require the use of a spectrometer.

Chromatography methods such as liquid chromatography in combination with mass spectrometry (LC-MS) offer an alternative to labelling and immobilising techniques. LC-MS monitors the formation of products from an enzyme reaction by detecting their mass and ionisation state and then correlating it to the concentrations of starting molecules (Maillard *et al.*, 2013). Whilst informative, some of the concerns with using LC-MS include degradation of products and loss of product during sample preparation (Chakravarti and Chakravarti, 2015), as well it not being suitable for application to continuous enzyme assays.

Continuous- or stopped-flow assays can also be used to study enzyme kinetics. These offer a tremendous advantage in increased instrument sensitivity and the ability to record rates for really fast reaction times (Hartwell and Grudpan, 2012). The basic principle relies on the rapid mixing of macromolecules in a mixing chamber and the detection of product formation using specialised detectors on a very fast (near physiological) timescale (Mitić *et al.*, 2017). These detectors allow for the monitoring of the unique spectral fingerprints of molecules to be detected (which includes fluorescence or absorption methods). This technique also offers the possibility of linking with structural characterisation methods, such as Circular Dichroism, nuclear magnetic resonance or pressure perturbations, thus allowing for a detailed characterisation of the catalytic reaction. However, continuous – or stopped-flow methods require high quantities of samples that can increase the cost of performing such experiments.

More recently, the kinetics of the TEM1 β-lactamase on conversion of a fluorogenic substrate CCF2 was monitored in *in vivo* in live HeLa cells using confocal microscopy (Zotter *et al.*, 2017). The authors report the detecting enzyme kinetics in live cells for the first time, and also highlight the importance of considering the result of *in vitro* studies that failed to take into account the complexity of the intracellular environment. Not all enzyme substrates contain a fluorogenic or chromogenic substrate, and as such studying enzyme kinetics through confocal microscopy cannot be applied to all systems.

4.4 The use of isothermal calorimetry to study enzyme kinetics

A common trait to all chemical reaction is the presence of heat, and as such they are classed as being either exothermic (generating heat) or endothermic (absorbing heat). The heat of chemical reactions has been used in calorimetry techniques to study protein interactions (Dębowski *et al.*, 2016; Dutta *et al.*, 2015), and more recently has also been applied to the understanding of enzyme kinetics (Atri *et al.*, 2015).

Calorimetry has been used as far back as the 1800s, with the first calorimeters used to measure metabolic heat produced in rodents (Black and Robinson, 1803). Modern calorimeters have been designed to display high levels of sensitivity and are coupled with advanced software to aid in the analysis of complex measurements (Keller *et al.*, 2012). Consequently, calorimetry measurements have many applications, including in therapeutics research (Brower *et al.*, 2010), validation of molecular dynamics simulations (Jensen *et al.*, 2010), in food science (McRae *et al.*, 2010), understanding protein-protein interactions (Long *et al.*, 2010), membrane association of proteins (Bartels *et al.*, 2010), and assembly of molecular complexes (Kononenko *et al.*, 2010).

The basic principle of isothermal calorimetry relies on small volumes of a molecule of interest being injected (known as titrant) at set intervals into a solution of another molecule. Following each addition of the titrant into the sample cell, the heat displacement of the reaction is determined for each injection. The power difference between the sample cell and a reference cell is then used to analyse the thermodynamic events that follow each injection. See Fig. 20 for schematic of a standard titration calorimeter.

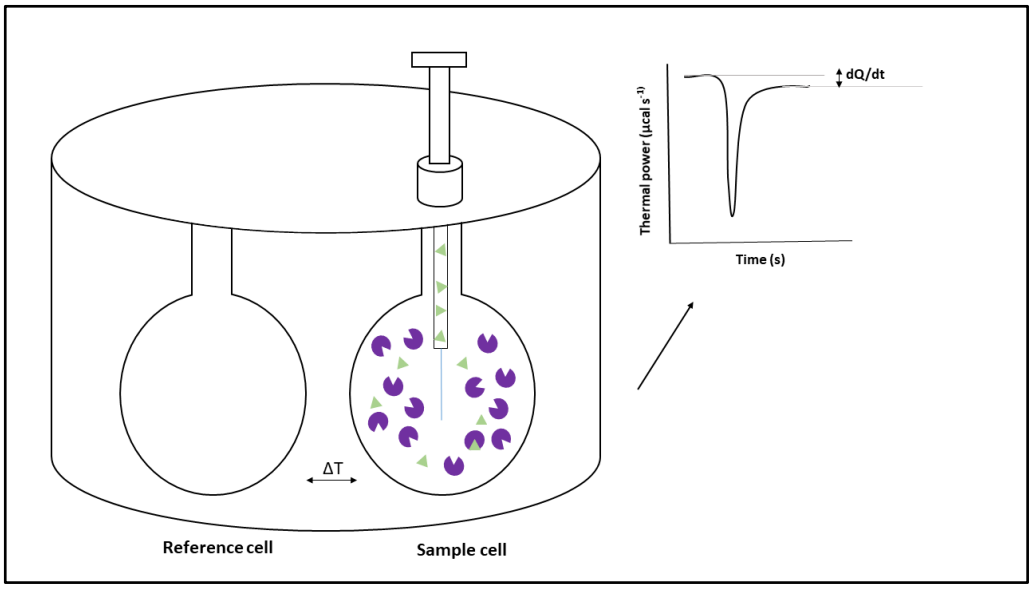

Figure 20. Schematic diagram of standard titration calorimeter where temperature is kept constant (isothermal calorimeter). Enzyme molecules shown in purple, substrate molecules shown in green. Inset, example of thermogram for a typical ITC kinetic measurement, where following each injection the return to baseline is not observed (as it would be for ITC binding experiments), but instead the power displacement (dQ/dt) is used to calculate enzyme rate.

The reference cell is usually filled with a solution of water and is kept at a constant temperature throughout the measurement. The sample cell contains one of the molecules studied and following addition of titrant the instrument will compensate for the heat change, depending on the nature of the reaction (endothermic or exothermic). The sample cell is also constantly stirred through the action of the syringe to ensure proper dispersal of the titrant.

For binding measurements, a set number of ITC injections of equal volume and equal spacing are used, with the first injection being of a small volume and often discarded due to potential of leaking of sample during thermal equilibration. Upon completion, a thermogram is generated, with each heat peak (positive for exothermic reaction and negative for endothermic reactions) corresponding to a single injection. The peaks correlate to the power applied by the instrument to ensure the temperature between the sample cell and reference cell is kept constant. Integration of these peaks generates information about the total the number of binding sites observed and the thermodynamics parameters of enthalpy and entropy (which can be used to calculate

heat capacity and Gibbs free energies for the binding events) (Lehoczki *et al.*, 2016). More recently, isothermal calorimetry has been applied to the study of enzyme kinetics (Bianconi, 2007; Rohatgi *et al.*, 2015). Even though it was first used more than 40 years ago (Spink and Wadsö, 1976), it did not become a common technique to study enzymatic reactions until more recently, greatly helped by the development of modern instruments and software.

Isothermal calorimetry for the study of enzyme kinetics can be used in two different ways, either through a single injection experiment or through multiple injections (Atri *et al.*, 2015). The functioning principle is similar to standard calorimetry measurements, with the difference being that in the case of kinetics, the measurement of instrument power or heat flow relates directly to the reaction rate and enthalpy of the experiment (Freyer and Lewis, 2008; Lonhienne *et al.*, 2001). Refer to Figure 21 for baseline shift differences in binding *vs* kinetic measurements using ITC.

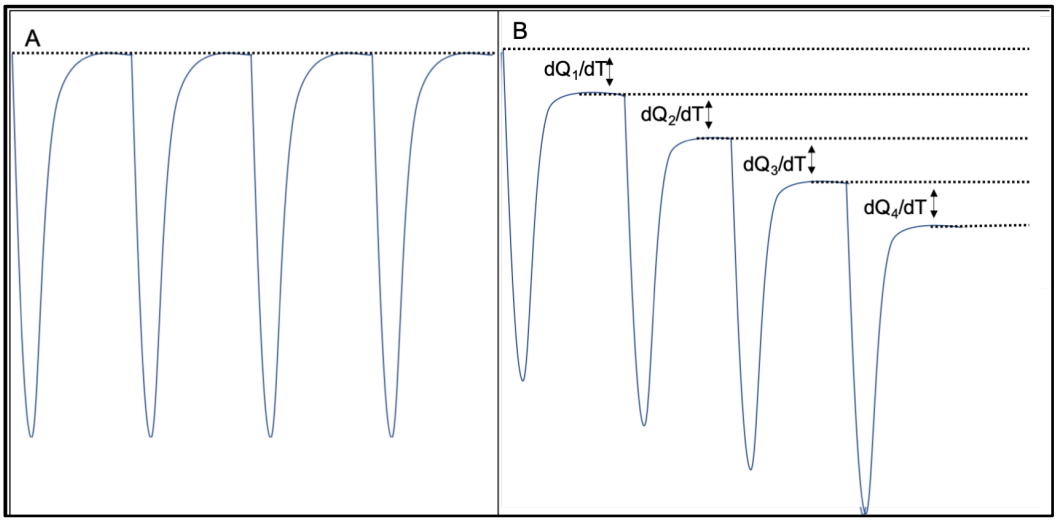

Figure 21. Cartoon of isothermal titration calorimetry baseline in binding measurements (A) and enzyme reaction (B). A, A simple binding experiment baseline signal returning to initial levels following each injection. B, in an enzyme kinetics experiment a baseline shift is observed under steady-state conditions, with changes the thermal power (dQ/dT) being used to calculate enzyme rate.

When analysing binding events using ITC, a return to baseline is an indication of stable reaction where no baseline drifting due to improper thermal equilibration or presence

of buffer contaminants can be detected (Duff, Jr. *et al.*, 2011). However, kinetic experiments are more complex, and it has been demonstrated that turnover events accompany baseline shifts for each new steady-state (Todd and Gomez, 2001; Rana *et al.*, 2016). However, this phenomenon is only observed in the case of using the multiple injection ITC method for enzyme kinetic and is not present in single-injection kinetics measurements (Transtrum *et al.*, 2015). This is due to the experimental setup differences in between the two methods, where steady-state kinetics are not required for the single-injection method.

In single injection measurements, a single injection (usually containing an enzyme solution) is added to the sample cell containing the enzyme of interest, and the reaction is monitored for a period of time (Transtrum *et al.*, 2015; Di Trani *et al.*, 2018). The data generated offer substantial details on the thermodynamics and kinetics of the reaction, but are often deemed too complex and require further analysis or control experiments (Transtrum *et al.*, 2015; Atri *et al.*, 2015).

The multiple injection method relies on two experiments being carried out to determine enzyme kinetics. The first injection experiment is a simple single injection of the substrate into sample cell, to measure the enthalpy of the reaction when the substrate was completely used up (Mazzei *et al.*, 2014; Rana *et al.*, 2016). This is obtained by integrating the area under the peak (corresponding to the injection) and dividing the value by the substrate concentration and the volume of the sample cell (Mazzei *et al.*, 2014). Following this, a second experiment is carried out where multiple injections of the substrate are used to monitor the heat rate at different substrate concentration and the reaction is kept in steady-state (Mazzei *et al.*, 2014). The calculated value for ΔH in the single injection experiment is used to calculate the reaction rate from the second experiment following Michaelis-Menten kinetics (Mazzei *et al.*, 2014). Whilst the analysis of the obtained isotherm is simpler compared to the single-injection technique, the limitations of the multiple injection kinetics relate to the high volume of sample required.

Despite the limitations of both techniques, calorimetry is emerging as an attractive alternative to many standard spectroscopic assays in the study of enzyme kinetics. Its

main advantages include the possibility of testing variable substrate concentration in one experiment, as well as no need for colourimetric or isotopic labelling (Noske *et al.*, 2010). However, complex data analyses and the high volumes of sample are two considerable disadvantages of the technique.

Chapter 3: The red edge excitation shift phenomenon can be used to unmask protein structural ensembles: implications for NEMO-ubiquitin interactions

Accompanying commentary for chapter 3:

Protein disorder is slowly emerging as a prevalent characteristic of many protein families, including proteins involved in signalling networks. Characterising the dynamics and structure of disordered proteins/proteins with disordered regions is proving challenging using traditional structural methods, as they pose size constraints and such proteins are too unstable to be used. As such, techniques that directly report on the dynamics of conformational change may employed. One such technique is the use of red edge excitation shift (REES) spectroscopy, as it allows for the characterisation of the dynamic nature of protein conformational change and can also be used to study molecule interactions (Chakraborty and Chattopadhyay, 2017; Haldar *et al.*, 2011).

NEMO is an important and medically relevant human protein, responsible for the activation of the NF-κB signalling pathway (Gilmore, 2006). NEMO controls the NF-κB response to a variety of stimuli, and it does by complex interactions with the IKK enzyme complex, specifically the enzyme IKKβ. To date, little consensus exists about the structure of NEMO, with new studies suggesting a dynamic protein, capable of undergoing conformational change when bound to various ligands (Hauenstein *et al.*, 2017).

We first established the use of REES as a probe to look at protein conformational change, by comparing the spectra of native, thermally denatured and chemically denatured protein. Our results showed great differences in the spectra of the three samples and validated the sensitivity of the REES probe (a single tryptophan residue located at the N-terminus of NEMO) to changes in the environment of the protein. Following this, the effect of molecular interaction was monitored using peptide mimics of two important *in vivo* binding partners, NBD as a mimic of the IKKβ enzyme, and IκBα as a mimic of the IκBα inhibitor. The results obtained show that the two peptides interact with NEMO differently, inducing a more compact NEMO conformation in the case of IκBα, whilst binding to NBD result in a more flexible conformation. NEMO conformation was also monitored in response to binding to linear poly-ubiquitin chains

of various lengths. This is an important interaction, as it thought to be one the main events activating cellular NEMO in response to stimuli binding (Napetschnig and Wu, 2013). Our results show that binding of poly-ubiquitin induced global conformational changes in NEMO, and further validate the single tryptophan probe, as the ubiquitin binding site is located in the C-terminus, not where the REES probe is. Finally, we also show that REES spectroscopy can be coupled with hydrostatic pressure perturbations to allow for a full thermodynamic characterisation of NEMO conformational change.

This declaration concerns the article entitled:									
The red edge excitation shift phenomenon can be used to unmask protein structural ensembles: implications for NEMO-ubiquitin interactions									
Publication status (tick one)									
draft manuscript		**Submitted**		**In review**		**Accepted**		**Published**	✓
Publication details (reference)	**Catici, D. A. M**., Amos, H. E., Yang, Y., van den Elsen, J. M. H., and Pudney, C. R., (2016) The red edge excitation shift phenomenon can be used to unmask protein structural ensembles: implications for NEMO–ubiquitin interactions. *FEBS J*. 10.1111/febs.13724								
Candidate's contribution to the paper (detailed, and also given as a percentage).	The candidate contributed to/ considerably contributed to/predominantly executed the… Formulation of ideas: DAMC, YY, JMHE, CRP Design of methodology: Laboratory experiments designed by: DAMC, CRP Experimental work: DAMC, HEA, YY, performed experiments Protein purification and expression of NEMO: DAMC Protein purification and expression of Sbi-III- IV: YY Red edge excitation and high-pressure measurements: DAMC Preliminary experimental work: HEA Data fitting: CRP Presentation of data in journal format: DAMC, JMHE, and CRP wrote the main manuscript text; DAMC and CRP prepared the figures;								
Statement from Candidate	This paper reports on original research I conducted during the period of my Higher Degree by Research candidature.								
Signed	**Dragana Catici**					**Date**	25th Jan 2019		

This research was originally published in the FEBS Journal. Catici, D.A.M., Amos, H.E., Yang, Y., van den Elsen, J.M.H.H., and Pudney, C.R., 2016. The red edge excitation shift phenomenon can be used to unmask protein structural ensembles: implications for NEMO-ubiquitin interactions. FEBS Journal, 283, pp.2272–2284.

The red edge excitation shift phenomenon can be used to unmask protein structural ensembles: implications for NEMO-ubiquitin interactions

***Dragana AM Catici**, Hope E Amos, Yi Yang, Jean MH van den Elsen and Christopher R Pudney**

Address. Department of Biology and Biochemistry, Faculty of Science, University of Bath, Bath, BA2 7AY, United Kingdom.

Running title: Unmasking protein conformational plasticity

Abbreviations: NEMO, NF-κB essential modulator; REES, Red edge excitation shift; FEL, Folding energy landscape; Sbi, second immunoglobulin-binding protein; CSM, center of spectral mass;

Keywords: Red edge excitation shift, free energy landscape, NEMO, protein dynamics, tryptophan fluorescence

ABSTRACT

To understand complex molecular interactions it is necessary to account for molecular flexibility and the available equilibrium of conformational states. Only a small number of experimental approaches can access such information. Potentially steady-state red edge excitation shift (REES) spectroscopy can act as a qualitative metric of changes to the protein free energy landscape (FEL) and the equilibrium of conformational states. First, we validate this hypothesis using a single Trp containing protein, NF-κB essential modulator (NEMO). We provide detailed evidence from chemical denaturation studies, macromolecular crowding studies and the first report of the pressure-dependence of the REES effect. Combined these data demonstrate that the REES effect can report on the 'ruggedness' of the FEL and we present a phenomenological model, based on realistic physical interpretations, for fitting steady-state REES data to allow quantification of this aspect of the REES effect. We test the conceptual framework we have developed by correlating findings from NEMO ligand binding studies with the REES data in a range of NEMO-ligand binary complexes. Our findings shed light on the nature of the interaction between NEMO and poly-ubiquitin, suggesting that NEMO is differentially regulated by poly-ubiquitin chain length and that this regulation occurs via a modulation of the available equilibrium of conformational states, rather than gross structural change. This study therefore demonstrates the potential of REES as a powerful tool for tackling contemporary issues in structural biology and biophysics and elucidates novel information on the structure-function relationship of NEMO and key interaction partners.

INTRODUCTION

There is an increasing realization that the molecular mechanism of many human proteins, particularly those involved in signaling networks, are governed by molecular flexibility and protein structural disorder. That is, proteins that mediate multiple signaling inputs may fold into ligand specific conformations, providing high specificity to a number of structurally dissimilar ligands (Uversky, 2013). Underpinning these notions is the free energy landscape (FEL) model of protein structure, which interprets molecular heterogeneity (structural disorder and flexibility) as a series of equilibrated energetic minima on a multi-dimensional free energy surface (Tsai *et al.*, 2001). Proteins that are highly flexible or exist as different discrete conformational states are considered to have a rather 'rugged' FEL. For signaling proteins, understanding how the FEL is altered on ligand binding is key to understanding the molecular mechanism of biological signaling networks.

Detecting ligand induced conformational change (folding) and the relationship to the equilibrium of protein conformational states is challenging. EPR (Sobolewska-Stawiarz *et al.*, 2014), single molecule (SM) (Laursen *et al.*, 2014; Ferreon *et al.*, 2013), Ion mobility mass spectrometry (IM-MS) (Ruotolo *et al.*, 2005) and NMR (Sugase *et al.*, 2007) studies can be used for this purpose with different levels of resolution. There is now evidence that an optical phenomenon called Red Edge Excitation Shift (REES) may provide unique information on protein conformational change and the equilibrium of conformational states (Chattopadhyay and Haldar, 2014). REES is a phenomenon where low energy excitation of a fluorophore leads to a red shift in the maximum of the emission intensity, $\Delta\lambda_{Em}^{max}$.This phenomenon may manifest where there are a range of discrete fluorophore solvation states and therefore potentially reflects the equilibrium of conformational states that are accessible to a protein (Chattopadhyay and Haldar, 2014; Demchenko, 2002).

The REES effect is governed by interactions between a fluorophore and the surrounding solvent in the ground and excited states. REES is observed as a result of the change in the dipole moment of the fluorophore following excitation and the speed at which solvent reorganisation occurs around the newly excited fluorophore (Chattopadhyay and Haldar, 2014; Demchenko, 2002). In a fully solvated environment,

the fluorescence lifetime (τ_F) occurs at higher rates compared to the lifetime of environmental relaxation (τ_S). In this case, the emission wavelength of the chromophore is independent of the excitation wavelength. When $\tau_F < \tau_S$, for example in a rigid molecular environment such as some folded protein states, the intermolecular interactions between the fluorophore and its environment do not change and dipolar relaxation does not occur during fluorescence emission (Weber and Shinitzky, 1970; Galley and Purkey, 1970). A consequence of this is that the fluorescence emission occurs at higher energy since photons are emitted from the excited state instead of a lower energy relaxed state. It is possible to select for individual solvation environments within an equilibrium by using low energy excitation (photoselection), for example by using lower energy photons or longer wavelengths located at the red edge of the excitation spectrum (Chattopadhyay and Mukherjee, 1999). Excitation at a lower energy selects for fluorophores in a solvent relaxed environment, which require less energy to become activated. Experimentally one observes a red shift in the emission maximum with respect to excitation wavelength.

There have been a few reports where emission arising from a single Trp residue gives an observable REES effect in the folded and molten globule like states (Kelkar *et al.*, 2010), while the REES effect disappears or is rather reduced in unfolded states (Mitra *et al.*, 2015; Chattopadhyay *et al.*, 2003). The REES effect is therefore a unique probe for proteins with a high degree of molecular flexibility resulting in an ensemble of solvent environments around the Trp probe. For proteins, such an ensemble may arise from a broad equilibrium of conformational states, such as in molten globule intermediates of highly flexible or dynamic proteins (Mitra *et al.*, 2015; Jain *et al.*, 2013; Rawat *et al.*, 2004).

NF-κB essential modulator is the key regulatory element in the NF-κB signaling pathway, controlling much of the nervous and immune system (Gilmore, 2006). NEMO regulates the activity of a kinase, IκB kinase-β (IKK-β), which has a diverse range of phosphorylation targets, for example, IκBα (Schröfelbauer *et al.*, 2012), huntingtin (Thompson *et al.*, 2009), and insulin receptor 1 (IRS-1) (Nakamori *et al.*, 2006). NEMO putatively ensures the specificity of IKK-β for IκBα, by facilitating the recruitment of IκBα to the kinase (Schröfelbauer *et al.*, 2012). Subsequent proteoasomal degradation

of IκBα then allows the NF-κB complex to enter the nucleus and induce expression of pro-inflammatory and anti-apoptotic genes. Despite the importance of NEMO to normal human health and disease associated processes, remarkably little is known about the molecular mechanism of action of NEMO and, in particular how NEMO is able to show specificity to a considerable number of interaction partners (Fenner *et al.*, 2010). We have recently provided evidence that NEMO is a flexible protein that undergoes ligand specific conformational change, and have hypothesized that the non-ligand bound protein adopts a broad equilibrium of conformational states (Catici *et al.*, 2015). We have previously used the emission of NEMO's single intrinsic Trp residue (W6) as a spectroscopic reporter of ligand-induced NEMO conformational change (Catici *et al.*, 2015).

Herein we explore the use of REES spectroscopy to inform on the structural and mechanistic determinants of NEMO-ligand binding. First, we develop a new framework for the quantitative interpretation of steady-state REES data, validated by folding and pressure perturbation studies. This then allows us to use the REES data quantitatively for a series of NEMO-ligand bound states. We develop our putative model for the molecular mechanism of NEMO's functional interactions, structure and how this connects to the NEMO free energy landscape and conformational change.

Results and Discussion.

NEMO W6 shows a detectable REES signal. Figure 22 shows the variation in emission spectrum (Figure 22A and Figure 22B) and center of spectral mass (CSM) (Figure 23B) of NEMO W6 *versus* excitation wavelength.

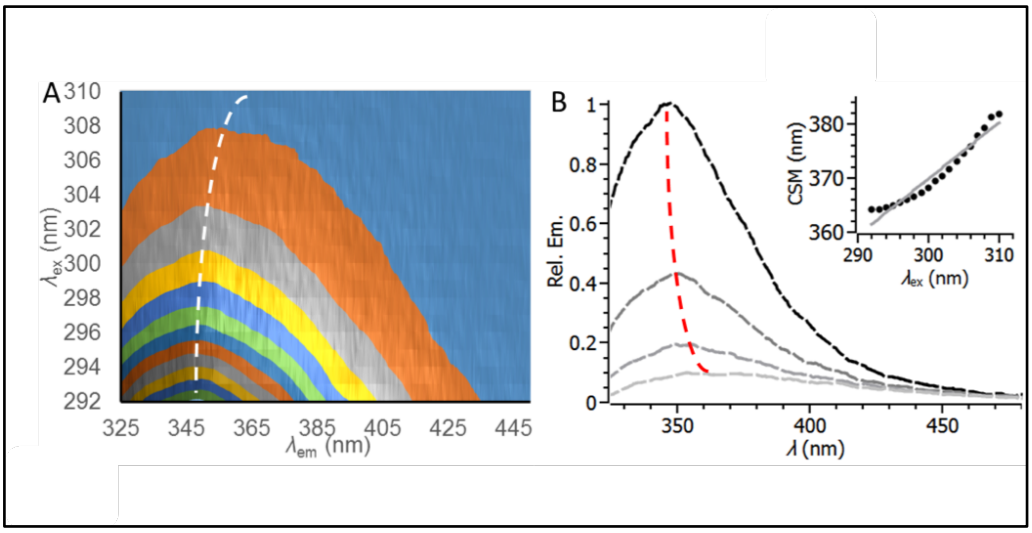

Figure 22. NEMO W6 REES effect A, Contour plot showing the change in the structure of the emissions spectra with increasing λ_{Ex}^{max} for NEMO W6 signal. The dashed white line shows the change in the λ_{Em}^{max} for each emission spectrum and is to aid the eye only. B, Relative change the intensity of W6 emission (λ_{Em}^{max} shown as a dashed red line to aid the eye) for increasing λ_{Ex}^{max}. *Inset*, the corresponding change in CSM with λ_{Ex}^{max} calculated from Eq. 11. Solid line is the fit to Eq. 11. The data plotted are the average of n=3 experimental repeats. All measurements were performed at 10° C.

Typically, the magnitude of the steady-state REES phenomenon is reported as the simple difference in CSM or $\Delta\lambda_{Em}^{max}$. From Figure 22, we observe a notable increase in red shift in the emission spectra (compared to other W REES values of 5 nm shift (Raghuraman and Chattopadhyay, 2006)), with an increase in CSM of 17.7 nm and an increase in $\Delta\lambda_{Em}^{max}$ of 15 nm from λ_{ex} 292-310 nm. Essentially, the data are treated by the linear function:

$$CSM = R\lambda_{ex} + CSM_0 \qquad [eq.\ 11]$$

where *R* is the REES magnitude expressed as the change in CSM per nm of the excitation wavelength, λ_{ex}. In this model the y-intercept, CSM_0, does not have an obvious physical meaning and is not typically reported. The solid grey line in Figure 23B *inset* shows the fit of the NEMO REES data to Eq. 11, giving *R* = 0.96.

The extracted REES signal with NEMO W6 is notable (17 nm shift) compared to other reported values (5 nm shift (Raghuraman and Chattopadhyay, 2006) and is even

more relevant given that NEMO W6 is already relatively solvent exposed. NEMO W6 is a class III Trp according to the Burstein classification (Reshetnyak *et al.*, 2001). Class III Trp residues are not typically thought to exhibit a detectable REES effect (Demchenko and Ladokhin, 1988) due to increased solvent exposure, thus giving rise to an essentially single solvated environment. However, we would point to the example of denatured spectrin which retains a measurable REES signature, despite being mainly solvent exposed (Mitra *et al.*, 2015). These findings have been rationalized as reflecting a partially 'unfolded' state with residual structure, comparable to a molten globule state. We have previously suggested that NEMO is a native molten globule (Catici *et al.*, 2015) and so our findings of a 17 nm REES effect for an already red-shifted tryptophan are consistent with our previous results of NEMO adopting a molten globule-like conformation .Physically, these findings suggest that NEMO adopts a very broad equilibrium of conformational states, where there are multiple discrete solvation environments for W6; this could arise both from a series of W6 micro-environments as well as from the stabilization of different Trp rotamers.

Pan *et al* have previously demonstrated that even solvent exposed Trp residues can display a broad range of $\Delta\lambda_{Em}^{max}$ values, arising from different Trp rotamers (Pan *et al.*, 2006) and calculate a range 344 – 365 nm from molecular dynamics simulations for a range of cyclic peptides. This would seem consistent with our data that show a similar range of $\Delta\lambda_{Em}^{max}$ values, with the highest value being $\Delta\lambda_{Em}^{max}$ = 363 nm at λ_{ex} = 310 nm. This value is the same as for free Trp in our buffer giving $\Delta\lambda_{Em}^{max}$ = 363 nm (Figure 24), suggesting this excitation wavelength is capturing essentially the most red-shifted (solvent exposed) conformational state. Further, Maglia *et al* reported a REES effect in a single Trp variant of DD-carboxypeptidase attributable to at least three different Trp rotamers (Maglia *et al.*, 2008) . These rotamers may be stabilized through differing H-bonding to the Trp amide carbonyl (Xu *et al.*, 2009). As such it is difficult to directly separate the contribution of differing Trp rotamers and increased conformational heterogeneity of the peptide backbone to the REES signal. Below, we explore the contribution of different Trp rotamers to the NEMO REES.

An artificial REES effect could arise if there is an observable convolution of our Trp signal with the background Tyr signal from NEMO. We excite NEMO from 292 nm

upwards specifically so that there is essentially no Tyr emission relative to Trp emission. However, we have explored how a small Tyr signal would affect our REES data by monitoring the REES data for 10 μM Tyr in buffered solution and subtracting this from our NEMO REES data. These data are shown in Figure 23 in detail.

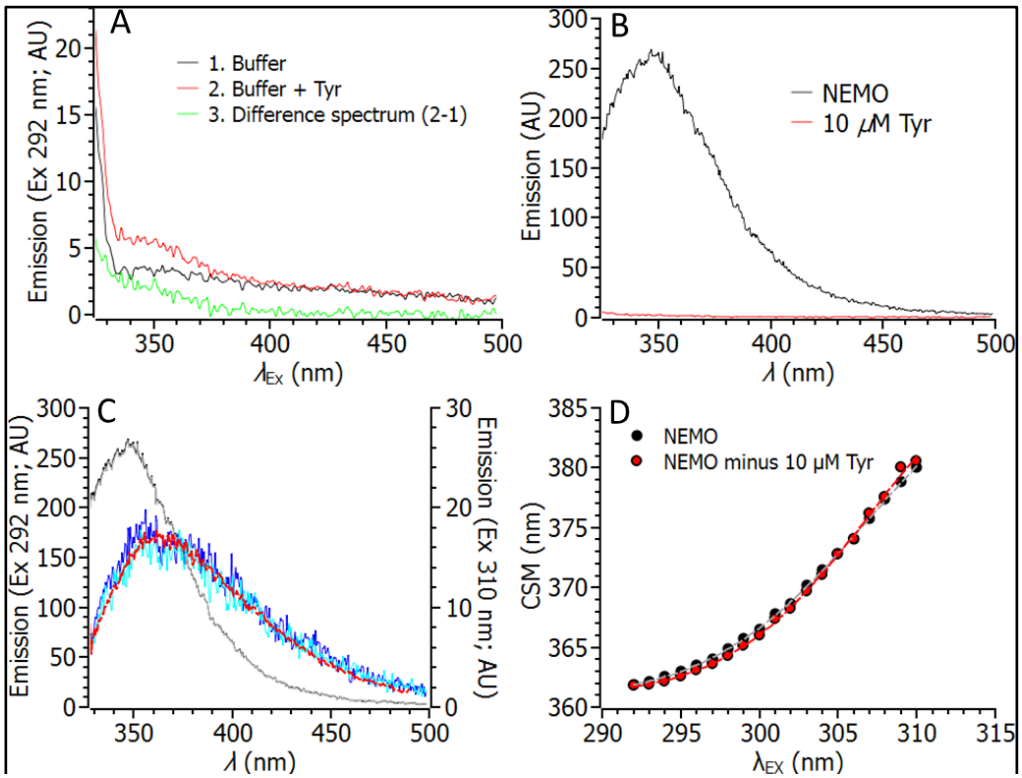

Figure 23.Emission spectra of tyrosine and NEMO W6. A, Emission spectra of tyrosine and buffer excited at 292 nm. The raw spectra, buffer spectra and difference spectrum are show in red, black, and green lines, respectively. B, The emission spectrum of 2 μM NEMO and 10 μM tyrosine (from A) excited at 292 nm. The total emission of Tyr is 0.5 % of the total NEMO emission. C, The emission spectrum of NEMO excited at 292 nm (black line; left axis) and 310 nm (blue line; right axis). The grey and cyan lines show the subtraction of the emission spectrum of 10 μM Tyr from the NEMO emission spectra at 292 nm and 310 nm, respectively. The red dashed line shows the emission spectrum of L-Trp (excitation at 310 nm) in the same buffer, with the intensity normalized for comparison. D, The resulting REES effect for NEMO (black) and for the Tyr subtracted spectra for 10 μM Tyr (red). All measurements were carried out at 10° C.

We find that accounting for the small Tyr signal arising from NEMO's intrinsic Tyr residues gives essentially no difference to our REES data. Further, we have monitored the REES signal from a single Tyr containing fragment of *Staphylococcus aureus* complement evasion second immunoglobulin-binding protein Sbi domain III and IV that, like NEMO, contains structurally disordered regions (Upadhyay *et al.*, 2008).

These data are shown in Figure 24. We do not find a detectable REES signal arising from Tyr emission as is expected because of the symmetrical nature of the Tyr ring system (0 nm shift). Together, these data demonstrate that the signal we monitor, as expected, arises essentially entirely from NEMO's single intrinsic Trp.

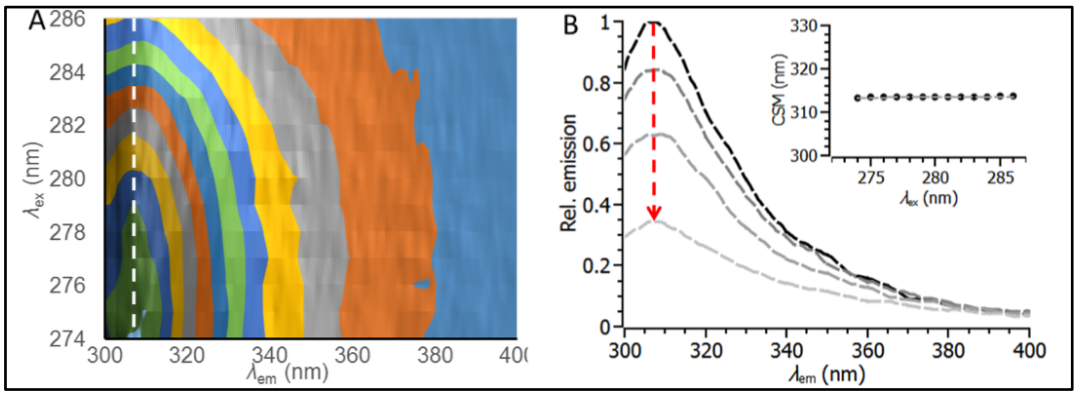

Figure 24. Sbi does not display a detectable REES effect. A, Contour plot showing the change in the structure of the emissions spectra with increasing λ_{Ex}^{max}. The dashed white line shows the change in the λ_{Em}^{max} for each emission spectrum to aid the eye only. B, Relative change the intensity of W6 emission (λ_{Em}^{max} shown as a dashed black lineto aid the eye for increasing λ_{Ex}^{max}. *Inset*, the corresponding change in CSM with λ_{Ex}^{max} calculated from Eq. 11. Solid line is the fit to Eq.11.

Establishing a quantitative analysis of REES data. The fit of our REES data to Eq.11 is poor and does not account for the curvature in the data. This is the case for all reported steady-state REES data where a high number of data point are collected (12-20 data points). For REES data to be used in comparative studies, the reporting of *R* in Eq. 11 will therefore be wildly inaccurate. To identify a numerical model that would best fit these data we have measured the change in the CSM of NEMO Trp emission across an extended range of Trp absorption (shown in Figure 26), incorporating the emission maximum of the Trp. The REES effect should be detectable at the far-red edge of the absorption spectrum, with little or no effect at the absorption maximum, since photoselection and hence REES will only occur under low energy excitation. From Figure 25, this trend is apparent.

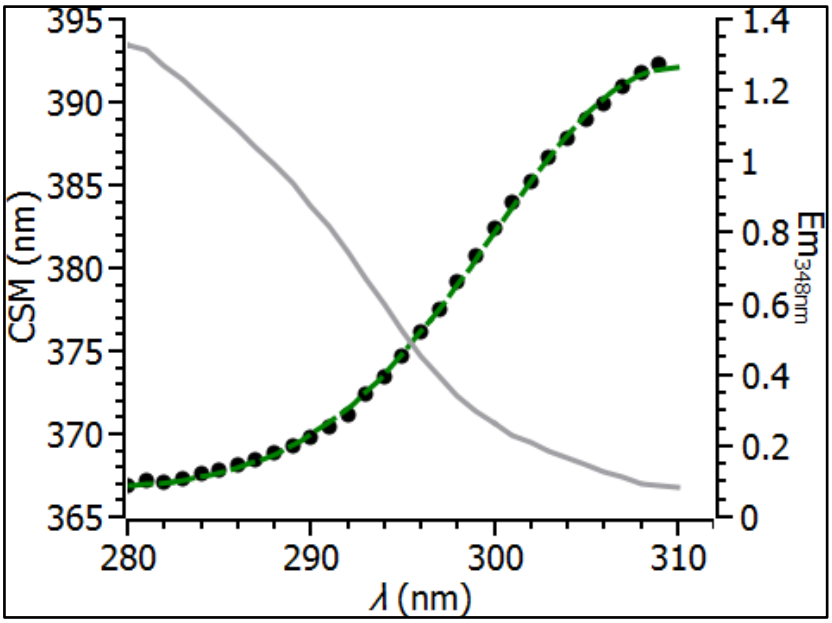

Figure 25. A phenomenological model to fit REES data. The excitation spectrum of NEMO W6 (emission at 348 nm) is shown as a grey line (right-hand axis) across an extended wavelength range. The variation in CSM with λ_{Ex}^{max} for NEMO W6 is shown as black circles (lef-hand axis) and the solid line is the fit to Eq. 12 but with a sum of two Gaussians to capture the ascending and descending limb of the REES data.

That is, we observe little or no REES effect occurring at the maximum of the excitation spectrum but a measurable REES effect at the red edge of the spectrum (17 nm shift in emission). We note that the observed changes in CSM are dominated by NEMO's intrinsic Trp residue and not convolved of contributions from Tyr emission since we have shown above that, consistent with theory, Tyr emission does not give a measurable REES effect and does not convolute our REES data (Figure 23). Indeed, we monitor emission from λ_{Ex} = 292 nm, where there is essentially no emission attributable to tyrosine as shown in Figure 24.

We find that the REES data in Figure 25 can be best represented by a Gaussian probability distribution of the form:

$$f(x) = R_0 + \frac{A\sqrt{2/\pi}}{w} exp\left(-2\left(\frac{x-m}{w}\right)^2\right) \qquad [eq.\,12]$$

Where *A* is the area, *w* is the full width at half-maximal (fwhm), *m* is the mid-point and R_0 is the y-intercept and $m = \lambda_{REES}^{max}$, where λ_{REES}^{max} is the excitation wavelength that gives the most notable change in the emission peak wavelength. The data in Figure 25

are fit to Eq. 12 and illustrate the low energy excitation at the red edge of the protein absorption spectrum. The fit of Eq. 12 to the experimental data is excellent and captures the expected relationship we describe above.

Potentially, the magnitude of *A* extracted from fitting Eq. 12 to a plot of excitation wavelength *versus* λ_{Em}^{max}, can be used as a qualitative comparator to assess changes in the extent of the REES phenomenon. The magnitude of R_0 should represent the minimum λ_{Em}^{max} value, in the absence of the REES effect. This magnitude is commonly used to reflect the degree of solvent exposure of Trp residues and can be used as a metric of folded/unfolded states. We discuss the interpretation of these values in more detail below. This simple model clearly neglects a range of contributing factors such as the proportion of excited molecules, the small contribution from changing excitation energy at different excitation wavelengths, the number of discrete conformational states that are photo-selectable and the contribution from dipole rotation in the excited electronic state. However, Eq. 12, unlike Eq. 11 is based on a realistic physical rationale and provides a means to extract meaningful quantitative data from the full range of REES data. We note that other distribution functions can and have been used in relation to extracting information from spectral features, including Lorentz and log-normal distributions (Djikanović *et al.*, 2007; Caarls *et al.*, 2010). Ultimately, we do not try and accurately recapitulate the absorbance/excitation spectrum of the fluorophore but instead wish to have a physically meaningful probe beyond the arbitrary use of a simple linear function.

Validating REES as a quantitative probe of molecular heterogeneity. Having established a quantitative model to compare REES data, we now test the hypothesis that REES can be used to reflect changes in the equilibrium of protein conformational states. To achieve this we monitor the REES effect with both denatured and stabilized NEMO as well as pressure-perturbation studies that systematically alter the equilibrium of conformational states and the extracted parameters from fitting the data are given in Table 1.

Table 1. Results of fitting NEMO-ligand complex REES data to Eq. 11 and Eq. 12.

	A^a	R_0 (nm)	R^a
Native, denatured, crowded			
$NEMO_{native}$	1 ± 0.1	363.2 ± 0.19	1 ± 0.13
$NEMO_{denat}$	0.37 ± 0.4	375.0 ± 0.5	0.21 ± 0.01
NEMO + Sbi (20 mg/ml)	2.24 ± 0.51	360.5 ± 0.45	1.07 ± 0.12
Binding partners			
NEMO + IκBα	0.85 ± 0.04	364.1 ± 0.62	1.35 ± 0.1
NEMO + NBD-Phe	1.33 ± 0.31	363.0 ± 1.5	0.98 ± 0.1
NEMO + Ub_4	0.77 ± 0.05	364.6 ± 0.77	1.06 ± 0.1
NEMO + Ub_{10}	1.23 ± 0.0.1	362.8 ± 0.25	0.93 ± 0.11

a, Values are relative to the extracted value for NEMO alone.

Typically denatured proteins do not give rise to an observable REES effect since the peptide backbone will become fully solvent accessible. In this case the solvent relaxation will be very rapid, and no REES effect observed, effectively because there is one discrete solvation state (fully solvated). We have incubated NEMO in 6M guanidine to denature the protein and the corresponding change in the center of spectral mass (CSM) *versus* λ_{ex} is shown in Figure 26. We favor the use of CSM instead of the magnitude of $\Delta\lambda_{Em}^{max}$ as we find this metric gives a more robust REES signal and the magnitude of $\Delta\lambda_{Em}^{max}$ may be highly error prone. However, we note the result using $\Delta\lambda_{Em}^{max}$ are essentially the same. A decrease and red-shift in Trp emission is typically grossly correlated with denaturation of proteins.

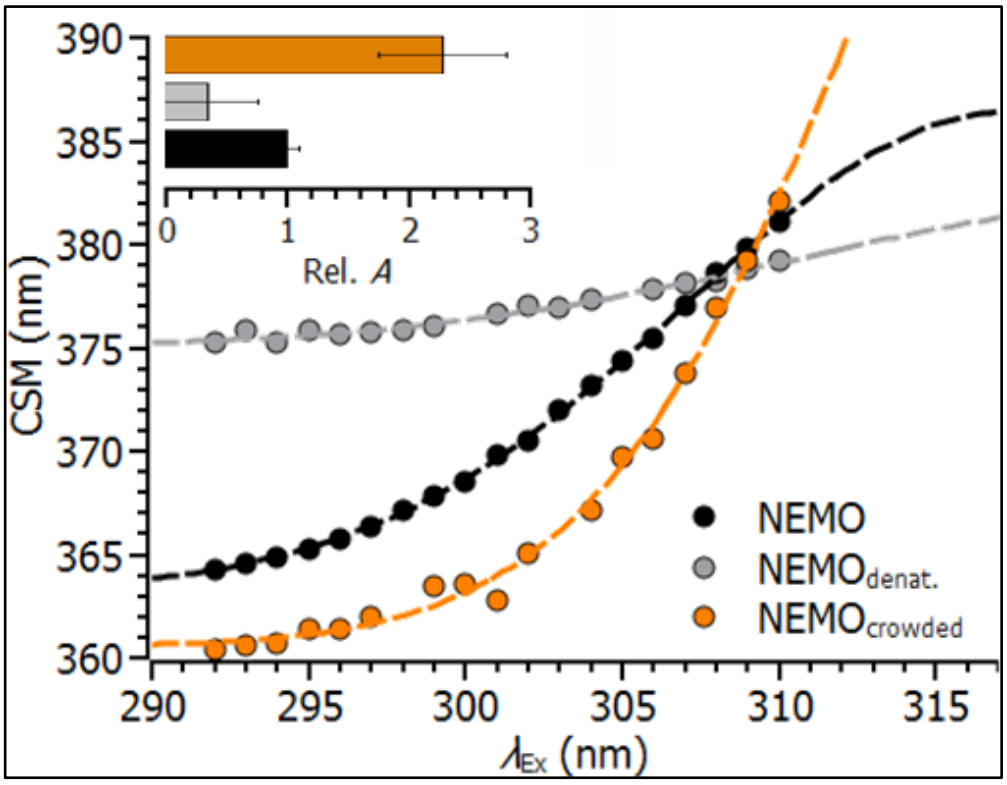

Figure 26. The effect of denaturation and crowding on NEMO REES. The REES data for native NEMO (black circles), denatured NEMO (grey circles) and crowded (20mg/ml Sbi) NEMO (orange circles) are fit to Eq.12 (solid lines). The inset shows the extracted value of *A* from Eq. 12. The error bars are the standard deviation from 3 measurements.

From Figure 26 the incubation with guanidine has resulted in denaturation of NEMO, with a red-shift in CSM giving R_0 = 363.2 ± 0.19 nm to R_0 = 375 ± 0.5 for the native and denatured protein, respectively. Note that this is not the REES effect but reflective of the solvent exposure of NEMO W6 on denaturation. The denatured NEMO shows a dramatically reduced REES effect. Denatured NEMO shows only a 4 nm shift from λ_{ex} 292 to 310 nm and fitting to Eq. 11 gives R = 0.21 ± 0.01 and a relative decrease compared to native NEMO of R = 1 ± 0.13. Fitting to Eq.12 also gives a notable decrease in the REES effect, A = 0.37 ± 0.4 (compared to A= 1 ± 0.1 for native NEMO). The relative change in the REES effect is similar using either approach and this argues strongly that our fitting approach using Eq.12 is robust.

Macromolecular crowding is a key feature of the intracellular milieu arising from the very high concentrations of other species in the cytosol. Crowding reduces the available solvent for other molecules in solution through the excluded volume effect, which effectively increase the concentration of e.g. protein and restricts the

accessible conformational states through hard-core repulsions between the crowding agent and the protein. Macromolecular crowding can alter protein conformation, typically inducing folding and stabilization (Dhar *et al.*, 2010). Crowding therefore potentially provides a means to explore the contrasting physical effect of denaturation on the REES effect, where the protein is more folded/stabilized. We have used a protein as the crowding agent, Sbi (reported above), instead of a synthetic crowding agent since protein is much more consistent with the intracellular environment. Sbi lacks any intrinsic Trp residues and does not give rise to a REES signal that would convolute our NEMO signal (Figure 24). Incubating NEMO with a high concentration of Sbi (20 mg/ml) gives a dramatic change to the both the absolute Trp emission and also the REES effect as shown in Figure 26. We note that the emission spectra have had the signal arising from Sbi subtracted and so there is no contribution from Sbi Tyr emission. The emission is blue shifted (R_0 = 360.5 ± 0.45 nm) compared to NEMO in the absence of Sbi (R_0 = 363.2 ± 0.19) and more intense (~1.4 times increased emission), suggesting that the NEMO Trp is less solvent exposed and therefore that NEMO is more 'folded' in the crowded environment. Intriguingly the REES effect is much prominent in the crowded environment giving a relative increase in *A* of 2.24 ± 0.51, compared to *A*= 1 ± 0.1 for native NEMO. These data therefore suggest that in a crowded environment, more similar to the intracellular milieu, NEMO has a more rugged FEL, able to explore a broader range of conformational states than observed in dilute buffered solution. This is consistent with findings from other studies, for example Dhar *et al* find the phosphoglycerate kinase shows an increase in conformational sampling in a crowded environment (Dhar *et al.*, 2010). This is consistent with our putative molecular model of NEMO activity that is based on allosterically regulated NEMO conformational change. Below, we consider the potential mechanistic role of an increased number of available conformational states with respect to ligand interactions.

Based on our native, denatured and stabilized protein analysis (Figure 26) as well as the theoretical basis of the REES effect, the magnitude of REES should be sensitive to changes in the number of discrete equilibrium conformational states. Testing this hypothesis is challenging since few experimental approaches give a direct

window into the equilibrium of conformational states. Non-denaturing pressure perturbation is an excellent tool for this purpose since it acts to perturb a pre-existing equilibrium of structural states characterized by different energy minima on the protein FEL (Akasaka, 2006) and has been used for this purpose in a number of studies (Pudney *et al.*, 2009; Hay *et al.*, 2010; Collins *et al.*, 2011). Crucially pressure, unlike temperature, does not alter the internal energy of the system, which might otherwise be a confounding factor for REES measurements. The observation of a pressure dependence on the REES effect itself would therefore be powerful evidence that REES is sensitive to the equilibrium of protein conformational states.

We have previously found that increasing pressure causes a decrease in W6 emission, suggesting increased solvent exposure (Catici *et al.*, 2015). This finding is corroborated by a red shift in the W6 CSM with increasing pressure (Figure 27A), giving an increase of 3.0 nm at λ_{ex} = 292 nm. The change in the magnitude of the value for our CSM this is due to a different spectral window used to calculate the CSM for the pressure studies. This was necessary due to the optical setup of the pressure cell. The $\Delta\lambda_{Em}^{max}$ value of W6 at 1 bar is similar to that reported above, giving $\Delta\lambda_{Em}^{max}$ = 348 nm at 10 °C, 1 bar and λ_{ex} = 295 nm. Increasing pressure leads to a higher reported value for CSM at higher λ_{ex} values, giving an increase of 8.9 nm at λ_{ex} = 310 nm from 1 to 2000 bar. These data suggest that the REES effect itself is pressure-dependent.

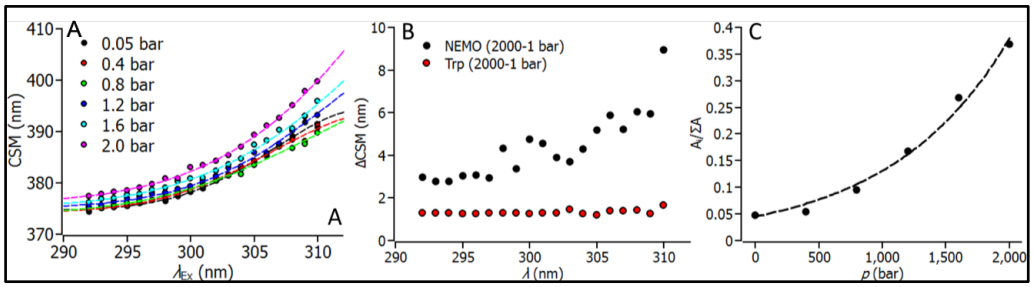

Figure 27. The REES effect is sensitive to pressure variation. A, Variation in REES with increasing pressure. Dashed lines are the fits to Eq.14. B, Comparison of low and high pressure REES data for NEMO W6 and free Trp. The data show the difference in CSM (ΔCSM) *versus* pressure. C, The pressure dependence of *A* extracted from the fits in panel A. The dashed line is the fit to Eq.13.

We note that we do not observe any REES effect with free Trp in buffered solution at any pressure (Figure 27B) and the changes we observe are protein specific. Fitting the REES data to Eq.13 gives the pressure dependence of *A,* shown in Figure 27C as the change in the fraction of *A* across the pressure range. The pressure dependence data

can be adequately fit to a simple, phenomenological model that implies a single transition between two states with changing hydrostatic pressure as used previously (Catici *et al.*, 2015):

$$\frac{A_i}{\sum A}(p,T) = \frac{K(p,T)}{1+K(p,T)} = \frac{\exp\left(lnK_0 - \Delta V_A p/R_p T\right)}{1+\exp\left(lnK_0 - \Delta V_A p/R_p T\right)} \qquad \text{[eq.13]}$$

where R_p = 83.13 cm3 mol^{-1} bar^{-1} K^{-1} when the pressure, p, is measured in bar, K_0 is the equilibrium constant for the change in the relative population of the ith conformational state represented by the magnitude of A from Eq.12, extrapolated to 0 bar and ΔV_A is the apparent difference in the volume associated with this equilibrium transition.

Fitting the data in Figure 28 to Eq.13 gives a negative activation volume ΔV = -24.7 ± 4.7 cm^3 mol^{-1}. We have previously measured ΔV for W6 emission and find (as we show here) that the emission decreases across the pressure range giving ΔV = 0.81 ± 0.03 cm^3 mol^{-1} (Catici *et al.*, 2015). The difference in sign is simply attributable to relative change in direction of the specific signal. What is important is that the magnitude of ΔV changing for REES effect compared to W6 emission. Indeed, this magnitude of pressure dependence is more consistent with global metrics of NEMO conformational change previously measured using the pressure dependence of 8-Anilinonaphthalene-1-sulfonic acid (ANS) emission (Catici *et al.*, 2015). The REES signal may therefore be reflective of the broader equilibrium of NEMO conformational states at sites distal to W6. That is, these two values are not necessarily comparable, reflecting different aspects of the W6 molecular environment. The key finding from the pressure data in the present context is that the REES effect itself is pressure-dependent with the magnitude of A increasing with pressure. Given that pressure acts to perturb the equilibrium of conformational states, this observation suggests that the magnitude of A extracted from Eq.12 is exquisitely sensitive to this equilibrium.

Our findings from denaturation, pressure and macromolecular crowding measurements suggest that the REES effect as monitored by Eq.12, is sensitive to changes in the equilibrium of conformational states, e.g. by unfolding (chemical denaturation), stabilization/folding (macromolecular crowding) or direct perturbation

(pressure). As such, we suggest that the magnitude of the REES effect can be used as a proxy for the protein free energy landscape (FEL), reflecting the distribution of discrete conformational sub-states. Based on our observations for NEMO REES and fits from Eq.12, we have developed a conceptual framework for interpreting protein REES data, shown in Figure 28. Our interpretation of the present data explicitly recognises the information content that arises from the curvature of the REES data, unlike other REES studies where data are fit to linear models only. Within this framework, the changing curvature of the REES data (reflected by the magnitude of *A* extracted from Eq.12) describes the progression to a greater or smaller number of discrete conformational states. In other words, this can be seen as changes in the FEL, with the FEL becoming more rugged or more flat depending on the change in the curvature of the data. In addition the intercept with the y-axis, R_0, describes whether the protein tends towards a folded or unfolded state, in exactly the same way as per the normal analysis of Trp emission in protein folding studies, but with the added benefit that it takes account of cases where the peak maximum of the emission band shifts with excitation wavelength. It is important to note that the terms folded and unfolded encompass more minor conformational changes also. So for highly flexible and dynamic proteins a blue shifted CSM may simply reflect a more compact conformational state (as we suggest is the case from the crowding experiment shown in Figure 26), without requiring global folding events.

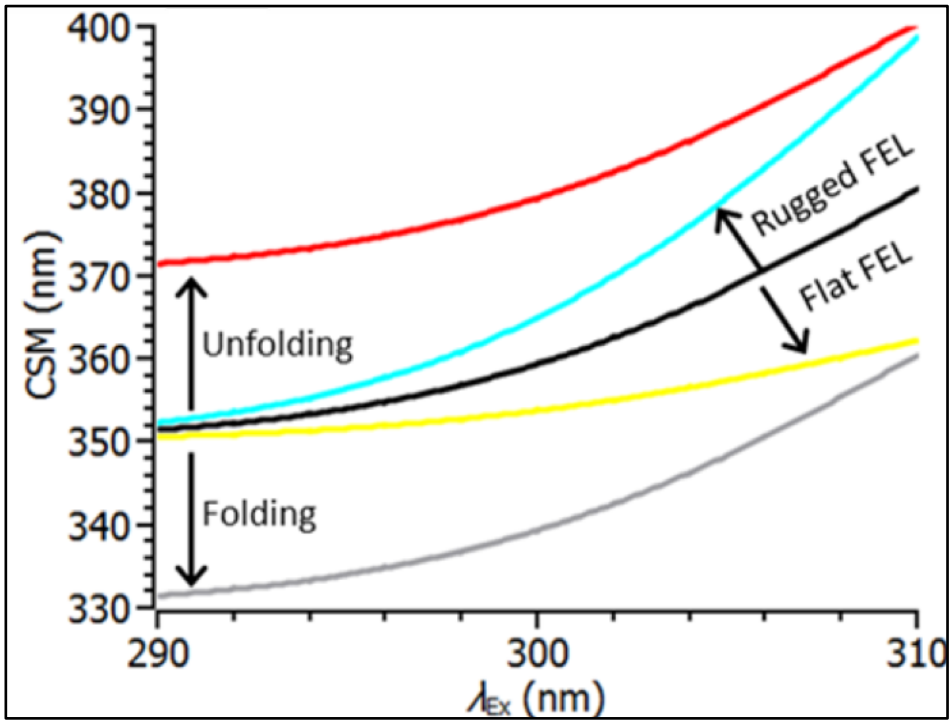

Figure 28.Conceptual framework for the interpretation of tryptophan REES data in proteins based on NEMO W6 experimental data. This model for REES data is based on the trends observed upon NEMO denaturation and presence of crowder, as seen in Fig 27.Depenidng on how the CSM plot changes, proteins are thought to transition to a 'more folded' conformation (flat FEL) upon the CSM becoming more less solvent exposed (lower λ seen on left axis) *vs* the proteins transitioning to a 'less folded' (rugged FEL) state upon the CSM becoming more solvent exposed (higher λ seen on left axis).

It is important to recognize that REES data from protein Trp residues will be convolved of the signal arising from different Trp rotamers (Pan *et al.*, 2006). However, our observations suggest that at least for NEMO, the REES signal is not convolved of a signal from Trp rotamers. That is, the pressure dependence of the REES gives an activation volume of V= -24.7 ± 4.7 cm^3 mol^{-1}, and different when compared to values obtained based on Trp emission alone (-1.6 ± 0.4 cm^3 mol^{-1}) and more consistent with measurements that reflect global NEMO conformational change (Catici *et al.*, 2015). Moreover, we demonstrate below that ligand binding at sites that are not located near the Trp residue alter the REES signal and this is powerful evidence that the NEMO REES signal is dominated by the protein's global structural ensemble.

Novel insight from REES on the nature of NEMO allostery and ligand induced conformational change. Having established that the REES effect, specifically the use of Eq.12, can be used as a proxy for the protein free energy landscape, we now consider

how the NEMO REES signal varies upon ligand binding. These data should give more direct insight into the mechanism of ligand induced conformational change and the relationship to the protein FEL. The REES data for NEMO ligand bound states are shown in Figure 29A and 29B with the solid lines representing the fit to Eq.12. The resulting extracted values of *A* from Eq.12 are given in Table 1 and also as an inset bar chart in Figure 30. For clarity, we report the *relative* change in *R* and *A* compared to NEMO alone, extracted from Eq. 11 and 2, respectively. Figure 30A shows NEMO alone and bound to either a peptide mimic of IκBα or IKK-β. The IKKβ peptide (termed the NEMO binding domain, NBD) contains two Trp residues and so is not suitable for the present study as the signal from the peptide would confound our analysis of the single NEMO Trp. Instead we have replaced these Trp residues with a conservative amino acid, Phe, and we call this peptide NBD-Phe. We find that this modified peptide binds to NEMO, giving a decrease in W6 emission of ~ 50 %. From Table 1 and Figure 30A there is a difference in the magnitude of *A* depending on the ligand bound form of NEMO. That is, *A* decreases on IκBα peptide binding ($A = 0.85 \pm 0.04$) but increases on NBD-Phe binding ($A = 1.33 \pm 0.3$). If we fit the ligand binding data shown in Figure 29A to the simple linear function described by Eq. 11 we find a different trend. That is, from Eq. 13, IκBα peptide binding increases the relative magnitude of the REES effect ($R = 1.35 \pm 0.1$) and IKK-β peptide binding gives essentially no change in the relative magnitude of the REES effect ($R = 0.98 \pm 0.1$).

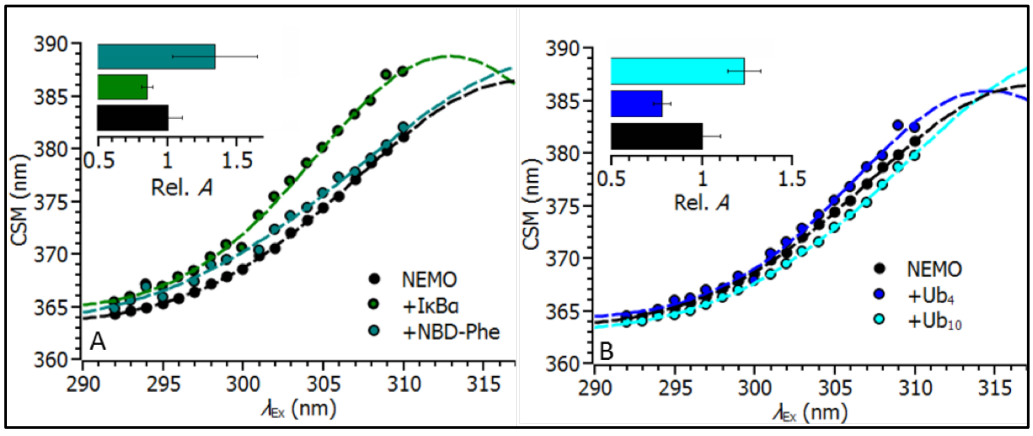

Figure 29. Ligand induced conformational change occurs by altering the existing equilibrium of NEMO conformational states. A, Change in NEMO W6 REES on binding IκBα and IKK-β peptides. Solid line is the fit to Eq.12. *Inset* the extracted relative magnitude of *A* from the fit. B, Change in NEMO W6 REES on binding different linear poly-ubiquitin chains, tetra-ubiquitin (cyan) and deca-ubiquitin (blue). Solid line is the fit to Eq.12. *Inset* the

extracted relative magnitude of *A* from the fit. The error bars are the standard deviation from 3 measurements.

From Figure 30A it is apparent that the REES data are not equivalent with NEMO bound to NBD-Phe and NEMO alone as suggested by the fit to Eq. 11. Instead the major difference is in the curvature of the data and this is captured by the use of Eq.12. Based on our findings from the pressure data discussed above, we suggest that these data reflect a decrease in the number of discrete conformational states on IκBα binding, but an increase in the number of discrete conformational states on IKK-β binding. This trend is supported by our previous NEMO-ligand binding studies monitoring the change in ANS emission (Catici *et al.*, 2015), which suggest the exposure of hydrophobic residues on IKK binding and the burying of hydrophobic residues on IκBα.

NEMO comprises a specific domain that non-covalently binds poly-ubiquitin. We have previously found that binding of long chain-length 'free' M1-linked poly-ubiquitin chains to NEMO allosterically regulates ligand affinity and potentially cellular localization based on evidence from stopped-flow and liposome binding assays (Catici *et al.*, 2015). Poly-ubiquitin is found as a range of chain-lengths in the cell and we have previously provided evidence from ANS binding studies that NEMO undergoes different conformational change depending on the chain-length of non-covalently bound poly-ubiquitin (Catici *et al.*, 2015). We have explored the REES effect on NEMO W6 in the presence of both short (4-mer; Ub_4) and long (10-mer; Ub_{10}) poly-ubiquitin chains, shown in Figure 30B. From the resulting values of *A*, given in Table 1, Ub_4 binding gives a decrease in *A* (*A* = 0.77 ± 0.05), but Ub_{10} gives an increase (*A* = 1.23 ± 0.1). A simple linear fit to Eq. 11 suggests no difference in REES with either chain length giving *R* of ~ 1 within error (Table 1), despite obvious differences in the curvature of the data sets. The absolute magnitude of the REES difference is small, and we would focus on the broad trend we observe that potentially suggests that longer chain lengths induce a broader range of accessible NEMO conformational states.

Based on the most current NEMO structural model the poly-ubiquitin binding site is not located near the native Trp residue (Catici *et al.*, 2015; Bagnéris *et al.*,

2015). That we observe a change in the REES effect for this Trp is consistent with the notion that poly-ubiquitin binding alters NEMO conformation or dynamics in an allosteric fashion. The trend for a decrease in REES with shorter poly-ubiquitin chain lengths and an increase at longer chain-lengths mirrors the binding of ANS that we have reported previously (Catici *et al.*, 2015). That is, we observe a decrease in ANS emission (suggesting burying of hydrophobic residues) at short chain lengths and an increase (suggesting exposure of hydrophobic residues) at longer chain lengths. Combined, these data suggest that shorter poly-ubiquitin chain lengths may drive compaction (burying of hydrophobics and a reduction in the equilibrium of conformational states) and longer chain lengths may drive expansion (exposure of hydrophobics and an increased equilibrium of conformational states) of NEMO. Our REES data further suggest that these changes are not large-scale folding or unfolding events since the R_0 values (Table 1) are essentially the same. Based on these data we hypothesise that the allosteric regulation of NEMO by poly-ubiquitin occurs by modulating the available equilibrium of conformational states, rather than gross structural change.

Mechanistic consequences for the NEMO-ubiquitin interaction. There is a great deal of contemporary interest in the relationship between the equilibrium of native protein conformational states and how this equilibrium changes upon ligand binding (Vogt and Di Cera, 2013; Nussinov *et al.*, 2014). Based on insight from our current data, we suggest that NEMO predominately utilizes a conformational selection model of ligand binding and we show this as a schematic in Figure 30. That is, NEMO adopts a range of equilibrated conformational states represented by discrete energetic minima on the protein FEL. Ligand binding occurs at one of these pre-existing conformers, shifting the equilibrium towards the ligand bound population. For example, as we show above, IκBα binding gives a reduction in the number of NEMO conformers, implying a less rugged FEL for the binary complex. However, we would extend this model to suggest that ligand binding may also induce new conformational states, as well as expanding the number of discrete states within the population (a more rugged FEL) as with NBD and Ub_{10}. A potential mechanistic rationale for this finding is that the new conformational space allows new molecular interactions, not accessible to the

non-ligand bound protein alone. Indeed, we have previously found that Ub_{10} enhances the affinity of NEMO for IKK-β and IκBα and promotes liposome association (Catici *et al.*, 2015). Based on our present data we would hypothesise that this allosteric effect is achieved by exposing new high affinity binding sites or additional binding determinants for these species.

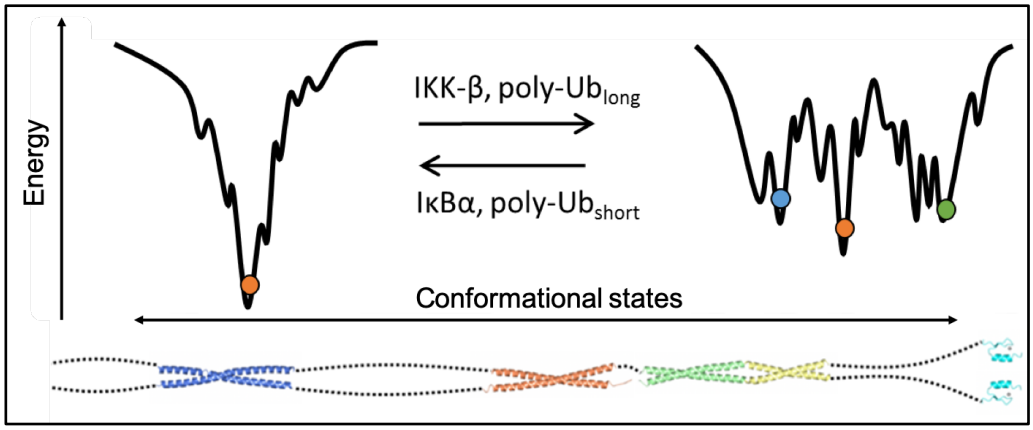

Figure 30. A schematic depiction of the putative change in NEMO's free energy landscape on interaction with IKK-β, IκBα and different chain-lengths of poly-ubiquitin. The black energy (E) barrier (left) represent the small number of discrete conformational states, tending towards a single major conformational state (orange circle) and the right-hand barrier represent an increased range of discrete conformational states (coloured circles). We suggest ligand binding modulates the available equilibrium of conformational states and that this acts as part of the molecular control of NEMO's functional interactions. The putative NEMO structure is shown as coloured ribbons (solved NEMO structures deposited in the PDB; 3BRV, 3CL3, 2ZVN and 2JVX; adapted from (Catici *et al.*, 2015)), connected by regions (dotted lines) which can change conformational state depending on the nature of the specific NEMO-ligand complex

A recent study by Bagnéris *et al* (Bagnéris *et al.*, 2015) have modeled the NEMO structure as a parallel coiled coil and have provided experimental evidence for this structural model from PELDOR (pulsed electron double resonance studies). We have previously found from far-UV CD studies that NEMO is composed primarily of α-helical (~50 %) and random coil (~40%) and our present data suggest that the NEMO structure occupies an equilibrium of conformational states. We suggest that these data can be resolved by a model where NEMO is in a dynamic equilibrium between well folded (coiled coil) and locally unfolded (random coil) states (the dotted connecting lines in Figure 31). This dynamic equilibrium can then be differently stabilized on ligand binding, with IκBα giving rise to an increased proportion of folded content and IKK-β/poly-ubiquitin giving more unstructured content. This model would then be

consistent with the PELDOR data, our previous ANS binding studies and the present REES data.

Methods

Protein expression and purification. Full length human NEMO was expressed and purified essentially as described previously (Catici *et al.*, 2015). Purified protein was dialysed extensively into a buffer comprising 50 mM Tris-Cl pH 8.0, 50 mM NaCl and 5 mM DTT. All measurements were made in this buffer unless otherwise stated. IKK-β and IκBα peptides were commercially synthesised by Genscript, having a purity of > 98 % and are of the sequence TALDFSFLQTE and DDRHDSGLDSMKD, respectively. The IKK-β peptide was modified such that the two native Trp residues were replaced with Phe residues. M1-linked poly-ubiquitin was purchased from Viva Bioscience. *Staphylococcus aureus* immune modulator protein fragment Sbi-III-IV K173A was expressed and purified essentially as described previously (Upadhyay *et al.*, 2008). Protein concentration used was between 1 and 5 µM. Peptide concentrations were 1 mM and poly-ubiquitin concentrations were 1 μM.

Red edge excitation and high-pressure measurements. All fluorescence measurements were performed using a Perkin Elmer LS50B Luminescence Spectrometer (Perkin Elmer, Waltham, MA, USA) connected to a circulating water bath for temperature regulation (± 1 °C). Samples were incubated for 5 minutes at the given conditions prior to recording measurements. Measurements were performed at 10°C, unless otherwise stated. Excitation and emission slit widths were 5 nm except for pressure experiments where they were 10 nm. The change in the slit width was required due to the optical setup of the pressure cell to ensure a low signal-to-noise for the W6 emission signal. For NEMO red edge excitation scans, tryptophan emission was monitored from 325 to 550 nm. The starting excitation wavelength was 292 nm and subsequently increased in 1nm steps for a total of 19 nm. For Sbi-III-IV, red edge excitation scans, tyrosine emission was monitored from 294 to 400 nm, with the excitation wavelength set at 274 nm. Similarly, the excitation wavelength was subsequently increased in 1nm steps for a total of 19 scans. The corresponding buffer or buffer and ligand control was subtracted from the spectra for each experimental condition. Specifically, we note that

for the crowding experiment with Sbi, we subtract the emission from the Sbi, so our signal is not convolved of Sbi Tyr emission in any way.

An ISS high-pressure cell (ISS, Champaign, UL, USA), fitted with a custom fiber optic mounting to the fluorimeter and connected to a circulating water bath for temperature regulation was used to record all high-pressure measurements. For NEMO high-pressure red edge excitation measurements, tryptophan emission was monitored between 325-450 nm.

The center of spectral mass (CSM) was calculated using the following equation:

$$CSM = \frac{\sum(f_i x\, \lambda_{Em})}{\sum(f_i)} \qquad \text{[Eq.14]}$$

where f_i is the measured fluorescence intensity and λ_{em} is the emission wavelength. We would stress the importance of using a consistent wavelength range when reporting CSM data, as the magnitude will be dependent on the wavelength range chosen. As such we report the CSM across the emission range 325 – 450 nm or 335 – 450 nm for pressure experiments.

Author Contributions

D.A.M.C, H.E.A, Y.Y and C.R.P performed experiments. D.A.M.C, J.M.H.E and C.R.P wrote the main manuscript text. D.A.M.C and C.R.P prepared the figures. All authors reviewed the manuscript.

Acknowledgements

We are grateful to Dr Ventsi Valev and Professor Joseph Lakowicz for helpful input and discussions. This work was funded by the UK Royal Society, the UK Biochemical Society, the University of Bath and the Engineering and Physical Sciences Research Council (EPSRC) fund DAMC's studentship.

Post-paper discussion:

Here we use REES spectroscopy to study NEMO functional conformational change, when bound to peptide mimics of two functional *in vivo* binding partners.

The peptide corresponding to the NEMO-binding domain of both IKK enzymes (NBD) is a target of interest for medical research. NBD has been shown to reduce the activation of NF-κB, whilst still allowing a weak NF- κB activity (May *et al.*, 2000). Many therapeutic attempts have looked at further characterising the mechanisms by which NBD selectively inhibits the activity of NF-κB, including in clinical trials (Habineza Ndikuyeze *et al.*, 2014). In a monkey model of Parkinson's disease, injections of NBD were reported to offer neuroprotection and improved motor functions (Mondal *et al.*, 2012). More recently in a murine model of Alzheimer's disease, the protective role of NBD was reported following intranasal administration of the peptide (Rangasamy *et al.*, 2015). In mice, treatment with NBD showed positive results which included: reduced levels of NF-κB in the hippocampus, neuroprotection and reduction in the detectable levels of amyloid-β, and better neurological functions (Rangasamy *et al.*, 2015). The promising results of many therapeutic studies using NBD suggest the importance of understanding the mechanism by which it modulates NF-κB activity, and more specifically understand its interactions with the IKK complex. Our findings highlight the effect of NEMO:NBD interaction, whereby it induces a more dynamic conformational change in NEMO. This is potentially an important factor to take into consideration when designing NEMO-based therapeutics.

This study also establishes the use of REES spectroscopy to detect protein changes following denaturation and molecular interactions, which illustrate the applicability of this technique to many protein systems, especially where issues arise due to disorder or size limitations. The use NEMO W6 emission for REES spectroscopy has proven be a good measure of NEMO global conformational change, which is not limited to the immediate environment of the fluorophore. We note that the data in Figure 23B do

not show a good fit and could have been refitted using the residuals to confirm that the fit is poor. However, this fit is just to guide the reader in observing the curvature of the data, and subsequent data fitting and discussion of NEMO REES incorporate a fit to capture the curvature of the REES data (eq.12).

The major advantage of using REES spectroscopy is the ability rapidly and easily access information about protein conformation without the need for extrinsic labels. Whilst other structural biology techniques such as Hydrogen deuterium exchange coupled with mass spectrometry (HDX-MS) and NMR are strong candidates, the lengthy experimental times coupled with relatively high protein concentrations required for NMR pose considerable risks of proteins undergoing unfolding or aggregation during data acquisition. REES measurements do not pose such issues as the experimental time requirements for REES measurements require between 10-30 mins, thus removing any concerns about stability of protein over time.

In terms of HDX-MS limitations include: poor sequence coverage due to presence of multiple disulphide bonds (Wang and Kaltashov, 2014) and gas-phase hydrogen scrambling (fast and uncontrolled relocation of the incorporated deuterium among backbone and side chains (Rand *et al.*, 2010)). NEMO has two important disulphide bonds, required for dimer formation and activation of the protein (Herscovitch *et al.*, 2008), and as such HDX-MS analysis of active protein is currently not achievable.

On the other hand, the main limitation of REES in lack of detail on the specific of the structural conformational changes observed, as it only conveys information about the changes in the solvation around the fluorophore. However, this technique is very powerful and sensitive to small changes in the environment: here we present data that show that binding of NEMO to a peptide mimic of the IKKβ enzyme (NBD) induces a more flexible conformation compared to unbound protein. These findings have recently been confirmed using X-ray crystallography and molecular simulations, with the authors proposing a structural model for NEMO where the protein exhibits a dynamic binding interface and allosteric regulation from ligand binding (Barczewski *et al.*, 2019), thus perfectly aligning with the results presented in chapter 3.

To our knowledge, this is the only the second study to investigate the effect of NEMO interacting with IκBα. Therefore, we can only speculate with regards to the functional conformational change observed upon NEMO-ligand binding. IκBα functions as an inhibitor of the NF-κB canonical pathway and its interaction with IKKβ results with its subsequent degradation and activation of the pathway (Traenckner *et al.*, 1995). NEMO is known to mediate the interaction between IKKβ and IκBα (Schröfelbauer *et al.*, 2012) and so potentially the conformational changes reported using REES show that upon binding to IκBα, NEMO undergoes a conformational change in preparation for binding to IKKβ.

We have described and analysed the kinetics of NEMO binding to IκBα, NBD, and various linear-ubiquitin chains using NEMO W6 fluorescence, ANS fluorescence and stopped-flow experiments (Catici *et al.*, 2015). The results show $K_{d(app)}$ for various NEMO:ligand complexes to be as follows: NEMO:NBD $K_{d(app)}$ = 2.0 ± 0.1 mM and NEMO:IκBα $K_{d(app)}$ = 0.6 ± 0.2 mM. The data show that binding to NBD induces a different NEMO conformational change compared to binding to IκBα, both globally verified using ANS fluorescence, as well different changes in the local environment of the W6 probe (Fig.31B). Stopped-flow binding experiments show a multiphasic trend indicative of an increase in the number of conformational substates, with both IκBα and NBD present (Fig.31C). These finding corroborate the results presented in Chapter 3, with binding of these two ligands allowing NEMO to access to more conformational states, with differences in their solvation, as shown by the ANS in Figure 31 and W6 REES data Figure 29.

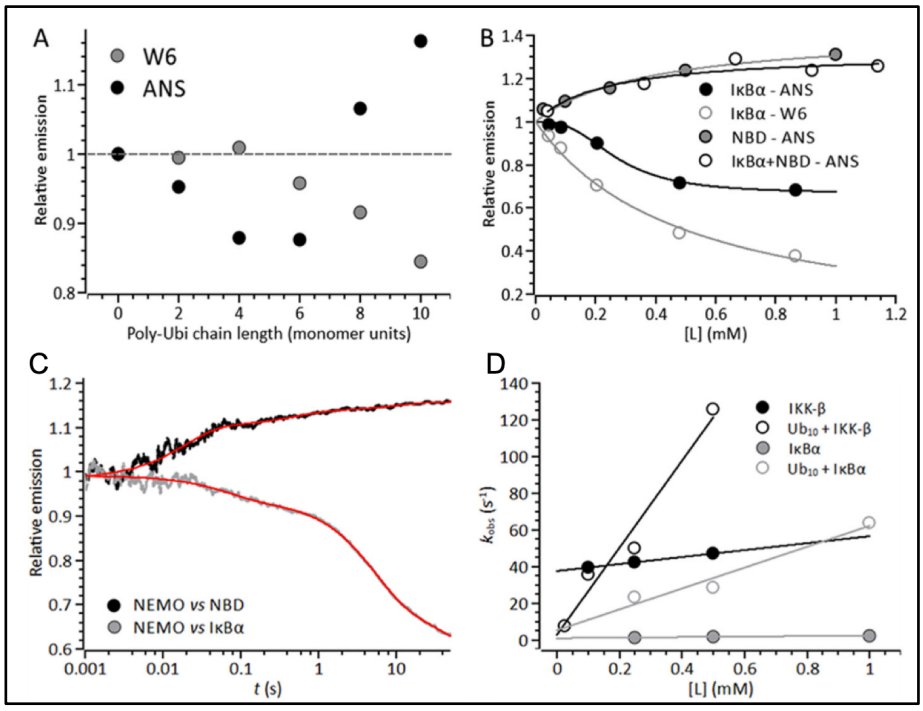

Figure 31. Ligand binding is coupled with NEMO conformational change. Solid lines are fits to specific equations, as described previously (Catici *et al.*, 2015). A, Relative NEMO W6 and ANS emission upon binding to 25 µg/ml polyubiquitin, linear poly-ubiquitin chains (monoubiquitin to decaubiquitin). B, Relative NEMO W6 and ANS emission upon binding to NBD and IκBα (0- 1.2 mM). C, NEMO conformational change following binding to NBD and IκBα (0.5 mM) analysed by stopped-flow. D, Concentration dependence of NBD and IκBα (0-1 mM) in the presence and absence of 25 µg/ml decaubiquitin. All measurements were carried out at 10 °C.

We have previously reported on chain length dependence of ubiquitin and binding to NEMO and how binding of ubiquitin induces conformational changes, as well as an increase in the affinity of NEMO for NBD and IκBα. In the presence of decaubiquitin, NEMO-Ubi10:NBD $K_{d(app)}$ = 0.01 ± 0.04 mM and NEMO-Ubi10:IκBα $K_{d(app)}$ = 0.09 ± 0.14 mM. In the cell, NEMO is activated by binding to ubiquitin in a non-proteolytic manor following which NEMO bind to (and possibly activates) IKKβ (*vide infra*) (Komander *et al.*, 2009). Based on previous reports (Figure 31 (Catici *et al.*, 2015)) and the findings presented in Chapter 3, we believe that the conformational changes observed in NEMO W6 REES upon binding to tetra- and decaubiquitin potentially allows NEMO access to functional conformational substates, not available to the unbound protein. Improved affinity for ligand binding further supports ubiquitin acting to 'prepare' NEMO for specific interactions, such as binding to IKKβ enzyme, for example. However,

we can only speculate as to what type of conformational states are available to NEMO upon ubiquitin binding, due to the limitation of REES spectroscopy. However, it is promising to observe changes in the N-terminus of NEMO (W6 location), upon binding of ubiquitin at the C-terminus, indicating that the ligand in capable on induces global changes in the structure of NEMO. This was recently confirmed also using SAXS measurements (Hauenstein *et al.*, 2017). Based on their structural findings, the authors observed that unbound NEMO exists in an 'auto-inhibited' state, whereby the C-terminus is capable of folding back upon itself, thus masking the ubiquitin binding region of NEMO. However, upon binding to ubiquitin, the protein adopts an *apo* conformation, with global conformational changes resulting in the elongation of NEMO (Hauenstein *et al.*, 2017). These findings offer structural evidence to support the changes a observed for NEMO ANS in the presence of ubiquitin reported in Chapter 3 (Catici *et al.*, 2016).

In conclusion, monitoring the REES arising from NEMO W6 fluorescence, this study offers detailed information of the dynamic nature of NEMO, and allosteric regulation following binding to various NF-κB proteins, further evidencing the ability of NEMO to undergo functional conformational change. This aligns with the aims of the PhD in understanding the nature of the protein conformational observed upon ligand binding and the potential functional importance of NEMO-ligand interactions. These results can be further tested and validated using SAXS measurements, to confirm the changes in protein conformation under the different conditions tested in Chapter 3 and allow for a detailed description of specific NEMO conformations.

Chapter 4: Mimicking the intracellular milieu exposes the molecular plasticity of NF-κB essential modulator

Accompanying commentary for chapter 4:

We have previously demonstrated the use of non-denaturing hydrostatic pressure to monitor NEMO conformational change using an intrinsic fluorophore (Catici *et al.*, 2016). Here we demonstrate the use of an extrinsic fluorophore, 1-anilino-8- naphthalene sulfonate (ANS), to study NEMO conformational change in response to pressure and temperature perturbations. In addition, we also monitor the NEMO functional conformational change in response to binding to a peptide mimic of the inhibitor IκBα.

ANS is a frequently used probe in studies focusing on protein conformational change (De *et al.*, 2005) membrane compositions (Haynes and Staerk, 1974; Slavík, 1982), and detection of protein aggregates (Kundu and Guptasarma, 2002; Finke and Jennings, 2001). The fluorophore offers a number of advantages such as low quantum yield (especially in polar environments) and increased sensitivity to the environment (Gasymov and Glasgow, 2007).

Early research on the photochemistry of ANS suggests that ANS emission is due to the presence of two distinct excited electronic states (Kosower and Kanety, 1983; Kosower and Huppert, 1986), depending on the polarity of the solvent. In addition, a third excited electronic state has been observed in aqueous environments; this allows for the solvation of the involving electrons, which return to their ground state without emitting any radiation, thus explaining the low quantum yield of the molecule (Kosower and Kanety, 1983; Kosower and Huppert, 1986). An increase in ANS quantum yield is observed in non-water polar environments, due to the different properties of water compared to non-water environments (Moore *et al.*, 1985).

ANS is thought to interact with proteins non-covalently, with the presence of hydrophobic (Stryer, 1965) and charged residues (Schonbrunn *et al.*, 2000) on proteins enabling this interaction. NEMO displays a proportion of ~40% disordered regions (Catici *et al.*, 2015), and as ANS was a very suitable probe to use to understand the behaviour of the protein in different environments.

In this study, we also investigate the effect of the physical parameters of the cell on the structure and dynamics of NEMO. These include viscosity, crowding, and presence of osmolytes, and their effect was studied on free NEMO, as well as NEMO:IκBα bound complex. These are important questions to answer, as more studies acknowledge and urge that the effect of the cellular environment not be ignored in structural and dynamic studies of macromolecules (Wirth and Gruebele, 2013; Monteith *et al.*, 2015). Most *in vitro* conditions fail to take into account the physical parameters of the intracellular milieu, which have been reported to exert an effect on protein structure, function, and dynamics.

The distribution of NEMO is the cell is heterogeneous, with the protein found in the cytoplasm (Gilmore, 2006), at the cell membrane (Nakamori *et al.*, 2006), and even inside the nucleus (Kim *et al.*, 2010). Considering the distribution of NEMO in the cells and the lack of consensus on the structure and dynamics of the protein, it is apparent that a thorough investigation of the effects of the intracellular milieu on NEMO is needed. Pressure and temperature perturbations are a suitable technique to study this as it offers detailed thermodynamics of protein conformational change and does not pose any size limitations compared to other techniques. We have previously established the use of it for monitoring NEMO intrinsic fluorescence and local conformational change (Catici *et al.*, 2015). The use of ANS will allow for monitoring of the global protein conformational change and thus offer a detailed image of NEMO dynamics and structure in a mimic of the intracellular environment.

This declaration concerns the article entitled:									
Mimicking the intracellular milieu exposes the molecular plasticity of NF-κB essential modulator									
Publication status (tick one)									
draft manuscript	✓	**Submitted**		**In review**		**Accepted**		**Published**	
Publication details (reference)	-								
Candidate's contribution to the paper (detailed, and also given as a percentage).	The candidate contributed to/ considerably contributed to/predominantly executed the… Formulation of ideas: DAMC, VLA, JMM, CRP Design of methodology: DAMC, JMM, CRP Experimental work: Protein purification and expression: DAMC Fluorescence and high-pressure measurements: DAMC Calculating predicted helical and coiled coil content: JMM Data fitting: VLA, CRP Presentation of data in journal format: DAMC, JMM, CRP								
Statement from Candidate	This paper reports on original research I conducted during the period of my Higher Degree by Research candidature.								
Signed	**Dragana Catici**				**Date**	25^{th} Jan 2019			

Mimicking the intracellular milieu exposes the molecular plasticity of NF-κB essential modulator

D A M Catici [1], J M Mason[1], V L Arcus[2]* and C R Pudney[1]*

Running title: The FEL in the cell

Abstract.

The intracellular milieu is a complex compartmentalized environment governed by a range of different physical factors including high concentrations of macromolecules, co-solutes and varying viscosities. Typically, protein structure and intra-molecular dynamics are considered in isolation as part of a simple buffered solution. However, there is building evidence that the thermodynamics of protein folding and motion can be affected by the individual physical factors governing the intracellular environment. There is an increasing awareness that protein intra-molecular dynamics, governed by the free energy landscape (FEL), are crucial to function. In particular, many signalling proteins are thought to be conformationally heterogeneous (flexible) in order to mediate multiple different ligand interactions. We wished to explore if the different physical factors of the intracellular milieu affected the thermodynamics that govern protein flexibility in a relevant model system. We have studied changes to the free energy landscape of NF-κB essential modulator (NEMO) under different conditions that mimic the intracellular milieu using combined pressure/temperature fluorescence studies. These studies allow us to go beyond simplistic descriptions of the FEL in terms of enthalpic and entropic contributions and expose the role of more crucial thermodynamic parameters such as heat capacity and expansivity. We find that the NEMO FEL responds differently to different environmental perturbations and dependent on ligand binding. Our data allow us to infer how the NEMO FEL varies in different cellular micro-environments and points to the intracellular milieu as an additional control parameter in determining protein structure, dynamics and function.

Introduction

Proteins have evolved to fold and function inside a complex and heterogeneous cellular environment. There are differences in the concentration of macromolecules (Rivas *et al.*, 2004), small organic molecules (osmolytes) (Street *et al.*, 2006) and viscosities (Sekhar *et al.*, 2014) depending on the specific cellular micro-environment and cell type (Guigas *et al.*, 2007). These different physical properties have been found to affect the structure, function, and dynamics of proteins (Gruebele *et al.*, 2016). Such studies point to the importance of protein quinary structure – the variance in structure arising through interaction with the solvated environment – in governing the fine detail of molecular structure and function (Wirth and Gruebele, 2013).Whilst the folded structure of most proteins is considered to be the same *in vitro* as *in vivo* (Gruebele *et al.*, 2016), notable differences in the thermodynamics of protein folding have been elegantly demonstrated primarily by whole-cell NMR studies (Danielsson *et al.*, 2015; Schlesinger *et al.*, 2011; Maldonado *et al.*, 2011). These studies suggest that the free energy landscape (FEL) - a series of energetic 'hills and valleys', separating discrete conformational sub-states - may be affected by the different physical factors of the intracellular milieu (Cheung *et al.*, 2004).

There is now broad appreciation that the intra-molecular dynamics of proteins is key to their normal function (Henzler-Wildman and Kern, 2007). Notionally conformational heterogeneity might provide some advantage to molecules that mediate multiple ligand interactions, for example those involved in signalling networks (Dunker *et al.*, 2005). Such conformationally flexible proteins could be described as having a 'rugged' FEL. In particular, the effect of macromolecular crowding (Stagg *et al.*, 2011; Hong and Gierasch, 2010) and the presence of osmolytes (Ferreon *et al.*, 2012) have been studied in the context of the protein FEL. These effects alter the hydration state of the protein, which also affect normal structure and dynamics (Xu and Cross, 1999; Sage *et al.*, 1996; Nakasako *et al.*, 2001; Gallat *et al.*, 2012; Beece *et al.*, 1980). Macromolecular crowding gives rise to the excluded volume effect, which disfavours protein hydration (Kuznetsova *et al.*, 2014). Similarly, osmolytes can give rise to an excluded volume effect or bury their osmophobic backbone in the protein core, which

can favour protein hydration (Kumar, 2009; Weatherly and Pielak, 2000). Additionally, the presence of other cellular components, including other proteins is also known to give rise to viscosity. Increased viscosity hydrates the protein indirectly, by favourably interacting with and stabilizing the protein solvation envelope (Gekko and Timasheff, 1981). Therefore, the intracellular milieu could potentially affect a proteins FEL through subtle changes to protein hydration state.

NF-κB essential modulator (NEMO) governs much of the human immune and nervous response, by regulating the interactions of the NF-κB proteins. Briefly, NF-κB is sequestered in the cytoplasm by IκBα. NEMO regulates the activity of the kinase IKK-β, which phosphorylates IκBα, targeting it for degradation and thus releasing NF-κB (Gilmore, 2006). We have provided evidence that NEMO exists in an equilibrium of inter-converting conformational sub-states, characterized by a rugged FEL (Catici *et al.*, 2015), and that the intrinsic flexibility of NEMO is functionally important (Catici *et al.*, 2015; Catici *et al.*, 2016). NEMO is found in a range of different intracellular micro-environments; in the cytoplasm (Gilmore, 2006), nucleus (Kim *et al.*, 2010) and at the plasma membrane (Nakamori *et al.*, 2006).

We hypothesize that the sensitivity of NEMO's FEL to the intracellular milieu may be so important that it affects not just the thermodynamics of protein folding but also the thermodynamics of the native dynamics and flexibility. Indeed, we have previously found that in the presence of a proteinaceous crowding agent NEMO becomes more compact, whilst maintaining its intrinsic flexibility (Catici *et al.*, 2016). Herein we combine the power of non-denaturing pressure/temperature (*p*/*T*) perturbation to examine the effect of the major physical factors of the intracellular milieu (crowding, presence of osmolyte, and viscosity) on the NEMO FEL, specifically relating to functional protein dynamics. We have opted for p/*T* studies because this allows us access to the full suite of thermodynamic parameters that govern the FEL. Crucially, the effects of these parameters are assessed for both ligand bound and unbound NEMO. We find that the different physical factors we study affect the FEL of NEMO in a condition specific manner, showing sensitivity to either the ligand bound or free protein. Given the extreme sensitivity of NEMO's FEL to the intracellular milieu we suggest a model where the different micro-environments of the cell act as an additional control parameter in governing the normal functional state of NEMO.

Results and Discussion

NEMO conformational state is affected by a mimicked intracellular milieu. We wish to understand how the different physical properties of the intracellular milieu affect NEMO conformational dynamics and the local FEL around the native state. To achieve this we monitor NEMO conformational change as the change in fluorescence emission arising from 1-anilinonaphthalene-8sulfonate (ANS) binding (Qadeer *et al.*, 2012) as we have demonstrated previously (Catici *et al.*, 2016) and used in similar studies. We focus our study on the effect of macromolecular crowding [polyethylene glycol (PEG; 100 g/L, MW 20,000)], and the presence of osmolyte (66 mM Betaine HCl). There are a range of potential crowding agents one could use, each with specific caveats, and no single crowding agent is 'optimal'. However, PEG is used very commonly in the literature (Samanta *et al.*, 2016). The use of crowding agents can be complex, leading to an increase in solution viscosity and also charge interactions (Christiansen *et al.*, 2013). We therefore also explore the effect of increasing viscosity (30% w/w glycerol; 2.17 cP at 25 °C) and the presence of the monomeric unit of the crowding agent (100 g/L ethylene glycol, EG). These different conditions therefore allow us to mimic the intracellular milieu and explore the conformational dynamic and thermodynamics though changes in ANS fluorescence.

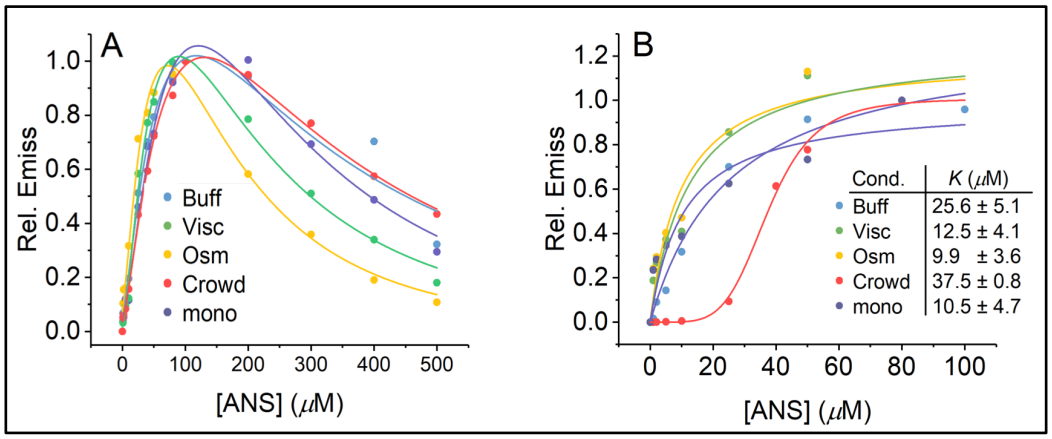

Figure 32. Relative emission of ANS following binding to NEMO under different conditions. The different conditions are as follows: simple buffer (blue), viscogen/glycerol (green), osmolyte/Betaine HCl (yellow), crowder/PEG (red), monomer/Ethylene glycol (purple). A, Binding of ANS (0-800 µM) to NEMO (25 µM) under the different conditions

studied. Relative emission is set to the emission intensity maximum for each condition. Solid lines are the fit to a skewed Gaussian function and are to aid the eye of the reader. B, ANS (0-100 µM) binding to NEMO (25µM) under the different conditions studied. The solid lines are the fit to a simple binding isotherm of the form, $E = E_{max}\cdot[ANS]/K+[ANS]$. Where E is the relative emission and *K* is the equilibrium constant for the binding of ANS to NEMO. The resulting values of *K* are given in the inset table. For the PEG data (red) we use a more complex function given the apparent sigmoidal nature of the binding in this case; $E = E_{max}\cdot[ANS]^n/K^n+[ANS]^n$, which is essentially the form of the Hill equation.

We have used 80 µM ANS for each of the conditions studied since above this concentration we observe a decrease in ANS emission (Figure 32A). This is most likely attributable to the inner filter effect or direct collisional quenching. Higher concentrations than ~80 µM will therefore potentially convolute our data with an emission signal that is difficult to account for. Titrating ANS against NEMO under the different conditions studied gives an effective equilibrium constant for the binding of ANS as shown in Figure 32B. We observe saturation behaviour of the ANS emission in the range < ~100 μM ANS, with the extracted equilibrium constants (fitting to a simple binding isotherm; Figure 32B) falling in the range K ~ 10-40 μM. We note that this is not a true K_d values (rather a K_{obs}) as we do not have a full understanding of the ANS:NEMO molar equivalent of binding, and as such treat it as equilibrium constant to inform on saturating ANS concentrations to use in this study.

The observation of signal saturation therefore implies we are capturing the ANS binding to NEMO under each of the conditions studied by using an ANS concentration of 80 μM. Ideally one would like to use an even higher concentration of ANS, but we note the limitation placed on the concentration that can be used given the observed quenching/inner filter effect for ANS described above (Figure 32A). We do not therefore rule out that our signal is convolved of ANS binding to very low affinity sites (K > 100 μM). Indeed, at the concentration of ANS we use, we are able to fully characterise the relatively 'complex' binding interaction in the presence of the crowding agent, where the data showing a sigmoidal, not hyperbolic relationship. However, we are mindful of the challenges using an extrinsic fluorophore as the observed signal and so we focus on the major trends in our data below, not the absolute magnitudes of extracted values.

Figure 33A shows the difference in ANS emission for the different conditions studied. ANS binding is broadly indicative of the exposure of hydrophobic patches on proteins (Stryer, 1965). We note that the data are background subtracted in all cases under the relevant control conditions and so the signals shown in Figure 32 and 33 arise solely from the ANS bound to NEMO. We label each condition as a subscript in the text i.e. NEMO in simple buffer, with crowding agent, osmolyte, viscogen and crowding monomer as $NEMO_{Buff}$, $NEMO_{Crowd}$, $NEMO_{Osm}$, $NEMO_{Visc}$, $NEMO_{mono}$, respectively. From Figure 33A, we find that $NEMO_{Crowd}$ and the $NEMO_{Osm}$ give an increase in ANS emission compared to $NEMO_{Buff}$, suggesting these conditions drive NEMO conformational change. Conversely, the control conditions ($NEMO_{Visc}$ and $NEMO_{EG}$) give essentially no change in the absolute magnitude of emission, suggesting any subsequent differences in our thermodynamic analysis for free NEMO (*vide infra*) are not the consequence of a different conformational state for these conditions. Figure 33B shows the ANS emission data for NEMO bound to a peptide mimic of IκBα, $IκBα_{27-39}$.

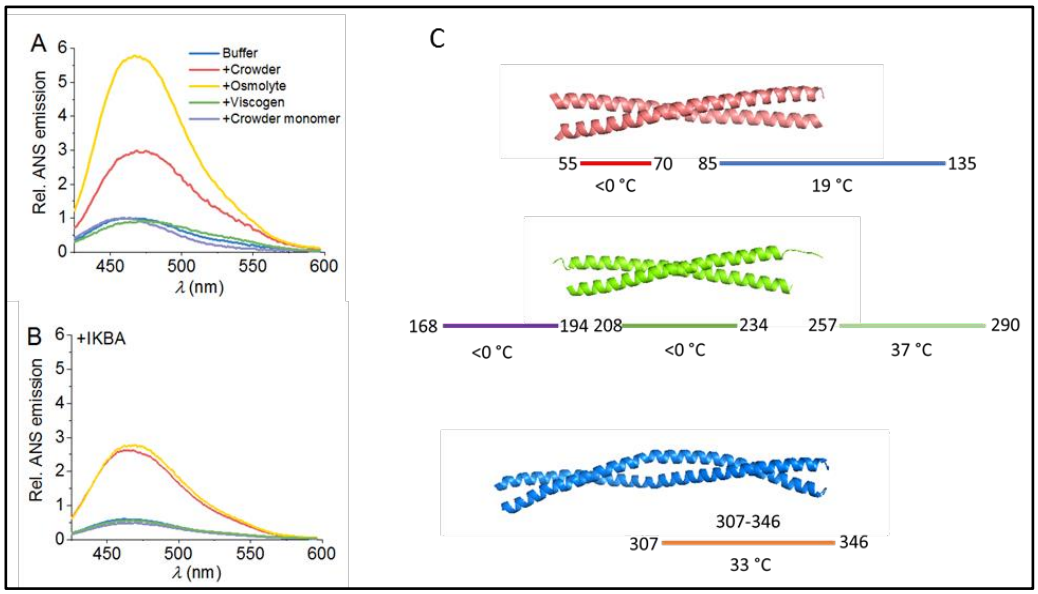

Figure 33. The change in NEMO-ANS emission (under different conditions (A) and with ligand bound (B)) and NEMO structures comparison with coiled-coil predictions. **A,B Values are relative to NEMO alone in simple buffer. NEMO concentration is 25μM and ANS concentration is 80 μM. C, Comparison of existing NEMO structures (each construct solved in isolation) with coiled-coil prediction. The C-terminal zinc finger is not shown. The values under each coloured line represent the calculated T_m for coiled coil breakdown and are a relative metric of coiled-coil probability and stability. Colours are to show different T_m ranges. The colours of the helices represent different regions of the protein.**

We use a peptide mimic because the background signal from ANS binding to the peptide is small and we subtract this signal in all cases. We have previously studied a peptide mimic of the NEMO binding region (NBD) from IKK-β but we found this complex was unstable, particularly during our *p/T* studies (below). The NEMO-IκBα$_{27\text{-}39}$ complex is stable on the ~days timescale. From Figure 33B, consistent with our previous reports (Catici *et al.*, 2016), binding of the IκBα$_{27\text{-}39}$ peptide to NEMO gives a decrease in ANS emission of approximately 25%. The magnitude of change is similar for all conditions, with the exception for NEMO$_{Crowd}$ which decrease by only ~ 5%. The smaller difference in ANS emission with PEG might suggest the presence of the crowding agent has affected NEMO-ligand binding. Alternatively, in the ligand bound form and in the presence of the crowding agent the breadth of available conformational states that NEMO are reduced and differently solvated compared to free NEMO or NEMO$_{Buff.}$

We wish to comment on what kind of conformational change we envisage our data represent. We have previously provided evidence that NEMO contains regions of structural disorder alongside extensive helical structure. To date, only crystal structures of partial constructs have been reported that all form a coiled-coil architecture composed of NEMO homodimers as shown in Figure 33C. Evidence from EPR studies and modelling based on helical register assignment have developed a picture when NEMO forms a rod-like coiled-coil architecture across nearly its entire length (Bagnéris *et al.*, 2015). From concentration dependence studies, NEMO has been shown to form concentration dependent oligomers (Ivins *et al.*, 2009) and these may be functionally relevant in forming lattice-like structures, particularly at the cell membrane (Scholefield *et al.*, 2016). The conformational changes we monitor below, and in our previous work (Catici *et al.*, 2015), do not appear to be consistent with an architecture as immobile as an extended, rod-like coiled-coil. Indeed, a recent small angle X-ray scattering (SAXS) model of NEMO, suggests that global conformational change is possible (Hauenstein *et al.*, 2017), mediated primarily by unordered loop regions (Muñoz and Luis, 1995). We have analysed the NEMO sequence (Figure 33C) using tools to detect both predicted helical and coiled coil content, Agadir (Muñoz and Serrano, 1995) and bCIPA (Mason *et al.*, 2006), respectively. It is clear from this

sequence analysis that NEMO cannot adopt a purely coiled coil architecture as has been hypothesized (Bagnéris *et al.*, 2015). Instead, we suggest three regions of coiled-coil structure, with predicted T_m values in the 19-37 °C range, consistent with µM levels of homodimeric affinity (Wiedersich *et al.*, 2008). These coiled-coil regions are interspersed by regions predicted to be disordered or isolated helices. The former are consistent Gly / Pro rich regions that are predicted to be non-helical and incapable of coiled coil formation. We therefore suggest that the conformational changes we monitor represent non-trivial variation in structure including transient unwinding of helices and coiled-coil, tertiary structural rearrangement and potentially oligomerisation state change (Mason *et al.*, 2006).

Probing the NEMO FEL in the mimicked intracellular milieu. The ANS binding data suggest changes in NEMO's environment (specifically those that affect the protein hydration state) can indeed affect NEMO conformation. We wish to probe if these changes affect the NEMO FEL. Combined pressure/temperature (*p*/*T*) denaturation studies have been used in a number of cases to extract the complete suite of thermodynamic parameters that define the FEL for protein folding, so called elliptical phase diagrams (Akasaka, 2006). In the present study we wish to explore the FEL specifically relating to native protein conformational change. Non-denaturing hydrostatic pressure is an excellent probe of native protein dynamics since it acts by perturbing the pre-existing equilibrium of states, favouring more compact conformations (Prabhu and Sharp, 2005). Non-denaturing pressure therefore gives access to the conformational changes that are natively accessible on the proteins FEL.
For a simple two state transition, e.g. equilibrium between two conformational sub-states, the temperature dependence of the equilibrium constant is given by,

$$\boldsymbol{lnK = \frac{-\Delta G}{RT}} \qquad [\boldsymbol{eq.15}]$$

The combined *p*/*T* dependence of Δ*G* is then given by,

$$\Delta G_{P,T} = \Delta G_0 + \Delta V_0(P - P_0) + \Delta \alpha'^{(P-P_0)(T-T_0)} + \frac{\Delta \beta'}{2}(P - P_0)^2 - \Delta S_0(T - T_0) - \Delta C_P \left[T\left(ln\left(\frac{T}{T_0}\right) - 1\right) + T_0\right] \qquad [eq.16]$$

where T_0 is a reference temperature. ΔH, ΔS, ΔG_0, ΔC_p, ΔV_0, $\Delta \beta$ and $\Delta \alpha$ reflect the changes in enthalpy, entropy, Gibbs free energy, heat capacity, activation volume, compressibility and expansivity between the two notional conformational sub-states that define the equilibrium, respectively. Note that this model assumes both ΔC_p and $\Delta \alpha$ are constant with respect to both pressure and temperature, and as such the values reported in the study reflect the changes in ΔC_p and $\Delta \alpha$ in response to changes in the experimental conditions tested (eg. presence of crowder or osmolyte) or in response to NEMO ligand binding. Fitting Eq. 16 to a plot of ΔG for a matrix of p/T values will therefore yield the breadth of different thermodynamic parameters. The equilibrium constant for NEMO conformational change is extracted from the relative change in ANS emission across the p/T matrix,

$$\frac{F_i}{\sum F}(p,T) = \frac{K(p,T)}{1 + K(p,T)} \qquad [eq.17]$$

where F_i is the integral of the emission intensity of ANS for a given pressure/temperature. These data are used to calculate ΔG (Eq. 15) across the p/T matrix and then fit to Eq. 16 to extract the thermodynamic parameters. From Figure 35 the fits of Eq. 16 to the experimental data are excellent, though given the high parameter space of Eq. 16, there are relatively increased error values associated with some of the extracted parameters. This is always the case in analyses of this type. That said, our data show clear difference, outside of error. For these reasons, we focus on the broad trends that allow us to characterise the FEL, namely ΔH, reflecting the barrier to conformational change; ΔG_0, reflecting the probability of conformational change; ΔC_p, reflecting the ruggedness of the FEL; and $\Delta \alpha$, reflecting changes in flexibility and solvation.

The major contribution to ΔC_p in the case of protein conformational change and protein folding is the difference in hydration state between the conformational states that are accessed (Prabhu and Sharp, 2005; Cooper *et al.*, 2007). Observing an increase

in the values of ΔC_p implies there is change in the distribution of ΔH values and by extension a range of barrier heights (governed by the magnitude of ΔH) separating discrete conformational states (i.e. a rugged FEL). Studies with model systems have found that the magnitude and sign of $\Delta\alpha$ is sensitive to the solvation environment (changes to water structure) and upon ligand binding (Royer, 2005; Mitra *et al.*, 2008). Zero values of $\Delta\alpha$ imply a 'rigid' protein (Mitra *et al.*, 2008) and positive $\Delta\alpha$ values are correlated with exposure of hydrophobic residues (Vasilchuk *et al.*, 2014; Schweiker *et al.*, 2009). These concepts are summarised as a cartoon in Figure 34, which links the changes in the thermodynamic parameters above and the 'shape' of the FEL. We note that the experimental error for ΔS and $\Delta\beta$ (below) is substantial and no trends could confidently be assigned and so we do not consider the trends of any in these data.

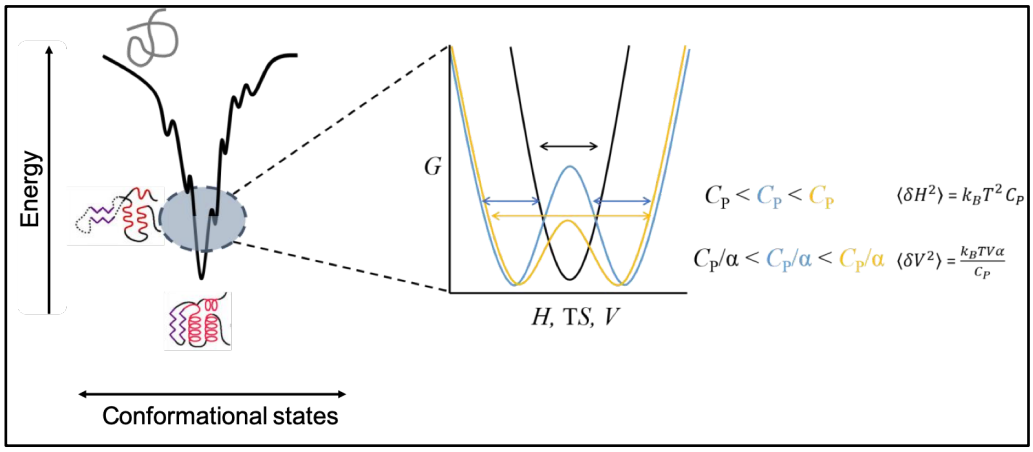

Figure 34. A schematic of how different thermodynamic parameters can be envisaged to affect a FEL. The grey line (at left) represents a model FEL where the size of the barriers is governed by *G*, the distribution of minima and their barrier sizes is governed by C_p and the hydration states associated with the energetic minima is governed by *α*. Changes to these parameters affect the shape of the FEL. At right, we show the change in the distribution of *H*, T*S* and *V* values associated with C_p and C_p/α. In black, a single narrow range of *H*, T*S* and *V* values results in low values of C_p and C_p/α. In blue are two interconverting states with a high barrier giving increased values of C_p and C_p/α. In yellow are two interconverting states with a low barrier which gives an even greater value of C_p and C_p/α.

The *p*/*T* matrix of ΔG values for each condition is shown as coloured planes in Figures 35A-F. Figure 36A-E shows the resulting parameters extracted from the fit to Eq. 16 for $NEMO_{Buff}$, $NEMO_{Crowd}$, $NEMO_{Osm}$ and the corresponding ligand bound states. The parameters for the control conditions $NEMO_{Visc}$ and $NEMO_{EG}$ are shown in 36F-I. All extracted values are given in Table 2. A comparison of the values for each extracted parameter is shown in Figures 35F-I.

Table 2. The extracted parameters from the fits of Eq. 16 to the data in Figure 35.

	$NEMO_{conc}$	$NEMO_{dil}$	$NEMO_{Crowd}$	$NEMO_{Osm}$	$NEMO_{Visc}$	$NEMO_{mono}$
ΔG_0 (kJ mol^{-1})[a]	8.7 ± 0.3	9.3 ± 0.8	-0.1 ± 0.8	10.0 ± 1.3	8.2 ± 0.2	11.8 ± 2.1
+ ligand	7.0 ± 1.6	-	8.6 ± 0.4	13.0 ± 0.8	11.7 ± 1.2	9.9 ± 2.3
ΔV_0 (cm^3 mol^{-1}) [a]	-4.7 ± 1.9	7.7 ± 3.9	-15 ± 4.8	2.9 ± 7.7	0.8 ± 1.2	5.5 ± 12.9
+ligand	8.5 ± 9.7	-	9.9 ± 2.3	4.5 ± 12.7	5.2 ± 7.2	4.2 ± 13.5
ΔC_p (kJ mol^{-1} K^{-1})	0.1 ± 0.4	0.5 ± 1.2	8.6 ± 0.9	1.5 ± 1.5	0.5 ± 0.2	-3.0 ± 2.5
+ligand	-4.1 ± 1.9	-	0.5 ± 0.4	-8.0 ± 1.0	-3.0 ± 1.4	-3.7 ± 2.6
$\Delta\alpha$ (K^{-1})	0.00 ± 0.05	-0.08 ± 0.14	-0.53 ± 0.14	0.01 ± 0.23	-0.20 ± 0.03	0.43 ± 0.37
+ligand	0.80 ± 0.34	-	0.12 ± 0.07	0.03 ± 0.15	0.21 ± 0.21	0.37 ± 0.39
ΔC_p / $\Delta\alpha$ (kJ mol^{-1})	59.4 ± 2600	-6.3 ± 19.6	-16.1 ± 4.6	15.8 ± 40.1	-50 ± 154	-7.0 ± 8.5
	-5.1 ± 3.0	-	4.3 ± 4.4	-250 ± 1100	-14.4 ± 16.2	-10 ± 12.6

[a,] Values reported at 1 bar and 37 °C.

We have previously measured (but not fit) the *p*/*T* matrix for a dilute solution of NEMO (5 μM) (Catici *et al.*, 2015). Here we use a more concentrated solution (25 μM) to ensure we capture a reasonable enough ANS signal for robust analysis, particularly since some signal changes are small. NEMO's oligomeric state is highly concentration dependent (Fontan *et al.*, 2007). The ANS *p*/*T* matrix is different at different NEMO concentrations (Figure 35D), suggesting the oligomeric state affects the thermodynamics of conformational change. Indeed, from Table 2 and Figure 36B, we find that the magnitude of ΔV_0 is negative for the more concentrated NEMO, but positive for the dilute NEMO. All other parameters are the same within experimental error. These data suggest that oligomerisation state change does not itself affect the flexibility of NEMO but does give access to a different equilibrium of conformational states.

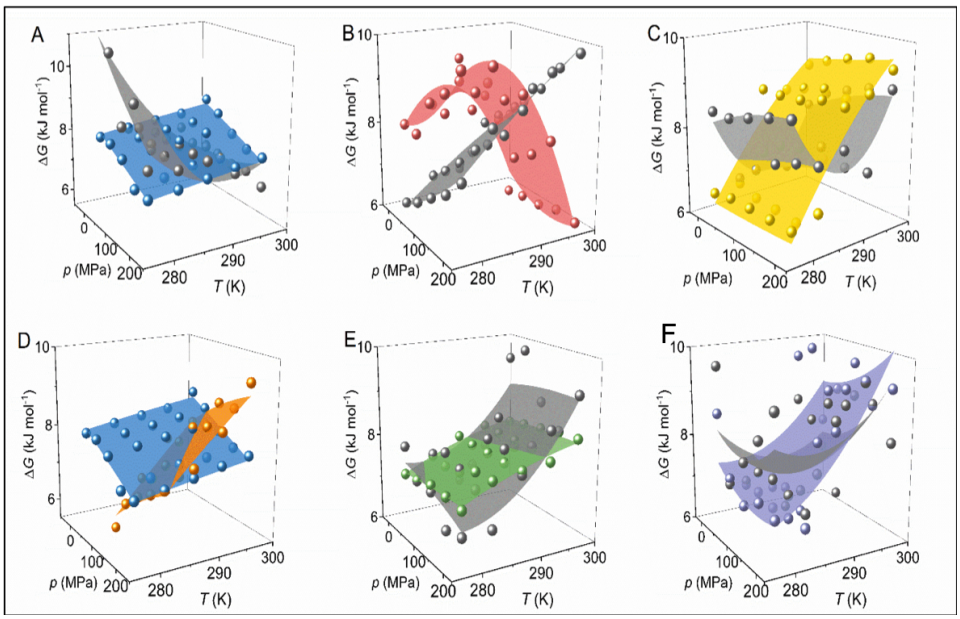

Figure 35. The combined *p/T* dependence of NEMO-ANS emission for the range of conditions studied. Concentrated $NEMO_{Buff}$ - blue (A), $NEMO_{Crowd}$ - red (B), $NEMO_{Osm}$ - yellow (C), dilute $NEMO_{Buff}$ - orange (D), $NEMO_{Visc}$ - green (E) and $NEMO_{mono}$ - purple (F). Surfaces are the fit to Eq. 16. Coloured surfaces are for free NEMO and the grey surface is the NEMO-IκBα_{27-39}complex.

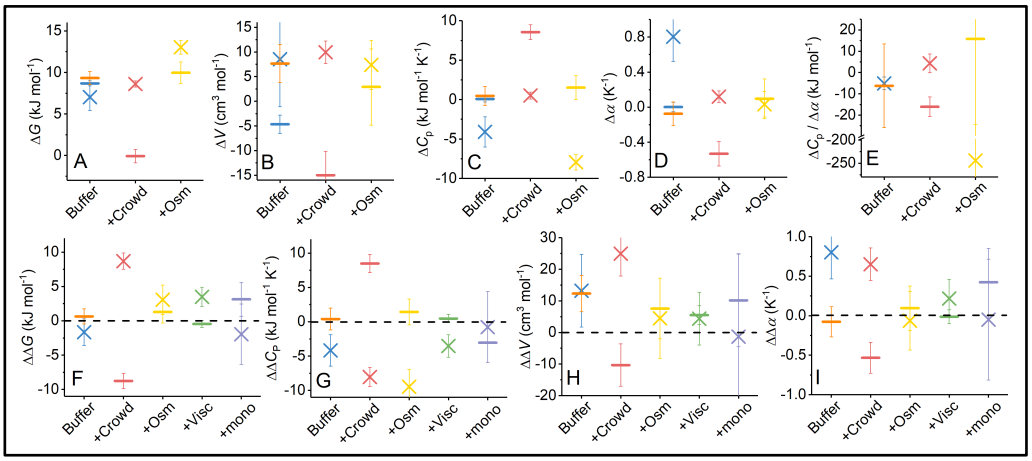

Figure 36.Magnitude of calculated thermodynamics parameters. A-E, The magnitude of Δ*G*, ΔC_p, Δ*V* and Δ*α* and ΔC_p/Δ*α*, extracted from fits of panels A-C to Eq. 16. Lines are free NEMO, stars are ligand bound. F-I, The magnitude of ΔΔ*G*, ΔΔC_P, ΔΔ*V* and ΔΔ*α*, showing the differences in Δ*G* between different conditions relative to $NEMO_{buff}$. A cartoon depiction of the data and how they relate to the shape of the FEL is shown in Figures 36A-F. The colours match the colour scheme in Figure 35.

Based on the relative ANS emission of concentrated NEMO *vs* more diluted protein, we have opted to study the range of conditions mimicking the intra-cellular milieu with the higher concentration NEMO, to improve the signal-to-noise ratio of our data. Moreover, recent evidence suggests that higher-order oligomers of NEMO are likely to

be functionally important (Scholefield *et al.*, 2016; Darwech *et al.*, 2010; Xie *et al.*, 2012) and so this species seems to be the most relevant to study. From Figure 36 and Table 2 there are clearly very important changes in thermodynamics for the different conditions studied and with respect to ligand binding.

The detailed description and discussion of the results is below, but to aid the reader the major trends are:

1. IκBα$_{27\text{-}39}$ generally makes ΔC_p more negative, for all conditions studied.
2. The osmolyte has very little effect on any thermodynamic parameter for the free NEMO but abrogates the effect of IκBα$_{27\text{-}39}$ biding.
3. The crowding agent has a profound effect on the thermodynamics of the system making ΔG_0, ΔV_0 and $\Delta\alpha$ more negative and ΔC_p more positive. However, IκBα$_{27\text{-}39}$ binding directly inverts these relationships, with a clear effect on both ΔV and $\Delta\alpha$ (see Table 2 for specific values).

Based on the cartoon in Figure 34, we have summarised these findings and how they relate to changes in the FEL shown in Figures 36A-I. From Figure 36G, ligand binding appears to primarily affect the magnitude of ΔC_p, giving a change from a zero/positive value to a negative value. These data suggest that the free NEMO FEL has a relatively narrow distribution of ΔH values, suggesting a relatively restricted range of conformational sub-states. On ligand binding, the observation of a negative ΔC_p suggests a transition to a FEL with a much broader distribution of ΔH values and so a broader range of conformational sub-states. That is, the NEMO FEL becomes more rugged when bound to the ligand IκBα$_{27\text{-}39}$ (depicted in Figure 37D). For NEMO$_{Crowd}$, NEMO$_{Osm}$ and NEMO$_{Visc}$ we observe an increase in ΔG for the ligand bound NEMO (Table 2). Therefore, while ΔC_p values argue that ligand binding gives access to more conformational substates, the increase in ΔG_0 suggests that the change in the height of the barriers has now changes such that these conformational changes are energetically unfavourable to occur (depicted in Figures 37D-F).

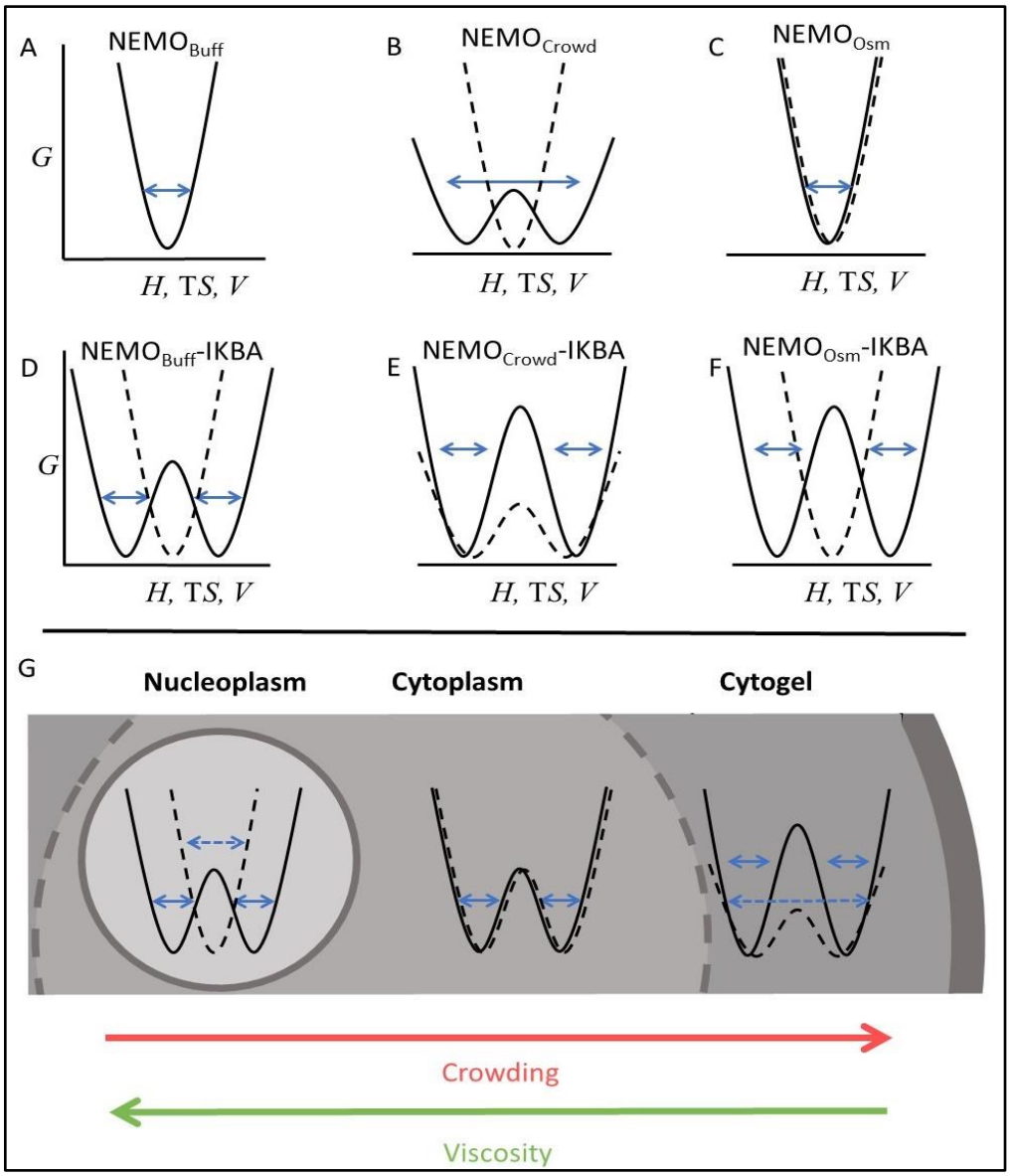

Figure 37. Cartoon showing the effect of the different conditions studied on the FEL. A, NEMO$_{Buff}$; B, NEMO$_{Crowd}$; C, NEMO$_{Osm}$ shown as a solid line, compared to NEMO$_{Buff}$ shown as a dashed line. D, NEMO$_{Buff}$-IκBα; E, NEMO$_{Crowd}$-IκBα$_{27-39}$; F, NEMO$_{Osm}$-IκBα$_{27-39}$ shown as a solid line, compared to the same ligand free condition shown as a dashed line. G, Model of the effect of variation in intracellular environment on the NEMO FEL. Dashed line is for free NEMO, solid line is for IκBα27-39 bound.

These data correlate well with our ANS emission data (Figure 32), where IκBα binding decreases ANS emission in all cases, suggesting conformational states with exposed hydrophobic residues are more restricted. PEG is used to mimic the excluded volume effect (NEMO$_{Crowd}$), but will also give rise to an increased solution viscosity (5.25 cP (Parker *et al.*, 2010)) and electrostatic effects from the monomeric unit. From Figures 36F-I, we find that the magnitude of ΔG_0, ΔC_p, ΔV_0 and $\Delta\alpha$ are essentially the same

within error for the viscogen ($NEMO_{Visc}$) and the PEG monomer ($NEMO_{mono}$) compared to $NEMO_{Buff}$. That is, changes in solution viscosity and electrostatic effects arising from the monomeric unit of PEG are not convolving our $NEMO_{Crowd}$ data and so the effects we observe are attributable to the excluded volume effect. We note that the viscosity of the glycerol solution will vary with temperature from ~3.5-2 cP across the temperature range studied, but the key is that the viscosity is increased relative to $NEMO_{Buff}$ (0.9 cP) and is of a similar magnitude to that found in the intracellular milieu (Auton *et al.*, 2011)

From Figures 36F-I, $NEMO_{Crowd}$ shows differences outside of error for ΔG_0 ($\Delta\Delta G_0$ = -8.8 ± 1.1 kJ mol^{-1}), ΔC_p ($\Delta\Delta C_p$ = 8.5 ± 1.3 kJ mol^{-1} K^{-1}), ΔV_0 ($\Delta\Delta V_0$ = 10.3 ± 6.7 kJ cm^3 mol^{-1}) and $\Delta\alpha$ ($\Delta\Delta\alpha$ = -0.52 ± 0.20 K^1). These data suggest a complex change to the NEMO FEL driven by the excluded volume effect, depicted in Figure 37B. The decrease in ΔG argues for lower barriers between conformational sub-states, suggesting a more flexible protein. This is mirrored in the measurably negative $\Delta\alpha$ value for $NEMO_{Crowd}$, which as we describe above, again would suggest a more flexible protein. The change in activation volume from a positive to a negative value suggests the conformational sub-states accessible to $NEMO_{Crowd}$ are structurally different. Finally, the positive value for ΔC_p could be indicative of a change in hydration state consistent with a less hydrated protein overall. This interpretation is consistent with the increased exposure of hydrophobic residues from our ANS studies (Figure 33A) and also the notional role of the excluded volume effect. As we discuss above, ligand binding has a global effect on ΔG_0 and ΔC_p. However, $NEMO_{Crowd}$-IκB$\alpha_{27\text{-}39}$ shows additional, condition specific changes. ΔV_0 increases, becoming positive ($\Delta\Delta V_0$ = 25.0 ± 7.1 kJ cm^3 mol^{-1}) and $\Delta\alpha$ increases, becoming positive ($\Delta\Delta\alpha$ = 0.65 ± 0.21 K^{-1}). From Figure 36H and 5I the increase in ΔV_0 and $\Delta\alpha$ is similar to that observed with $NEMO_{Buff}$ ($\Delta\Delta V_0$ = 13.2 ± 11.5 kJ cm^3 mol^{-1} and $\Delta\Delta\alpha$ = 0.80 ± 0.34 K^{-1}). Finally, there is an increase in ΔG_0, but we also see an increase arising from $NEMO_{Visc}$-IκB$\alpha_{27\text{-}39}$ and so we do not attribute the effect on ΔG_0 with $NEMO_{Crowd}$-IκB$\alpha_{27\text{-}39}$ to the excluded volume effect. In summary, despite the observed change to the NEMO FEL for $NEMO_{Crowd}$, the effect is to some extent abrogated on ligand binding, at least with respect to ΔV_0 and $\Delta\alpha$.

Binding of osmolytes has been shown in other systems to alter Δ*H* and Δ*S*, indirectly stabilising proteins by lowering ΔG_0 (Verma *et al.*, 2004). From Figures 36A-E and Table 2 there is no difference outside of error between $NEMO_{Osm}$ and $NEMO_{Buff}$ for any of the extracted thermodynamic parameters. That is, the NEMO FEL hardly varies for $NEMO_{Osm}$ and $NEMO_{Buff}$ (Figure 37C). However, $NEMO_{Osm\text{-}I\kappa B\alpha 27\text{-}39}$ suppresses the effect of ligand binding observed for both $NEMO_{Buff}$ and $NEMO_{Crowd}$. Instead of increases in Δ*V* and Δ*α* on ligand binding, we find that these parameters become invariant within error in the presence of the osmolyte ($\Delta\Delta V_0$ = 4.5 ± 12.7 kJ cm^3 mol^{-1} and $\Delta\Delta\alpha$ = -0.06 ± 0.37 K^{-1}) shown in Figures 36H and 36I. We find a similar pattern of invariance in both ΔV_0 and Δ*α* with $NEMO_{Visc}$ ($\Delta\Delta V_0$ = 4.4 ± 8.3 kJ cm^3 mol^{-1} and $\Delta\Delta\alpha$ = -0.22 ± 0.24 K^{-1}). That is, both the osmolyte and viscogen, which both notionally increase the protein hydration state, disrupts the ligand induced changes to the NEMO FEL, at least with respect to ΔV_0 and Δ*α.* Similar to the crowding agent, both the osmolyte and viscogen increase the magnitude of ΔG_0 for the ligand bound complex (Figure 37F).

Taken together (as summarised in Figure 37A-F) our study illustrates a complex interplay between the different physical factors that govern the intracellular milieu and NEMO's FEL. We do not find that hydration state change associated with the osmolyte, viscosity change or the monomer of the crowding agent, have an effect on the free NEMO FEL outside of error. The only condition that appears to affect the free NEMO FEL (within the error of our measurements) is the presence of a crowding agent and specifically the excluded volume effect. We find that the excluded volume effect alters the barrier between different conformational sub-states, giving both a broader distribution of states and lower barriers between sub-states, a more 'rugged' FEL. That is, the excluded volume effect tends to make NEMO more flexible. Similarly, we find that ligand binding ($I\kappa B\alpha_{27\text{-}39}$) induces a more rugged FEL, with burying of hydrophobic residues. Ligand induced changes to the NEMO FEL are affected by the crowding agent only to increase the magnitude of ΔG_0. However, both the osmolyte and viscogen suppress the effects of ligand binding specifically with respect to changes in Δ*V* and Δ*α.* In summary, the major trends in our data are for desolvation (the excluded volume effect) to affect the free NEMO FEL and for solvation (binding of osmolyte and

increased viscosity) to affect the ligand bound FEL. These findings are summarised as a cartoon in Figure 37.

Conclusions

The complexity and ubiquity of the NF-κB signalling pathway means that NEMO experiences a variety of cellular environments. The protein is usually found in the cytoplasm in unstimulated cells, but also in the nucleus and near the plasma membrane (Bicknese *et al.*, 1993). We have previously found evidence for a model where free NEMO exists in an equilibrium of conformational states, but ligand binding potentially 'functionalises' NEMO for subsequent molecular interactions, by inducing specific NEMO conformations; with different ligands inducing different conformations, thus selecting for different functional conformations (Catici *et al.*, 2015). Our present study extends this model, suggesting that the ligand bound NEMO is hyper responsive to the intracellular milieu, particularly to solvation state change.

There have been a number of efforts to quantify the viscosity and crowding in different sub-cellular locations, broadly studying the nucleus, cytoplasm, near the plasma membrane and within the plasma membrane. These data suggest, in a simplified scheme (Figure 35) that near the PM (the cytogel), the viscosity is only slightly increased than in water (~ 3-4 times higher (Liang *et al.*, 2009)), is higher in the cytoplasm proper (~ double than in water(Auton *et al.*, 2011)) and is relatively higher still in the nucleoplasm (~4 times higher than water) (Spitzer and Poolman, 2013; Liang *et al.*, 2009).

Conversely, the degree of crowding in the cytogel is thought to be extremely high, referred to as 'supercrowded' (Spitzer and Poolman, 2013), but is rather smaller in the cytoplasm and less still in the nucleoplasm (Guigas *et al.*, 2007). Based on this simplified model of the cell and our experimental findings regarding the effect of crowding and viscosity on NEMO's FEL, we suggest how the FEL will differ for NEMO in different sub-cellular compartments, shown in Figure 37G. Our data suggests that at the PM, free NEMO exposes hydrophobic residues and binding to IκBα does not affect this. However, away from the PM, in the cyto/nucleoplasm, NEMO-IκBα will be relatively flexible, adopting a broad range of conformational

states. Potentially the different FEL's and conformational states 'prime' NEMO for subsequent molecular interactions, specific to the local cellular micro-environment. We cannot project how such changes would affect NEMO's functional activity in terms of regulating NF-κB signalling since one cannot independently perturb the physical factors we have studied inside the cell. However, given our previous findings that NEMO flexibility and conformational change are key to ligand binding, the present findings point to the importance of understanding these principles when considering NEMO's intracellular activity.

Given the apparent sensitivity of NEMO's FEL to hydration-state change, and the variable cellular localisation of NEMO, we suggest that the intracellular milieu acts as an additional control parameter, ensuring the proper protein conformation is achieved and ultimately, proper functioning. In other words, the intracellular milieu is capable of modulating the NEMO FEL and allows the protein to explore a number of conformational states. We suggest this ensures a fine balance between NEMO flexibility, stability, and function is achieved inside the cell.

Materials & Methods

***Protein expression and purification*.** Full-length human NEMO was expressed and purified using a previously described method (Catici *et al.*, 2015). Purified protein was dialysed in a buffer containing 50 mM Tris-HCl (pH 8.0), 50 mM NaCl, 5 mM DTT.

Fluorescence and high-pressure measurements. All fluorescence measurements were performed using a Perkin Elmer LS50B Spectrometer (Perkin Elmer, Waltham, MA, USA) connected to a circulating water bath for temperature regulation (± 1 °C). All pressure measurements were performed using an ISS high pressure cell (ISS, Champaign, IL, USA), fitted with a custom fibre optic mounting to the fluorimeter and connected to a circulating water bath for temperature control (± 1 °C). For high-pressure measurements, NEMO ANS emission was monitored from was monitored from 425 nm to 600 nm, with excitation at 390 nm. The emission and excitation slits were set to 15 nm for high-pressure measurements (in order to reduce the signal to noise ratio due to the optical setup of the pressure cell). The starting temperature was set to 5 °C, and increased in 5 °C increments up to 25 °C. The pressure dependence at

each temperature was monitored at 50, 500, 1000, 1500, and 2000 bar. For all fluorescence measurements the appropriate buffer controls were subtracted from each protein scan prior to data processing.

Post-paper discussion:

The cellular environment plays an important role in modulating the structure, function, and dynamics of many proteins. Many *in vitro* conditions do not account for the physical parameters of the cell and so do not offer a true image of the macromolecules studied. In this study we investigated the role of viscosity, crowding, and presence of osmolytes on the structure and dynamics of the human protein NEMO. To our knowledge, this study is the first of its kind, reporting on the thermodynamics of NEMO conformational change in conditions that mimic the intracellular environment. Here we also discuss the effect of the physical parameters of the cell on NEMO ligand binding, as illustrated by interactions the IκBα peptide, a mimic of an important NF-κB inhibitor. *In vivo* studies of NEMO have been previously published, with the aim of understanding the oligomeric state of the protein (Scholefield *et al.*, 2016). Here, the authors report a complex NEMO structure to be found inside cells, but do not mention how the intracellular environment may affect it.

Hydrostatic pressure and temperature perturbations are frequently used in studies aiming to understand the thermodynamics of protein conformational change. More recently they have been combined with NMR (Kremer *et al.*, 2011) and X-ray crystallography (Kurpiewska and Lewiński, 2010) to help understand the thermodynamics of specific protein conformations. As this PhD did not aim to elucidate specific NEMO conformations but rather understand the breath of conformational states NEMO can access under specific conditions, *p*/*T* perturbations were the most appropriate method. In-cell NMR studies should be considered in the future to describe the NEMO conformations observed in the intracellular environment and understand the functional significance of any protein conformational change. As the NEMO interactome is considerably extensive, future studies should consider probing the effect of NEMO binding to a variety of NF-κB ligands for a comprehensive structural and functional understanding of NEMO. Similarly, single-molecule FRET measurements inside live cells (Sustarsic and Kapanidis, 2015) may also be considered to complement NMR and fluorescence studies and, ultimately offer a comprehensive image of the structure, dynamics, and function of NEMO in the cell. With the recent

developments in increasing the size limit of molecules subjected to NMR studies (Sugiki *et al.*, 2017) and improvements in data analysis software for single molecule FRET (LeBlanc *et al.*, 2018) now including intrinsically disordered proteins, NMR and FRET studies on NEMO can certainly be pursued in future studies.

The present study illustrates the importance of considering viscosity and crowding in future NEMO structural and functional studies; the results clearly that compared to simple buffered conditions, the presence of a crowder affects the dynamic of free-NEMO, as well as ligand bound-NEMO. This is an important consideration especially when attempting to resolve any signal arising from NEMO disorder during NMR or FRET. Additionally, the results from this study also which specific conditions give rise to less flexible NEMO conformations, which should be used when stability issues arise when studying NEMO.

Taking into account all results, it can be concluded that in the case of NEMO, the intracellular milieu acts as an additional control to modulate the structure and function of the protein. These findings also shed light onto one possible reason for the lack of consensus about the conformation of NEMO, as many studies investigate the structure and dynamics of NEMO in different conditions (Agou *et al.*, 2004; Rothwarf *et al.*, 1998; Tegethoff *et al.*, 2003; Fontan *et al.*, 2007; Lo *et al.*, 2008). The present study also answers one of the aims of this PhD project, in contributing towards the understanding of the effects on the intracellular environment on the medically relevant NEMO. Further studies are advised to consider these when investigating the structure and dynamics of NEMO.

Chapter 5: Understanding the role of NF-κB essential modulator (NEMO) in mediating the IKKβ: IκBα interaction

Accompanying commentary for chapter 5:

Activation of the canonical NF-κB signalling pathway relies on the activation of NEMO, which facilitates the interaction between the IKKβ enzyme and the inhibitor IκBα (Gilmore, 2006). In this study, we attempt to better understand the role of NEMO in mediating the interaction between IKKβ and IκBα. In order to do so, isothermal titration calorimetry (ITC) is used to understand the kinetics of the IKKβ:IκBα interaction, both in the presence and absence of NEMO. In the event that NEMO only functions as a scaffold, no change in the measurable reaction kinetics should be observed. If, however, the role of NEMO extends beyond this, a change in the reaction rate and/or binding affinity should be detected. The importance of IKKβ:NEMO interaction for activation of the enzyme is well known (Schröfelbauer *et al.*, 2012), but the role of NEMO in the IKKβ:IκBα has not been thoroughly investigated to date.

ITC offers an excellent alterative to classic biochemical enzyme assays, as the IKKβ:IκBα enzymatic reaction does not produce a colourimetric product that can be easily monitored using spectroscopy methods. Using ITC also removed the need for further tagging of the enzyme or substrate, as the method only measures the heat associated with the enzymatic reaction, which is subsequently converted into reaction rate. The use of ITC for the study of enzyme reactions has been previously demonstrated (Mazzei *et al.*, 2014; Di Trani *et al.*, 2017), and the binding of truncated IKKβ:NEMO complexes have also been determined using ITC (Lo *et al.*, 2008). Previous studies have reported the kinetics of IKKβ:IκBα using immunoprecipitation labelling (Zandi *et al.*, 1998). This is the first study that uses ITC kinetic measurements and successfully captures the complexity of the IKKβ: IκBα interaction. The results show that NEMO plays an important role during the phosphorylation of IκBα, allowing for the reaction to proceed at a faster rate and with an increase in the affinity of the reaction.

This declaration concerns the article entitled:									
Understanding the role of NF-κB essential modulator (NEMO) in mediating IKKβ: IκBα interaction									
Publication status (tick one)									
draft manuscript	✓	**Submitted**		**In review**		**Accepted**		**Published**	
Publication details (reference)	-								
Candidate's contribution to the paper (detailed, and also given as a percentage).	The candidate contributed to/ considerably contributed to/predominantly executed the… Formulation of ideas: DAMC, CRP Design of methodology: DAMC, CRP Experimental work: Protein expression and purification: DAMC ITC kinetic experiments: DAMC Data fitting: DAMC, CRP Presentation of data in journal format: DAMD, CRP								
Statement from Candidate	This paper reports on original research I conducted during the period of my Higher Degree by Research candidature.								
Signed	**Dragana Catici**					**Date**	25^{th} Jan 2019		

Understanding the role of NF-κB essential modulator (NEMO) in mediating IKKβ: IκBα interaction

Dragana A.M. Catici, and Christopher R. Pudney,
Department of Biology and Biochemistry, Faculty of Science, University of Bath, UK

Abstract

The control and regulation of the canonical NF-κB signalling pathway in response to specific stimuli is a complex process and it involves the interaction between three key proteins: NEMO, the enzyme IKKβ and the NF-κB inhibitor IκBα. Whilst it is known that IKKβ phosphorylates IκBα thus ensuring the first step towards its proteoasomal degradation, the role of NEMO in mediating this interaction is unclear. Here we use isothermal calorimetry (ITC) to measure the kinetics of the IKKβ:IκBα interaction, both in the presence and absence of NEMO to better understand its role in activating the NF-κB pathway. Our results show that NEMO improves the kinetics of this interaction and potentially acts as an additional control in ensuring a dose-depending phosphorylation of IκBα. This is the first study that uses full-length human NEMO as well as full-length IKKβ for ITC measurements, and manages to capture the complexity of the IKKβ: IκBα interaction both in the presence and absence of NEMO.

Introduction

The NF-κB signalling pathway is an important regulatory human pathway in charge of modulating the response of the immune and nervous systems (Gilmore, 2006; Mémet, 2006). Canonical activation of the pathway is triggered in response to mostly pathogenic stimuli (Israël, 2010) and the reaction is quick, but short-lived (Thompson *et al.*, 1995; Tarantino *et al.*, 2014). In contrast, the alternative activation pathway of NF-κB is characterised by a slower response and it controls very specific functions, such as: organ development (eg. lymph nodes) (Flister *et al.*, 2010; Gerondakis and Siebenlist, 2010), B-cell functioning and growth (Kaileh and Sen, 2012; Sasaki and Iwai, 2015), specific neuronal stimulation and protection (Ade *et al.*, 2007; Dresselhaus *et al.*, 2018), and even bone development (Boyce *et al.*, 2010; Abu-Amer, 2013).

In the absence of a stimulus, NF-κB proteins maintain their cytoplasmic localisation due to the action of specific inhibitors (known as IκBs) being bound to them. During canonical activation of the pathway, degradation of the IκBs is achieved by interactions with the IKK complex. Two kinases, IKKβ and IKKα, and non-catalytic IKKγ or NEMO, make up the IKK complex. Following binding of canonical stimulus to their specific receptor, activation of the IKK complex is triggered. Non-covalent binding of ubiquitin to NEMO ensure activation of NEMO; this in turn is thought to induce the activation of the IKKβ enzyme by a mechanism which is not yet fully understood (Tegethoff *et al.*, 2003; Wang *et al.*, 2001; Fang *et al.*, 2017). Once activated, the IKK complex now targets the NF-κB-bound inhibitors for proteoasomal degradation, though phosphorylation at two specific serine residues (Ser 32 & Ser 36) by IKKβ (Verma *et al.*, 1995; Zandi *et al.*, 1998; DiDonato *et al.*, 1996), followed by ubiquitination by other enzymes (Hatakeyama *et al.*, 1999). These steps ensure the proteoasomal degradation of the IκB inhibitors (IκBα in this case), with the cytoplasmic NF-κB proteins now free to translocate to the nucleus and initiate gene regulation.

NEMO, or the NF-κB essential modulator, is the main activator of the canonical NF-κB pathway (Rothwarf *et al.*, 1998; Shoji Yamaoka *et al.*, 1998; Mercurio *et al.*, 1999; Y. Li *et al.*, 1999). However, the mechanisms by which this is achieved are not fully understood. Most studies assign NEMO the function of a scaffold protein, ensuring that IKKβ and IκBα are located near enough to ensure the phosphorylation of IκBα (Schröfelbauer *et al.*, 2012; Weil *et al.*, 2003). Before this process can occur, activation of both NEMO and IKKβ needs to occur. For NEMO, this is achieved through non-covalent binding of free (Catici *et al.*, 2015; Rahighi *et al.*, 2009; Ivins *et al.*, 2009) or linear chains of ubiquitin (Kensche *et al.*, 2012; Ngadjeua *et al.*, 2013), facilitated by the NEMO LZ and NOA domain (Chiaravalli *et al.*, 2011; Laplantine *et al.*, 2009).

That NEMO plays in important role in NF-κB signalling is also evidenced by clinical reports of male embryonic death in the absence of the NEMO gene (Scheuerle and Ursini, 1993), with similar result recorded for NEMO deficient mice (Rudolph *et al.*, 2000; Tanaka *et al.*, 1999; Q. Li *et al.*, 1999). Surviving females with NEMO mutations exhibit neurological and immune conditions (Fusco *et al.*, 2008; Hadj-Rabia *et al.*, 2003).

It is clear from these findings that the role of scaffold protein for NEMO is an unsatisfactory definition and requires a better investigated. Here we aim to answer if the presence of NEMO leads to changes in the kinetics of the IKKβ: IκBα interaction. To our knowledge, this is the first study to attempt this, and also the first study to determine the kinetics of IκBα phosphorylation by IKKβ through the use of isothermal titration calorimetry.

Previous studied have employed radiolabelled IκBα peptides (Huynh *et al.*, 2000) or radioisotope labelled γ-ATP analysed by immunoprecipitation/gel electrophoresis to quantify the amount of phosphorylation present (Heilker *et al.*, 1999). Although informative, these studies do not take into account the role of NEMO in mediating this interaction. Similarly, issues with detection and loss of signal during the washing steps pose concerns about the reliability and accuracy of these techniques (Ma *et al.*, 2008).

Isothermal titration calorimetry (ITC), a technique often used to study molecular binding (Duff, Jr. *et al.*, 2011), has more recently been demonstrated as an alternative for enzyme assays (Mazzei *et al.*, 2014). ITC does not require any labelling of ATP or substrate, which removes concerns about labelling interfering with protein function, or loss of signal due to detection sensitivity. The principle of ITC is to measure the amount of heat released or absorbed during chemical reactions. For the study of enzyme kinetics, two ITC methods are available: single injection or multiple injections (Atri *et al.*, 2015; Mazzei *et al.*, 2014). Both methods function by titrating the substrate into the enzyme (or mixture of enzyme plus molecule(s) of interest) and recording the heat flow; this can be used to directly calculate the reaction rate (Morin and Freire, 1991; Freyer and Lewis, 2008; Lonhienne *et al.*, 2001). For the multiple injection method, an additional measurement is carried out to determine the enthalpy of the reaction needed to calculate the final rate (Mazzei *et al.*, 2014; Rana *et al.*, 2016; Transtrum *et al.*, 2015). ITC offers the best option to answer fundamental questions about the role of NEMO in mediating the phosphorylation of IκBα by IKKβ.

The phosphorylation of the NF-κB inhibitor protein IκBα by the IKKβ enzyme is a critical step in ensuring activation of the NF-κB signalling pathway in response to specific stimuli (T. D. Gilmore, 2006). Phosphorylation is an important cellular process, as it is the basis of many crucial survival-associated responses, including: cell differentiation (Van Hoof *et al.*, 2009), cell signalling (Ardito *et al.*, 2017), control of metabolism (Humphrey *et al.*, 2015) and apoptotic responses (Niemi and MacKeigan, 2013), as well as vital for the proper functioning of the immune (Swamy *et al.*, 2016) and nervous systems (Sweatt, 2001), and even used in therapeutic formulations for cancer treatment and detection (Nayak *et al.*, 2018). Studies estimate that approximately 30% of all proteins undergo phosphorylation (Hunter, 1995), this reversible process whereby a phosphate group (PO_4) is added to specific proteins residues (usually aromatic amino acids) by specific proteins known as kinases (Burnett and Kenedy, 1954; Tan, 2011; Ardito *et al.*, 2017). In eukaryotes, Serine residues are most commonly phosphorylated (~79 %), followed by threonine (~17 %), and tyrosine (~4%) (Olsen *et al.*, 2006). The relatively high number of phosphorylated proteins is thought to be due to phosphorylation being a reversible process that has been shown to induce

modulate the structure, function, and localisation of proteins (Johnson and Barford, 1993; Jenal and Galperin, 2009; Nishi *et al.*, 2011; Bononi *et al.*, 2011; Hunter, 2012), and in some cases even promote disorder⇔order switches in protein conformations (Antz *et al.*, 1999; Collins *et al.*, 2008).

Uncontrolled canonical NF-κB activation has been linked to a number of medical conditions, including various types of cancer (Jost *et al.*, 2007; Zhou *et al.*, 2015; Nakagawa and Rathinam, 2018). Thus, understanding the phosphorylation of IκBα is important for the development of better therapeutic agents and disease markers for NF-κB associated conditions. Figures 38-42 present the phosphorylation data for IκBα by the IKKβ enzyme as determined by ITC. Herein we set to better understand the role NEMO plays in mediating the interaction between the IKKβ enzyme and a peptide mimic of the inhibitor IκBα, and thus better characterise the role of NEMO as NF-κB essential modulator.

Materials and Methods

***Protein expression and purification*.** Full-length human NEMO was expressed and purified as previously described (Catici *et al.*, 2015). NEMO expression plasmid was purchased from Addgene (catalog no. 11966), containing the full-length human IKKγ (NEMO) gene also containing a N-terminal His6 tag incorporated onto a pET28a expression vector. *Escherichia coli* BL21 T7 Express cells (New England Biolabs, catalog no. C25661) were used for plasmid transformation. Protein expression was induced using 0.5mM Isopropyl β-D-1-thiogalactopyranoside (IPTG) at 25 °C for 12hrs. NEMO was purified from lysed cells using nickel affinity chromatography (HisTrap FF crude 1ml column) in the presence of 1mM adenosine triphosphate (ATP). Purified protein was dialysed in 50 mM Tris/Cl pH 8.0, 50 mM NaCl, and 5 mM TCEP. NEMO was previously purified using 5 mM DTT instead (Catici *et al.*, 2015), but this reducing agent is not compatible with the use of ITC due its oxidation and subsequent ring-closing which gives rise to artificial baseline signal until the reduced state is no longer formed (Salim and Feig, 2009). In order to avoid this, TCEP was used instead.

Recombinant full-length constitutively active IKKβ enzyme was purchased from MRC PPU Reagents Dundee (catalogue no. DU316). All IκBα peptides were purchased from GenScript, purity level >95% (seq: LDDRHDSGLDSMKDEEY). Linear polyubiquitin chains

were purchased from Enzo Life Sciences (catalogue no. BML-UW0825-0001). All samples were dialysed and subsequent ITC measurements were all carried out in the following buffer system: 50 mM KCl, 2 mM MgCl2 ,2 mM MnCl2 ,10 mM NaF, 25 mM Hepes buffer, 1 mM TCEP, pH. 7.6. It is advised to keep concentration of reducing agents ≤ 1mM when performing calorimetry measurements (Keeler *et al.*, 2013).

Isothermal titration calorimetry. Measurement were recorded at 20 °C on a MicroCal VP-ITC isothermal titration calorimeter (Malvern Panalytical). All samples were degassed by vacuum aspiration for approximately 10 minutes prior to loading. Reference cell was regularly cleaned, with water solution replaced every two weeks. Enzymatic experiments were set up as follows: first, a simple kinetic experiment was performed (M1 experiment), where one concentration of IκBα (39µM) was titrated into a solution of either IKKβ (30nM) or IKKβ (30nM):NEMO (1µM) in order to calculate the enthalpy (Δ*H*) of total substrate conversion. A total of three replicate injection of 39 µM IκBα (with 1200s spacing in between each) were performed and the substrate conversion reaction was deemed complete upon a complete return of the baseline to the initial pre-injection levels.

Secondly, a more complex experiment (M2 experiment) was set up, where increasing concentrations of IκBα (0µM-800µM) were titrated into the sample cell either loaded with IKKβ (30nM) or IKKβ (30nM):NEMO (1µM). The injection set-up was as follows:

Table 3. Isothermal titration calorimetry experimental set-up for IκBα turnover measurements (M2 experiment).

Injection	Concentration of IκBα (μM)	Spacing in between each injection (s)
1	2.78	400
2	5.57	400
3	11.12	600
4	16.68	600
5	30.52	600
6	52.57	800
7	79.95	800
8	120.67	1000
9	187.56	1000
10	292.06	1200
11	418.32	1200
12	563.44	1400
13	746.07	1400

For M1 experiments, an average Δ*H* was calculated using the method described previously (Mazzei *et al.*, 2014):

$$\boldsymbol{\Delta H = \frac{\int_{t=0}^{\infty} \frac{dQ}{dt}\, dt}{V[S]_{t=0}}} \qquad [\boldsymbol{eq.18}]$$

where, $\frac{dQ}{dt}$ is heat flow measured at each substrate concentration (essentially the area under the curve for each M1 injection), V is the volume of the sample cells (expressed in L), and $[S]$ is the concentration of IκBα injection (expressed in μM). The Δ*H* obtained from M1 experiment was used to calculate the enzyme rate from the M2 experiment, by fitting the data to the following equation [Eq.19]:

$$\boldsymbol{v = \frac{dP}{dt} = \frac{1}{V * \Delta H} * \frac{dQ}{dt}} \qquad [\boldsymbol{eq.19}]$$

where, *v* is the rate of the reaction, $\frac{dP}{dt}$ is the product formation with respect to time, *V* is the volume (expressed in L), *ΔH* is the enthalpy as calculated from M1 experiment, and $\frac{dQ}{dt}$ is heat flow measured at each substrate concentration. The term $\frac{dQ}{dt}$ relates to the differences in the baseline after each injection: as the baseline change directly reports on the kinetic reactions recorder, $\frac{dQ}{dt}$ is the difference between the baseline recorded after each new injection and the initial baseline level at the start of each injection.

Essentially, using ITC to measure enzyme kinetics using the multiple-injection methods requires first determining the enthalpy - Δ*H* - for the complete substrate conversion (M1 experiment) and determination of the thermal power - $\frac{dQ}{dt}$ - variation from the continuous conversion of substrate to product (M2 experiment). The amount of heat observed during catalysis (d*Q*) is equal to the number of moles of product produced times the enthalpy of the reaction (Mazzei *et al.*, 2014; Rana *et al.*, 2016).

RESULTS & DISCUSSION

For each experiment, the corresponding control thermogram was subtracted to give thermograms de-convolved of background signals. To achieve this, we used a control 'reaction' where the serine residues in the IκBα were both mutated to alanine, rendering the peptide non-phosphorylatable (S32A and S36A). The control thermograms are shown in Figure 38. These data show a return to baseline that is non-zero both in the absence and presence of NEMO and, crucially, with the variant IκBα (IκBα$_{S32A,S36A}$). Since IκBα$_{S32A,S36A}$ does not contain any threonine residues, potentially the data in Figure 38 might reflect a background of phosphorylation of tyrosine residues (one tyrosine residue present in the control IκBα). Indeed, tyrosine phosphorylation of IκBα has previously been reported (Fan *et al.*, 2003; Gallagher *et al.*, 2007; Cullen *et al.*, 2015), but not part of the canonical or alternative NF-κB signalling. Activation of the NF-κB pathway through phosphorylation of Tyr42 is poorly defined and involves the dissociation from NF-κB complexes (Béraud *et al.*, 1999). However, the phosphorylation rate of tyrosine residues on proteins is considerably lower compared to serine (<4% *vs* >79%) (Olsen *et al.*, 2006) and so Tyr

phosphorylation does not seem likely. That said, we are mindful that this could be a convolving factor in the observed background signal. A further potential convolving factor is phosphorylation of NEMO (Palkowitsch *et al.*, 2008; Prajapati and Gaynor, 2002) or IKKβ (Shambharkar *et al.*, 2007; Delhase *et al.*, 1999). We consider these possibilities in more detail below.

NEMO is a protein capable of undergoing conformational change upon binding to various ligands (Catici *et al.*, 2015; Catici *et al.*, 2016; Hauenstein *et al.*, 2017), and the thermal fluctuations observed in the control experiment with NEMO in Figure 38 may reflect conformational change of NEMO upon binding to IKKβ.

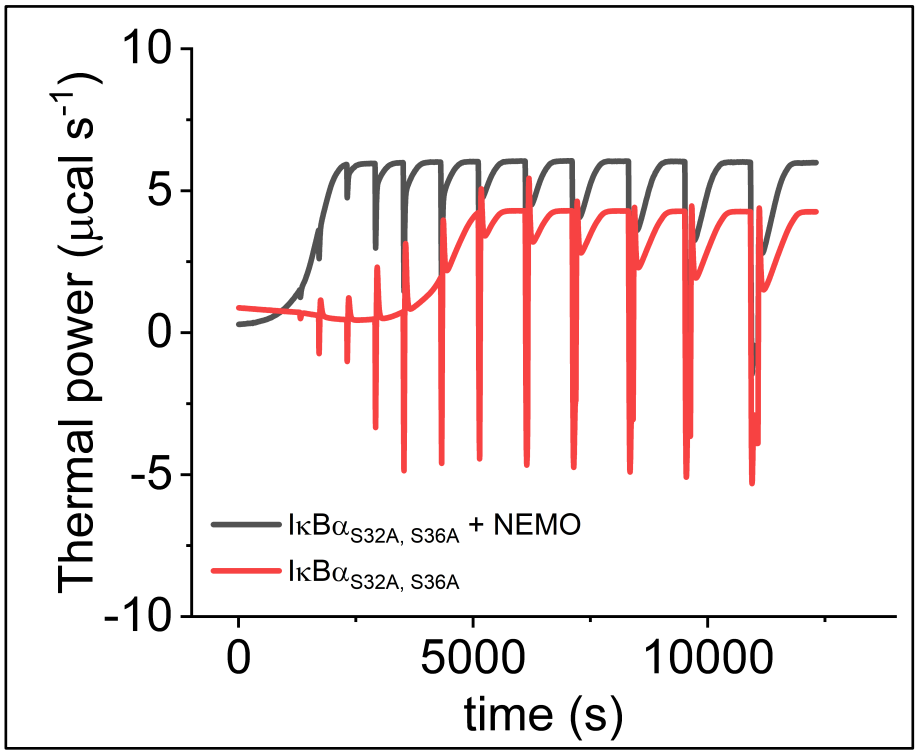

Figure 38. Thermal power recorded for control experiments as measured by isothermal titration calorimetry. All measurements were carried out in the presence of 1 mM ATP, 20 °C and with IκBα double serine mutant ($IκBα_{S32A,S36A}$). Shown in red is the corresponding experiment for titration of $IκBα_{S32A,S36A}$ (0-800 µM) into a solution of 30 nM IKKβ . Shown in grey is the corresponding experiment for titration of $IκBα_{S32A,S36A}$ (0-800 µM) into a solution of 30 nM IKKβ and 1 µM NEMO. Each peak (positive and negative) corresponds to an injection of IκBα set at specific times and concentrations. See Table 3 for detailed experimental set-up. The data are averages of n=3 biological replicates.

We have previously demonstrated that a peptide mimic of IKKβ is capable of inducing a NEMO conformational change whereby the degree of flexibility in the protein has increased (Catici *et al.*, 2016), which could contribute to the thermal fluctuations observed in Figure 38. However, these could also be due to IKKβ undergoing conformational change upon binding to NEMO. A model for activation of IKKβ through interactions with NEMO has previously been proposed but is poorly understood. Potentially binding of NEMO induces a conformational change in IKKβ whereby it promotes the binding of substrate (IκBα) (Schröfelbauer *et al.*, 2012). We consider the information content of the thermograms, related to protein conformational change in more detail below.

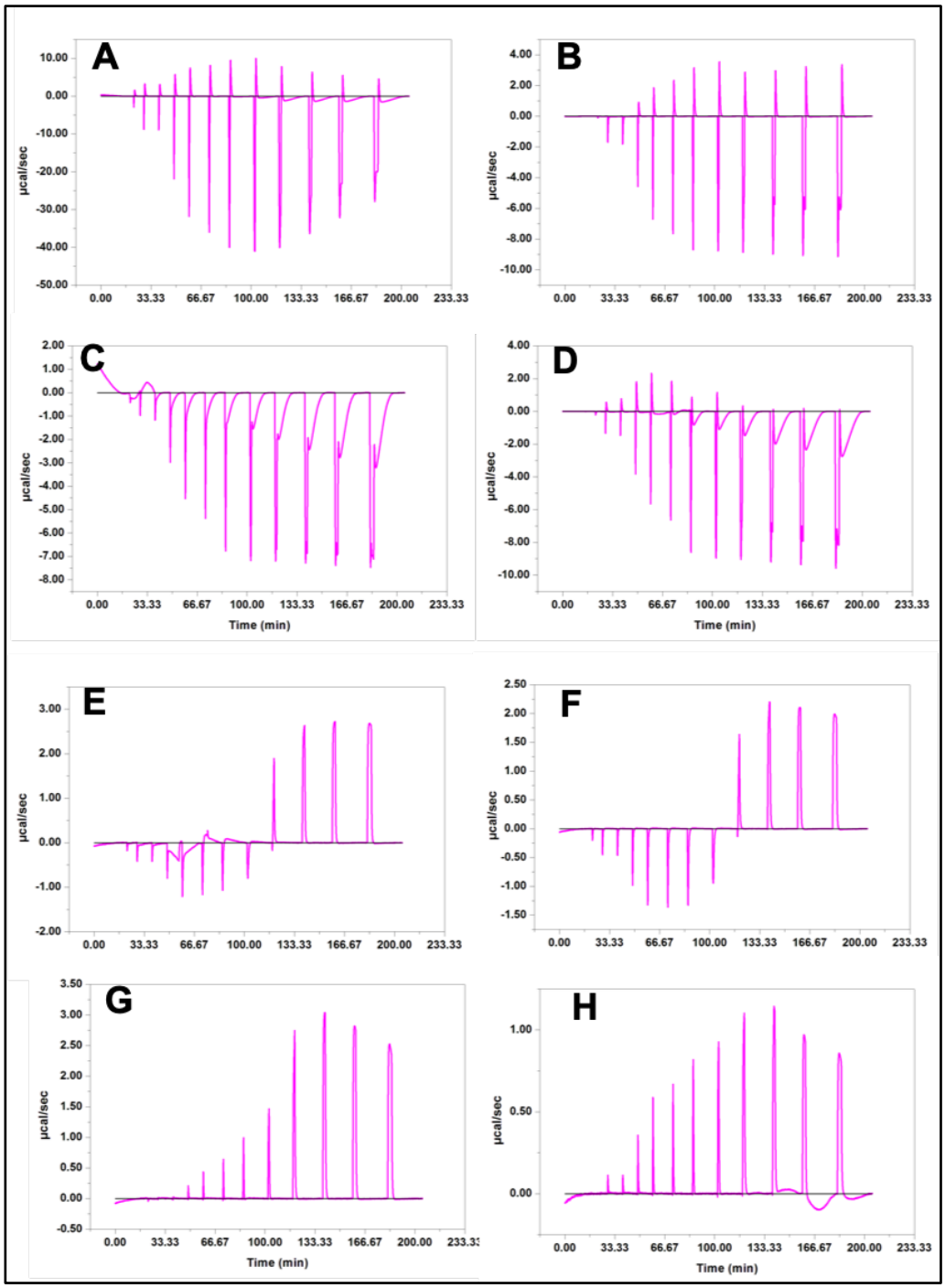

Figure 39. Thermal power recorded for all IκBα phosphorylation experiments as measured by isothermal titration calorimetry. All conditions were tested in presence of 1µM NEMO, 1mM ATP, 30 nM IKKβ**.** A, **IκBα with NEMO.** B, **IκBα no NEMO.** C, **IκBα$_{S32A,S36A}$ variant with NEMO.** D, **IκBα$_{S32A,S36A}$ variant no NEMO.** E, **IκBα$_{S32A}$ NEMO.** F, **IκBα$_{S36A}$ no NEMO.** G, **IκBα$_{S36A}$ with NEMO.** H, **IκBα$_{S36A}$ no NEMO. All data are averages of n=3 biological replicates. For each condition the baseline shifts have been minimised in order to understand the origin of the positive and negative peaks observed in the kinetic experiments. This was done using the "Create final ITC figure" feature on the OriginMicroCal software, which creates a zeroed baseline for each thermogram without altering the peaks.**

The use of ITC to monitor IKKβ enzyme turnover also affords further information relating to the thermodynamic changes accompanying turnover, represented by the heat spikes separating the injection and the return to baseline. Specifically, one can extract information on the magnitude and sign (exothermic/endothermic) of these heat spikes by integrating the individual peaks. Figure 39 shows the baseline corrected thermograms for each of the experimental conditions above (black line). That is, we remove the information that allows the calculation of the observed rate to focus on the changes in the heat spikes of the thermograms.

Figure 39A-H shows the baseline corrected thermograms for all experiments, including controls. These thermograms are dominated by negative spikes intervening the return to baseline, with some positive spikes at low IκBα$_{S32A,S36A}$ concentrations. In the presence of the IκBα peptide with both serines present (Figure 39A and Figure 39B; with and without NEMO, respectively) one now observes positive heat spikes at all concentrations of IκBα. These data suggest that phosphorylation of the serines manifests as positive heat spikes intervening the return to baseline. Figures 39E-H confirm this, showing positive heat spikes at high concentration of the single serine variants, IκBα$_{S36A}$ (Figure 39E and Figure 39F; IκBα$_{S36A}$ with and without NEMO, respectively) and IκBα$_{S32A}$ (Figure 39G and Figure 39H; IκBα$_{S32A}$ with and without NEMO, respectively. Indeed, with IκBα$_{S36A}$ no negative heat spikes are observed at all, implying that the positive heat spikes are offsetting the negative heat spikes observed in the control experiments (Figure 39C-D). Given that the phosphorylation events appear to manifest positive heat spikes, and that our control experiments show predominately negative heat spikes, it seems unlikely that the background signal we observe in Figure 38 is attributable to Tyr phosphorylation on IκBα or Ser phosphorylation on either IKKβ or NEMO.

Given that the thermograms (Figure 39) suggest that our background signal is not chemical turnover, we consider that part of the signal may be attributable to protein conformational change associated with IκBα binding. Indeed, a number of studies have demonstrated that NEMO undergoes ligand (Catici *et al.*, 2015; Hauenstein *et al.*, 2017) and environment induced conformational change (also Chapter 3 and 4 in this

thesis). These data therefore suggest that the observed kinetic arising from our ITC studies, whilst dominantly convolved of chemical turnover associated with phosphorylation of IκBα serines, may well also be convolved of conformational change associated with IκBα binding to IKKβ and or NEMO. Without a more detailed kinetic study we cannot confidently assert whether putative conformational changes are kinetically coupled to chemical turnover.

Regardless of the precise origin of the background thermograms, these control experiments allow us to capture turnover of IKKβ, de-convolved from this background signal. Additionally, Figure 47 shows the baseline shifts characteristic of the product formation during enzyme turnover when analysed by ITC (Figure 47A and 47B). These show the baseline shift recorder during phosphorylation of IκBα by IKKβ, both in the presence and absence of NEMO. As previously demonstrated, these are indicative of stead-state kinetics and enzyme turnover (Lonhienne *et al.*, 2001; Freyer and Lewis, 2008), and are absent in the data where no phosphorylation of IκBα is observed (such as in the control experiment for $IκBα_{S32A,S36A}$ (Figure 47C). The results from Figure 47 combined with the preliminary results from LC-MS analysis of the phosphorylation of IκBα, we are confident that we are capturing the kinetics of IKKβ: IκBα using ITC.

The concentration dependence of IκBα *versus* the observed rate from our ITC assay is shown in Figures 40-42 and the data extracting from fitting is given in Table 4. In the absence of NEMO (red data set), turnover appears to follow a sigmoidal relationship with respect to substrate concentration. These data therefore imply non-Michaelis-Menten type turnover, most likely suggesting cooperativity.

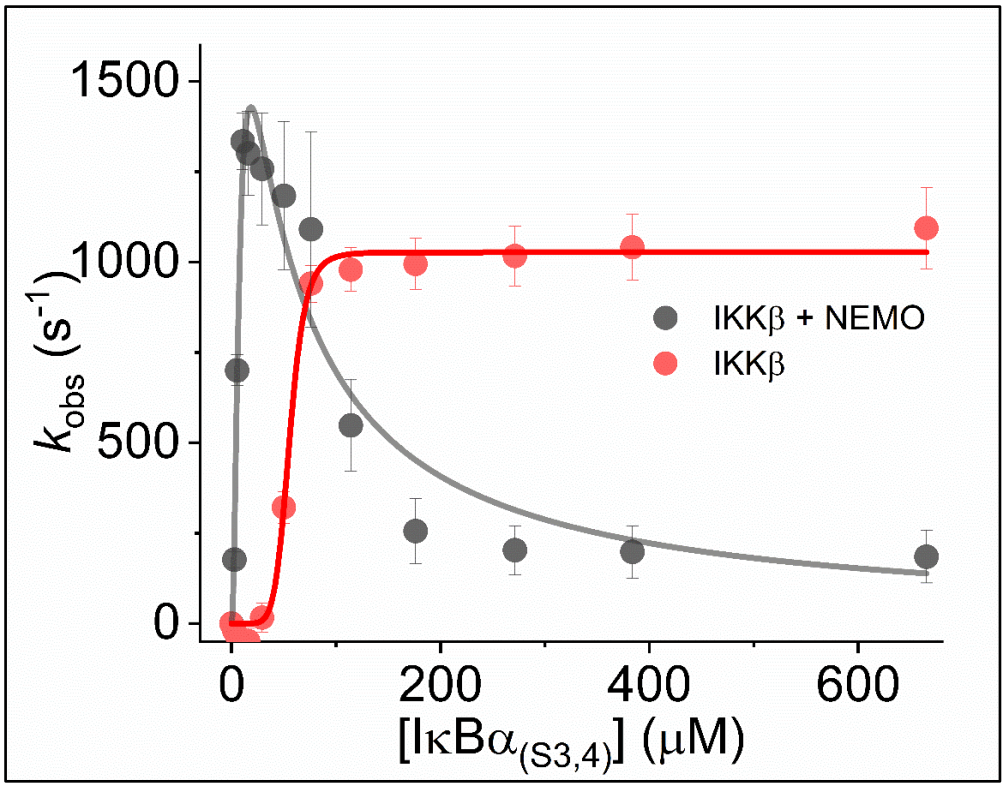

Figure 40. Phosphorylation of IκBα by IKKβ in the presence and absence of NEMO as measured by isothermal titration calorimetry. All measurements were carried out at 20 °C and with 1mM ATP. Shown in red is the corresponding experiment for the phosphorylation of IκBα$_{S32,S36}$ (0-800 μM) into a solution of 30 nM IKKβ . Shown in grey is the corresponding experiment for phosphorylation of IκBα$_{S32,S36}$ (0-800 μM) into a solution of 30 nM IKKβ and 1 μM NEMO. The data in the absence of NEMO are fit to equation 20 are shown in red, and the data for phosphorylation in presence of NEMO fit to equation 21 are shown in grey. Solid lines are the fits to Eq 20 and Eq 21. All data are averages of n=3 biological replicates.

$$v = \frac{k_{cat}[E]_0[S]^n}{K_M + [S]^n} \qquad [eq.\,20]$$

where , *n* is essentially the Hill number, reflecting the degree of cooperativity and, under some scenarios, the number of species involved in the cooperative interaction.

In the presence of NEMO, there is a similar sigmoidal relationship, but now also apparent inhibition at higher substrate concentrations, potentially reflecting substrate inhibition. This is a complex kinetic scheme; cooperativity and putative substrate inhibition, and can be modelled,

$$v = \frac{k_{cat}[E]_0[S]^n}{K_m^n + [S]^n + \left(\frac{1+[S]^n}{K_i}\right)} \qquad [eq.21]$$

Where, K_i reflects the inhibition constant, putatively for the substrate. We note such a relationship is not uncommon, for example as typified by aspartate transcarbamylase (LiCata and Allewell, 1997). The data resulting from the fits to Eq.210and Eq.21 (shown in Figure 40) are given in Table 4.

Table 4. Results of fitting data shown in Figures 40-42 for IκBα phosphorylation to Eq.20 and Eq.21.

	k_{cat} (s^{-1})	K_M (μM)	n	K_i (μM)
IκBα	1027.2 ± 17.6	55.62 ± 1.4	7.4 ± 1.2	-
IκBα + NEMO	2443.3± 895.0	8.71 ± 3.9	1.8 ± 0.6	40.0 ± 23.2
$IκBα_{S32}$	881.9 ± 20.0	53.53 ± 3.4	12.8 ± 11.8	-
$IκBα_{S36}$	863.3 ± 22.7	53.0 ± 7.9	15.5 ± 40.0	-
$IκBα_{S32}$+NEMO	1246.3 ± 16.9	5.1 ± 0.2	3.5 ± 0.4	>5000
$IκBα_{S36}$+NEMO	1454.1 ± 16.9	5.10 ± 0.1	3.5 ± 0.3	>5000

From Figure 40 and Table 4, The calculated k_{cat} values in the presence and absence of NEMO shows some difference, with k_{cat} showing a ~2-fold increase in the presence of NEMO 1027.2 ± 17.6 s^{-1}, compared to 2443.3 ± 895.0 s^{-1} in the absence. These data suggest that the addition of NEMO increases the phosphorylation rate of the IκBα peptide. Previous studies report much smaller values for rate of IκBα phosphorylation, ranging from 3.7 x 10^{-2} s^{-1} (Heilker *et al.*, 1999) to 18 s^{-1} (Li *et al.*, 1998). The differences in these values might be explained by the low ATP values used in previous studies, 50 μM (Heilker *et al.*, 1999) and 1.3 μM (Li *et al.*, 1998), suggesting the observed rate might not be saturated in these studies. It has been reported that ATP depletion can affect the rate of phosphorylation, with de-phosphorylation observed in other protein system upon depletion of ATP (Sturani *et al.*, 1988). It is precisely for this

reason we use a relatively high concentration of ATP (1 mM). Similarly, the differences in the rates observed may also be due to the sensitivity of the detection method used. Previous studies have relied on autoradiography and used very low concentration of peptide 0.5-8 μM substrate (Heilker *et al.*, 1999), compared to the values presented in Table 4, ranging from 2.7 -746 μM. ITC is a highly sensitive method, offering direct measurement of the kinetic reaction studied, especially compared to autoradiography methods, which report on the kinetic parameters indirectly and have poor sensitivity.

Despite the differences in reported rate constants, previous studies are in agreement with our findings, also reporting an increase in the rate of phosphorylation under conditions where NF-κB proteins are present during the phosphorylation reaction; their reported values show a 5-fold increase in the phosphorylation rate (Zandi *et al.*, 1998), whereas we observe a two-fold increase in the rate, as discussed above. We note that NEMO and the NF-κB proteins are distinct, but it is of interest that both appear to increase the rate of IKKβ turnover. The increase in k_{cat} upon addition of NF-κB proteins has been suggested to arise from stabilisation of the IKKβ: IκBα interaction, which would also allow for a more efficient phosphorylation reaction. We propose that NEMO behaves similarly in ensuring the formation of a more stable IKKβ: IκBα complex. Studies exploring the half-life of cytoplasmic IκBα report that in stimulated cells, IκBα is rapidly degraded, with unstimulated cells showing a three orders of magnitude decrease in the degradation of IκBα (O'Dea *et al.*, 2007). While our conditions studied using ITC do not take into account the presence of a NF-κB stimulus, the hallmark of such would be the presence of NEMO and its interaction with IKKβ, which we believe allows for a similar effect to be observed whilst also decreasing the complexity of the experimental conditions. Our results show a similar trend, with the rate of IκBα phosphorylation being much slower in the absence of NEMO (indirect mimic of 'unstimulated' cells).

From Table 4, there is a decrease in the $K_{m,}$ from K_M = 55.62 ± 1.40 μM in the absence of NEMO to K_M = 8.7 ± 3.9 when NEMO was present. Potentially the difference in K_m could be due to an increased affinity of IKKβ for IκBα in the presence of NEMO. However, without knowing the intrinsic rate constants for the 'on' and 'off' rate of

ligand binding, this interpretation should be treated extremely cautiously. That said, previous studies report the K_M for the IKKβ: IκBα complex to also increase in the presence of NF-κB proteins, from 2.2 μM → 1.4 μM (Zandi *et al.*, 1998).

The data in Figure 40 show a kinetic scheme for IKKβ:IκBα interactions, with apparent cooperativity both in the presence and absence of NEMO. The value of *n* is increased in the absence of NEMO and decreases in the presence of NEMO, *n* = 7.4 ± 1.2 and 1.8 ± 0.6, respectively. At a simple level, evidence for cooperativity might suggest a cooperative relationship between IκBα or cooperativity for each of the two serine residues present on a single IκBα peptide (inter / intra-peptide cooperativity). Potentially, the magnitude of *n* can be used to infer the number of species involved in the cooperative interaction. The number increased in the absence of NEMO and it is difficult to construct a realistic model where 7/8 species are involved. In the presence of NEMO *n* ~ 2 and this might further suggest the origin of the putative cooperativity is based on the two available serines on IκBα or two monomers the IκBα peptide.

The most striking difference between the kinetic data in the presence/absence of NEMO is that in the presence of NEMO there is apparent substrate inhibition, or at least the data fit to a model that includes an inhibitory affect with increasing substrate concentration. The extracted K_i value only shows ~4 times increase compared to the K_m, K_i = 40.0 ± 23.2 and K_m = 8.7 ± 3.9, respectively. This leads to a relatively 'sharp' concentration dependence on k_{obs}, where the maximal observed rate is restricted to a relatively small window of IκBα concentrations (Figure 40). It is tempting to speculate that this 'restriction of function' of IKKβ by NEMO might be an important biologically relevant control mechanism and we discuss this further below.

Given the potential for kinetic complexity arising from the phosphorylation of S32 and S36 on the IκBα peptide, and in the context of the putative cooperativity observed in the kinetic plots (as above), the turnover with single serine variant IκBα was explored in the presence and absence of NEMO, shown in Figures 41 and 42, respectively. The resulting data from the fits is given in Table 4. The peptides, $IκBα_{S36A}$ and $IκBα_{S32A}$ are single serine to alanine mutants, S36A and S32A, respectively. We note that previous

studies have reported phosphorylation of S32 of IκBα by IKKβ to proceed at 3.7 x 10^{-2} s^{-1}, in the presence of 50 µM ATP, with K_M 1.7 ± 0.6 µM (Heilker *et al.*, 1999).

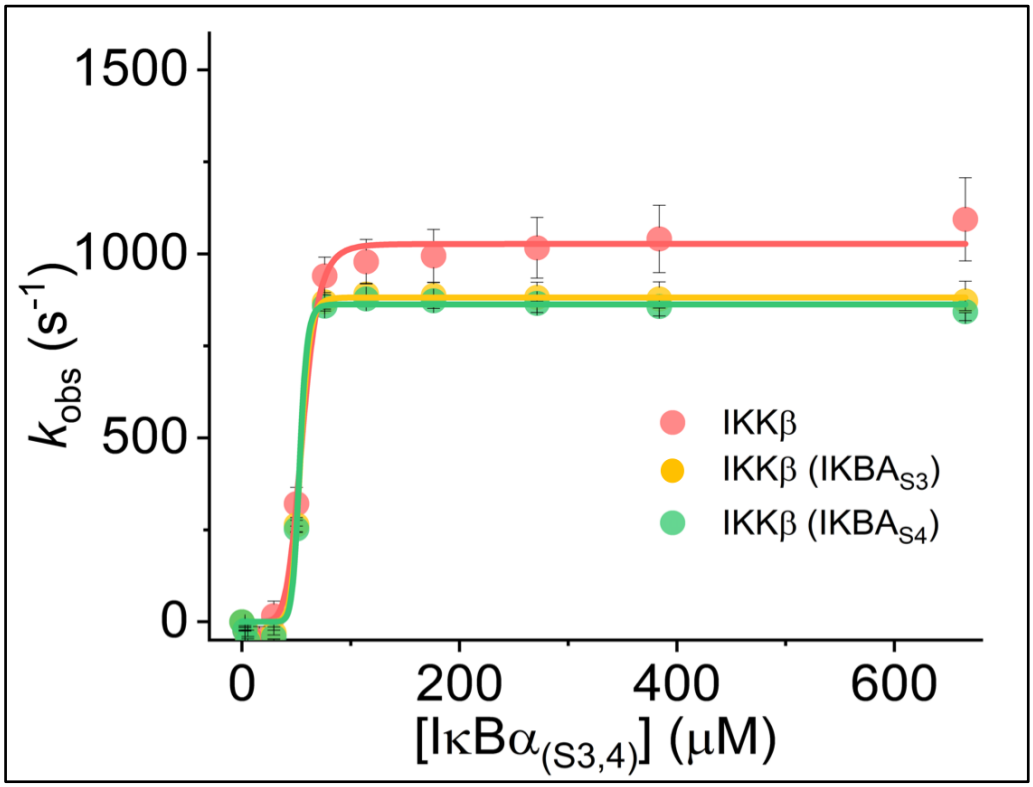

Figure 41. Phosphorylation of IκBα peptides by IKKβ in absence of NEMO as measured by isothermal titration calorimetry. All measurements were carried out at 20 °C and with 1mM ATP. Shown in red is the corresponding experiment for phosphorylation of IκBα$_{S32,S36}$ (0-800 µM) by 30 nM IKKβ. Shown in red is the corresponding experiment for the phosphorylation of IκBα$_{S32,S36}$ (0-800 µM) by 30 nM IKKβ. The phosphorylation of IκBα$_{S32A}$ and IκBα$_{S36A}$ by 30 nM IKKβ in presence of 1 µM NEMO in shown in yellow and green, respectively. The solid lines are the fits to Eq.20. All data are averages of n=3 biological replicates. The data for phosphorylation of IκBα$_{S32,S36}$ (red dataset) is the data presented in Figure 39 but superimposed onto the traces obtained from phosphorylation of single serine phosphorylation of IκBα peptides to emphasize the similarity in the overall trend observed.

We note that our calculated k_{cat} is much higher (1027.2 ± 17.6 s^{-1}) compared to previous studies (3.7 x 10^{-2} s^{-1} and 18 s^{-1}) and believe this is due to the detection methods used and potentially the rather higher concentration of ATP as described above. Moreover, Heilker *et al* have calculated the value of k_{cat} based on association and dissociation data obtained from surface plasmon resonance studies (Heilker *et al.*, 1999) and not directly as we have though ITC.

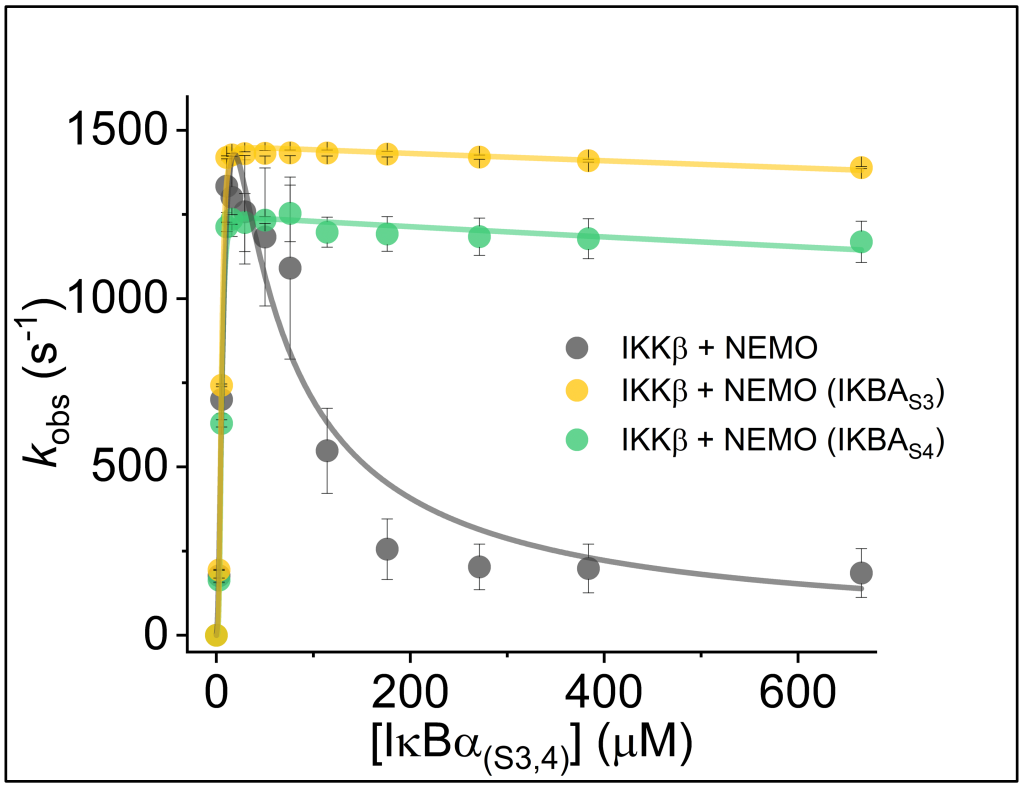

Figure 42. Phosphorylation of IκBα peptides by IKKβ in presence of NEMO as measured by isothermal titration calorimetry. All measurements were carried out at 20 °C and with 1mM ATP. Shown in grey is the corresponding experiment for phosphorylation of IκBα$_{S32,S36}$ (0-800 μM) by 30 nM IKKβ in the presence of In yellow and green The phosphorylation of IκBα$_{S32A}$ and IκBα$_{S36A}$ by 30 nM IKKβ in presence of 1 μM NEMO in shown in yellow and green, respectively. The solid lines are fits to Eq. 20 for IκBα$_{S32,S36}$ phosphorylation, and Eq.21 for IκBα$_{S32A}$ and IκBα$_{S36A}$. All data are averages of n=3 biological replicates. The data for phosphorylation of IκBα$_{S32,S36}$ (grey dataset) is the data presented in Figure 39 but superimposed onto the traces obtained from phosphorylation of single serine phosphorylation of IκBα peptides to emphasize the differences in the overall trend observed between the peptides tested.

From Figure 41 and 42 and Table 4 we find that the serine deletion variants of IκBα show a decrease in the extracted k_{cat} values both in the presence and absence of NEMO. In the absence of NEMO, the decrease is relatively small, being 881.93 ± 20.01 μM s^{-1} for IκBα$_{S3}$ and 863.20 ± 22.69 μM s^{-1} for IκBα$_{S4}$, compared to 1027.21 ± 17.56 μM s^{-1} for IκBα peptide. However, when NEMO is added, k_{cat} =1246.3 ± 16.9 s^{-1} for IκBα$_{S3}$ and k_{cat} = 1454.1 ± 16.9 s^{-1} for IκBα$_{S4}$ compared to k_{cat} =2443.3 ± 895.0 s^{-1} for the two Ser IκBα in the presence of NEMO. Despite these differences in calculated k_{cat}, we find there is no difference within error for the K_m values in the presence and absence of NEMO.

Above, we hypothesised that the putative cooperativity observed both in the absence and presence of NEMO might arise due to the presence of two phosphorylatable serines on the IκBα peptide, with the first phosphorylation potentially enhancing the propensity for phosphorylation of the next serine. From Table 4, the magnitude of *n* increases (approximately doubles) both in absence and presence of NEMO for single serine peptides. However, we note the error values in the absence of NEMO for single serine peptides potentially make this trend difficult to interpret. In the presence of NEMO, the magnitude of *n* approximately doubles *outside* of calculated error, suggesting this finding is *bone fide*. These data therefore suggest that the presence of only a single phosphorylatable serine *increases* the degree of cooperativity. It therefore does not appear likely that the observed cooperative relationships are attributable to intra-peptide cooperativity arising from different phosphorylatable serines on the same peptide, but more likely, inter-peptide cooperativity, where cooperativity arises from individual IκBα monomers. Cooperativity is a common control mechanism that ensures a specific dose-response relationship and one could easily envisage that this might have a biological role in the context of NFKB signalling. We consider this in more detail below.

Finally, from Figures 42 and Table 4, we find that single serine variant IκBα peptides essentially ablate the putative substrate inhibition in the presence of NEMO. That is, the extracted K_i values increase (> 5 mM), essentially tending toward no effective substrate inhibition. These data suggest that the presence of multiple serines on IκBα induce substrate inhibition but only in the presence of NEMO. One of the potential functions of NEMO is to present the substrate (IκBα) to the enzyme (IKKβ). These data suggest that indeed NEMO does alter the geometry of IκBα relative to IKKβ, since the presence of NEMO induces substrate inhibition. Most likely this arises due to a non-(less) productive binding geometry between IκBα and IKKβ that becomes accessible in the presence of NEMO. As we discuss above, the presence of substrate inhibition has potential benefits in terms of control and regulation of IKKβ activity. Our hypothesis was that NEMO might enhance the interaction between IκBα and IKKβ, possibly increasing affinity. However, it appears that NEMO also may have a role in presenting

a non-productive geometry of IκBα and IKKβ, induces a further layer of regulatory control.

Conclusions.

NEMO is classically considered to function as a scaffold protein, with most reports suggesting a role in sub-cellular localisation of IKKβ. It is however intriguing that NEMO is able to bind both IKKβ, but also the substrate of IKKβ, IκBα. We hypothesised that NEMO might play an additional role in regulating the enzyme activity of IKKβ. Our study suggests that NEMO may alter the rate of IKKβ turnover somewhat (~2 fold), but in terms of a catalytic advantage this would seem relatively minimal. Instead we find the more major changes are in the equilibrium constants that govern the substrate interaction with IKKβ. Specifically, we find that the presence of NEMO 'tunes' the *K*m and induces substrate inhibition, such that the IKKβ enzyme operates in a relatively narrow window of IκBα concentrations. We suggest that this represents a regulation of IKKβ function at the level of substrate concentration. Such a model suggestion chimes well with the regulatory behaviour of very many enzymes involved in human metabolism and signalling. It is interesting to note that our data points to a role for conformational change (both ligand induced and NEMO mediated) within the control exerted by NEMO in activation of the NF-κB signalling pathway.

Post-paper discussion:

This study aimed to resolve the role NEMO in mediating the interaction between IKKβ and IκBα. While published reports characterise NEMO as a scaffold protein, we believe its role in activating the signalling pathway in response to canonical stimuli extends beyond this. This study is the first to report the inhibitory effect of NEMO on IκBα phosphorylation by the IKKβ enzyme, and points to NEMO controlling not only the activation of NF-κB signalling, as well as modulating the length of the response. This is potentially important for the development of therapeutics targeting the uncontrolled activation of NF-κB, which fail to take into account the role of NEMO.

Many previous attempts at characterising the IKKβ:IκBα interaction have been carried out using indirect phosphorylation detection methods. The results in Chapter 5 offer a new alternative through the use of ITC kinetic measurements. The main advantages consist of elimination of need to labelling or the use of coupled-assay, and the ability to continuously monitor the enzymatic reaction. However, this is to say that by no means ITC offers the best methods for this analysis. This study offers an excellent premise for future kinetic measurements, showing for the first time the kinetics of the IKKβ:IκBα in the presence of full-length IKKβ enzyme and NEMO. Future studies should aim to corroborate these findings with other assays, such as stopped- or continuous-flow assays, or even in-cell assays. The kinetics of TEM1 β-lactamase was monitored *in vivo* in HeLa cells using confocal microscopy, by using fluorogenic substrate and monitoring the product formation at a specific wavelength (Zotter *et al.*, 2017). This techniques potentially offers a better understanding of the cellular role of NEMO in mediating the IKKβ:IκBα interaction, seen as the intracellular milieu acts as an additional control to modulate NEMO structure and dynamics (Chapter 4).

Understanding the role of NEMO oligomerisation for IKKβ kinetics should also be the focus of future studies. NEMO oligomeric state is still a matter of active debate, with no clear understanding of the relationship between oligomeric state and cellular roles. Cys54 and Cys347 are required for intermolecular disulphide bond formation in NEMO (Herscovitch *et al.*, 2008); the effect disruption of these on the ability of NEMO mediate the IKKβ:IκBα interaction and kinetics should also be considered for a more in-

depth analysis. In addition, structural studies should be used alongside enzyme assays to better characterise the IKKβ:IκBα complex in association with NEMO. Recent advances in the field of cryo-electron microscopy allow for better a resolution of dynamic proteins (Bonomi *et al.*, 2018), and such a complete characterisation of the NEMO: IKKβ:IκBα using cryo-EM should be attempted in the future fir a comprehensive analysis of the mechanistic activation of the IKK complex, which to date has yet to be fully understood.

To validate the results from Chapter 5, a coupled enzyme assay should be carried out. As ATP is required for the kinetics of IKKβ, an assay measuring the consumption of ATP during phosphorylation of IκBα, as ATP is required for the kinetics of the phosphorylation reaction. Similarly, monitoring the kinetics of IKKβ can in theory also be achieved using chromatography methods coupled with mass-spectrometry, such as ion exchange chromatography or liquid chromatography coupled with MS. This technique offers increased sensitivity and is now frequently used to study enzyme kinetics (Winkler *et al.*, 2013; Perna *et al.*, 2018). However, many studies report that MS methods pose a series of limitation when used to detect and quantify peptide phosphorylation (Arnott *et al.*, 2003; Molina *et al.*, 2007). Specifically, phosphorylation may have an effect on the enzymatic digestion of peptides prior to MS analysis (Steen *et al.*, 2005). Similarly, phosphorylated and unphosphorylated peptides exhibit different ionisation efficiencies which may limit the comparison of measured ion currents for quantification of phosphorylation (Wu *et al.*, 2018).

We have previously attempted to detect phosphorylation of IκBα using LC-MS (See figure 43). However, we were only able to detect phosphorylation of the single serine peptides, and due to the limitations of LC-MS discussed above, no further measurements were attempted. However, with the development of new improvements to sample preparations and software analysis, LC-MS may offer an alternative to radiolabelled assays or western blotting to study the phosphorylation of IκBα and the kinetics of the IKKβ enzyme.

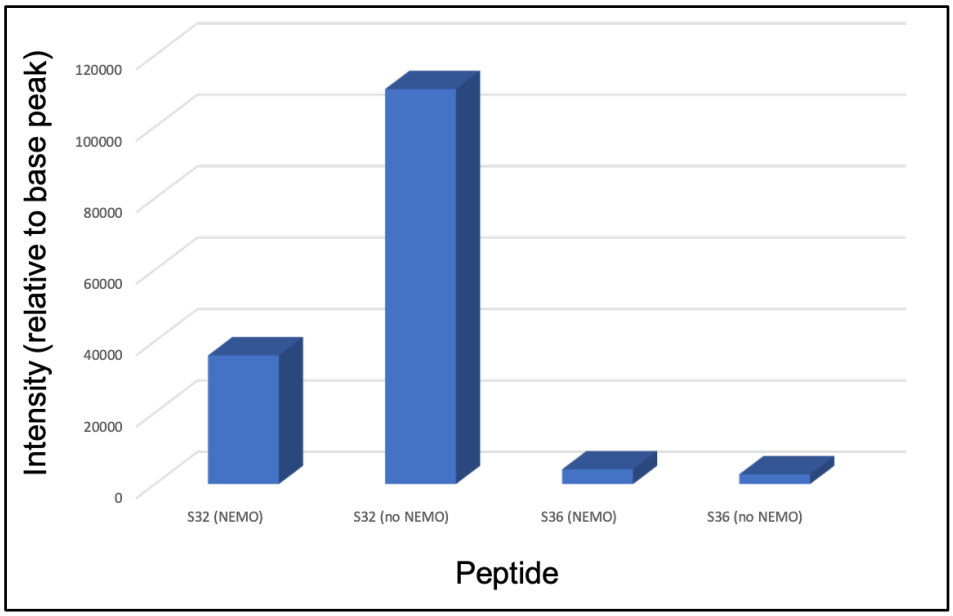

Figure 43. Preliminary LC-MS data for phosphorylation of IκBα by IKKβ. The data show the phosphorylation in the presence and absence of NEMO, and the intensity detected for the phosphorylation of single serines. No detection for the phosphorylation of the double serine IκBα was detected using LC-MS. The experimental setup was: 1 mM ATP, 30 nM IKKβ, 1 µM NEMO, 1 mM IκBα. The data are from one single measurement.

In summary, the results presented in Chapter 5 show align with the original aims of this PhD in better understanding the role of cytoplasmic NEMO in the activation of the NF-κB signalling pathway. The data presented here demonstrate the extensive scaffold role of NEMO in mediating the interaction between the IKKβ enzyme and its substrate IκBα, as well improving the kinetics of IκBα phosphorylation *in vitro*

.

Chapter 6: General Conclusions

This PhD project aimed to understand the effects of the biophysical factors governing the structure, function, and dynamics of the relevant human protein NEMO. Firstly, we established the use of an optical phenomenon known as Red edge excitation shift (REES) as a tool for monitoring and quantifying NEMO conformational change. Using intrinsic NEMO fluorescence (W6), we captured the protein conformational change in response to binding of NEMO different peptides, NDB and IκBα. Using REES, we were able to establish that the two binding events induced different NEMO conformational changes, suggesting NEMO functional regulation by ligand binding, as well offering evidence for the dynamic nature of the protein. Much debate still exists around the structure of NEMO, with some reports suggesting a more rigid NEMO conformation (Bagnéris *et al.*, 2015). A united view on the dynamic structure of NEMO is hopefully achievable in the near future. Improvements to more robust structural characterisation techniques such as SAXS or cry-EM microscopy are being carried out to allow for better sensitivity and incorporation of protein dynamics in the data analysis. The notion of NEMO existing as a dynamic molecule as proposed by our REES W6 data (Chapter 3), was recently also confirmed by different structural biology techniques and computational methods. Using SAXS the structure of NEMO has been shown to be undergo conformational change upon ligand binding (Hauenstein *et al.*, 2017), with the protein in general adopting a more dynamic conformation than the previously rigid structure (Bagnéris *et al.*, 2015). Similarly, our proposed mechanism for ubiquitin-induced NEMO conformational change potentially selecting for functional NEMO conformations has also been verified using SAXS (Hauenstein *et al.*, 2017). More recently, the flexibility of the NEMO N-terminal (W6 region) has also been validated using X-ray crystallography and MD simulations (Barczewski *et al.*, 2019). Here the authors report that NEMO exhibits a dynamic ligand binding interface and is capable of undergoing ligand-induced conformational change. The validation of the REES data presented in Chapter 3 using a number of structural techniques illustrates the sensitivity of the REES W6 probe and its application in understanding protein dynamics and conformational change without the need for labelling or extensive data refinement.

The effect of the intracellular milieu on protein dynamics and stability is slowly emerging as an important factor to consider in structural studies (Monteith *et al.*, 2015). The results presented in Chapter 4 describe the effect of the physical parameters of the intracellular environment on the structure and dynamics of NEMO. It was also important to compare free NEMO to ligand bound to understand whether the intracellular milieu exerted different effects on the free protein *vs* a functional NEMO conformation. The data show that the intracellular environment acts as an additional control for NEMO conformational change, with different cellular compartments either affecting the free or ligand bound protein. As a high proportion of NEMO is thought to be disordered (Catici *et al.*, 2015), awareness of the regulatory nature of the intracellular milieu is potentially essential in understanding the current lack of consensus of NEMO structure and function. Our results from Chapter 4 offer guidelines for future structural and functional studies, by describing in thermodynamics details the conditions that induce changes in the dynamics of the protein. These could potentially be important for future structural studies where protein stability is an issues, thus knowing which conditions induced less solvent exposure in the NEMO structure could prove beneficial for choosing appropriate buffer systems.

These findings are also important for studies looking to develop NEMO-based therapeutic targets, as they offer detailed description of *in vivo* conditions where the protein exists in more flexible, potentially more energetically favourable conformations. We understand the limitations that arise from using a mimic of the physical parameters of the intracellular environment. With improvements to whole cell methods (such as in cell-NMR), future studies should apply these to better understanding how the *in vivo* conditions influence the structure and dynamics of proteins (including NEMO) and improve *in vitro* methodologies to better mimic the effect of the intracellular environment. However, to date this is the first study to comprehensively describe the thermodynamics of NEMO conformational change in response to the intracellular environment, showing a potentially new regulatory role of the intracellular milieu on the dynamics and potentially function of NEMO.

This study also offer a comprehensive analysis of the role of NEMO in activating the NF-κB pathway, by specifically mediating the interaction between the IKKβ and its substrate, the inhibitor IκBα. Based on the result from Chapter 5, we propose that NEMO functions to ensure activation of the pathway through mediating the IKKβ:IκBα interactions, as well control the length of the response by acting as an inhibitor of the IKKβ enzyme. We acknowledge that these results require further validation using other enzyme assays, but they also offer a better understating on the role of cytoplasmic NEMO and the molecular basis of canonical NF-κB activation. To our knowledge, no other NEMO functional studies have reported on the potential inhibitory role of NEMO during NF-κB activation. However, the results from Chapter 5 could potentially help account for the lack of consensus on the characterisation of IKKβ kinetics, as no other reports have analysed the effect of NEMO on the IKKβ kinetics. Taking into account our data, we propose that the role of NEMO in the cytoplasm is not just a scaffold, but also an additional modulator of the phosphorylation of IκBα, controlling the activation of the NF-κB pathway, as well as the duration of the response. This is a potentially important notion to consider when designing therapeutics that target abnormal NF-κB activation, which ultimately results in a number of clinical conditions (Staudt, 2010; Nakagawa and Rathinam, 2018).

Based on the results from Chapters 3-5 we propose a new model for the dynamics and function of NEMO in the intracellular milieu, shown in Figure 44. The scaffold role, we believe is attributable to NEMO when the protein is located at the cell membrane or possibly when inside the nucleus. Although not analysed in this study, all evidence for NEMO presence at these locations points to NEMO functioning to facilitate protein interactions; at the cell membrane, ubiquitinated NEMO is believed to recruit IKKβ at the membrane to allow for it to be activated by its corresponding kinases (Wang *et al.*, 2001; Zhang *et al.*, 2014; Catici *et al.*, 2015). Is it also possible that NEMO functions as a scaffold in the cytoplasm, mediating the interactions between the functional IKK complex and their targets (as discussed in Chapter 5). The data for the role of NEMO inside the nucleus is scarce, but evidence suggests that it functions

to stabilise specific proteins, such as c-myc (Kim *et al.*, 2010). Other studies have confirmed the presence of NEMO in the nucleus where it is thought to competitively bind to cAMP-responsive element-binding protein-binding protein or CBP and block the interaction between other NF-κB proteins and CBP (Verma *et al.*, 2004).For example, IKKα association with CBP is essential in ensuring transcription of NF-κB genes during cytokine stimulation (Yamamoto *et al.*, 2003; Anest *et al.*, 2003).

Based on recently published NEMO findings and the results from Chapter 3-5, we proposed that depending on its subcellular localisation, NEMO is assigned different roles. A scaffold role at the cell membrane and nucleus, where the intracellular milieu affects ligand binding and induces a more 'flexible' conformation. Based on these, potentially NEMO functions to mediate specific interactions with other proteins and offers a stabilising role. A similar role may also be observed in the cytoplasm, where NEMO has also been shown to associate with the IKK complex and allow for its activation and subsequent activation of the NF-κB pathway signalling pathway. Here the intracellular milieu affects both ligand binding and unbound-NEMO. Seen as the interactome of NEMO contains over 150 members (Fenner *et al.*, 2010), potentially the intracellular milieu acting as an additional control for NEMO structure and dynamics allows for specific selection of NEMO functional conformations, depending on the nature of the NEMO-ligand interaction. Finally, based on the findings discussed in Chapter 5 we propose that NEMO functions to control the interaction between IKKβ and its substrate IκBα, specifically controlling the length of the phosphorylation of IκBα by IKKβ. This has considerable implications for the development of NF-κB therapeutics of targets and shows the essential role in activating and modulating the response of canonical NF-κB.

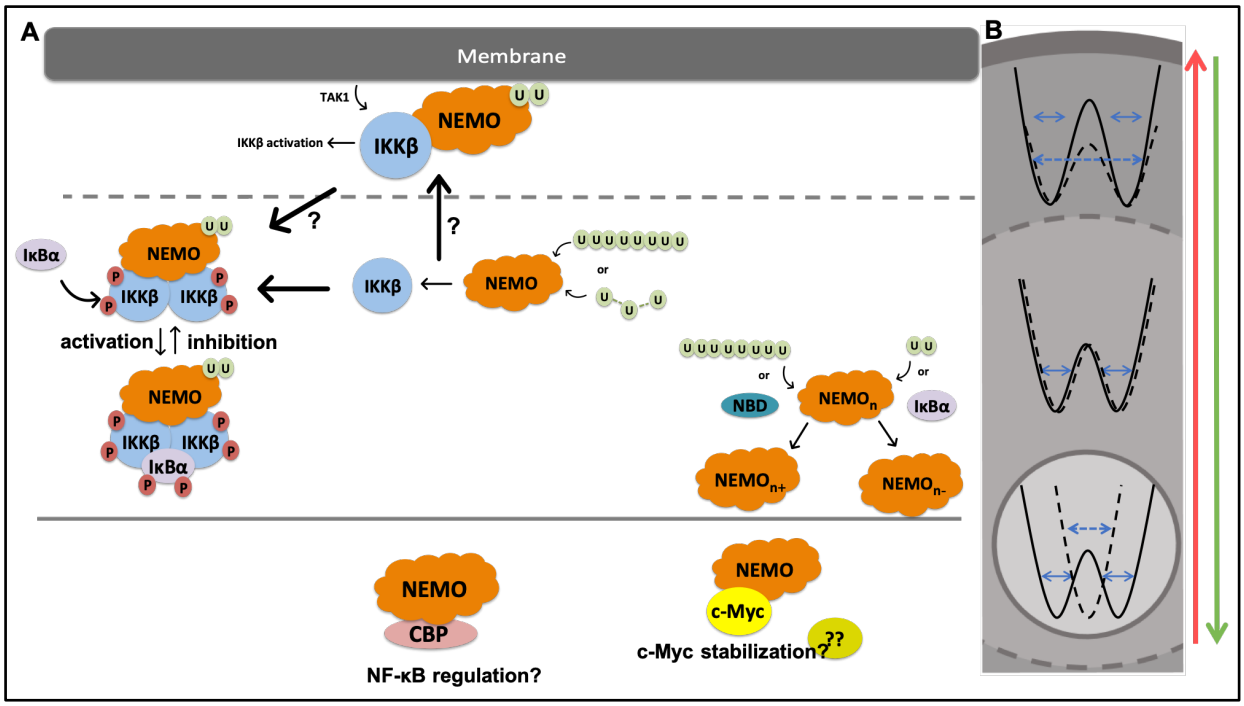

Figure 44. Proposed mechanism for NEMO conformational change cellular functions based on findings presented in Chapters 3-5. A, NEMO conformational changes observed upon ligand binding and due to the effect of physical parameters of the intracellular milieu (based on results presented in Chapter 3 and 5). B, Cartoon representation of NEMO FEL changes taking into account the effect of the physical parameters of the intracellular environment and following ligand binding based on results presented in Chapter 4.

In summary, based on the result presented in Chapter 3-5, we now know that NEMO is a dynamic protein, capable of undergoing conformational change in response to ligand binding or under the effect of the intracellular environment. Binding of ligands to NEMO allosterically modulates the protein, which can have important implications in activating the protein and ultimately NF-κB or even promote the formation of complex molecular complexes with NEMO and other cytoplasmic proteins. In the activation of NF-κB, the role of NEMO extends beyond its 'scaffold only' definition, with the protein not only required to activate the pathways by mediating the between the IKKβ and its substrate IκBα, but also having a regulatory role in controlling the length of the response of the NF-κB. The role of NEMO as the NF-κB essential modulator is thus two-fold, mediating the interaction between the activating enzyme IKKβ and the inhibitors sequestering the NF-κB transcription factors in the absence of a stimulus, as well as ensure the correct response time to safeguard the appropriate response and

limit the development of any clinical conditions associated with abnormal NF-κB canonical activation.

Appendix

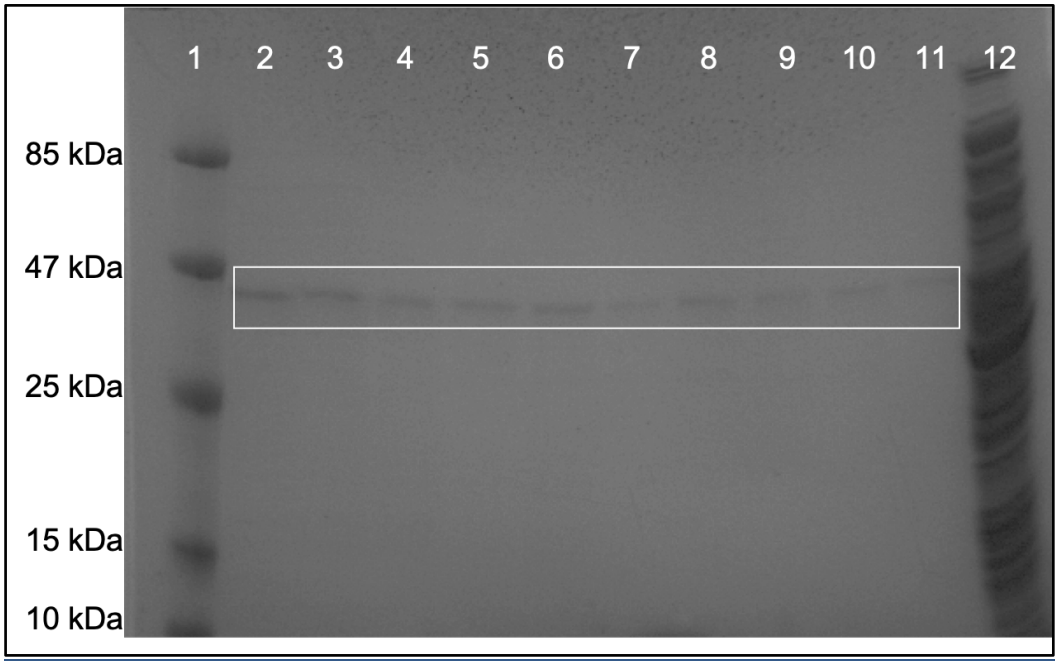

Figure 45. SDS-PAGE (12%) analysis by Coomassie blue stain of NEMO purification. The samples are: 1, Molecular weight marker; 2-11 NEMO purified fraction following affinity chromatography; 12, cell lysate prior to purification. White box to guide the reader in identifying NEMO samples.

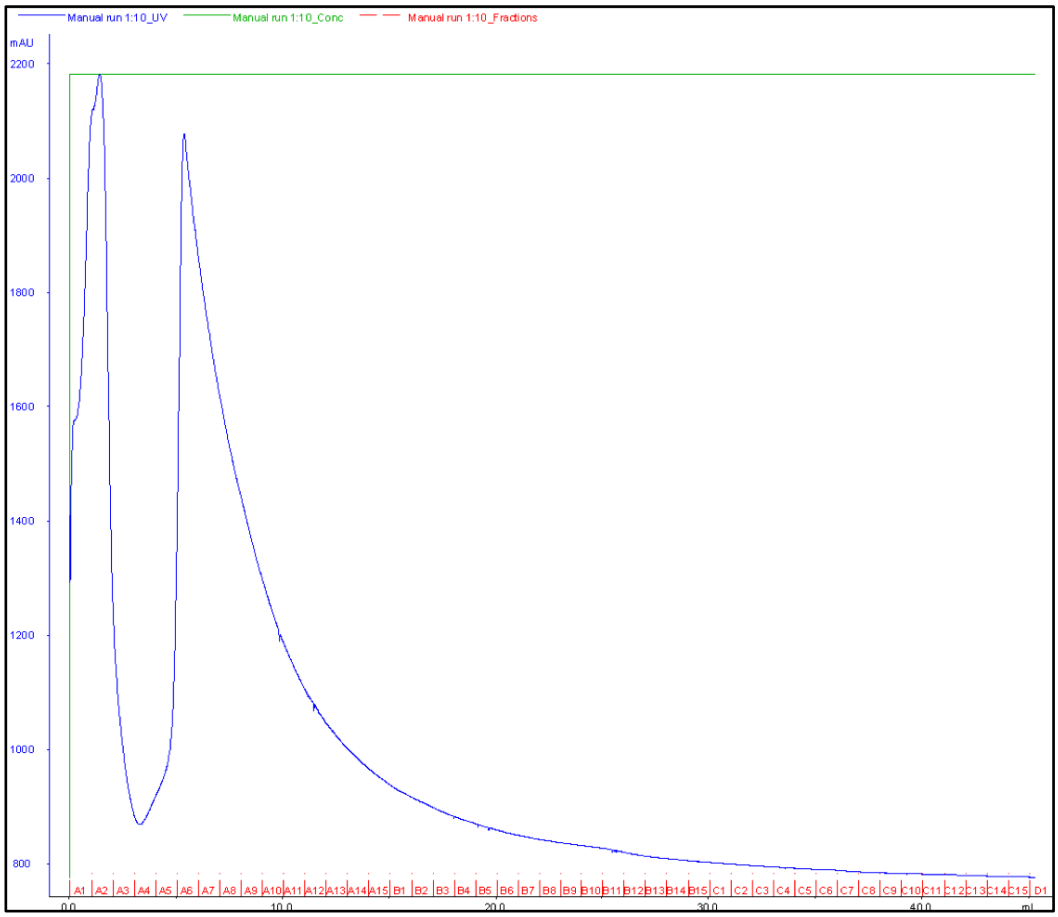

Figure 46. NEMO affinity chromatography purification profile following purification on a HisTrap FF crude 1ml column. Shown in blue is the trace shows the UV absorbance at 280 nm, green trace shown the % increase from 0-96 % 500mM Imidazole, and in red from A1-D1 are the sample fractions collected following purification and analysed using SDS-PAGE (See Figure 43).

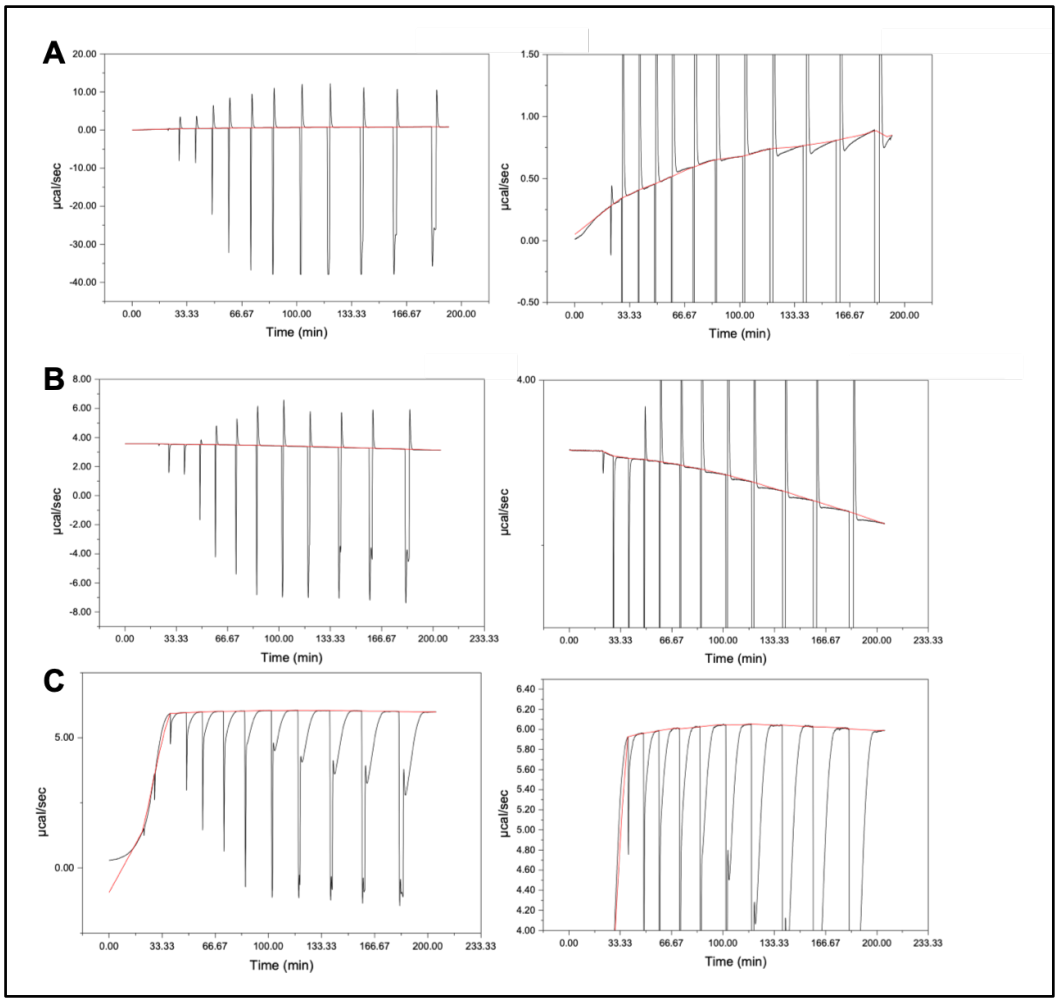

Figure 47. Raw thermograms for IKKβ kinetics in presence (A) and absence of NEMO (B). **The data show the baseline shift accompanying kinetic measurement using ITC during phosphorylation of IκBα, in the presence and absence of NEMO, as µcal/sec *vs* duration of the experiment (min). The experimental setup is as described in figure 40. C, no baseline shift observed in the control experiment with IκBα$_{S32A,S36A}$. This is due to the IκBα$_{S32A,S36A}$ peptide not containing any serine residues and as such no phosphorylation and no baseline shifts are detected. The data on the right-hand side show a close-up of both experiments in order to observe the kinetic baseline shifts. The red line is to guide the reader in following the baseline shifts.**

References

Abbyad, P., Childs, W., Shi, X., and Boxer, S.G., 2007. Dynamic Stokes shift in green fluorescent protein variants [Online]. *Proceedings of the National Academy of Sciences*, 104(51), pp.20189–20194.

Abu-Amer, Y., 2013. NF-κB signaling and bone resorption. *Osteoporosis international : a journal established as result of cooperation between the European Foundation for Osteoporosis and the National Osteoporosis Foundation of the USA*, 24(9), pp.2377–86.

Acuña, A.U., Amat-Guerri, F., Morcillo, P., Liras, M., and Rodríguez, B., 2009. Structure and Formation of the Fluorescent Compound of *Lignum nephriticum* . *Organic Letters*, 11(14), pp.3020–3023.

Ade, N., Antonios, D., Kerdine-Romer, S., Boisleve, F., Rousset, F., and Pallardy, M., 2007. NF-κB Plays a Major Role in the Maturation of Human Dendritic Cells Induced by NiSO4 but not by DNCB . *Toxicological Sciences*, 99(2), pp.488–501.

Adli, M., Merkhofer, E., Cogswell, P., and Baldwin, A.S., 2010. IKKalpha and IKKbeta each function to regulate NF-kappaB activation in the TNF-induced/canonical pathway. *PloS one*, 5(2), p.e9428.

Agou, F., Traincard, F., Vinolo, E., Courtois, G., Yamaoka, S., Israël, A., and Véron, M., 2004. The trimerization domain of NEMO is composed of the interacting C-terminal CC2 and LZ coiled-coil subdomains . *Journal of Biological Chemistry*, 279(27), pp.27861–27869.

Agou, F., Ye, F., Goffinont, S., Courtois, G., Yamaoka, S., Israël, A., and Véron, M., 2002. NEMO trimerizes through its coiled-coil C-terminal domain. *Journal of Biological Chemistry*, 277(20), pp.17464–17475.

Akasaka, K., 2003. Highly fluctuating protein structures revealed by variable-pressure nuclear magnetic resonance. *Biochemistry*, 42(37), pp.10875–10885.

Akasaka, K., 2006. Probing conformational fluctuation of proteins by pressure perturbation. *Chemical Reviews*, 106(5), pp.1814–1835.

Amir, R.E., Haecker, H., Karin, M., and Ciechanover, A., 2004. Mechanism of processing of the NF-κB2 p100 precursor: identification of the specific polyubiquitin chain-anchoring lysine residue and analysis of the role of NEDD8-modification on the SCFβ-TrCP ubiquitin ligase. *Oncogene*, 23(14), pp.2540–2547.

Anest, V., Hanson, J.L., Cogswell, P.C., Steinbrecher, K.A., Strahl, B.D., and Baldwin, A.S., 2003. A nucleosomal function for IκB kinase-α in NF-κB-dependent gene expression. *Nature*, 423(6940), pp.659–663.

Antz, C., Bauer, T., Kalbacher, H., Frank, R., Covarrubias, M., Kalbitzer, H.R., Ruppersberg, J.P., Baukrowitz, T., and Fakler, B., 1999. Control of K+channel gating by protein phosphorylation: Structural switches of the inactivation gate. *Nature Structural Biology*, 6(2), pp.146–150.

Ardito, F., Giuliani, M., Perrone, D., Troiano, G., and Lo Muzio, L., 2017. The crucial role of protein phosphorylation in cell signaling and its use as targeted therapy (Review). *International journal of molecular medicine*, 40(2), pp.271–280.

Arenzana-Seisdedos, F., Turpin, P., Rodriguez, M., Thomas, D., Hay, R.T., Virelizier, J.L., and Dargemont, C., 1997. Nuclear localization of I kappa B alpha promotes active transport of NF-kappa B from the nucleus to the cytoplasm. *Journal of cell science*, 110 (Pt 3), pp.369–78.

Ariafard, A. and Yates, B.F., 2009. In-depth insight into the electronic and steric effects of phosphine ligands on the mechanism of the R–R reductive elimination from (PR3)2PdR2. *Journal of Organometallic Chemistry*, 694(13), pp.2075–2084.

Arnott, D., Gawinowicz, M.A., Grant, R.A., Neubert, T.A., Packman, L.C., Speicher, K.D., Stone, K., and Turck, C.W., 2003. ABRF-PRG03: phosphorylation site determination. *Journal of biomolecular techniques : JBT*, 14(3), pp.205–15.

Atri, M.S., Saboury, A.A., and Ahmad, F., 2015. Biological Applications of Isothermal Titration Calorimetry. *Physical Chemistry Research*, 3(4), pp.319–330.

Aubin, J.E., 1979. Autofluorescence of viable cultured mammalian cells. [Online]. *Journal of Histochemistry & Cytochemistry*, 27(1), pp.36–43.

Auton, M., Rösgen, J., Sinev, M., Holthauzen, L.M.F., and Bolen, D.W., 2011. Osmolyte effects on protein stability and solubility: a balancing act between backbone and side-chains. [Online]. *Biophysical chemistry*, 159(1), pp.90–9.

Azumi, T., Itoh, K.I., and Shiraishi, H., 1976. Shift of emission band upon the excitation at the long wavelength absorption edge. III. Temperature dependence of the shift and correlation with the time dependent spectral shift. *The Journal of Chemical Physics*, 65(7), pp.2550–2555.

Baeuerle, P.A. and Baltimore, D., 1988. IkappaB: a specific inhibitor of the NF-kappaB transcription factor. *Science*, 242(1987), p.540.

Bagnéris, C., Ageichik, A. V, Cronin, N., Wallace, B., Collins, M., Boshoff, C., Waksman, G., and Barrett, T., 2008. Crystal structure of a vFlip-IKKgamma complex: insights into viral activation of the IKK signalosome. *Molecular cell*, 30(5), pp.620–31.

Bagnéris, C., Rogala, K.B., Baratchian, M., Zamfir, V., Kunze, M.B.A., Dagless, S., Pirker, K.F., Collins, M.K., Hall, B.A., Barrett, T.E., and Kay, C.W.M., 2015. Probing the solution structure of IκB kinase (IKK) subunit γ and its interaction with Kaposi sarcoma-associated herpes virus flice-interacting protein and IKK subunit β by EPR spectroscopy. *Journal of Biological Chemistry*, 290(27), pp.16539–16549.

Barczewski, A.H., Ragusa, M.J., Mierke, D.F., and Pellegrini, M., 2019. The IKK-binding domain of NEMO is an irregular coiled coil with a dynamic binding interface. *Scientific Reports*, 9(1), p.2950.

Bartels, T., Ahlstrom, L.S., Leftin, A., Kamp, F., Haass, C., Brown, M.F., and Beyer, K., 2010. The N-Terminus of the Intrinsically Disordered Protein α-Synuclein Triggers Membrane Binding and Helix Folding. *Biophysical Journal*, 99(7), pp.2116–2124.

Baruah, M., Qin, W., Flors, C., Hofkens, J., Vallée, R.A.L., Beljonne, D., Van Der Auweraer, M., De Borggraeve, W.M., and Boens, N., 2006. Solvent and pH dependent fluorescent properties of a dimethylaminostyryl borondipyrromethene dye in solution. *Journal of Physical Chemistry A*, 110(18), pp.5998–6009.

Baxter, N.J. and Williamson, M.P., 1997. Temperature dependence of 1H chemical shifts in proteins. *Journal of Biomolecular NMR*, 9(4), pp.359–369.

Beece, D., Eisenstein, L., Frauenfelder, H., Good, D., Marden, M.C., Reinisch, L., Yue, K.T., Reynolds, A.H., and Sorensen, L.B., 1980. Solvent Viscosity and Protein Dynamics. *Biochemistry*, 19(23), pp.5147–5157.

Beg, A.A., Ruben, S.M., Scheinman, R.I., Haskill, S., Rosen, C.A., and Baldwin, A.S., 1992. I kappa B interacts with the nuclear localization sequences of the subunits of NF-kappa B: a mechanism for cytoplasmic retention. *Genes & development*, 6(10), pp.1899–913.

Benson, R.C., Meyer, R.A., Zaruba, M.E., and Mckhann, G.M., 1979. *Cellular Autofluorescence-Is It due to flavins? J Histochem Cytochem*. 27(1), pp44-8.

Béraud, C., Henzel, W.J., and Baeuerle, P.A., 1999. Involvement of regulatory and catalytic subunits of phosphoinositide 3-kinase in NF-kappaB activation. *Proceedings of the National Academy of Sciences of the United States of America*, 96(2), pp.429–34.

Berezin, M.Y. and Achilefu, S., 2010. Fluorescence lifetime measurements and biological imaging. *Chemical Reviews*, 110(5), pp.2641–2684.

Betts, J.C. and Nabel, G.J., 1996. Differential regulation of NF-kappaB2(p100) processing and control by amino-

terminal sequences. *Molecular and cellular biology*, 16(11), pp.6363–71.

Bhak, G., Lee, J., Kim, T.-H., Lee, S., Lee, D., and Paik, S.R., 2014. Molecular inscription of environmental information into protein suprastructures: temperature effects on unit assembly of α-synuclein oligomers into polymorphic amyloid fibrils. *The Biochemical journal*, 464(2), pp.259–69.

Bianconi, M.L., 2007. Calorimetry of enzyme-catalyzed reactions. *Biophysical Chemistry*, 126(1–3), pp.59–64.

Bicknese, S., Periasamy, N., Shohet, S.B., and Verkman, A.S., 1993. Cytoplasmic viscosity near the cell plasma membrane: measurement by evanescent field frequency-domain microfluorimetry. *Biophysical Journal*, 65(3), pp.1272–1282.

Birks, J.B., 1971. Photophysics of aromatic molecules. *Journal of Luminescence*, 4(1), pp.69–71.

Black, J. and Robinson, J., 1803. *Lectures on the elements of chemistry, delivered in the University of Edinburgh.* Printed by Mundell and son, for Longman and Rees, London, and W. Creech, Edinburgh.

Blank, V., Kourilsky, P., and Israël, A., 1991. Cytoplasmic retention, DNA binding and processing of the NF-kappa B p50 precursor are controlled by a small region in its C-terminus. *The EMBO journal*, 10(13), pp.4159–4167.

Bloor, S., Ryzhakov, G., Wagner, S., Butler, P.J.G., Smith, D.L., Krumbach, R., Dikic, I., and Randow, F., 2008. Signal processing by its coil zipper domain activates IKK gamma. *Proceedings of the National Academy of Sciences of the United States of America*, 105(4), pp.1279–84.

Bonomi, M., Pellarin, R., and Vendruscolo, M., 2018. Simultaneous Determination of Protein Structure and Dynamics Using Cryo-Electron Microscopy. *Biophysical Journal*, 114(7), pp.1604–1613.

Bononi, A., Agnoletto, C., De Marchi, E., Marchi, S., Patergnani, S., Bonora, M., Giorgi, C., Missiroli, S., Poletti, F., Rimessi, A., and Pinton, P., 2011. Protein kinases and phosphatases in the control of cell fate. *Enzyme research*, 2011, p.329098.

Boskey, A.L. and Villarreal-Ramirez, E., 2016. Intrinsically disordered proteins and biomineralization. *Matrix Biology*, 52–54, pp.43–59.

Boyce, B.F., Yao, Z., and Xing, L., 2010. Functions of nuclear factor κB in bone. *Annals of the New York Academy of Sciences*, 1192(1), pp.367–375.

Brambilla, R., Bracchi-Ricard, V., Hu, W.-H., Frydel, B., Bramwell, A., Karmally, S., Green, E.J., and Bethea, J.R., 2005. Inhibition of astroglial nuclear factor κB reduces inflammation and improves functional recovery after spinal cord injury. *The Journal of Experimental Medicine*, 202(1), pp.145–156.

Brandt, J.A., Churchill, L., Rehman, A., Ellis, G., Mémet, S., Israël, A., and Krueger, J.M., 2004. Sleep deprivation increases the activation of nuclear factor kappa B in lateral hypothalamic cells. *Brain Research*, 1004(1–2), pp.91–97.

Bremm, A., Freund, S.M. V, and Komander, D., 2010. Lys11-linked ubiquitin chains adopt compact conformations and are preferentially hydrolyzed by the deubiquitinase Cezanne. *Nature Structural & Molecular Biology*, 17(8), pp.939–947.

Bridgman, P., 1914. The coagulation of albumin by pressure. *J. Biol. Chem.*, 19, pp.511–512.

Brower, E.T., Schön, A., and Freire, E., 2010. Naturally occurring variability in the envelope glycoprotein of HIV-1 and development of cell entry inhibitors. *Biochemistry*, 49(11), pp.2359–67.

Bull, J.J., 2015. Evolutionary reversion of live viral vaccines: Can genetic engineering subdue it?. *Virus evolution*, 1(1).

Burnett, G. and Kenedy, E.., 1954. The enzymatic phosphorylation of proteins. *The Journal of biological chemistry*, 211, pp.969–980.

Caarls, W., Soledad Celej, M., Demchenko, A.P., and Jovin, T.M., 2010. Characterization of coupled ground state and

excited state equilibria by fluorescence spectral deconvolution. *Journal of fluorescence*, 20(1), pp.181–90.

Campbell, J.A., 1985. Le Châtelier's principle, temperature effects, and entropy. *Journal of Chemical Education*, 62(3), p.231.

Cassandri, M., Smirnov, A., Novelli, F., Pitolli, C., Agostini, M., Malewicz, M., Melino, G., and Raschellà, G., 2017. Zinc-finger proteins in health and disease . *Cell Death Discovery*, 3, p.17071.

Catici, D.A.M., Amos, H.E., Yang, Y., van den Elsen, J.M.H.H., and Pudney, C.R., 2016. The red edge excitation shift phenomenon can be used to unmask protein structural ensembles: implications for NEMO-ubiquitin interactions. *FEBS Journal*, 283, pp.2272–2284.

Catici, D.A.M., Horne, J.E., Cooper, G.E., and Pudney, C.R., 2015. Poly-ubiquitin drives the molecular interactions of NF-κB essential modulator by allosteric regulation. *Journal of Biological Chemistry*, 290(22), pp.14130–14139.

Černý, J. and Hobza, P., 2007. Non-covalent interactions in biomacromolecules. *Physical Chemistry Chemical Physics*, 9(39), p.5291.

Chadli, A., Bouhouche, I., Sullivan, W., Stensgard, B., McMahon, N., Catelli, M.G., and Toft, D.O., 2000. Dimerization and N-terminal domain proximity underlie the function of the molecular chaperone heat shock protein 90. [Online]. *Proceedings of the National Academy of Sciences of the United States of America*, 97(23), pp.12524–9.

Chakraborty, H. and Chattopadhyay, A., 2017. Sensing Tryptophan Microenvironment of Amyloid Protein Utilizing Wavelength-Selective Fluorescence Approach. *Journal of Fluorescence*, 27(6), pp.1995–2000.

Chakravarti, B. and Chakravarti, D.N., 2015. Liquid Chromatography - Tandem Mass Spectrometry - Application for Clinical Chemistry Laboratory. *Journal of Molecular Biomarkers & Diagnosis*, 06(05).

Chan, K.T., Tong, G.S.M., To, W.-P., Yang, C., Du, L., Phillips, D.L., and Che, C.-M., 2017. The interplay between fluorescence and phosphorescence with luminescent gold(i) and gold(iii) complexes bearing heterocyclic arylacetylide ligands. *Chemical science*, 8(3), pp.2352–2364.

Chattopadhyay, A. and Haldar, S., 2014. Dynamic insight into protein structure utilizing red edge excitation shift. *Accounts of Chemical Research*, 47(1), pp.12–19.

Chattopadhyay, A. and Mukherjee, S., 1999. Red Edge Excitation Shift of a Deeply Embedded Membrane Probe: Implications in Water Penetration in the Bilayer. *The Journal of Physical Chemistry B*, 103(38), pp.8180–8185.

Chattopadhyay, A., Rawat, S.S., Kelkar, D. a, Ray, S., and Chakrabarti, A., 2003. Organization and dynamics of tryptophan residues in erythroid spectrin: novel structural features of denatured spectrin revealed by the wavelength-selective fluorescence approach. *Protein science : a publication of the Protein Society*, 12(11), pp.2389–2403.

Chen, C.R. and Makhatadze, G.I., 2017. Molecular determinant of the effects of hydrostatic pressure on protein folding stability. *Nature Communications*, 8, p.14561.

Chen, G., Song, F., Xiong, X., and Peng, X., 2013. Fluorescent nanosensors based on fluorescence resonance energy transfer (FRET) [Online]. *Industrial and Engineering Chemistry Research*, 52(33), pp.11228–11245.

Chen, R., Tang, Y., Wan, Y., Chen, T., Zheng, C., Qi, Y., Cheng, Y., and Huang, W., 2017. Promoting Singlet/triplet Exciton Transformation in Organic Optoelectronic Molecules: Role of Excited State Transition Configuration. *Scientific reports*, 7(1), p.6225.

Cheng, M.-X., Gong, J.-P., Chen, Y., Liu, Z.-J., Tu, B., and Liu, C.-A., 2012. NBD peptides protect against ischemia reperfusion after orthotopic liver transplantation in rats. [Online]. *The Journal of surgical research*, 176(2), pp.666–71.

Cheng, Y., LeGall, T., Oldfield, C.J., Mueller, J.P., Van, Y.Y.J., Romero, P., Cortese, M.S., Uversky, V.N., and Dunker, A.K., 2006. Rational drug design via intrinsically disordered protein. *Trends in Biotechnology*, 24(10), pp.435–442.

Cheung, M.S., Chavez, L.L., and Onuchic, J.N., 2004. The energy landscape for protein folding and possible connections to function. *Polymer*, 45(2), pp.547–555.

Chiaravalli, J., Fontan, E., Fsihi, H., Coic, Y.M., Baleux, F., Véron, M., and Agou, F., 2011. Direct inhibition of NF-κB activation by peptide targeting the NOA ubiquitin binding domain of NEMO. *Biochemical Pharmacology*, 82(9), pp.1163–1174.

Cho, M., Gwak, J., Park, S., Won, J., Kim, D.-E., Yea, S.S., Cha, I.-J., Kim, T.K., Shin, J.-G., and Oh, S., 2005. Diclofenac attenuates Wnt/β-catenin signaling in colon cancer cells by activation of NF-κB. *FEBS Letters*, 579(20), pp.4213–4218.

Christian, F., Smith, E., and Carmody, R., 2016. The Regulation of NF-κB Subunits by Phosphorylation. *Cells*, 5(1), p.12.

Christiansen, A., Wang, Q., Cheung, M.S., and Wittung-Stafshede, P., 2013. *Effects of macromolecular crowding agents on protein folding in vitro and in silico*. *Biophys Rev*. 5(2), pp137-145

Chuang, H.-C., Lan, J.-L., Chen, D.-Y., Yang, C.-Y., Chen, Y.-M., Li, J.-P., Huang, C.-Y., Liu, P.-E., Wang, X., and Tan, T.-H., 2011. The kinase GLK controls autoimmunity and NF-κB signaling by activating the kinase PKC-θ in T cells. *Nature Immunology*, 12(11), pp.1113–1118.

Cioni, P. and Gabellieri, E., 2011. Biochimica et Biophysica Acta Protein dynamics and pressure : What can high pressure tell us about protein structural flexibility ? *BBA - Proteins and Proteomics*, 1814(8), pp.934–941.

Collins, M.D., Hummer, G., Quillin, M.L., Matthews, B.W., and Gruner, S.M., 2005. Cooperative water filling of a nonpolar protein cavity observed by high-pressure crystallography and simulation. *Proceedings of the National Academy of Sciences*, 102(46), pp.16668–16671.

Collins, M.D., Kim, C.U., and Gruner, S.M., 2011. High-pressure protein crystallography and NMR to explore protein conformations. *Annual review of biophysics*, 40(1), pp.81–98.

Collins, M.O., Yu, L., Campuzano, I., Grant, S.G.N., and Choudhary, J.S., 2008. Phosphoproteomic Analysis of the Mouse Brain Cytosol Reveals a Predominance of Protein Phosphorylation in Regions of Intrinsic Sequence Disorder. *Molecular & Cellular Proteomics*, 7(7), pp.1331–1348.

Considine, K.M., Kelly, A.L., Fitzgerald, G.F., Hill, C., and Sleator, R.D., 2008. High-pressure processing â€“ effects on microbial food safety and food qualit.y *FEMS Microbiology Letters*, 281(1), pp.1–9.

Cooper, A., Cameron, D., Jakus, J., and Pettigrew, G.W., 2007. Pressure perturbation calorimetry, heat capacity and the role of water in protein stability and interactions. *Biochemical Society Transactions*, 35(6), pp.1547–1550.

Cordier, F., Grubisha, O., Traincard, F., Véron, M., Delepierre, M., and Agou, F., 2009. The zinc finger of NEMO is a functional ubiquitin-binding domain. *Journal of Biological Chemistry*, 284(5), pp.2902–7.

Cordier, F., Vinolo, E., Véron, M., Delepierre, M., and Agou, F., 2008. Solution structure of NEMO zinc finger and impact of an anhidrotic ectodermal dysplasia with immunodeficiency-related point mutation. *Journal of molecular biology*, 377(5), pp.1419–32.

Correa, R.G., Tergaonkar, V., Izpisua-Belmonte, J.C., and Verma, I.M., 2004. Characterization of NF-kappa B/I kappa B proteins in zebra fish and their involvement in notochord development. *Molecular and cellular biology*, 24(12), pp.5257–5268.

Cortese, M.S., Uversky, V.N., and Keith Dunker, A., 2008. Intrinsic disorder in scaffold proteins: Getting more from less. *Progress in Biophysics and Molecular Biology*, 98(1), pp.85–106.

Cote, S.M., Gilmore, T.D., Shaffer, R., Weber, U., Bollam, R., Golden, M.S., Glover, K., Herscovitch, M., Ennis, T., Allen, K.N., and Whitty, A., 2013. Mutation of nonessential cysteines shows that the NF-κB essential modulator forms a constitutive noncovalent dimer that binds IκB kinase-β with high affinity. *Biochemistry*, 52(51), pp.9141–54.

Croy, C.H., Bergqvist, S., Huxford, T., Ghosh, G., and Komives, E.A., 2004. Biophysical characterization of the free IκBα ankyrin repeat domain in solution. *Protein Science*, 13(7), pp.1767–1777.

Cullen, S., Ponnappan, S., and Ponnappan, U., 2015. Redox-regulated pathway of tyrosine phosphorylation underlies NF-κB induction by an atypical pathway independent of the 26S proteasome. *Biomolecules*, 5(1), pp.95–112.

Dang, Y.-Q., Li, Q., Wang, K., Wu, Y., Lian, L., and Zou, B., 2012. Hydrostatic Pressure Effects on the Fluorescence and FRET Behavior of Cy3-Labeled Phycocyanin System. *The Journal of Physical Chemistry B*, 116(36), pp.11010–11016.

Danielsson, J., Mu, X., Lang, L., Wang, H., Binolfi, A., Theillet, F.-X., Bekei, B., Logan, D.T., Selenko, P., Wennerström, H., and Oliveberg, M., 2015. Thermodynamics of protein destabilization in live cells. *Proceedings of the National Academy of Sciences*, 112(40), pp.12402–12407.

Darwech, I., Otero, J.E., Alhawagri, M.A., and Abu-Amer, Y., 2010. Tyrosine Phosphorylation Is Required for IκB Kinase-β (IKKβ) Activation and Function in Osteoclastogenesis. *Journal of Biological Chemistry*, 285(33), pp.25522–25530.

Day, R. and García, A.E., 2008. Water penetration in the low and high pressure native states of ubiquitin. *Proteins: Structure, Function and Genetics*, 70(4), pp.1175–1184.

De, S., Girigoswami, A., and Das, S., 2005. Fluorescence probing of albumin–surfactant interaction. *Journal of Colloid and Interface Science*, 285(2), pp.562–573.

Dębowski, D., Wyrzykowski, D., Lubos, M., and Rolka, K., 2016. Interactions between trypsin and its peptidic inhibitors studied by isothermal titration calorimetry (ITC). *Journal of Thermal Analysis and Calorimetry*, 123(1), pp.807–812.

Dejardin, E., 2006. The alternative NF-κB pathway from biochemistry to biology: Pitfalls and promises for future drug development. *Biochemical Pharmacology*, 72(9 SPEC. ISS.), pp.1161–1179.

Delhase, M., Hayakawa, M., Chen, Y., and Karin, M., 1999. Positive and negative regulation of I kappa B kinase activity through IKK beta subunit phosphorylation. *Science*, 284(5412), pp.309–313.

Dellarole, M., Kobayashi, K., Rouget, J.B., Caro, J.A., Roche, J., Islam, M.M., Garcia-Moreno E., B., Kuroda, Y., and Royer, C.A., 2013. Probing the physical determinants of thermal expansion of folded proteins. *Journal of Physical Chemistry B*, 117(42), pp.12742–12749.

Demchenko, A.P., 2002. The red-edge effects: 30 years of exploration. *Luminescence*, 17(1), pp.19–42.

Demchenko, A.P. and Ladokhin, A.S., 1988. Red-edge-excitation fluorescence spectroscopy of indole and tryptophan [Online]. *European Biophysics Journal*, 15(6), pp.369–379.

Denny, S.E., Nazeer, S.S., T.T., S., Nair, B.J., and Jayasree, R.S., 2018. Forensic application of fluorescence spectroscopy: An efficient technique to predict the presence of human saliva. *Journal of Luminescence*, 203, pp.696–701.

Devi-Kesavan, L.S. and Gao, J., 2003. Combined QM/MM study of the mechanism and kinetic isotope effect of the nucleophilic substitution reaction in haloalkane dehalogenase. *Journal of the American Chemical Society*, 125(6), pp.1532–1540.

Deyl, Z., Macek, K., Adam, M., and Vancíková, O., 1980. Studies on the chemical nature of elastin fluorescence. *Biochimica et biophysica acta*, 625(2), pp.248–54.

Dhar, A., Samiotakis, A., Ebbinghaus, S., Nienhaus, L., Homouz, D., Gruebele, M., and Cheung, M.S., 2010. Structure, function, and folding of phosphoglycerate kinase are strongly perturbed by macromolecular crowding. *Proceedings of the National Academy of Sciences of the United States of America*, 107(41), pp.17586–91.

DiDonato, J., Mercurio, F., Rosette, C., Wu-Li, J., Suyang, H., Ghosh, S., and Karin, M., 1996. Mapping of the inducible IkappaB phosphorylation sites that signal its ubiquitination and degradation. *Molecular and cellular biology*, 16(4), pp.1295–304.

Djikanović, D., Kalauzi, A., Jeremić, M., Mićić, M., and Radotić, K., 2007. Deconvolution of fluorescence spectra: contribution to the structural analysis of complex molecules. *Colloids and surfaces. B, Biointerfaces*, 54(2), pp.188–92.

Döffinger, R., Smahi, A., Bessia, C., Geissmann, F., Feinberg, J., Durandy, A., Bodemer, C., Kenwrick, S., Dupuis-Girod, S., Blanche, S., Wood, P., Rabia, S.H., Headon, D.J., Overbeek, P.A., Le Deist, F., Holland, S.M., Belani, K., Kumararatne, D.S., Fischer, A., Shapiro, R., Conley, M.E., Reimund, E., Kalhoff, H., Abinun, M., Munnich, A., Israël, A., Courtois, G., and Casanova, J.-L., 2001. X-linked anhidrotic ectodermal dysplasia with immunodeficiency is caused by impaired NF-κB signaling. *Nature Genetics*, 27(3), pp.277–285.

Dolcet, X., Llobet, D., Encinas, M., Pallares, J., Cabero, A., Schoenenberger, J.A., Comella, J.X., and Matias-Guiu, X., 2006. Proteasome Inhibitors Induce Death but Activate NF-κB on Endometrial Carcinoma Cell Lines and Primary Culture Explants. *Journal of Biological Chemistry*, 281(31), pp.22118–22130.

Dresselhaus, E.C., Boersma, M.C.H., and Meffert, M.K., 2018. Targeting of NF-κB to Dendritic Spines Is Required for Synaptic Signaling and Spine Development. *The Journal of neuroscience : the official journal of the Society for Neuroscience*, 38(17), pp.4093–4103.

Du, X.-L., Kong, L.-S., Meng, Q.-Y., Qian, A., Li, W.-D., Chen, H., Li, X.-Q., and Li, C.-L., 2015. Safety and Efficacy of Low Dosage of Urokinase for Catheter-directed Thrombolysis of Deep Venous Thrombosis. *Chinese medical journal*, 128(13), pp.1787–92.

Duckworth, E.A.M., Butler, T., Collier, L., Collier, S., and Pennypacker, K.R., 2006. NF-κB protects neurons from ischemic injury after middle cerebral artery occlusion in mice. *Brain Research*, 1088(1), pp.167–175.

Duff, Jr., M.R., Grubbs, J., and Howell, E.E., 2011. Isothermal Titration Calorimetry for Measuring Macromolecule-Ligand Affinity. *Journal of Visualized Experiments*, 7(55), pp.5–8.

Dumstrei, K., Mennecke, R., and Raz, E., 2004. Signaling pathways controlling primordial germ cell migration in zebrafish. *Journal of Cell Science*, 117(20), pp.4787–4795.

Dunker, A.K., Cortese, M.S., Romero, P., Iakoucheva, L.M., and Uversky, V.N., 2005. Flexible nets: The roles of intrinsic disorder in protein interaction networks. *FEBS Journal*, 272(20), pp.5129–5148.

Dunker, A.K., Oldfield, C.J., Meng, J., Romero, P., Yang, J.Y., Chen, J.W., Vacic, V., Obradovic, Z., and Uversky, V.N., 2008. The unfoldomics decade: An update on intrinsically disordered proteins. In: *BMC Genomics*.

Dutta, A.K., Rösgen, J., and Rajarathnam, K., 2015. Using Isothermal Titration Calorimetry to Determine Thermodynamic Parameters of Protein–Glycosaminoglycan Interactions. In: *Methods in Molecular Biology*. NIH Public Access, pp.315–324.

Ea, C.-K., Deng, L., Xia, Z.-P., Pineda, G., and Chen, Z.J., 2006. Activation of IKK by TNFalpha requires site-specific ubiquitination of RIP1 and polyubiquitin binding by NEMO. *Molecular cell*, 22(2), pp.245–57.

Easterby, J.S., 1973. Coupled enzyme assays: A general expression for the transient. *Biochimica et Biophysica Acta (BBA) - Enzymology*, 293(2), pp.552–558.

Emmerich, C.H., Ordureau, A., Strickson, S., Arthur, J.S.C., Pedrioli, P.G.A., Komander, D., and Cohen, P., 2013. Activation of the canonical IKK complex by K63/M1-linked hybrid ubiquitin chains. *Proceedings of the*

National Academy of Sciences, 110(38), pp.15247–15252.

Eom, K.S., Cheong, J.S., and Lee, S.J., 2016. Structural Analyses of Zinc Finger Domains for Specific Interactions with DNA. *Journal of Microbiology and Biotechnology*, 26(12), pp.2019–2029.

Fairchild, K.D., Singh, I.S., Carter, H.C., Hester, L., and Hasday, J.D., 2005. Hypothermia enhances phosphorylation of IκB kinase and prolongs nuclear localization of NF-κB in lipopolysaccharide-activated macrophages. *American Journal of Physiology-Cell Physiology*, 289(5), pp.C1114–C1121.

Fan, C., Li, Q., Ross, D., and Engelhardt, J.F., 2003. Tyrosine phosphorylation of I kappa B alpha activates NF kappa B through a redox-regulated and c-Src-dependent mechanism following hypoxia/reoxygenation. *The Journal of biological chemistry*, 278(3), pp.2072–80.

Fang, R., Wang, C., Jiang, Q., Lv, M., Gao, P., Yu, X., Mu, P., Zhang, R., Bi, S., Feng, J.-M., and Jiang, Z., 2017. NEMO–IKKβ Are Essential for IRF3 and NF-κB Activation in the cGAS–STING Pathway. *The Journal of Immunology*, 199, p.ji1700699.

Fenimore, P.W., Frauenfelder, H., McMahon, B.H., and Parak, F.G., 2002. Slaving: Solvent fluctuations dominate protein dynamics and functions. *Proceedings of the National Academy of Sciences*, 99(25), pp.16047–16051.

Fenner, B.J., Scannell, M., and Prehn, J.H.M., 2010. Expanding the substantial interactome of NEMO using protein microarrays. *PloS one*, 5(1), p.e8799.

Ferreon, A.C.M., Ferreon, J.C., Wright, P.E., and Deniz, A.A., 2013. Modulation of allostery by protein intrinsic disorder *Nature*, 498(7454), pp.390–394.

Ferreon, A.C.M., Moosa, M.M., Gambin, Y., and Deniz, A.A., 2012. Counteracting chemical chaperone effects on the single-molecule -synuclein structural landscape. *Proceedings of the National Academy of Sciences*, 109(44), pp.17826–17831.

Filipe-Santos, O., Bustamante, J., Haverkamp, M.H., Vinolo, E., Ku, C.-L., Puel, A., Frucht, D.M., Christel, K., von Bernuth, H., Jouanguy, E., Feinberg, J., Durandy, A., Senechal, B., Chapgier, A., Vogt, G., de Beaucoudrey, L., Fieschi, C., Picard, C., Garfa, M., Chemli, J., Bejaoui, M., Tsolia, M.N., Kutukculer, N., Plebani, A., Notarangelo, L., Bodemer, C., Geissmann, F., Israël, A., Véron, M., Knackstedt, M., Barbouche, R., Abel, L., Magdorf, K., Gendrel, D., Agou, F., Holland, S.M., and Casanova, J.-L., 2006. X-linked susceptibility to mycobacteria is caused by mutations in NEMO impairing CD40-dependent IL-12 production. *The Journal of Experimental Medicine*, 203(7), pp.1745–1759.

Finke, J.M. and Jennings, P.A., 2001. Early aggregated States in the folding of interleukin-1β. *Journal of Biological Physics*, 27(2/3), pp.119–131.

Flister, M.J., Wilber, A., Hall, K.L., Iwata, C., Miyazono, K., Nisato, R.E., Pepper, M.S., Zawieja, D.C., and Ran, S., 2010. Inflammation induces lymphangiogenesis through up-regulation of VEGFR-3 mediated by NF- B and Prox1. *Blood*, 115(2), pp.418–429.

Fontan, E., Traincard, F., Levy, S.G., Yamaoka, S., Véron, M., and Agou, F., 2007. NEMO oligomerization in the dynamic assembly of the IκB kinase core complex. *FEBS Journal*, 274(10), pp.2540–2551.

Forman-Kay, J.D. and Mittag, T., 2013. From Sequence and Forces to Structure, Function, and Evolution of Intrinsically Disordered Proteins. *Structure*, 21(9), pp.1492–1499.

Förster, T., 1948. Zwischenmolekulare Energiewanderung und Fluoreszenz. *Annalen der Physik*, 437(1–2), pp.55–75.

Frauenfelder, H., Alberding, N. a, Ansari, A., Braunstein, D., Cowen, B.R., Hong, M.K., Iben, I.E.T., Johnson, J.B., Luck, S., Marden, M.C., Mourant, J.R., Ormos, P., Reinisch, L., Scholl, R., Schulte, A., Shyamsunder, E., Soremen, L.B., Steinbach, P.J., Xie, A., and Young, R.D., 1990. Proteins and Pressure. *J. Phys. Chem.*, 94(3), pp.1024–1037.

Freyer, M.W. and Lewis, E.A., 2008. Isothermal Titration Calorimetry: Experimental Design, Data Analysis, and Probing Macromolecule/Ligand Binding and Kinetic Interactions. *Methods in Cell Biology*, 84, pp.79–113.

Fridmacher, V., Kaltschmidt, B., Goudeau, B., Ndiaye, D., Rossi, F.M., Pfeiffer, J., Kaltschmidt, C., Israël, A., and Mémet, S., 2003. Forebrain-specific neuronal inhibition of nuclear factor-kappaB activity leads to loss of neuroprotection. *The Journal of neuroscience : the official journal of the Society for Neuroscience*, 23(28), pp.9403–8.

Fu, Y., Kasinath, V., Moorman, V.R., Nucci, N. V., Hilser, V.J., and Wand, A.J., 2012. Coupled Motion in Proteins Revealed by Pressure Perturbation [Online]. *Journal of the American Chemical Society*, 134(20), pp.8543–8550.

Fujita, H., Rahighi, S., Akita, M., Kato, R., Sasaki, Y., Wakatsuki, S., and Iwai, K., 2014. Mechanism underlying IκB kinase activation mediated by the linear ubiquitin chain assembly complex. *Molecular and cellular biology*, 34(7), pp.1322–35.

Fusco, F., Pescatore, A., Bal, E., Ghoul, A., Paciolla, M., Lioi, M.B., D'Urso, M., Rabia, S.H., Bodemer, C., Bonnefont, J.P., Munnich, A., Miano, M.G., Smahi, A., and Ursini, M.V., 2008. Alterations of the IKBKG locus and diseases: An update and a report of 13 novel mutations. *Human Mutation*, 29(5), pp.595–604.

Galea, C.A., Wang, Y., Sivakolundu, S.G., and Kriwacki, R.W., 2008. Regulation of cell division by intrinsically unstructured proteins: Intrinsic flexibility, modularity, and signaling conduits. *Biochemistry*, 47(29), pp.7598–7609.

Galitski, V. and Spielman, I.B., 2013. Spin-orbit coupling in quantum gases. *Nature*, 494(7435), pp.49–54.

Gallagher, D., Gutierrez, H., Gavalda, N., O'Keeffe, G., Hay, R., and Davies, A.M., 2007. Nuclear factor-kappaB activation via tyrosine phosphorylation of inhibitor kappaB-alpha is crucial for ciliary neurotrophic factor-promoted neurite growth from developing neurons. *The Journal of neuroscience : the official journal of the Society for Neuroscience*, 27(36), pp.9664–9.

Gallat, F.X., Laganowsky, A., Wood, K., Gabel, F., Van Eijck, L., Wuttke, J., Moulin, M., Härtlein, M., Eisenberg, D., Colletier, J.P., Zaccai, G., and Weik, M., 2012. Dynamical coupling of intrinsically disordered proteins and their hydration water: Comparison with folded soluble and membrane proteins. *Biophysical Journal*, 103(1), pp.129–136.

Galley, W.C. and Purkey, R.M., 1970. Role of heterogeneity of the solvation site in electronic spectra in solution. *Proceedings of the National Academy of Sciences of the United States of America*, 67(3), pp.1116–21.

Gamble, C., McIntosh, K., Scott, R., Ho, K.H., Plevin, R., and Paul, A., 2012. Inhibitory kappa B kinases as targets for pharmacological regulation [Online]. *British Journal of Pharmacology*, 165(4), pp.802–819.

Gamsjaeger, R., Liew, C.K., Loughlin, F.E., Crossley, M., and Mackay, J.P., 2007. Sticky fingers: zinc-fingers as protein-recognition motifs. *Trends in Biochemical Sciences*, 32(2), pp.63–70.

Gao, J. and Xu, D., 2012. Correlation between posttranslational modification and intrinsic disorder in protein. *Pacific Symposium on Biocomputing. Pacific Symposium on Biocomputing*, pp.94–103.

Gao, Z., Hao, Y., Zheng, M., and Chen, Y., 2017. A fluorescent dye with large Stokes shift and high stability: synthesis and application to live cell imaging. *RSC Advances*, 7(13), pp.7604–7609.

Garcia-Viloca, M., Gao, J., Karplus, M., and Truhlar, D.G., 2004. How Enzymes Work: Analysis by Modern Rate Theory and Computer Simulations. *Science*, 303(5655), pp.186–195.

Garçon, F., Patton, D.T., Emery, J.L., Hirsch, E., Rottapel, R., Sasaki, T., and Okkenhaug, K., 2008. CD28 provides T-cell costimulation and enhances PI3K activity at the immune synapse independently of its capacity to interact with the p85/p110 heterodimer. *Blood*, 111(3), pp.1464–71.

Gasymov, O.K. and Glasgow, B.J., 2007. ANS fluorescence: potential to augment the identification of the external binding sites of proteins. *Biochimica et biophysica acta*, 1774(3), pp.403–11.

Gautheron, J. and Courtois, G., 2010. 'Without Ub I am nothing': NEMO as a multifunctional player in ubiquitin-mediated control of NF-kappaB activation. *Cellular and molecular life sciences : CMLS*, 67(18), pp.3101–13.

Gauthier, M. and Degnan, B.M., 2008. The transcription factor NF-κB in the demosponge Amphimedon queenslandica: insights on the evolutionary origin of the Rel homology domain. *Development Genes and Evolution*, 218(1), pp.23–32.

Gekko, K. and Timasheff, S.N., 1981. Mechanism of Protein Stabilization by Glycerol: Preferential Hydration in Glycerol-Water Mixtures. *Biochemistry*, 20(16), pp.4667–4676.

Gerondakis, S. and Siebenlist, U., 2010. Roles of the NF-kappaB pathway in lymphocyte development and function. *Cold Spring Harbor perspectives in biology*, 2(5), p.a000182.

Ghisaidoobe, A.B.T. and Chung, S.J., 2014. Intrinsic tryptophan fluorescence in the detection and analysis of proteins: a focus on Förster resonance energy transfer techniques. *International journal of molecular sciences*, 15(12), pp.22518–38.

Ghosh, S., May, M.J., and Kopp, E.B., 1998. NF-κB AND REL PROTEINS: Evolutionarily Conserved Mediators of Immune Responses. *Annual Review of Immunology*, 16(1), pp.225–260.

Giese, K.C. and Vierling, E., 2002. Changes in oligomerization are essential for the chaperone activity of a small heat shock protein in vivo and in vitro.*The Journal of biological chemistry*, 277(48), pp.46310–8.

Gijsbers, A., Nishigaki, T., and Sánchez-Puig, N., 2016. Fluorescence Anisotropy as a Tool to Study Protein-protein Interactions. *Journal of Visualized Experiments*, (116).

Gilmore, T D, 2006. Introduction to NF-κB: Players, pathways, perspectives. *Oncogene*, 25(51), pp.6680–6684.

Gilmore, T.D. and Wolenski, F.S., 2012. NF-κB: Where did it come from and why? *Immunological Reviews*, 246(1), pp.14–35.

Golub, M., Lehofer, B., Martinez, N., Ollivier, J., Kohlbrecher, J., Prassl, R., and Peters, J., 2017. High hydrostatic pressure specifically affects molecular dynamics and shape of low-density lipoprotein particles. *Scientific Reports*, 7(1), p.46034.

Gómez, J., Hilser, V.J., Xie, D., and Freire, E., 1995. The heat capacity of proteins. *Proteins: Structure, Function, and Bioinformatics*, 22(4), pp.404–412.

Gong, H., Murphy, P.W., Langille, G.M., Minielly, S.J., Murphy, A., McMaster, C.R., and Byers, D.M., 2008. Tryptophan fluorescence reveals induced folding of Vibrio harveyi acyl carrier protein upon interaction with partner enzymes. *Biochimica et biophysica acta*, 1784(11), pp.1835–43.

Gorinstein, S., Goshev, I., Moncheva, S., Zemser, M., Weisz, M., Caspi, A., Libman, I., Lerner, H.T., Trakhtenberg, S., and Martín-Belloso, O., 2000. Intrinsic Tryptophan Fluorescence of Human Serum Proteins and Related Conformational Changes. *Journal of Protein Chemistry*, 19(8), pp.637–642.

Gorovits, B.M. and Horowitz, P.M., 1998. High Hydrostatic Pressure Can Reverse Aggregation of Protein Folding Intermediates and Facilitate Acquisition of Native Structure. *Biochemistry*, 37(17), pp.6132–6135.

Gozani, O., Karuman, P., Jones, D.R., Ivanov, D., Cha, J., Lugovskoy, A.A., Baird, C.L., Zhu, H., Field, S.J., Lessnick, S.L., Villasenor, J., Mehrotra, B., Chen, J., Rao, V.R., Brugge, J.S., Ferguson, C.G., Payrastre, B., Myszka, D.G., Cantley, L.C., Wagner, G., Divecha, N., Prestwich, G.D., and Yuan, J., 2003. The PHD finger of the chromatin-associated protein ING2 functions as a nuclear phosphoinositide receptor. *Cell*, 114(1), pp.99–111.

Grubisha, O., Kaminska, M., Duquerroy, S., Fontan, E., Cordier, F., Haouz, A., Raynal, B., Chiaravalli, J., Delepierre, M., Israël, A., Véron, M., and Agou, F., 2010. DARPin-Assisted Crystallography of the CC2-LZ Domain of NEMO

Reveals a Coupling between Dimerization and Ubiquitin Binding. *Journal of Molecular Biology*, 395(1), pp.89–104.

Gruebele, M., Dave, K., and Sukenik, S., 2016. Globular Protein Folding In Vitro and In Vivo. *Annual Review of Biophysics*, 45(1), pp.233–251.

Grumont, R.J. and Gerondakis, S., 1994. *Alternative splicing of RNA transcripts encoded by the murine p105 NF-cB gene generates IKcBy isoforms with different inhibitory activities. Proc Natl Acad Sci U S A. 91(10), pp4367-71.*

Guigas, G., Kalla, C., and Weiss, M., 2007. The degree of macromolecular crowding in the cytoplasm and nucleoplasm of mammalian cells is conserved. *FEBS Letters*, 581(26), pp.5094–5098.

Guo, B., Audu, C.O., Cochran, J.C., Mierke, D.F., and Pellegrini, M., 2014. Protein engineering of the n-terminus of NEMO: Structure stabilization and rescue of ikkβ binding. *Biochemistry*, 53(43), pp.6776–6785.

Habineza Ndikuyeze, G., Gaurnier-Hausser, A., Patel, R., Baldwin, A.S., May, M.J., Flood, P., Krick, E., Propert, K.J., and Mason, N.J., 2014. A phase I clinical trial of systemically delivered NEMO binding domain peptide in dogs with spontaneous activated B-cell like diffuse large B-cell lymphoma.. *PloS one*, 9(5), p.e95404.

Hadian, K., Griesbach, R.A., Dornauer, S., Wanger, T.M., Nagel, D., Metlitzky, M., Beisker, W., Schmidt-Supprian, M., and Krappmann, D., 2011. NF-κB essential modulator (NEMO) interaction with linear and Lys-63 ubiquitin chains contributes to NF-κB activation. *Journal of Biological Chemistry*, 286(29), pp.26107–26117.

Hadj-Rabia, S., Froidevaux, D., Bodak, N., Hamel-Teillac, D., Smahi, A., Touil, Y., Fraitag, S., de Prost, Y., and Bodemer, C., 2003. Clinical Study of 40 Cases of Incontinentia Pigmenti. *Archives of Dermatology*, 139(9), pp.1163–70.

Haglund, K. and Dikic, I., 2005. Ubiquitylation and cell signaling. *The EMBO Journal*, 24(19), pp.3353–3359.

Haidekker, M.A., Brady, T.P., Lichlyter, D., and Theodorakis, E.A., 2005. Effects of solvent polarity and solvent viscosity on the fluorescent properties of molecular rotors and related probes [Online]. *Bioorganic Chemistry*, 33(6), pp.415–425.

Hakoshima, T., 2005. Leucine Zippers. In: *Encyclopedia of Life Sciences*.

Haldar, S., Chaudhuri, A., and Chattopadhyay, A., 2011. *Organization and dynamics of membrane probes and proteins utilizing the red edge excitation shift.* J Phys Chem B.115(19), pp5693-706

Hall, T.M.T., 2005. Multiple modes of RNA recognition by zinc finger proteins. *Current Opinion in Structural Biology*, 15(3), pp.367–373.

Hanson, E.P., Monaco-Shawver, L., Solt, L.A., Madge, L.A., Banerjee, P.P., May, M.J., and Orange, J.S., 2008. Hypomorphic nuclear factor-κB essential modulator mutation database and reconstitution system identifies phenotypic and immunologic diversity. *Journal of Allergy and Clinical Immunology*, 122(6), pp.1169-1177.e16.

Harhaj, E.W. and Dixit, V.M., 2011. Deubiquitinases in the regulation of NF-κB signaling. *Cell research*, 21(1), pp.22–39.

Harhaj, E.W. and Sun, S.-C., 1999. *Regulation of RelA Subcellular Localization by a Putative Nuclear Export Signal and p50* . Mol Cell Biol. 19(10), pp7088-95.

Hartwell, S.K. and Grudpan, K., 2012. Flow-Based Systems for Rapid and High-Precision Enzyme Kinetics Studies [Online]. *Journal of Analytical Methods in Chemistry*, 2012, pp.1–10.

Hatakeyama, S., Kitagawa, M., Nakayama, K., Shirane, M., Matsumoto, M., Hattori, K., Higashi, H., Nakano, H., Okumura, K., Onoé, K., Good, R.A., and Nakayama, K., 1999. Ubiquitin-dependent degradation of IkappaBalpha is mediated by a ubiquitin ligase Skp1/Cul 1/F-box protein FWD1. *Proceedings of the National Academy of Sciences of the United States of America*, 96(7), pp.3859–63.

Hauenstein, A. V, Xu, G., Kabaleeswaran, V., and Wu, H., 2017. Evidence for M1-Linked Polyubiquitin- Mediated

Conformational Change in NEMO. *Journal of Molecular Biology*, 429, pp.3793–3800.

Hawe, A., Sutter, M., and Jiskoot, W., 2008. Extrinsic fluorescent dyes as tools for protein characterizatio. *Pharmaceutical Research*, 25(7), pp.1487–1499.

Hay, S., Pudney, C.R., Sutcliffe, M.J., and Scrutton, N.S., 2010. Probing active site geometry using high pressure and secondary isotope effects in an enzyme-catalysed 'deep' H-tunnelling reaction.. *Journal of physical organic chemistry*, 23(7), pp.696–701.

Hayden, M.S. and Ghosh, S., 2012. NF-κB, the first quarter-century: remarkable progress and outstanding questions. *Genes & development*, 26(3), pp.203–34.

Hayden, M.S. and Ghosh, S., 2014. Regulation of NF-κB by TNF family cytokines.*Seminars in immunology*, 26(3), pp.253–66.

Haynes, C., Oldfield, C.J., Ji, F., Klitgord, N., Cusick, M.E., Radivojac, P., Uversky, V.N., Vidal, M., and Iakoucheva, L.M., 2006. Intrinsic Disorder Is a Common Feature of Hub Proteins from Four Eukaryotic Interactomes. *PLoS Computational Biology*, 2(8), p.e100.

Haynes, D.H. and Staerk, H., 1974. 1-Anilino-8-naphthalenesulfonate: A fluorescent probe of membrane surface structure, composition and mobility. *The Journal of Membrane Biology*, 17(1), pp.313–340.

He, C. and Klionsky, D.J., 2009. Regulation mechanisms and signaling pathways of autophagy. *Annual review of genetics*, 43, pp.67–93.

Hei, D.J. and Clark, D.S., 1994. Pressure stabilization of proteins from extreme thermophiles [Online]. *Applied and Environmental Microbiology*, 60(3), pp.932–939.

Heilker, R., Freuler, F., Vanek, M., Pulfer, R., Kobel, T., Peter, J., Zerwes, H.G., Hofstetter, H., Eder, J., and Eder., 1999. The kinetics of association and phosphorylation of IkB isoforms by IkB kinase 2 correlate with their cellular regulation in human endothelial cells. *Biochemistry*, 38, pp.6231–6238.

Henzler-Wildman, K. and Kern, D., 2007. Dynamic personalities of proteins. *Nature*, 450(7172), pp.964–972.

Herberhold, H., Marchal, S., Lange, R., Scheyhing, C.H., Vogel, R.F., and Winter, R., 2003. Characterization of the Pressure-induced Intermediate and Unfolded State of Red-shifted Green Fluorescent Protein—A Static and Kinetic FTIR, UV/VIS and Fluorescence Spectroscopy Study. *Journal of Molecular Biology*, 330(5), pp.1153–1164.

Heremans, K. and Smeller, L., 1998. Protein structure and dynamics at high pressure. *Biochim Biophys Acta.* 1386(2), pp353-70.

Heremans, L. and Heremans, K., 1989. Raman spectroscopic study of the changes in secondary structure of chymotrypsin: effect of pH and pressure on the salt bridge. *Biochimica et biophysica acta*, 999(2), pp.192–7.

Herscovitch, M., Comb, W., Ennis, T., Coleman, K., Yong, S., Armstead, B., Kalaitzidis, D., Chandani, S., and Gilmore, T.D., 2008. Intermolecular disulfide bond formation in the NEMO dimer requires Cys54 and Cys347. *Biochemical and biophysical research communications*, 367(1), pp.103–8.

Hetru, C. and Hoffmann, J.A., 2009. NF-kappaB in the immune response of Drosophila. *Cold Spring Harbor perspectives in biology*, 1(6), p.a000232.

Ho, T.-Y., Yan, W., and Bagnell, C.A., 2007. Relaxin-induced matrix metalloproteinase-9 expression is associated with activation of the NF-κB pathway in human THP-1 cells. *Journal of Leukocyte Biology*, 81(5), pp.1303–1310.

Hoesel, B. and Schmid, J. a, 2013. The complexity of NF-κB signaling in inflammation and cancer. *Molecular cancer*, 12(1), p.86.

Hoffmann, A. and Baltimore, D., 2006. Circuitry of nuclear factor kappaB signaling. *Immunological reviews*, 210, pp.171–186.

Hoffmann, A., Natoli, G., and Ghosh, G., 2006. Transcriptional regulation via the NF-kappaB signaling module. *Oncogene*, 25(51), pp.6706–16.

Hong, J. and Gierasch, L.M., 2010. Macromolecular crowding remodels the energy landscape of a protein by favoring a more compact unfolded state. *Journal of the American Chemical Society*, 132(30), pp.10445–10452.

Van Hoof, D., Muñoz, J., Braam, S.R., Pinkse, M.W.H., Linding, R., Heck, A.J.R., Mummery, C.L., and Krijgsveld, J., 2009. Phosphorylation Dynamics during Early Differentiation of Human Embryonic Stem Cells. *Cell Stem Cell*, 5(2), pp.214–226.

Hu, Y., Baud, V., Delhase, M., Zhang, P., Deerinck, T., Ellisman, M., Johnson, R., and Karin, M., 1999. Abnormal morphogenesis but intact IKK activation in mice lacking the IKKalpha subunit of IkappaB kinase. *Science (New York, N.Y.)*, 284(5412), pp.316–20.

Hua Li, Hiroaki Yamada, and, and Akasaka*, K., 1998. Effect of Pressure on Individual Hydrogen Bonds in Proteins. Basic Pancreatic Trypsin Inhibitor. *Biochemistry*. 37(5), pp1167-73.

Huang, G.J., Zhang, Z.Q., and Jin, D.Y., 2002. Stimulation of IKK-γ oligomerization by the human T-cell leukemia virus oncoprotein Tax. *FEBS Letters*, 531(3), pp.494–498.

Huang, J., Li, L., Yuan, W., Zheng, L., Guo, Z., and Huang, W., 2016. NEMO-Binding Domain Peptide Attenuates Lipopolysaccharide-Induced Acute Lung Injury by Inhibiting the NF-κB Signaling Pathway.. *Mediators of inflammation*, 2016, p.7349603.

Huang, T.T. and Miyamoto, S., 2001. Postrepression Activation of NF-B Requires the Amino-Terminal Nuclear Export Signal Specific to IB . *Molecular And Cellular Biology*, 21(14), pp.4737–4747.

Huggins, D.J., 2016. Studying the role of cooperative hydration in stabilizing folded protein states. *Journal of structural biology*, 196(3), pp.394–406.

Hummer, G., Garde, S., García, A.E., Paulaitis, M.E., Pratt, L.R., Garcia, A.E., Paulaitis, M.E., and Pratt, L.R., 1998. The pressure dependence of hydrophobic interactions is consistent with the observed pressure denaturation of proteins. *Proceedings of the National Academy of Sciences*, 95(4), pp.1552–1555.

Humphrey, S.J., James, D.E., and Mann, M., 2015. Protein Phosphorylation: A Major Switch Mechanism for Metabolic Regulation. *Trends in endocrinology and metabolism: TEM*, 26(12), pp.676–687.

Hunter, T., 1995. Protein kinases and phosphatases: the yin and yang of protein phosphorylation and signaling. *Cell*, 80(2), pp.225–36.

Hunter, T., 2012. Why nature chose phosphate to modify proteins [Online]. *Philosophical Transactions of the Royal Society B: Biological Sciences*, 367(1602), pp.2513–2516.

Huxford, T. and Ghosh, G., 2009. A structural guide to proteins of the NF-kappaB signaling module. *Cold Spring Harbor perspectives in biology*, 1(3), p.a000075.

Huxford, T., Huang, D.B., Malek, S., and Ghosh, G., 1998. The crystal structure of the IkappaBalpha/NF-kappaB complex reveals mechanisms of NF-kappaB inactivation. *Cell*, 95(6), pp.759–70.

Huynh, Q.K., Boddupalli, H., Rouw, S.A., Koboldt, C.M., Hall, T., Sommers, C., Hauser, S.D., Pierce, J.L., Combs, R.G., Reitz, B.A., Diaz-Collier, J.A., Weinberg, R.A., Hood, B.L., Kilpatrick, B.F., and Tripp, C.S., 2000. Characterization of the recombinant IKK1/IKK2 heterodimer: Mechanisms regulating kinase activity. *Journal of Biological Chemistry*, 275(34), pp.25883–25891.

Hyun, J.S., Satsu, H., and Shimizu, M., 2007. Cadmium induces Interleukin-8 production via NF-κB activation in the human intestinal epithelial cell, Caco-2. *Cytokine*, 37(1), pp.26–34.

Ikeda, F., Deribe, Y.L., Skånland, S.S., Stieglitz, B., Grabbe, C., Franz-Wachtel, M., van Wijk, S.J.L., Goswami, P., Nagy,

V., Terzic, J., Tokunaga, F., Androulidaki, A., Nakagawa, T., Pasparakis, M., Iwai, K., Sundberg, J.P., Schaefer, L., Rittinger, K., Macek, B., and Dikic, I., 2011. SHARPIN forms a linear ubiquitin ligase complex regulating NF-κB activity and apoptosis. *Nature*, 471(7340), pp.637–641.

Imbert, V., Rupec, R.A., Livolsi, A., Pahl, H.L., Traenckner, E.B., Mueller-Dieckmann, C., Farahifar, D., Rossi, B., Auberger, P., Baeuerle, P.A., and Peyron, J.-F.F., 1996. Tyrosine phosphorylation of I kappa B-alpha activates NF-kappa B without proteolytic degradation of I kappa B-alpha. *Cell*, 86, pp.787–798.

Irazoqui, J.E., Urbach, J.M., and Ausubel, F.M., 2010. Evolution of host innate defence: insights from Caenorhabditis elegans and primitive invertebrates. *Nature reviews. Immunology*, 10(1), pp.47–58.

Ishikawa, H., Asano, M., Kanda, T., Kumar, S., Gélinas, C., and Ito, Y., 1993. Two novel functions associated with the Rel oncoproteins: DNA replication and cell-specific transcriptional activation. *Oncogene*, 8(11), pp.2889–96.

Ishimaru, D., Andrade, L.R., Teixeira, L.S.P., Quesado, P.A., Maiolino, L.M., Lopez, P.M., Cordeiro, Y., Costa, L.T., Heckl, W.M., Weissmüller, G., Foguel, D., and Silva, J.L., 2003. Fibrillar aggregates of the tumor suppressor p53 core domain. *Biochemistry*, 42(30), pp.9022–9027.

Israël, A., 2010. The IKK Complex, a Central Regulator of NF- B Activation. *Cold Spring Harbor Perspectives in Biology*, 2(3), pp.a000158–a000158.

Itoh, K. and Azumi, T., 1973. Shift of emission band upon excitation at the long wavelength absorptio edge. 1. A preliminary survey for quinine and related compounds. *Chemical Physics Letters*, 22(2), pp.395–399.

Itoh, K.I. and Azumi, T., 1975. Shift of the emission band upon excitation at the long wavelength absorption edge. II. Importance of the solute-solvent interaction and the solvent reorientation relaxation process. *The Journal of Chemical Physics*, 62(9), pp.3431–3438.

Ivanyi-Nagy, R., Davidovic, L., Khandjian, E.W., and Darlix, J.-L., 2005. Disordered RNA chaperone proteins: from functions to disease. *Cellular and Molecular Life Sciences*, 62(13), pp.1409–1417.

Ivins, F.J., Montgomery, M.G., Smith, S.J.M., Morris-Davies, A.C., Taylor, I.A., and Rittinger, K., 2009. NEMO oligomerization and its ubiquitin-binding properties. *Biochemical Journal*, 421(2), pp.243–251.

Iwadate, M., Asakura, T., Dubovskii, P. V, Yamada, H., Akasaka, K., and Williamson, M.P., 2001. Pressure-dependent changes in the structure of the melittin α-helix determined by NMR. *Journal of Biomolecular NMR*, 19(2), pp.115–124.

Jacobs, M.D. and Harrison, S.C., 1998. Structure of an IkappaBalpha/NF-kappaB complex. *Cell*, 95(6), pp.749–58.

Jain, N., Bhasne, K., Hemaswasthi, M., and Mukhopadhyay, S., 2013. Structural and Dynamical Insights into the Membrane-Bound α-Synuclein . *PLoS ONE*, 8(12), p.e83752.

Jenal, U. and Galperin, M.Y., 2009. Single domain response regulators: molecular switches with emerging roles in cell organization and dynamics. *Current Opinion in Microbiology*, 12(2), pp.152–160.

Jenner, R.G., Alba, M.M., Boshoff, C., and Kellam, P., 2001. Kaposi's Sarcoma-Associated Herpesvirus Latent and Lytic Gene Expression as Revealed by DNA Arrays. *Journal of Virology*, 75(2), pp.891–902.

Jensen, L.B., Mortensen, K., Pavan, G.M., Kasimova, M.R., Jensen, D.K., Gadzhyeva, V., Nielsen, H.M., and Foged, C., 2010. Molecular Characterization of the Interaction between siRNA and PAMAM G7 Dendrimers by SAXS, ITC, and Molecular Dynamics Simulations. *Biomacromolecules*, 11(12), pp.3571–3577.

Ji, X.-L. and Liu, S.-Q., 2011. Is stoichiometry-driven protein folding getting out of thermodynamic control? *Journal of biomolecular structure & dynamics*, 28(4), pp.621–3; discussion 669-674.

Jiang, Z., Ninomiya-Tsuji, J., Qian, Y., Matsumoto, K., and Li, X., 2002. Interleukin-1 (IL-1) receptor-associated kinase-dependent IL-1-induced signaling complexes phosphorylate TAK1 and TAB2 at the plasma membrane and activate TAK1 in the cytosol. *Molecular and cellular biology*, 22(20), pp.7158–67.

Johnson, L.N. and Barford, D., 1993. The Effects of Phosphorylation on the Structure and Function of Proteins. *Annual Review of Biophysics and Biomolecular Structure*, 22(1), pp.199–232.

Johnson, M.P., 2016. Photosynthesis. *Essays in biochemistry*, 60(3), pp.255–273.

Jost, P.J., Ruland, J., Krappmann, D., Emmerich, F., Mapara, M.Y., Bommert, K., Royer, H.D., Scheidereit, C., and Dörken, B., 2007. Aberrant NF-kappaB signaling in lymphoma: mechanisms, consequences, and therapeutic implications. *Blood*, 109(7), pp.2700–7.

Kaileh, M. and Sen, R., 2012. NF-κB function in B lymphocyte.s. *Immunological Reviews*, 246(1), pp.254–271.

Kamatari, Y.O., Kitahara, R., Yamada, H., Yokoyama, S., and Akasaka, K., 2004. High-pressure NMR spectroscopy for characterizing folding intermediates and denatured states of proteins *Methods*, 34(1), pp.133–143.

Kamerlin, S.C.L., Chu, Z.T., and Warshel, A., 2010. On catalytic preorganization in oxyanion holes: highlighting the problems with the gas-phase modeling of oxyanion holes and illustrating the need for complete enzyme models. *The Journal of organic chemistry*, 75(19), pp.6391–401.

Kang, J.-A., Choi, H., Yang, T., Cho, S.K., Park, Z.-Y., and Park, S.-G., 2017. PKCθ-Mediated PDK1 Phosphorylation Enhances T Cell Activation by Increasing PDK1 Stability. *Molecules and cells*, 40(1), pp.37–44.

Kang, J.Y., Nan, X., Jin, M.S., Youn, S.-J., Ryu, Y.H., Mah, S., Han, S.H., Lee, H., Paik, S.-G., and Lee, J.-O., 2009. Recognition of Lipopeptide Patterns by Toll-like Receptor 2-Toll-like Receptor 6 Heterodimer. *Immunity*, 31(6), pp.873–884.

Kao, S.-J., Lei, H.-C., Kuo, C.-T., Chang, M.-S., Chen, B.-C., Chang, Y.-C., Chiu, W.-T., and Lin, C.-H., 2005. Lipoteichoic acid induces nuclear factor-kappaB activation and nitric oxide synthase expression via phosphatidylinositol 3-kinase, Akt, and p38 MAPK in RAW 264.7 macrophages *Immunology*, 115(3), pp.366–374.

Kasha, M., 1950. Characterization of electronic transitions in complex molecules. *Discussions of the Faraday Society*, 9(0), p.14.

Kauzmann, W., 1987. Thermodynamics of unfolding . *Nature*, 325(6107), pp.763–764.

Kawai, T. and Akira, S., 2007. Signaling to NF-κB by Toll-like receptors. *Trends in Molecular Medicine*, 13(11), pp.460–469.

Keeler, C., Poon, G., Kuo, I.Y., Ehrlich, B.E., and Hodsdon, M.E., 2013. An Explicit Formulation Approach for the Analysis of Calcium Binding to EF-Hand Proteins Using Isothermal Titration Calorimetry. *Biophysical Journal*, 105(12), p.2843.

Kelkar, D.A., Chaudhuri, A., Haldar, S., and Chattopadhyay, A., 2010. Exploring tryptophan dynamics in acid-induced molten globule state of bovine α-lactalbumin: A wavelength-selective fluorescence approach. *European Biophysics Journal*, 39(10), pp.1453–1463.

Keller, S., Vargas, C., Zhao, H., Piszczek, G., Brautigam, C.A., and Schuck, P., 2012. High-Precision Isothermal Titration Calorimetry with Automated Peak-Shape Analysi.s *Analytical Chemistry*, 84(11), pp.5066–5073.

Kensche, T., Tokunaga, F., Ikeda, F., Goto, E., Iwai, K., and Dikic, I., 2012. Analysis of nuclear factor-κB (NF-κB) essential modulator (NEMO) binding to linear and lysine-linked ubiquitin chains and its role in the activation of NF-κB [Online]. *Journal of Biological Chemistry*, 287(28), pp.23626–23634.

Kharakoz, D.P., 2000. Protein compressibility, dynamics, and pressure. *Biophysical Journal*, 79(1), pp.511–525.

Kharakoz, D.P. and Sarvazyan, A.P., 1993. Hydrational and intrinsic compressibilities of globular proteins. *Biopolymers*, 33(1), pp.11–26.

Kida, Y., Kobayashi, M., Suzuki, T., Takeshita, A., Okamatsu, Y., Hanazawa, S., Yasui, T., and Hasegawa, K., 2005. Interleukin-1 stimulates cytokines, prostaglandin E 2 and matrix metalloproteinase-1 production via activation of MAPK/AP-1 and NF-κB in human gingival fibroblasts. *Cytokine*, 29(4), pp.159–168.

Kim, B.-Y., Yang, J.-S., Kwak, S.-Y., Zhang, X., and Han, Y.-H., 2010. NEMO stabilizes c-Myc through direct interaction in the nucleus. *FEBS Letters*, 584(22), pp.4524–4530.

Kim, M.L., Jeong, H.G., Kasper, C.A., and Arrieumerlou, C., 2010. IKKα contributes to canonical NF-κB activation downstream of Nod1-mediated peptidoglycan recognition. *PLoS ONE*, 5(10), p.e15371.

Kitahara, R., Yamada, H., Akasaka, K., and Wright, P.E., 2002. High Pressure NMR Reveals that Apomyoglobin is an Equilibrium Mixture from the Native to the Unfolded. *Journal of Molecular Biology*, 320(2), pp.311–319.

Kleinpoppen, H. and Becker, U., 1999. Interactions of polarized electrons and polarized photons with atoms and molecules. *Philosophical Transactions of the Royal Society A: Mathematical, Physical and Engineering Sciences*, 357(1755), pp.1229–1258.

Komander, D. and Rape, M., 2012. The Ubiquitin Code. *Annual Review of Biochemistry*, 81(1), pp.203–229.

Komander, D., Reyes-Turcu, F., Licchesi, J.D.F., Odenwaelder, P., Wilkinson, K.D., and Barford, D., 2009. Molecular discrimination of structurally equivalent Lys 63-linked and linear polyubiquitin chains. *EMBO reports*, 10(5), pp.466–73.

Konig, H.-G., Fenner, B.J., Byrne, J.C., Schwamborn, R.F., Bernas, T., Jefferies, C.A., and Prehn, J.H.M., 2012. Fibroblast growth factor homologous factor 1 interacts with NEMO to regulate NF- B signaling in neurons. *Journal of Cell Science*, 125(24), pp.6058–6070.

König, H.G., Watters, O., Kinsella, S., Ameen, M., Fenner, B.J., and Prehn, J.H.M., 2018. A constitutively-active IKK-complex at the axon initial segment. *Brain Research*, 1678, pp.356–366.

Kononenko, A. V., Mitkevich, V.A., Atkinson, G.C., Tenson, T., Dubovaya, V.I., Frolova, L.Y., Makarov, A.A., and Hauryliuk, V., 2010. GTP-dependent structural rearrangement of the eRF1:eRF3 complex and eRF3 sequence motifs essential for PABP binding. *Nucleic Acids Research*, 38(2), pp.548–558.

Koo, J.W., Russo, S.J., Ferguson, D., Nestler, E.J., and Duman, R.S., 2010. Nuclear factor- B is a critical mediator of stress-impaired neurogenesis and depressive behavior. *Proceedings of the National Academy of Sciences*, 107(6), pp.2669–2674.

Kornegay, J.N., Peterson, J.M., Bogan, D.J., Kline, W., Bogan, J.R., Dow, J.L., Fan, Z., Wang, J., Ahn, M., Zhu, H., Styner, M., and Guttridge, D.C., 2014. NBD delivery improves the disease phenotype of the golden retriever model of Duchenne muscular dystrophy. *Skeletal muscle*, 4, p.18.

Kosower, E.M. and Huppert, D., 1986. Excited State Electron and Proton Transfers. *Annual Review of Physical Chemistry*, 37(1), pp.127–156.

Kosower, E.M. and Kanety, H., 1983. Intramolecular donor-acceptor systems. 10. Multiple fluorescences from 8-(N-phenylamino)-1-naphthalenesulfonates. *Journal of the American Chemical Society*, 105(20), pp.6236–6243.

Kovalenko, A., Chable-Bessia, C., Cantarella, G., Israël, A., Wallach, D., and Courtois, G., 2003. The tumour suppressor CYLD negatively regulates NF-κB signalling by deubiquitination. *Nature*, 424(6950), pp.801–805.

Kremer, W., Arnold, M., Munte, C.E., Hartl, R., Erlach, M.B., Koehler, J., Meier, A., and Kalbitzer, H.R., 2011. Pulsed Pressure Perturbations, an Extra Dimension in NMR Spectroscopy of Proteins. *Journal of the American Chemical Society*, 133(34), pp.13646–13651.

Kumar, Aseem, Kumar, Anand, Michael, P., Brabant, D., Parissenti, A.M., Ramana, C. V., Xu, X., and Parrillo, J.E., 2005. Human Serum from Patients with Septic Shock Activates Transcription Factors STAT1, IRF1, and NF-κB and Induces Apoptosis in Human Cardiac Myocytes. *Journal of Biological Chemistry*, 280(52), pp.42619–42626.

Kumar, R., 2009. Role of naturally occurring osmolytes in protein folding and stability. *Arch Biochem Biophys*. 491(1-2),pp 1-6.

Kundu, B. and Guptasarma, P., 2002. Use of a hydrophobic dye to indirectly probe the structural organization and conformational plasticity of molecules in amorphous aggregates of carbonic anhydrase . *Biochemical and Biophysical Research Communications*, 293(1), pp.572–577.

Kurpiewska, K. and Lewiński, K., 2010. High pressure macromolecular crystallography for structural biology: a review. *Open Life Sciences*, 5(5), pp.531–542.

Kuznetsova, I.M., Turoverov, K.K., and Uversky, V.N., 2014. What macromolecular crowding can do to a protein. *International Journal of Molecular Sciences*, 15(12), pp.23090–23140.

Kwak, Y.T., Guo, J., Shen, J., and Gaynor, R.B., 2000. Analysis of Domains in the IKK and IKK Proteins That Regulate Their Kinase Activity. *J Biol Chem*. 275(19),pp.14752-9.

Lakowicz, J.R., 2006. *Principles of Fluorescence Spectroscopy Principles of Fluorescence Spectroscopy*.

Lakowicz, J.R. and Weber, G., 1973. Quenching of fluorescence by oxygen. Probe for structural fluctuations in macromolecules. *Biochemistry*, 12(21), pp.4161–4170.

Laplantine, E., Fontan, E., Chiaravalli, J., Lopez, T., Lakisic, G., Véron, M., Agou, F., and Israël, A., 2009. NEMO specifically recognizes K63-linked poly-ubiquitin chains through a new bipartite ubiquitin-binding domain. *The EMBO journal*, 28(19), pp.2885–95.

Larabi, A., Devos, J.M., Ng, S.-L., Nanao, M.H., Round, A., Maniatis, T., and Panne, D., 2013. Crystal structure and mechanism of activation of TANK-binding kinase 1. *Cell reports*, 3(3), pp.734–46.

Latz, E., Verma, A., Visintin, A., Gong, M., Sirois, C.M., Klein, D.C.G., Monks, B.G., McKnight, C.J., Lamphier, M.S., Duprex, W.P., Espevik, T., and Golenbock, D.T., 2007. Ligand-induced conformational changes allosterically activate Toll-like receptor 9. *Nature Immunology*, 8(7), pp.772–779.

Laursen, T., Singha, A., Rantzau, N., Tutkus, M., Borch, J., Hedegård, P., Stamou, D., Møller, B.L., and Hatzakis, N.S., 2014. Single molecule activity measurements of cytochrome P450 oxidoreductase reveal the existence of two discrete functional states. *ACS Chem Biol*. 9(3)pp.630-4.

Laverdant, J., de Marcillac, W.D., Barthou, C., Chinh, V.D., Schwob, C., Coolen, L., Benalloul, P., Nga, P.T., and Maitre, A., 2011. Experimental Determination of the Fluorescence Quantum Yield of Semiconductor Nanocrystals. *Materials*, 4(7), pp.1182–1193.

Lawrence, T., 2009. The nuclear factor NF-kappaB pathway in inflammation.*Cold Spring Harbor perspectives in biology*, 1(6), p.a001651.

LeBlanc, S., Kulkarni, P., and Weninger, K., 2018. Single Molecule FRET: A Powerful Tool to Study Intrinsically Disordered Proteins. *Biomolecules*, 8(4), p.140.

Lee, D.F., Kuo, H.P., Chen, C. Te, Hsu, J.M., Chou, C.K., Wei, Y., Sun, H.L., Li, L.Y., Ping, B., Huang, W.C., He, X., Hung, J.Y., Lai, C.C., Ding, Q., Su, J.L., Yang, J.Y., Sahin, A.A., Hortobagyi, G.N., Tsai, F.J., Tsai, C.H., and Hung, M.C., 2007. IKKβ Suppression of TSC1 Links Inflammation and Tumor Angiogenesis via the mTOR Pathway. *Cell*, 130(3), pp.440–455.

Lee, D.L., Ivaninskii, S., Burkhard, P., and Hodges, R.S., 2003. Unique stabilizing interactions identified in the two-stranded alpha-helical coiled-coil: crystal structure of a cortexillin I/GCN4 hybrid coiled-coil peptide. *Protein science : a publication of the Protein Society*, 12(7), pp.1395–405.

Lehoczki, G., Szabó, K., Takács, I., Kandra, L., and Gyémánt, G., 2016. Simple ITC method for activity and inhibition studies on human salivary α-amylase. *Journal of Enzyme Inhibition and Medicinal Chemistry*, 31(6), pp.1648–1653.

Lerch, M.T., López, C.J., Yang, Z., Kreitman, M.J., Horwitz, J., and Hubbell, W.L., 2015. Structure-relaxation mechanism for the response of T4 lysozyme cavity mutants to hydrostatic pressure. *Proceedings of the*

National Academy of Sciences, 112(19), pp.E2437–E2446.

Lernbecher, T., Müller, U., and Wirth, T., 1993. Distinct NF-κB/Rel transcription factors are responsible for tissue-specific and inducible gene activation. *Nature*, 365(6448), pp.767–770.

Levy, Y. and Onuchic, J.N., 2004. Water and proteins: A love-hate relationship. *Proceedings of the National Academy of Sciences*, 101(10), pp.3325–3326.

Lewis, E.K., Haaland, W.C., Nguyen, F., Heller, D.A., Allen, M.J., MacGregor, R.R., Berger, C.S., Willingham, B., Burns, L.A., Scott, G.B.I., Kittrell, C., Johnson, B.R., Curl, R.F., and Metzker, M.L., 2005. Color-blind fluorescence detection for four-color DNA sequencing. *Proceedings of the National Academy of Sciences of the United States of America*, 102(15), pp.5346–51.

Li, J., Peet, G.W., Pullen, S.S., Schembri-king, J., Warren, T.C., Marcu, K.B., Kehry, M.R., Barton, R., and Jakes, S., 1998. Recombinant IκB Kinases α and β Are Direct Kinases of IκBα. *The Journal of Biological Chemistry*, 273(46), pp.30736–30741.

Li, J., Yin, Q., and Wu, H., 2013. Structural basis of signal transduction in the TNF receptor superfamily. *Advances in immunology*, 119, pp.135–53.

Li, Q., Van Antwerp, D., Mercurio, F., Lee, K.F., and Verma, I.M., 1999. Severe liver degeneration in mice lacking the IkappaB kinase 2 gene. *Science (New York, N.Y.)*, 284(5412), pp.321–5.

Li, Y., Kang, J., Friedman, J., Tarassishin, L., Ye, J., Kovalenko, A., Wallach, D., and Horwitz, M.S., 1999. Identification of a cell protein (FIP-3) as a modulator of NF-B activity and as a target of an adenovirus inhibitor of tumor necrosis factor-induced apoptosis. *Proc Natl Acad Sci U S A.* 96(3)pp.1042-7.

Liang, L., Wang, X., Xing, D., Chen, T., and Chen, W.R., 2009. Noninvasive determination of cell nucleoplasmic viscosity by fluorescence correlation spectroscopy. *Journal of biomedical optics*, 14(2), p.024013.

LiCata, V.J. and Allewell, N.M., 1997. Is substrate inhibition a consequence of allostery in aspartate transcarbamylase? *Biophysical chemistry*, 64(1–3), pp.225–34.

Lin, L.-N., Brandts, J.F., Brandts, J.M., and Plotnikov, V., 2002. Determination of the Volumetric Properties of Proteins and Other Solutes Using Pressure Perturbation Calorimetry. *Analytical Biochemistry*, 302(1), pp.144–160.

Lin, S.-C., Chung, J.Y., Lamothe, B., Rajashankar, K., Lu, M., Lo, Y.-C., Lam, A.Y., Darnay, B.G., and Wu, H., 2008. Molecular basis for the unique deubiquitinating activity of the NF-kappaB inhibitor A20.. *Journal of molecular biology*, 376(2), pp.526–40.

Ling, L., Cao, Z., and Goeddel, D. V, 1998. NF-κB-inducing kinase activates IKK-α by phosphorylation of Ser-176 . *Proceedings of the National Academy of Sciences*, 95(7), pp.3792–3797.

Liu, L., Botos, I., Wang, Y., Leonard, J.N., Shiloach, J., Segal, D.M., and Davies, D.R., 2008. Structural Basis of Toll-Like Receptor 3 Signaling with Double-Stranded RNA . *Science*, 320(5874), pp.379–381.

Liu, R., Wang, Z.-H., Xu, Q., Yu, N., and Cao, M.-C., 2014. Combined use of infrared and Raman spectra in the characterization of orthoclase under various hydrostatic pressures. *Guang pu xue yu guang pu fen xi.* 34(2), pp.426–30.

Liu, S., Misquitta, Y.R., Olland, A., Johnson, M.A., Kelleher, K.S., Kriz, R., Lin, L.L., Stahl, M., and Mosyak, L., 2013. Crystal structure of a human IκB kinase β asymmetric dimer. *The Journal of biological chemistry*, 288(31), pp.22758–67.

Liu, T., Wang, Y., Luo, X., Li, J., Reed, S.A., Xiao, H., Young, T.S., and Schultz, P.G., 2016. Enhancing protein stability with extended disulfide bonds. *Proceedings of the National Academy of Sciences of the United States of America*, 113(21), pp.5910–5.

Lo, Y.-C., Lin, S.-C., Rospigliosi, C.C., Conze, D.B., Wu, C.-J., Ashwell, J.D., Eliezer, D., and Wu, H., 2009. Structural basis for recognition of diubiquitins by NEMO. *Molecular cell*, 33(5), pp.602–15.

Lo, Y.C., Maddineni, U., Chung, J.Y., Rich, R.L., Myszka, D.G., and Wu, H., 2008. High-affinity interaction between IKKβ and NEMO. *Biochemistry*, 47(10), pp.3109–3116.

Lombardi, M., Canter, J., Patrick, P.A., and Altman, R., 2015. Is Fluorescence Under an Alternate Light Source Sufficient to Accurately Diagnose Subclinical Bruising? *Journal of Forensic Sciences*, 60(2), pp.444–449.

Long, J., Garner, T.P., Pandya, M.J., Craven, C.J., Chen, P., Shaw, B., Williamson, M.P., Layfield, R., and Searle, M.S., 2010. Dimerisation of the UBA Domain of p62 Inhibits Ubiquitin Binding and Regulates NF-κB Signalling . *Journal of Molecular Biology*, 396(1), pp.178–194.

Lonhienne, T., Baise, E., Feller, G., Bouriotis, V., and Gerday, C., 2001. Enzyme activity determination on macromolecular substrates by isothermal titration calorimetry: Application to mesophilic and psychrophilic chitinases. *Biochimica et Biophysica Acta - Protein Structure and Molecular Enzymology*, 1545(1–2), pp.349–356.

Luedde, T., Beraza, N., Kotsikoris, V., van Loo, G., Nenci, A., De Vos, R., Roskams, T., Trautwein, C., and Pasparakis, M., 2007. Deletion of NEMO/IKKγ in Liver Parenchymal Cells Causes Steatohepatitis and Hepatocellular Carcinoma. *Cancer Cell*, 11(2), pp.119–132.

Luong, T.Q. and Winter, R., 2015. Combined pressure and cosolvent effects on enzyme activity - a high-pressure stopped-flow kinetic study on α-chymotrypsin. *Physical chemistry chemical physics : PCCP*, 17(35), pp.23273–8.

Lymperopoulos, A., Karkoulias, G., Koch, W.J., and Flordellis, C.S., 2006. α2-Adrenergic receptor subtype-specific activation of NF-κB in PC12 cells *Neuroscience Letters*, 402(3), pp.210–215.

Ma, H., Deacon, S., and Horiuchi, K., 2008. The challenge of selecting protein kinase assays for lead discovery optimization. *Expert opinion on drug discovery*, 3(6), pp.607–621.

Ma, L. and Cui, Q., 2006. The temperature dependence of salt-protein association is sequence specific.. *Biochemistry*, 45(48), pp.14466–72.

Ma, L., Yang, F., and Zheng, J., 2014. Application of fluorescence resonance energy transfer in protein studies.. *Journal of molecular structure*, 1077, pp.87–100.

Mabb, A.M., Wuerzberger-Davis, S.M., and Miyamoto, S., 2006. PIASγ mediates NEMO sumoylation and NF-κB activation in response to genotoxic stress. *Nature Cell Biology*, 8(9), pp.986–993.

Madge, L.A., Kluger, M.S., Orange, J.S., and May, M.J., 2008. Lymphotoxin- 1 2 and LIGHT Induce Classical and Noncanonical NF- B-Dependent Proinflammatory Gene Expression in Vascular Endothelial Cells *The Journal of Immunology*, 180(5), pp.3467–3477.

Madonna, R., Massaro, M., Pandolfi, A., Consoli, A., and De Caterina, R., 2007. The prominent role of p38 mitogen-activated protein kinase in insulin-mediated enhancement of VCAM-1 expression in endothelial cells. *International journal of immunopathology and pharmacology*, 20(3), pp.539–55.

Magde, D., Rojas, G.E., and Seybold, P.G., 1999. Solvent Dependence of the Fluorescence Lifetimes of Xanthene Dyes *Photochemistry and Photobiology*, 70(5), pp.737–744.

Maglia, G., Jonckheer, A., De Maeyer, M., Frère, J.-M., and Engelborghs, Y., 2008. An unusual red-edge excitation and time-dependent Stokes shift in the single tryptophan mutant protein DD-carboxypeptidase from Streptomyces: the role of dynamics and tryptophan rotamers. *Protein science : a publication of the Protein Society*, 17(2), pp.352–61.

Mahoney, D.J., Cheung, H.H., Mrad, R.L., Plenchette, S., Simard, C., Enwere, E., Arora, V., Mak, T.W., Lacasse, E.C.,

Waring, J., and Korneluk, R.G., 2008. Both cIAP1 and cIAP2 regulate TNF -mediated NF- B activation *Proceedings of the National Academy of Sciences*, 105(33), pp.11778–11783.

Maillard, M.C., Dominguez, C., Gemkow, M.J., Krieger, F., Park, H., Schaertl, S., Winkler, D., and Muñoz-Sanjuán, I., 2013. A label-free LC/MS/MS-based enzymatic activity assay for the detection of genuine caspase inhibitors and SAR development. *Journal of Biomolecular Screening*, 18(8), pp.868–878.

Makris, C., Roberts, J.L., and Karin, M., 2002. The Carboxyl-Terminal Region of I B Kinase (IKK) Is Required for Full IKK Activation. *Molecular and Cellular Biology*, 22(18), pp.6573–6581.

Maldonado, A.Y., Burz, D.S., and Shekhtman, A., 2011. Progress in Nuclear Magnetic Resonance Spectroscopy In-cell NMR spectroscopy. *Progress in Nuclear Magnetic Resonance Spectroscopy*, 59(3), pp.197–212.

Malek, S., Huang, D.-B., Huxford, T., Ghosh, S., and Ghosh, G., 2003. X-ray crystal structure of an IkappaBbeta x NF-kappaB p65 homodimer complex. *The Journal of biological chemistry*, 278(25), pp.23094–100.

Malgieri, G., Palmieri, M., Russo, L., Fattorusso, R., Pedone, P. V., and Isernia, C., 2015. The prokaryotic zinc-finger: Structure, function and comparison with the eukaryotic counterpart. *FEBS Journal*, 282(23), pp.4480–4496.

Malinin, N.L., Boldin, M.P., Kovalenko, A. V., and Wallach, D., 1997. MAP3K-related kinase involved in NF-KB induction by TNF, CD95 and IL-1. *Nature*, 385(6616), pp.540–544.

Martinez, O., Valmas, C., and Basler, C.F., 2007. Ebola virus-like particle-induced activation of NF-κB and Erk signaling in human dendritic cells requires the glycoprotein mucin domain. *Virology*, 364(2), pp.342–354.

Martini, S., Bonechi, C., Foletti, A., and Rossi, C., 2013. Water-protein interactions: the secret of protein dynamics. *TheScientificWorldJournal*, 2013, p.138916.

Mason, J.M., Schmitz, M.A., Muller, K.M., and Arndt, K.M., 2006. Semirational design of Jun-Fos coiled coils with increased affinity: Universal implications for leucine zipper prediction and design .*Proceedings of the National Academy of Sciences*, 103(24), pp.8989–8994.

Masson, P., Cléry, C., Guerra, P., Redslob, A., Albaret, C., and Fortier, P.L., 1999. Hydration change during the aging of phosphorylated human butyrylcholinesterase: importance of residues aspartate-70 and glutamate-197 in the water network as probed by hydrostatic and osmotic pressures. *The Biochemical journal*, 343 Pt 2, pp.361–9.

Matsuda, A., Suzuki, Y., Honda, G., Muramatsu, S., Matsuzaki, O., Nagano, Y., Doi, T., Shimotohno, K., Harada, T., Nishida, E., Hayashi, H., and Sugano, S., 2003. Large-scale identification and characterization of human genes that activate NF-kappaB and MAPK signaling pathways. *Oncogene*, 22(21), pp.3307–18.

Matsuo, N., Goda, N., Shimizu, K., Fukuchi, S., Ota, M., and Hiroaki, H., 2018. Discovery of cryoprotective activity in human genome-derived intrinsically disordered proteins. *International Journal of Molecular Sciences*, 19(2).

Matta, H., Sun, Q., Moses, G., and Chaudhary, P.M., 2003. Molecular Genetic Analysis of Human Herpes Virus 8-encoded Viral FLICE Inhibitory Protein-induced NF-κB Activation [Online]. *Journal of Biological Chemistry*, 278(52), pp.52406–52411.

Mátyus, L., Szöllősi, J., and Jenei, A., 2006. Steady-state fluorescence quenching applications for studying protein structure and dynamics. *Journal of Photochemistry and Photobiology B: Biology*, 83(3), pp.223–236.

Maubach, G. and Naumann, M., 2017. NEMO Links Nuclear Factor-kB to Human Diseases [Online]. *Tends in molecular medicine*, 23(12), pp.1138–1155.

May, M.J., D'Acquisto, F., Madge, L.A., Glöckner, J., Pober, J.S., and Ghosh, S., 2000. Selective inhibition of NF-KB Activation by a Peptide That Blocks the Interaction of NEMO with the IKB Kinase Complex. *Science*, 289(5484), pp.1550–4.

Mazzei, L., Ciurli, S., and Zambelli, B., 2014. Hot Biological Catalysis: Isothermal Titration Calorimetry to Characterize

Enzymatic Reactions. *Journal of Visualized Experiments*, (86), pp.514873791–51487.

McCarthy, A.N. and Grigera, J.R., 2006. Pressure denaturation of apomyoglobin: A molecular dynamics simulation study. *Biochimica et Biophysica Acta (BBA) - Proteins and Proteomics*, 1764(3), pp.506–515.

McClure, W.R., 1969. A Kinetic Analysis of Coupled Enzyme Assays. *Biochemistry*, 8(7), pp.2782–2786.

McKenzie, F.R., Connelly, M. a, Balzarano, D., Müller, J.R., Geleziunas, R., and Marcu, K.B., 2000. Functional isoforms of IkappaB kinase alpha (IKKalpha) lacking leucine zipper and helix-loop-helix domains reveal that IKKalpha and IKKbeta have different activation requirements. *Molecular and cellular biology*, 20(8), pp.2635–49.

McRae, J.M., Falconer, R.J., and Kennedy, J.A., 2010. Thermodynamics of Grape and Wine Tannin Interaction with Polyproline: Implications for Red Wine Astringency. *Journal of Agricultural and Food Chemistry*, 58(23), pp.12510–12518.

Mémet, S., 2006. NF-κB functions in the nervous system: From development to disease. *Biochemical Pharmacology*, 72(9 SPEC. ISS.), pp.1180–1195.

Menter, J.M., 2006. Temperature dependence of collagen fluorescence. *Photochemical & Photobiological Sciences*, 5(4), p.403.

Mercurio, F., Murray, B.W., Shevchenko, A., Bennett, B.L., Young, D.B., Li, J.W., Pascual, G., Motiwala, A., Zhu, H., Mann, M., and Manning, A.M., 1999. IkappaB kinase (IKK)-associated protein 1, a common component of the heterogeneous IKK complex. *Molecular and cellular biology*, 19(2), pp.1526–38.

Mercurio, F., Zhu, H., Murray, B.W., Shevchenko, A., Bennett, B.L., Li, J.W., Young, D.B., Barbosa, M., Mann, M., Manning, A., and Rao, A., 1997. IKK-1 and IKK-2: Cytokine-activated IκB kinases essential for NF-κB activation. *Science*, 278(5339), pp.860–866.

Metallo, S.J., 2010. Intrinsically disordered proteins are potential drug target.s *Current Opinion in Chemical Biology*, 14(4), pp.481–488.

Meyer, E., Aglyamova, G. V, Wang, S., Buchanan-Carter, J., Abrego, D., Colbourne, J.K., Willis, B.L., and Matz, M. V, 2009. Sequencing and de novo analysis of a coral larval transcriptome using 454 GSFlx *BMC Genomics*, 10(1), p.219.

Michels, P.C. and Clark, D.S., 1997. Pressure-enhanced activity and stability of a hyperthermophilic protease from a deep-sea methanogen. *Applied and environmental microbiology*, 63(10), pp.3985–91.

Middleton, G., Hamanoue, M., Enokido, Y., Wyatt, S., Pennica, D., Jaffray, E., Hay, R.T., and Davies, A.M., 2000. Cytokine-induced nuclear factor kappa B activation promotes the survival of developing neurons. *The Journal of cell biology*, 148(2), pp.325–32.

Millero, F.J., Ward, G.K., and Chetirkin, P., 1976. Partial specific volume, expansibility, compressibility, and heat capacity of aqueous lysozyme solutions *The Journal of biological chemistry*, 251(13), pp.4001–4.

Minor, P.D., 2015. Live attenuated vaccines: Historical successes and current challenges. *Virology*, 479–480, pp.379–392.

Mitić, S., Strampraad, M.J.F., Hagen, W.R., and de Vries, S., 2017. Microsecond time-scale kinetics of transient biochemical reactions. *PloS one*, 12(10), p.e0185888.

Mitra, L., Rouget, J.B., Garcia-Moreno, B., Royer, C.A., and Winter, R., 2008. Towards a quantitative understanding of protein hydration and volumetric properties. *ChemPhysChem*, 9(18), pp.2715–2721.

Mitra, L., Smolin, N., Ravindra, R., Royer, C., and Winter, R., 2006. Pressure perturbation calorimetric studies of the solvation properties and the thermal unfolding of proteins in solution—experiments and theoretical interpretation. *Physical Chemistry Chemical Physics*, 8(11), p.1249.

Mitra, M., Chaudhuri, A., Patra, M., Mukhopadhyay, C., Chakrabarti, A., and Chattopadhyay, A., 2015. Organization

and dynamics of tryptophan residues in brain spectrin: novel insight into conformational flexibility. *Journal of fluorescence*, 25(3), pp.707–17.

Molina, H., Horn, D.M., Tang, N., Mathivanan, S., and Pandey, A., 2007. Global proteomic profiling of phosphopeptides using electron transfer dissociation tandem mass spectrometry .*Proceedings of the National Academy of Sciences*, 104(7), pp.2199–2204.

Mondal, S., Roy, A., Jana, A., Ghosh, S., Kordower, J.H., and Pahan, K., 2012. Testing NF-κB-based Therapy in Hemiparkinsonian Monkeys. *Journal of Neuroimmune Pharmacology*, 7(3), pp.544–556.

Monteith, W.B., Cohen, R.D., Smith, A.E., Guzman-Cisneros, E., Pielak, G.J., Designed, G.J.P., and Performed, C, 2015. Quinary structure modulates protein stability in cells. *Proc Natl Acad Sci U S A* 10(6), pp.1739–1742.

Moore, R.A., Lee, J., and Robinson, G.W., 1985. Hydration dynamics of electrons from a fluorescent probe molecule [Online]. *The Journal of Physical Chemistry*, 89(17), pp.3648–3654.

Morin, P.E. and Freire, E., 1991. Direct Calorimetric Analysis of the Enzymatic Activity of Yeast Cytochrome c Oxidase1.. *Biochemistry*, 30, pp.8494–8500.

Morrison, M.D., Reiley, W., Zhang, M., and Sun, S.-C., 2005. An Atypical Tumor Necrosis Factor (TNF) Receptor-associated Factor-binding Motif of B Cell-activating Factor Belonging to the TNF Family (BAFF) Receptor Mediates Induction of the Noncanonical NF-κB Signaling Pathway. *Journal of Biological Chemistry*, 280(11), pp.10018–10024.

Mosavi, L.K., Cammett, T.J., Desrosiers, D.C., and Peng, Z.-Y., 2004. The ankyrin repeat as molecular architecture for protein recognition. *Protein science : a publication of the Protein Society*, 13(6), pp.1435–48.

Mozhaev, V. V, Heremans, K., Frank, J., Masson, P., and Balny, C., 1996. High pressure effects on protein structure and function. *Proteins: Structure, Function and Genetics*, 24(1), pp.81–91.

Munishkina, L.A. and Fink, A.L., 2007. Fluorescence as a method to reveal structures and membrane-interactions of amyloidogenic proteins. *Biochimica et Biophysica Acta (BBA) - Biomembranes*, 1768(8), pp.1862–1885.

Muñoz-Pinedo, C., 2012. Signaling Pathways that Regulate Life and Cell Death: Evolution of Apoptosis in the Context of Self-Defense. In: *Advances in experimental medicine and biology*. pp.124–143.

Muñoz, V. and Luis, S., 1995. Elucidating the Folding Problem of Helical Peptides using Empirical Parameters. III. Temperature and pH Dependence. *J. Mol. Biol*, 245, pp.297–308.

Muñoz, V. and Serrano, L., 1995. Elucidating the folding problem of helical peptides using empirical parameters. II†. Helix macrodipole effects and rational modification of the helical content of natural peptides. *Journal of Molecular Biology*, 245(3), pp.275–296.

Nakagawa, M.M. and Rathinam, C.V., 2018. Constitutive Activation of the Canonical NF-κB Pathway Leads to Bone Marrow Failure and Induction of Erythroid Signature in Hematopoietic Stem Cells. *Cell Reports*, 25, pp.2094-2109.e4.

Nakamori, Y., Emoto, M., Fukuda, N., Taguchi, A., Okuya, S., Tajiri, M., Miyagishi, M., Taira, K., Wada, Y., and Tanizawa, Y., 2006. Myosin motor Myo1c and its receptor NEMO/IKK-γ promote TNF-α-induced serine307phosphorylation of IRS-1. *Journal of Cell Biology*, 173(5), pp.665–671.

Nakasako, M., Fujisawa, T., Adachi, S.-I., Kudo, T., and Higuchi, S., 2001. Large-Scale Domain Movements and Hydration Structure Changes in the Active-Site Cleft of Unligated Glutamate Dehydrogenase from Thermococcus profundus Studied by Cryogenic X-ray Crystal Structure Analysis and Small-Angle X-ray Scattering. *Biochemistry*, 40, pp.3069–3079.

Napetschnig, J. and Wu, H., 2013. Molecular Basis of NF-κB Signaling . *Annual Review of Biophysics*, 42(March), pp.443–68.

Náray-Szabó, G., Oláh, J., and Krámos, B., 2013. Quantum Mechanical Modeling: A Tool for the Understanding of Enzyme Reactions. *Biomolecules*, 3(4), pp.662–702.

Nayak, A., Kapur, A., Barroilhet, L., Patankar, M., Nayak, A.P., Kapur, A., Barroilhet, L., and Patankar, M.S., 2018. Oxidative Phosphorylation: A Target for Novel Therapeutic Strategies Against Ovarian Cancer. *Cancers*, 10(9), p.337.

Ngadjeua, F., Chiaravalli, J., Traincard, F., Raynal, B., Fontan, E., and Agou, F., 2013. Two-sided ubiquitin binding of NF-κB essential modulator (NEMO) zinc finger unveiled by a mutation associated with anhidrotic ectodermal dysplasia with immunodeficiency syndrome. *The Journal of biological chemistry*, 288(47), pp.33722–37.

Nick Pace, C., Scholtz, J.M., and Grimsley, G.R., 2014. Forces stabilizing proteins. *FEBS Letters*, 588(14), pp.2177–2184.

Niemi, N.M. and MacKeigan, J.P., 2013. Mitochondrial phosphorylation in apoptosis: flipping the death switch. *Antioxidants & redox signaling*, 19(6), pp.572–82.

Nieuwenhuysen, P., Heremans, K., and Clauwaert, J., 1980. High-pressure scattering study of Artemia salina ribosomes and polysomes. *Biochimica et biophysica acta*, 606(2), pp.292–303.

Nishi, H., Hashimoto, K., and Panchenko, A.R., 2011. Phosphorylation in protein-protein binding: effect on stability and function. *Structure (London, England : 1993)*, 19(12), pp.1807–15.

Nisius, L. and Grzesiek, S., 2012. Key stabilizing elements of protein structure identified through pressure and temperature perturbation of its hydrogen bond network. *Nature Chemistry*, 4(9), pp.711–717.

Noraini, M.Y., Ong, H.C., Badrul, M.J., and Chong, W.T., 2014. A review on potential enzymatic reaction for biofuel production from algae. *Renewable and Sustainable Energy Reviews*, 39, pp.24–34.

Noske, R., Cornelius, F., and Clarke, R.J., 2010. Investigation of the enzymatic activity of the Na+,K+-ATPase via isothermal titration microcalorimetry. *Biochimica et Biophysica Acta - Bioenergetics*, 1797(8), pp.1540–1545.

Nussinov, R., Ma, B., and Tsai, C.-J., 2014. Multiple conformational selection and induced fit events take place in allosteric propagation. *Biophysical Chemistry*, 186, pp.22–30.

O'Dea, E. and Hoffmann, A., 2009. NF-κB signaling. *Wiley interdisciplinary reviews. Systems biology and medicine*, 1(1), pp.107–15.

O'Dea, E.L., Barken, D., Peralta, R.Q., Tran, K.T., Werner, S.L., Kearns, J.D., Levchenko, A., and Hoffmann, A., 2007. A homeostatic model of IkappaB metabolism to control constitutive NF-kappaB activity. *Molecular systems biology*, 3, p.111.

O'Dea, E.L., Kearns, J.D., and Hoffmann, A., 2008. UV as an amplifier rather than inducer of NF-kappaB activity. *Molecular cell*, 30(5), pp.632–41.

Okazaki, K., Sato, T., and Takano, M., 2012. Temperature-Enhanced Association of Proteins Due to Electrostatic Interaction: A Coarse-Grained Simulation of Actin–Myosin Binding *Journal of the American Chemical Society*, 134(21), pp.8918–8925.

Oliveira, A.C., Gaspar, L.P., Da Poian, A.T., and Silva, J.L., 1994. Arc Repressor will not Denature Under Pressure in the Absence of Water. *Journal of Molecular Biology*, 240(3), pp.184–187.

Olsen, J. V., Blagoev, B., Gnad, F., Macek, B., Kumar, C., Mortensen, P., and Mann, M., 2006. Global, In Vivo, and Site-Specific Phosphorylation Dynamics in Signaling Networks. *Cell*, 127(3), pp.635–648.

Pabis, A. and Kamerlin, S.C.L., 2016. Promiscuity and electrostatic flexibility in the alkaline phosphatase superfamily. *Current Opinion in Structural Biology*, 37, pp.14–21.

Pace, C.N., Grimsley, G.R., Thomson, J.A., and Barnett, B.J., 1988. Conformational stability and activity of ribonuclease T1 with zero, one, and two intact disulfide bonds. *The Journal of biological chemistry*, 263(24),

pp.11820–5.

Paci, E. and Marchi, M., 1996. Intrinsic compressibility and volume compression in solvated proteins by molecular dynamics simulation at high pressure. *Proceedings of the National Academy of Sciences of the United States of America*, 93(21), pp.11609–11614.

Palkowitsch, L., Leidner, J., Ghosh, S., and Marienfeld, R.B., 2008. Phosphorylation of serine 68 in the IkappaB Kinase (IKK)-binding domain of NEMO interferes with the structure of the IKK complex and tumor necrosis factor-kappa-induced NF-kappB activity. *Journal of Biological Chemistry*, 283(1), pp.76–86.

Pan, C.-P., Callis, P.R., and Barkley, M.D., 2006. Dependence of tryptophan emission wavelength on conformation in cyclic hexapeptides. *The journal of physical chemistry. B*, 110(13), pp.7009–16.

Pancsa, R. and Tompa, P., 2012. Structural disorder in eukaryotes. [Online]. *PloS one*, 7(4), p.e34687.

Pandya, C., Farelli, J.D., Dunaway-Mariano, D., and Allen, K.N., 2014. Enzyme promiscuity: engine of evolutionary innovation. *The Journal of biological chemistry*, 289(44), pp.30229–36.

Pant, S., Tripathi, H.B., and Pant, D.D., 1995. Solvent polarity and viscosity effect on the fluorescence spectrum and excited state lifetime of quinine dication. *Journal of Photochemistry and Photobiology A: Chemistry*, 85(1–2), pp.33–38.

Park, M. and Hong, J., 2016. Roles of NF-κB in Cancer and Inflammatory Diseases and Their Therapeutic Approaches . *Cells*, 5(2), p.15.

Parker, W.C., Chakraborty, N., Vrikkis, R., Elliott, G., Smith, S., and Moyer, P.J., 2010. High-resolution intracellular viscosity measurement using time-dependent fluorescence anisotropy. *Optics express*, 18(16), pp.16607–17.

Paul, S. and Schaefer, B.C., 2013. A new look at T cell receptor signaling to nuclear factor-κB. *Trends in immunology*, 34(6), pp.269–81.

Pauli, W., 1946. *Exclusion principle and quantum mechanics. Nobel lecture* .

Payens, T.A.J. and Heremans, K., 1969. Effect of pressure on the temperature-dependent association of β-casein. *Biopolymers*, 8(3), pp.335–345.

Peng, Z., Oldfield, C.J., Xue, B., Mizianty, M.J., Dunker, A.K., Kurgan, L., and Uversky, V.N., 2014. A creature with a hundred waggly tails: intrinsically disordered proteins in the ribosome. *Cellular and Molecular Life Sciences*, 71(8), pp.1477–1504.

Pennington, C., Dunn, J., Li, C., Ha, T., and Browder, W., 2000. Nuclear factor kappaB activation in acute appendicitis: a molecular marker for extent of disease? *The American surgeon*, 66(10), pp.914–8; discussion 918-9.

Perna, V., Agger, J.W., Holck, J., and Meyer, A.S., 2018. Multiple Reaction Monitoring for quantitative laccase kinetics by LC-MS.. *Scientific Reports*, 8(1), p.8114.

Peterson, J., Kline, W., Canan, B.D., Ricca, D.J., Kaspar, B., Delfín, D.A., DiRienzo, K., Clemens, P.R., Robbins, P.D., Baldwin, A.S., Flood, P., Kaumaya, P., Freitas, M., Kornegay, J.N., Mendell, J.R., Rafael-Fortney, J.A., Guttridge, D.C., and Janssen, P.M.L., 2011. Peptide-based inhibition of NF-κB rescues diaphragm muscle contractile dysfunction in a murine model of Duchenne muscular dystrophy. *Molecular Medicine*, 17(5–6), p.1.

Piatkevich, K.D., Malashkevich, V.N., Morozova, K.S., Nemkovich, N.A., Almo, S.C., and Verkhusha, V. V, 2013. Extended Stokes shift in fluorescent proteins: chromophore-protein interactions in a near-infrared TagRFP675 variant. *Scientific reports*, 3, p.1847.

Pickart, C.M., 2004. Back to the future with ubiquitin. [Online]. *Cell*, 116(2), pp.181–90.

Pobezinskaya, Y.L. and Liu, Z., 2012. The role of TRADD in death receptor signaling. *Cell cycle* 11(5), pp.871–6.

Da Poian, A.T., Gomes, A.M., Oliveira, R.J., and Silva, J.L., 1996. Migration of vesicular stomatitis virus glycoprotein

to the nucleus of infected cells. *Proceedings of the National Academy of Sciences of the United States of America*, 93(16), pp.8268–73.

Polley, S., Huang, D.-B., Hauenstein, A. V., Fusco, A.J., Zhong, X., Vu, D., Schröfelbauer, B., Kim, Y., Hoffmann, A., Verma, I.M., Ghosh, G., and Huxford, T., 2013. A Structural Basis for IκB Kinase 2 Activation Via Oligomerization-Dependent Trans Auto-Phosphorylation. *PLoS Biology*, 11(6), p.e1001581.

Polley, S., Passos, D.O., Huang, D. Bin, Mulero, M.C., Mazumder, A., Biswas, T., Verma, I.M., Lyumkis, D., and Ghosh, G., 2016. Structural Basis for the Activation of IKK1/α. *Cell Reports*, 17(8), pp.1907–1914.

Pontes, L., Cordeiro, Y., Giongo, V., Villas-Boas, M., Barreto, A., Araújo, J.R., and Silva, J.L., 2001. Pressure-induced formation of inactive triple-shelled rotavirus particles is associated with changes in the spike protein VP411 . *Journal of Molecular Biology*, 307(5), pp.1171–1179.

Prabhu, N. V. and Sharp, K.A., 2005. Heat Capacity In Proteins. *Annual Review of Physical Chemistry*, 56(1), pp.521–548.

Prajapati, S. and Gaynor, R.B., 2002. Regulation of Ikappa B kinase (IKK)gamma /NEMO function by IKKbeta -mediated phosphorylation. *The Journal of biological chemistry*, 277(27), pp.24331–9.

Preciado, D., Lin, J., Wuertz, B., and Rose, M., 2008. Cigarette Smoke Activates NFκB and Induces *Muc5b* Expression in Mouse Middle Ear Cells. *The Laryngoscope*, 118(3), pp.464–471.

Pu, Y., Wang, W., Yang, Y., and Alfano, R.R., 2013. Stokes shift spectroscopic analysis of multifluorophores for human cancer detection in breast and prostate tissues. [*Journal of biomedical optics*, 18(1), p.17005.

Pudney, C.R., Hay, S., Levy, C., Pang, J., Sutcliffe, M.J., Leys, D., and Scrutton, N.S., 2009. Evidence to support the hypothesis that promoting vibrations enhance the rate of an enzyme catalyzed H-tunneling reaction. *Journal of the American Chemical Society*, 131(47), pp.17072–3.

Pujol, N., Link, E.M., Liu, L.X., Kurz, C.L., Alloing, G., Tan, M.W., Ray, K.P., Solari, R., Johnson, C.D., and Ewbank, J.J., 2001. A reverse genetic analysis of components of the Toll signaling pathway in Caenorhabditis elegans. *Current biology : CB*, 11(11), pp.809–21.

Qadeer, A., Rabbani, G., Zaidi, N., Ahmad, E., Khan, J.M., and Khan, R.H., 2012. 1-Anilino-8-naphthalene sulfonate (ANS) is not a desirable probe for determining the molten globule state of chymopapain.. *PloS one*, 7(11), p.e50633.

Radivojac, P., Iakoucheva, L.M., Oldfield, C.J., Obradovic, Z., Uversky, V.N., and Dunker, A.K., 2007. Intrinsic disorder and functional proteomics. *Biophysical journal*, 92(5), pp.1439–56.

Raghuraman, H. and Chattopadhyay, A., 2006. Effect of ionic strength on folding and aggregation of the hemolytic peptide melittin in solution. *Biopolymers*, 83(2), pp.111–121.

Rahighi, S., Ikeda, F., Kawasaki, M., Akutsu, M., Suzuki, N., Kato, R., Kensche, T., Uejima, T., Bloor, S., Komander, D., Randow, F., Wakatsuki, S., and Dikic, I., 2009. Specific recognition of linear ubiquitin chains by NEMO is important for NF-kappaB activation. *Cell*, 136(6), pp.1098–109.

Rahman, M.M. and McFadden, G., 2011. Modulation of NF-κB signalling by microbial pathogens [Online]. *Nature Reviews Microbiology*, 9(4), pp.291–306.

Rana, H., Moussatche, P., Rocha, L.S., Abdellaoui, S., Minteer, S.D., and Moomaw, E.W., 2016. Isothermal titration calorimetry uncovers substrate promiscuity of bicupin oxalate oxidase from Ceriporiopsis subvermispora . *Biochemistry and Biophysics Reports*, 5, pp.396–400.

Rand, K.D., Zehl, M., Jensen, O.N., and Jørgensen, T.J.D., 2010. Loss of Ammonia during Electron-Transfer Dissociation of Deuterated Peptides as an Inherent Gauge of Gas-Phase Hydrogen Scrambling. *Analytical Chemistry*, 82(23), pp.9755–9762.

Rangasamy, S.B., Corbett, G.T., Roy, A., Modi, K.K., Bennett, D.A., Mufson, E.J., Ghosh, S., and Pahan, K., 2015. Intranasal Delivery of NEMO-Binding Domain Peptide Prevents Memory Loss in a Mouse Model of Alzheimer's Disease. *Journal of Alzheimer's Disease*, 47(2), pp.385–402.

Rawat, S.S., Kelkar, D.A., and Chattopadhyay, A., 2004. Monitoring Gramicidin Conformations in Membranes: A Fluorescence Approach. *Biophysical Journal*, 87(2), pp.831–843.

Razani, B., Zarnegar, B., Ytterberg, A.J., Shiba, T., Dempsey, P.W., Ware, C.F., Loo, J.A., and Cheng, G., 2010. Negative Feedback in Noncanonical NF- B Signaling Modulates NIK Stability Through IKK -Mediated Phosphorylation. *Science Signaling*, 3(123), pp.ra41–ra41.

Reay, D.P., Yang, M., Watchko, J.F., Daood, M., O'Day, T.L., Rehman, K.K., Guttridge, D.C., Robbins, P.D., and Clemens, P.R., 2011. Systemic delivery of NEMO binding domain/IKKγ inhibitory peptide to young mdx mice improves dystrophic skeletal muscle histopathology. *Neurobiology of Disease*, 43(3), pp.598–608.

Régnier, C.H., Song, H.Y., Gao, X., Goeddel, D. V, Cao, Z., and Rothe, M., 1997. Identification and characterization of an IkappaB kinase. *Cell*, 90(2), pp.373–83.

Reichmann, D., Xu, Y., Cremers, C.M., Ilbert, M., Mittelman, R., Fitzgerald, M.C., and Jakob, U., 2012. Order out of Disorder: Working Cycle of an Intrinsically Unfolded Chaperone . *Cell*, 148(5), pp.947–957.

Reshetnyak, Y.K., Koshevnik, Y., and Burstein, E.A., 2001. Decomposition of protein tryptophan fluorescence spectra into log-normal components. III. Correlation between fluorescence and microenvironment parameters of individual tryptophan residues. *Biophysical Journal*, 81(3), pp.1735–1758.

Rhodes, C.A., Dougherty, P.G., Cooper, J.K., Qian, Z., Lindert, S., Wang, Q.E., and Pei, D., 2018. Cell-Permeable Bicyclic Peptidyl Inhibitors against NEMO-IκB Kinase Interaction Directly from a Combinatorial Library. *Journal of the American Chemical Society*, 140(38), pp.12102–12110.

Rittinger, K. and Ikeda, F., 2017. Linear ubiquitin chains: enzymes, mechanisms and biology. *Open biology*, 7(4).

Rivas, G., Ferrone, F., and Herzfeld, J., 2004. Life in a crowded world. *EMBO reports*, 5(1), pp.23–27.

Roche, J., Caro, J.A., Norberto, D.R., Barthe, P., Roumestand, C., Schlessman, J.L., Garcia, A.E., Garcia-Moreno E., B., and Royer, C.A., 2012. Cavities determine the pressure unfolding of proteins. *Proceedings of the National Academy of Sciences*, 109(18), pp.6945–6950.

Roche, J., Dellarole, M., Royer, C.A., and Roumestand, C., 2015. Exploring the Protein Folding Pathway with High-Pressure NMR: Steady-State and Kinetics Studies. *Sub-cellular biochemistry*.72, pp.261–278.

Rogers, S., Wells, R., Rechsteiner, M., Franzoso, G., and Siebenlist, U., 1986. Amino acid sequences common to rapidly degraded proteins: the PEST hypothesis. *Science* 234(4774), pp.364–8.

Rohatgi, N., Gudmundsson, S., and Rolfsson, Ó., 2015. Kinetic analysis of gluconate phosphorylation by human gluconokinase using isothermal titration calorimetry *FEBS Letters*, 589(23), pp.3548–3555.

Romanelli, R.G., Petrai, I., Robino, G., Efsen, E., Novo, E., Bonacchi, A., Pagliai, G., Grossi, A., Parola, M., Navari, N., Delogu, W., Vizzutti, F., Rombouts, K., Gentilini, P., Laffi, G., and Marra, F., 2006. Thrombopoietin stimulates migration and activates multiple signaling pathways in hepatoblastoma cells. *American Journal of Physiology-Gastrointestinal and Liver Physiology*, 290(1), pp.G120–G128.

Rothwarf, D.M. and Karin, M., 1999. The NF- B Activation Pathway:A Paradigm in Information Transfer from Membrane to Nucleus. *Science Signaling*, 1999(5), pp.re1–re1.

Rothwarf, D.M., Zandi, E., Natoli, G., and Karin, M., 1998. IKK-gamma is an essential regulatory subunit of the IkappaB kinase complex. *Nature*, 395(6699), pp.297–300.

Royer, C.A., 2005. Insights into the role of hydration in protein structure and stability obtained through hydrostatic pressure studies. *Brazilian journal of medical and biological research = Revista brasileira de pesquisas*

médicas e biológicas / Sociedade Brasileira de Biofísica ... [et al.], 38(8), pp.1167–73.

Ruan, K., Xu, C., Li, T., Li, J., Lange, R., and Balny, C., 2003. The thermodynamic analysis of protein stabilization by sucrose and glycerol against pressure-induced unfolding: The typical example of the 33-kDa protein from spinach photosystem II. *European Journal of Biochemistry*, 270(8), pp.1654–1661.

Ruan, K., Xu, C., Yu, Y., Li, J., Lange, R., Bec, N., and Balny, C., 2001. Pressure-exploration of the 33-kDa protein from the spinach photosystem II particle [Online]. *European Journal of Biochemistry*, 268(9), pp.2742–2750.

Rudolph, D., Yeh, W.-C., Wakeham, A., Rudolph, B., Nallainathan, D., Potter, J., Elia, A.J., and Mak, T.W., 2000. Severe liver degeneration and lack of NF-B activation in NEMO/IKK-deficient mice. *Genes Dev*. 14(7)pp,854-62.

Ruotolo, B.T., Giles, K., Campuzano, I., Sandercock, A.M., Bateman, R.H., and Robinson, C. V, 2005. Evidence for macromolecular protein rings in the absence of bulk water. *Science* 310(5754), pp.1658–61.

Rushe, M., Silvian, L., Bixler, S., Chen, L.L., Cheung, A., Bowes, S., Cuervo, H., Berkowitz, S., Zheng, T., Guckian, K., Pellegrini, M., and Lugovskoy, A., 2008. Structure of a NEMO/IKK-associating domain reveals architecture of the interaction site. *Structure (London, England : 1993)*, 16(5), pp.798–808.

Ryseck, R.P., Bull, P., Takamiya, M., Bours, V., Siebenlist, U., Dobrzanski, P., and Bravo, R., 1992. RelB, a new Rel family transcription activator that can interact with p50-NF-kappa B. *Molecular and cellular biology*, 12(2), pp.674–84.

Saccani, S., Pantano, S., and Natoli, G., 2003. Modulation of NF-κB activity by exchange of dimers. *Molecular Cell*, 11(6), pp.1563–1574.

Sage, C.R., Rutenber, E.E., Stout, T.J., and Stroud, R.M., 1996. An Essential Role for Water in an Enzyme Reaction Mechanism: The Crystal Structure of the Thymidylate Synthase Mutant E58Q .*Biochemistry*, 35(50), pp.16270–16281.

Salim, N.N. and Feig, A.L., 2009. Isothermal titration calorimetry of RNA. *Methods.* 47(3), pp.198–205.

Samanta, N., Luong, T.Q., Das Mahanta, D., Mitra, R.K., and Havenith, M., 2016. Effect of Short Chain Poly(ethylene glycol)s on the Hydration Structure and Dynamics around Human Serum Albumin. *Langmuir*, 32(3), pp.831–837.

Sanders, R., Gerritsen, H.C., Draaijer, A., Houpt, P.M., and Levine, Y.K., 1994. Fluorescence lifetime imaging of free calcium in single cells . *Bioimaging*, 2(3), pp.131–138.

Sanderson, M.J., Smith, I., Parker, I., and Bootman, M.D., 2014. Fluorescence microscopy. *Cold Spring Harbor protocols*, 2014(10), p.pdb.top071795.

Santoro, M.G., Rossi, A., and Amici, C., 2003. NF-κB and virus infection: Who controls whom [Online]. *EMBO Journal*, 22(11), pp.2552–2560.

Sasaki, C., Naito, H., Iwata, M., Kudo, H., Yamada, Y., Taguchi, T., Jyouichi, T., Okagawa, H., Tadatomo, K., and Tanaka, H., 2003. Temperature dependence of Stokes shift in InxGa1−xN epitaxial layers. *Journal of Applied Physics*, 93(3), pp.1642–1646.

Sasaki, Y. and Iwai, K., 2015. Roles of the NF-κB Pathway in B-Lymphocyte Biology. In: *Current topics in microbiology and immunology*. pp.177–209.

Schad, E., Tompa, P., and Hegyi, H., 2011. The relationship between proteome size, structural disorder and organism complexity. *Genome biology*, 12(12), p.R120.

Scheuerle, A.E. and Ursini, M.V., 1993. *Incontinentia Pigmenti*. University of Washington, Seattle.

Schlesinger, A.P., Wang, Y., Tadeo, X., Millet, O., and Pielak, G.J., 2011. Macromolecular Crowding Fails To Forld a Globular Protein in Cells. *J. Am. Chem. Soc.*, 133, pp.8082–8085.

Schmitz, M.L., Stelzer, G., Altmann, H., Meisterernst, M., and Baeuerle, P.A., 1995. Interaction of the COOH-terminal transactivation domain of p65 NF-kappa B with TATA-binding protein, transcription factor IIB, and coactivators. *The Journal of biological chemistry*, 270(13), pp.7219–26.

Schneider, G., Henrich, A., Greiner, G., Wolf, V., Lovas, A., Wieczorek, M., Wagner, T., Reichardt, S., von Werder, A., Schmid, R.M., Weih, F., Heinzel, T., Saur, D., and Krämer, O.H., 2010. Cross talk between stimulated NF-κB and the tumor suppressor p53. *Oncogene*, 29(19), pp.2795–2806.

Scholefield, J., Henriques, R., Savulescu, A.F., Fontan, E., Boucharlat, A., Laplantine, E., Smahi, A., Israël, A., Agou, F., and Mhlanga, M.M., 2016. Super-resolution microscopy reveals a preformed NEMO lattice structure that is collapsed in incontinentia pigmenti. *Nature Communications*, 7(1), p.12629.

Schonbrunn, E., Eschenburg, S., Luger, K., Kabsch, W., and Amrhein, N., 2000. Structural basis for the interaction of the fluorescence probe 8-anilino-1-naphthalene sulfonate (ANS) with the antibiotic target MurA. *Proceedings of the National Academy of Sciences*, 97(12), pp.6345–6349.

Schröfelbauer, B., Polley, S., Behar, M., Ghosh, G., and Hoffmann, A., 2012. NEMO Ensures Signaling Specificity of the Pleiotropic IKKβ by Directing Its Kinase Activity toward IκBα. *Molecular Cell*, 47(1), pp.111–121.

Schulze-Luehrmann, J. and Ghosh, S., 2006. Antigen-Receptor Signaling to Nuclear Factor κB. *Immunity*, 25(5), pp.701–715.

Schweiker, K.L., Fitz, V.W., and Makhatadze, G.I., 2009. Universal convergence of the specific volume changes of globular proteins upon unfolding [Online]. *Biochemistry*, 48(46), pp.10846–10851.

Sebban, H., Yamaoka, S., and Courtois, G., 2006. Posttranslational modifications of NEMO and its partners in NF-κB signaling. *Trends in Cell Biology*, 16(11), pp.569–577.

Sebé-Pedrós, A., de Mendoza, A., Lang, B.F., Degnan, B.M., and Ruiz-Trillo, I., 2011. Unexpected repertoire of metazoan transcription factors in the unicellular holozoan Capsaspora owczarzaki. [Online]. *Molecular biology and evolution*, 28(3), pp.1241–1254.

Seigner, J., Basilio, J., Resch, U., and de Martin, R., 2018. CD40L and TNF both activate the classical NF-κB pathway, which is not required for the CD40L induced alternative pathway in endothelial cells. *Biochemical and Biophysical Research Communications*, 495(1), pp.1389–1394.

Sekar, R.B. and Periasamy, A., 2003. Fluorescence resonance energy transfer (FRET) microscopy imaging of live cell protein localizations. *Journal of Cell Biology*, 160(5), pp.629–633.

Sekhar, A., Latham, M.P., Vallurupalli, P., and Kay, L.E., 2014. Viscosity-Dependent Kinetics of Protein Conformational Exchange: Microviscosity Effects and the Need for a Small Viscogen. *The Journal of Physical Chemistry B*, 118, pp.4546–4551.

Sen, R. and Baltimore, D., 1986. Multiple nuclear factors interact with the immunoglobulin enhancer sequences. *Cell*, 46(5), pp.705–716.

Shambharkar, P.B., Blonska, M., Pappu, B.P., Li, H., You, Y., Sakurai, H., Darnay, B.G., Hara, H., Penninger, J., and Lin, X., 2007. Phosphorylation and ubiquitination of the IkappaB kinase complex by two distinct signaling pathways. *The EMBO journal*, 26(7), pp.1794–805.

Shanker, N. and Bane, S.L., 2008. Basic Aspects of Absorption and Fluorescence Spectroscopy and Resonance Energy Transfer Methods. *Methods in Cell Biology*, 84(07), pp.213–242.

Sharma, C.S., Sarkar, S., Periyakaruppan, A., Ravichandran, P., Sadanandan, B., Ramesh, V., Thomas, R., Hall, J.C., Wilson, B.L., and Ramesh, G.T., 2008. Simulated microgravity activates apoptosis and NF-κB in mice testis. *Molecular and Cellular Biochemistry*, 313(1–2), pp.71–78.

Shembade, N., Pujari, R., Harhaj, N.S., Abbott, D.W., and Harhaj, E.W., 2011. The kinase IKKα inhibits activation of

the transcription factor NF-κB by phosphorylating the regulatory molecule TAX1BP1. *Nature immunology*, 12(9), pp.834–43.

Shih, R.-H., Wang, C.-Y., and Yang, C.-M., 2015. NF-kappaB Signaling Pathways in Neurological Inflammation: A Mini Review. *Frontiers in Molecular Neuroscience*, 8(December), pp.1–8.

Shih, V.F.-S., Tsui, R., Caldwell, A., and Hoffmann, A., 2011. A single NFκB system for both canonical and non-canonical signaling. *Cell research*, 21(1), pp.86–102.

Shiraga, K., Ogawa, Y., and Kondo, N., 2016. Hydrogen Bond Network of Water around Protein Investigated with Terahertz and Infrared Spectroscopy. *Biophysical Journal*, 111(12), pp.2629–2641.

Siddiqui, K.S., Poljak, A., Guilhaus, M., Feller, G., D'Amico, S., Gerday, C., and Cavicchioli, R., 2005. Role of disulfide bridges in the activity and stability of a cold-active alpha-amylase. *Journal of bacteriology*, 187(17), pp.6206–12.

Silva, J.L., Oliveira, A.C., Vieira, T.C.R.G., de Oliveira, G.A.P., Suarez, M.C., and Foguel, D., 2014. High-Pressure Chemical Biology and Biotechnology. *Chemical Reviews*, 114(14), pp.7239–7267.

Slavík, J., 1982. Anilinonaphthalene sulfonate as a probe of membrane composition and function. *Biochimica et biophysica acta*, 694(1), pp.1–25.

Smahi, A., Courtois, G., Rabia, S.H., Doffinger, R., Bodemer, C., Munnich, A., Casanova, J.L., Israel, A., Smahi, A., Courtois, G., Rabia, S.H., and Do, R., 2002. The NF-kappa B signalling pathway in human disease: from incontinentia pigmenti to ectodermal dysplasias and immune-deficiency syndromes. *Human Molecular Genetics*, 11(20), pp.2371–2375.

Smahi, A., Courtois, G., Vabres, P., Yamaoka, S., Heuertz, S., Munnich, A., Israël, A., Heiss, N.S., Klauck, S.M., Kioschis, P., Wiemann, S., Poustka, A., Esposito, T., Bardaro, T., Gianfrancesco, F., Ciccodicola, A., D'Urso, M., Woffendin, H., Jakins, T., Donnai, D., Stewart, H., Kenwrick, S.J., Aradhya, S., Yamagata, T., Levy, M., Lewis, R.A., and Nelson, D.L., 2000. Genomic rearrangement in NEMO impairs NF-κB activation and is a cause of incontinentia pigmenti. *Nature*, 405(6785), pp.466–472.

Smith-Garvin, J.E., Koretzky, G.A., and Jordan, M.S., 2009. T Cell Activation. *Annual Review of Immunology*, 27(1), pp.591–619.

Sobolewska-Stawiarz, A., Leferink, N.G.H., Fisher, K., Heyes, D.J., Hay, S., Rigby, S.E.J., and Scrutton, N.S., 2014. Energy landscapes and catalysis in nitric-oxide synthase. *J Biol Chem.* 289(17),pp.11725-38.

Spink, C. and Wadsö, I., 1976. Calorimetry as an analytical tool in biochemistry and biology. *Methods of biochemical analysis*, 23(0), pp.1–159.

Spitzer, J. and Poolman, B., 2013. How crowded is the prokaryotic cytoplasm? [Online]. *FEBS Letters*, 587(14), pp.2094–2098.

Stagg, L., Christiansen, A., and Wittung-Stafshede, P., 2011. Macromolecular crowding tunes folding landscape of parallel α/β protein, apoflavodoxin. *Journal of the American Chemical Society*, 133(4), pp.646–648.

Staudt, L.M., 2010. Oncogenic activation of NF-kappaB. [Online]. *Cold Spring Harbor perspectives in biology*, 2(6), p.a000109.

Steen, H., Jebanathirajah, J.A., Springer, M., and Kirschner, M.W., 2005. Stable isotope-free relative and absolute quantitation of protein phosphorylation stoichiometry by MS. *Proceedings of the National Academy of Sciences*, 102(11), pp.3948–3953.

Stokes, G.G., 1852. On the change of refrangibility of light. *Phil Trans R Soc*, 142, pp.463–562.

Stopel, M.H.W., Blum, C., and Subramaniam, V., 2014. Excitation Spectra and Stokes Shift Measurements of Single Organic Dyes at Room Temperature. *The Journal of Physical Chemistry Letters*, 5(18), pp.3259–3264.

Størmer, L., 1952. PHYLOGENY AND TAXONOMY OF FOSSIL HORSESHOE CRABS. *JOURNAL OF PALEONTOLOGY*, 26(4), pp.630–639.

Street, T.O., Bolen, D.W., and Rose, G.D., 2006. A molecular mechanism for osmolyte-induced protein stability. *Proceedings of the National Academy of Sciences*, 103(38), pp.13997–14002.

Stryer, L., 1965. The interaction of a naphthalene dye with apomyoglobin and apohemoglobin: a fluorescent probe of non-polar binding sites. *Journal of Molecular Biology*, 13(2), pp.482–495.

Sturani, E., Zippel, R., Toschi, L., Morello, L., Comoglio, P.M., and Alberghina, L., 1988. Kinetics and regulation of the tyrosine phosphorylation of epidermal growth factor receptor in intact A431 cells. *Molecular and Cellular Biology*, 8(3), pp.1345–1351.

Sue, S.-C., Alverdi, V., Komives, E.A., and Dyson, H.J., 2011. Detection of a ternary complex of NF-kappaB and IkappaBalpha with DNA provides insights into how IkappaBalpha removes NF-kappaB from transcription sites. *Proceedings of the National Academy of Sciences of the United States of America*, 108(4), pp.1367–72.

Sue, S.-C., Cervantes, C., Komives, E.A., and Dyson, H.J., 2008. Transfer of flexibility between ankyrin repeats in IkappaB* upon formation of the NF-kappaB complex. [*Journal of molecular biology*, 380(5), pp.917–31.

Sugase, K., Dyson, H.J., and Wright, P.E., 2007. Mechanism of coupled folding and binding of an intrinsically disordered protein. *Nature*, 447(7147), pp.1021–1025.

Sugiki, T., Kobayashi, N., and Fujiwara, T., 2017. Modern Technologies of Solution Nuclear Magnetic Resonance Spectroscopy for Three-dimensional Structure Determination of Proteins Open Avenues for Life Scientists.. *Computational and Structural Biotechnology Journal*, 15, pp.328–339.

Sullivan, J.C., Kalaitzidis, D., Gilmore, T.D., and Finnerty, J.R., 2007. Rel homology domain-containing transcription factors in the cnidarian Nematostella vectensis. *Development Genes and Evolution*, 217(1), pp.63–72.

Sun, M.M., Caillot, R., Mak, G., Robb, F.T., and Clark, D.S., 2001. Mechanism of pressure-induced thermostabilization of proteins: studies of glutamate dehydrogenases from the hyperthermophile Thermococcus litoralis. *Protein science : a publication of the Protein Society*, 10(9), pp.1750–7.

Sun, M.M., Tolliday, N., Vetriani, C., Robb, F.T., and Clark, D.S., 1999. Pressure-induced thermostabilization of glutamate dehydrogenase from the hyperthermophile Pyrococcus furiosus. *Protein science : a publication of the Protein Society*, 8(5), pp.1056–63.

Sun, S.-C., 2011. Non-canonical NF-κB signaling pathway. *Cell research*, 21(1), pp.71–85.

Sustarsic, M. and Kapanidis, A.N., 2015. Taking the ruler to the jungle: single-molecule FRET for understanding biomolecular structure and dynamics in live cells. *Current Opinion in Structural Biology*, 34, pp.52–59.

Swamy, M., Beck-Garcia, K., Beck-Garcia, E., Hartl, F.A., Morath, A., Yousefi, O.S., Dopfer, E.P., Molnár, E., Schulze, A.K., Blanco, R., Borroto, A., Martín-Blanco, N., Alarcon, B., Höfer, T., Minguet, S., and Schamel, W.W.A., 2016. A Cholesterol-Based Allostery Model of T Cell Receptor Phosphorylation. *Immunity*, 44(5), pp.1091–101.

Sweatt, J.D., 2001. Memory mechanisms: The yin and yang of protein phosphorylation. *Current Biology*, 11(10), pp.R391–R394.

Szabó, Á., Szendi-Szatmári, T., Ujlaky-Nagy, L., Rádi, I., Vereb, G., Szöllősi, J., and Nagy, P., 2018. The Effect of Fluorophore Conjugation on Antibody Affinity and the Photophysical Properties of Dyes. *Biophysical journal*, 114(3), pp.688–700.

Takada, Y., Mukhopadhyay, A., Kundu, G.C., Mahabeleshwar, G.H., Singh, S., and Aggarwal, B.B., 2003. Hydrogen peroxide activates NF-κB through tyrosine phosphorylation of IBκα and serine phosphorylation of p65. Evidence for the involvement of IκBαkinase and Syk protein-tyrosine kinase. *Journal of Biological Chemistry*,

278(26), pp.24233–24241.

Tan, C.S.H., 2011. Sequence, structure, and network evolution of protein phosphorylation. *Science signaling*, 4(182), p.mr6.

Tanaka, M., Fuentes, M.E., Yamaguchi, K., Durnin, M.H., Dalrymple, S.A., Hardy, K.L., and Goeddel, D. V, 1999. Embryonic lethality, liver degeneration, and impaired NF-kappa B activation in IKK-beta-deficient mice. *Immunity*, 10(4), pp.421–9.

Tantos, A., Han, K.H., and Tompa, P., 2012. Intrinsic disorder in cell signaling and gene transcription. *Molecular and Cellular Endocrinology*, 348(2), pp.457–465.

Tarantino, N., Tinevez, J.-Y.Y., Crowell, E.F., Boisson, B., Henriques, R., Mhlanga, M., Agou, F., Israël, A., and Laplantine, E., 2014. Tnf and il-1 exhibit distinct ubiquitin requirements for inducing NEMO-IKK supramolecular structures. *Journal of Cell Biology*, 204(2), pp.231–245.

Teale, F.W. and Weber, G., 1957. Ultraviolet fluorescence of the aromatic amino acids. *The Biochemical journal*, 65(3), pp.476–82.

Tegethoff, S., Behlke, J., and Scheidereit, C., 2003. Tetrameric oligomerization of IkappaB kinase gamma (IKKgamma) is obligatory for IKK complex activity and NF-kappaB activation. *Molecular and cellular biology*, 23(6), pp.2029–41.

Ten, R.M., Paya, C. V, Israël, N., Le Bail, O., Mattei, M.G., Virelizier, J.L., Kourilsky, P., and Israël, A., 1992. The characterization of the promoter of the gene encoding the p50 subunit of NF-kappa B indicates that it participates in its own regulation. *The EMBO journal*, 11(1), pp.195–203.

Thompson, J.E., Phillips, R.J., Erdjument-Bromage, H., Tempst, P., and Ghosh, S., 1995. I kappa B-beta regulates the persistent response in a biphasic activation of NF-kappa B. *Cell*, 80(4), pp.573–82.

Thompson, L.M., Aiken, C.T., Kaltenbach, L.S., Agrawal, N., Illes, K., Khoshnan, A., Martinez-Vincente, M., Arrasate, M., O'Rourke, J.G., Khashwji, H., Lukacsovich, T., Zhu, Y.-Z., Lau, A.L., Massey, A., Hayden, M.R., Zeitlin, S.O., Finkbeiner, S., Green, K.N., LaFerla, F.M., Bates, G., Huang, L., Patterson, P.H., Lo, D.C., Cuervo, A.M., Marsh, J.L., and Steffan, J.S., 2009. IKK phosphorylates Huntingtin and targets it for degradation by the proteasome and lysosome. *The Journal of Cell Biology*, 187(7), pp.1083–1099.

Tian, S.M., Ruan, K.C., Qian, J.F., Shao, G.Q., and Balny, C., 2000. Effects of hydrostatic pressure on the structure and biological activity of infectious bursal disease virus. *European journal of biochemistry*, 267(14), pp.4486–94.

Tiangco, D.A., Lattanzio, F.A., Osgood, C.J., Beebe, S.J., Kerry, J.A., and Hargrave, B.Y., 2005. 3,4-Methylenedioxymethamphetamine Activates Nuclear Factor-κB, Increases Intracellular Calcium, and Modulates Gene Transcription in Rat Heart Cells. *Cardiovascular Toxicology*, 5(3), pp.301–310.

Todd, M.J. and Gomez, J., 2001. Enzyme kinetics determined using calorimetry: A general assay for enzyme activity?. *Analytical Biochemistry*, 296(2), pp.179–187.

Tokunaga, F., Nishimasu, H., Ishitani, R., Goto, E., Noguchi, T., Mio, K., Kamei, K., Ma, A., Iwai, K., and Nureki, O., 2012. Specific recognition of linear polyubiquitin by A20 zinc finger 7 is involved in NF-κB regulation.. *The EMBO journal*, 31(19), pp.3856–70.

Tokunaga, F., Sakata, S.I., Saeki, Y., Satomi, Y., Kirisako, T., Kamei, K., Nakagawa, T., Kato, M., Murata, S., Yamaoka, S., Yamamoto, M., Akira, S., Takao, T., Tanaka, K., and Iwai, K., 2009. Involvement of linear polyubiquitylation of NEMO in NF-κB activation. *Nature Cell Biology*, 11(2), pp.123–132.

Tolani, B., Matta, H., Gopalakrishnan, R., Punj, V., and Chaudhary, P.M., 2014. NEMO is essential for Kaposi's sarcoma-associated herpesvirus-encoded vFLIP K13-induced gene expression and protection against death receptor-induced cell death, and its N-terminal 251 residues are sufficient for this process. *Journal of*

virology, 88(11), pp.6345–54.

Tompa, P., Szász, C., and Buday, L., 2005. Structural disorder throws new light on moonlighting [Online]. *Trends in Biochemical Sciences*, 30(9), pp.484–489.

Traenckner, E.B., Pahl, H.L., Henkel, T., Schmidt, K.N., Wilk, S., and Baeuerle, P.A., 1995. Phosphorylation of human I kappa B-alpha on serines 32 and 36 controls I kappa B-alpha proteolysis and NF-kappa B activation in response to diverse stimuli. *The EMBO journal*, 14(12), pp.2876–83.

Traenckner, E.B., Wilk, S., and Baeuerle, P.A., 1994. A proteasome inhibitor prevents activation of NF-κB and stabilizes a newly phosphorylated form of IκBα that is still bound to NF-κB. *The EMBO journal*, 13(22), pp.5433–41.

Di Trani, J.M., De Cesco, S., O'Leary, R., Plescia, J., do Nascimento, C.J., Moitessier, N., and Mittermaier, A.K., 2018. Rapid measurement of inhibitor binding kinetics by isothermal titration calorimetry. *Nature Communications*, 9(1), p.893.

Di Trani, J.M., Moitessier, N., Mittermaier, A.K., Trani, J.M. Di, Moitessier, N., and Mittermaier, A.K., 2017. Measuring Rapid Time-Scale Reaction Kinetics Using Isothermal Titration Calorimetry *Analytical Chemistry*, 89(13), pp.7022–7030.

Transtrum, M.K., Hansen, L.D., and Quinn, C., 2015. Enzyme kinetics determined by single-injection isothermal titration calorimetry.. *Methods*, 76, pp.194–200.

Trelle, M.B., Ramsey, K.M., Lee, T.C., Zheng, W., Lamboy, J., Wolynes, P.G., Deniz, A., and Komives, E.A., 2016. Binding of NFκB Appears to Twist the Ankyrin Repeat Domain of IκBα . *Biophys J*. 110(4),pp.887-95

Treweek, T.M., Rekas, A., Walker, M.J., and Carver, J.A., 2010. A quantitative NMR spectroscopic examination of the flexibility of the C-terminal extensions of the molecular chaperones, αA- and αB-crystallin. *Experimental Eye Research*, 91(5), pp.691–699.

Truhlar, S.M.E., Torpey, J.W., and Komives, E.A., 2006. Regions of IkappaBalpha that are critical for its inhibition of NF-kappaB.DNA interaction fold upon binding to NF-kappaB. [Online]. *Proceedings of the National Academy of Sciences of the United States of America*, 103(50), pp.18951–6.

Tsai, A.M., Udovic, T.J., and Neumann, D.A., 2001. The inverse relationship between protein dynamics and thermal stability. *Biophys. J.*, 81(4), pp.2339–2343.

Tsukamoto, H., Fukudome, K., Takao, S., Tsuneyoshi, N., and Kimoto, M., 2010. Lipopolysaccharide-binding protein-mediated Toll-like receptor 4 dimerization enables rapid signal transduction against lipopolysaccharide stimulation on membrane-associated CD14-expressing cells. *International Immunology*, 22(4), pp.271–280.

Uckelmann, M. and Sixma, T.K., 2017. Histone ubiquitination in the DNA damage response. *DNA Repair*, 56, pp.92–101.

Uhlen, M., Oksvold, P., Fagerberg, L., Lundberg, E., Jonasson, K., Forsberg, M., Zwahlen, M., Kampf, C., Wester, K., Hober, S., Wernerus, H., Björling, L., and Ponten, F., 2010. Towards a knowledge-based Human Protein Atlas. *Nature Biotechnology*, 28(12), pp.1248–1250.

Upadhyay, A., Burman, J.D., Clark, E.A., Leung, E., Isenman, D.E., Van Den Elsen, J.M.H., and Bagby, S., 2008. Structure-function analysis of the C3 binding region of Staphylococcus aureus immune subversion protein Sbi. *Journal of Biological Chemistry*, 283(32), pp.22113–22120.

Uversky, V.N., 2011. Intrinsically disordered proteins from A to Z. *The international journal of biochemistry & cell biology*, 43(8), pp.1090–103.

Uversky, V.N., 2013. A decade and a half of protein intrinsic disorder: Biology still waits for physics. *Protein Science*, 22(6), pp.693–724.

Uversky, V.N., Davé, V., Iakoucheva, L.M., Malaney, P., Metallo, S.J., Pathak, R.R., and Joerger, A.C., 2014. Pathological unfoldomics of uncontrolled chaos: Intrinsically disordered proteins and human diseases. *Chemical Reviews*, 114(13), pp.6844–6879.

Valeur, B., 2001. *Molecular Fluorescence*. Weinheim, FRG: Wiley-VCH Verlag GmbH.

Valeur, B. and Berberan-Santos, M.N., 2011. A brief history of fluorescence and phosphorescence before the emergence of quantum theory. *Journal of Chemical Education*, 88(6), pp.731–738.

Vasilchuk, D., Pandharipande, P.P., Suladze, S., Sanchez-Ruiz, J.M., and Makhatadze, G.I., 2014. Molecular determinants of expansivity of native globular proteins: A pressure perturbation calorimetry study. *Journal of Physical Chemistry B*, 118(23), pp.6117–6122.

Verma, I.M., Stevenson, J.K., Schwarz, E.M., and Antwerp, D. Van, 1995. Rel/NF-KB /IKB family: intimate tales of association and dissociation. *Genes & Development*, pp.2723–2735.

Verma, U.N., Yamamoto, Y., Prajapati, S., and Gaynor, R.B., 2004. Nuclear Role of IκB Kinase-γ/NF-κB Essential Modulator (IKKγ/NEMO) in NF-κB-dependent Gene Expression. *Journal of Biological Chemistry*, 279(5), pp.3509–3515.

Verstrepen, L., Bekaert, T., Chau, T.-L., Tavernier, J., Chariot, A., and Beyaert, R., 2008. TLR-4, IL-1R and TNF-R signaling to NF-κB: variations on a common theme. *Cellular and Molecular Life Sciences*, 65(19), pp.2964–2978.

Vincendeau, M., Hadian, K., Messias, A.C., Brenke, J.K., Halander, J., Griesbach, R., Greczmiel, U., Bertossi, A., Stehle, R., Nagel, D., Demski, K., Velvarska, H., Niessing, D., Geerlof, A., Sattler, M., and Krappmann, D., 2016. Inhibition of Canonical NF-κB Signaling by a Small Molecule Targeting NEMO-Ubiquitin Interaction. *Scientific Reports*, 6(1), p.18934.

Voet, D. and Voet, J.G., 2011. *Biochemistry*. John Wiley & Sons.

Vogt, A.D. and Di Cera, E., 2013. Conformational selection is a dominant mechanism of ligand binding. *Biochemistry*, 52(34), pp.5723–9.

Vyšniauskas, A., Qurashi, M., Gallop, N., Balaz, M., Anderson, H.L., and Kuimova, M.K., 2015. Unravelling the effect of temperature on viscosity-sensitive fluorescent molecular rotors. *Chemical Science*, 6(10), pp.5773–5778.

Wan, F. and Lenardo, M.J., 2009. Specification of DNA binding activity of NF-kappaB proteins. [Online]. *Cold Spring Harbor perspectives in biology*, 1(4), p.a000067.

Wang, C., Deng, L., Hong, M., Akkaraju, G.R., Inoue, J., and Chen, Z.J., 2001. TAK1 is a ubiquitin-dependent kinase of MKK and IKK . *Nature*, 412(6844), pp.346–351.

Wang, G. and Kaltashov, I.A., 2014. Approach to characterization of the higher order structure of disulfide-containing proteins using hydrogen/deuterium exchange and top-down mass spectrometry. [Online]. *Analytical chemistry*, 86(15), pp.7293–8.

Wang, T., Zou, D., Zhang, J., and Chen, Y., 2016. Application of Microbeam X-Ray Fluorescence Spectrometry in the Diagnosis of Suspected Electrocution by High-Voltage Direct Current.*The American Journal of Forensic Medicine and Pathology*, 37(3), pp.190–193.

Wang, V.Y.-F., Huang, W., Asagiri, M., Spann, N., Hoffmann, A., Glass, C., and Ghosh, G., 2012. The transcriptional specificity of NF-κB dimers is coded within the κB DNA response elements. *Cell reports*, 2(4), pp.824–39.

Wang, X.W., Tan, N.S., Ho, B., and Ding, J.L., 2006. Evidence for the ancient origin of the NF-kappaB/IkappaB cascade: its archaic role in pathogen infection and immunity. *Proceedings of the National Academy of Sciences of the United States of America*, 103(11), pp.4204–9.

Ward, J.J., Sodhi, J.S., McGuffin, L.J., Buxton, B.F., and Jones, D.T., 2004. Prediction and Functional Analysis of Native

Disorder in Proteins from the Three Kingdoms of Life. *Journal of Molecular Biology*, 337(3), pp.635–645.

Warshel, A., Aqvist, J., and Creighton, S., 1989. Enzymes work by solvation substitution rather than by desolvation. *Proceedings of the National Academy of Sciences*, 86(15), pp.5820–5824.

Watanabe, T., Takahashi, K., Shimura, K., and Kim, D., 2017. Influence of carrier localization at the core/shell interface on the temperature dependence of the Stokes shift and the photoluminescence decay time in CdTe/CdS type-II quantum dots. *Physical Review B*, 96(3), p.035305.

Weatherly, G.T. and Pielak, G.J., 2000. Second virial coefficients as a measure of protein–osmolyte interactions. *Protein Science*, 10, pp.12–16.

Webb, J.N., Webb, S.D., Cleland, J.L., Carpenter, J.F., and Randolph, T.W., 2001. Partial molar volume, surface area, and hydration changes for equilibrium unfolding and formation of aggregation transition state: High-pressure and cosolute studies on recombinant human IFN-gamma. *Proceedings of the National Academy of Sciences*, 98(13), pp.7259–7264.

Weber, G. and Shinitzky, M., 1970. Failure of Energy Transfer between Identical Aromatic Molecules on Excitation at the Long Wave Edge of the Absorption Spectrum. *Proceedings of the National Academy of Sciences of the United States of America*, 65(4), pp.823–30.

Van De Weert, M. and Stella, L., 2011. Fluorescence quenching and ligand binding: A critical discussion of a popular methodology. *Journal of Molecular Structure*, 998(1–3), pp.145–150.

Weil, R., Schwamborn, K., Alcover, A., Bessia, C., Di Bartolo, V., and Israël, A., 2003. Induction of the NF-κB cascade by recruitment of the scaffold molecule NEMO to the T cell receptor. *Immunity*, 18(1), pp.13–26.

Wessells, J., Baer, M., Young, H.A., Claudio, E., Brown, K., Siebenlist, U., and Johnson, P.F., 2004. BCL-3 and NF-κB p50 Attenuate Lipopolysaccharide-induced Inflammatory Responses in Macrophages. *Journal of Biological Chemistry*, 279(48), pp.49995–50003.

Wettke-Schäfer, R. and Kantner, G., 1983. X-linked dominant inherited diseases with lethality in hemizygous males. *Human genetics*, 64(1), pp.1–23.

Wiedersich, J., Kohler, S., Skerra, A., and Friedrich, J., 2008. Temperature and pressure dependence of protein stability: The engineered fluorescein-binding lipocalin FluA shows an elliptic phase diagram. *Proceedings of the National Academy of Sciences*, 105(15), pp.5756–5761.

Williams, S.A., Chen, L.F., Kwon, H., Fenard, D., Bisgrove, D., Verdin, E., and Greene, W.C., 2004. Prostratin antagonizes HIV latency by activating NF-κB. *Journal of Biological Chemistry*, 279(40), pp.42008–42017.

Winkler, D., Beconi, M., Toledo-Sherman, L.M., Prime, M., Ebneth, A., Dominguez, C., and Muñoz-Sanjuan, I., 2013. Development of LC/MS/MS, High-Throughput Enzymatic and Cellular Assays for the Characterization of Compounds That Inhibit Kynurenine Monooxygenase (KMO). *Journal of Biomolecular Screening*, 18(8), pp.879–889.

Wirth, A.J. and Gruebele, M., 2013. Quinary protein structure and the consequences of crowding in living cells: Leaving the test-tube behind. *Bioessays*, 35(11), pp.984–993.

Wolenski, F.S., Garbati, M.R., Lubinski, T.J., Traylor-Knowles, N., Dresselhaus, E., Stefanik, D.J., Goucher, H., Finnerty, J.R., and Gilmore, T.D., 2011. Characterization of the Core Elements of the NF- B Signaling Pathway of the Sea Anemone Nematostella vectensis . *Molecular and Cellular Biology*, 31(5), pp.1076–1087.

Wu, Z., Tiambeng, T.N., Cai, W., Chen, B., Lin, Z., Gregorich, Z.R., and Ge, Y., 2018. Impact of Phosphorylation on the Mass Spectrometry Quantification of Intact Phosphoproteins. *Analytical Chemistry*, 90(8), pp.4935–4939.

Wu, Z.H., Wong, E.T., Shi, Y., Niu, J., Chen, Z., Miyamoto, S., and Tergaonkar, V., 2010. ATM- and NEMO-dependent ELKS ubiquitination coordinates TAK1-Mediated IKK activation in response to genotoxic stress.*Molecular Cell*,

40(1), pp.75–86.

Wuerzberger-Davis, S.M., Nakamura, Y., Seufzer, B.J., and Miyamoto, S., 2007. NF-κB activation by combinations of NEMO SUMOylation and ATM activation stresses in the absence of DNA damage. *Oncogene*, 26(5), pp.641–651.

Xia, Y.-L., Sun, J.-H., Ai, S.-M., Li, Y., Du, X., Sang, P., Yang, L.-Q., Fu, Y.-X., and Liu, S.-Q., 2018. Insights into the role of electrostatics in temperature adaptation: a comparative study of psychrophilic, mesophilic, and thermophilic subtilisin-like serine proteases. *RSC Advances*, 8(52), pp.29698–29713.

Xia, Z.-P., Sun, L., Chen, X., Pineda, G., Jiang, X., Adhikari, A., Zeng, W., and Chen, Z.J., 2009. Direct activation of protein kinases by unanchored polyubiquitin chains. *Nature*, 461(7260), pp.114–119.

Xiao, G., Harhaj, E.W., and Sun, S.C., 2001. NF-kappaB-inducing kinase regulates the processing of NF-kappaB2 p100.*Molecular cell*, 7(2), pp.401–9.

Xie, D., Jules, S., Weng, Y., Zhou, Y., Sidner, R.A., and Pescovitz, M., 2012. Poly(ethylene glycol) and poly(N-vinlypyrrolidone) for improved porcine islet cryopreservation. *Journal of Biomedical Science and Engineering*, 05(05), pp.263–269.

Xie, H., Vucetic, S., Iakoucheva, L.M., Oldfield, C.J., Dunker, A.K., Uversky, V.N., and Obradovic, Z., 2007. Functional anthology of intrinsic disorder. 1. Biological processes and functions of proteins with long disordered regions. *Journal of Proteome Research*, 6(5), pp.1882–1898.

Xie, P., 2013. TRAF molecules in cell signaling and in human diseases. *Journal of molecular signaling*, 8(1), p.7.

Xu, F. and Cross, T.A., 1999. Water: foldase activity in catalyzing polypeptide conformational rearrangements. *Proceedings of the National Academy of Sciences of the United States of America*, 96(16), pp.9057–9061.

Xu, G., Lo, Y.C., Li, Q., Napolitano, G., Wu, X., Jiang, X., Dreano, M., Karin, M., and Wu, H., 2011. Crystal structure of inhibitor of κb kinase β . *Nature*, 472(7343), pp.325–330.

Xu, J., Chen, J., Toptygin, D., Tcherkasskaya, O., Callis, P., King, J., Brand, L., and Knutson, J.R., 2009. Femtosecond fluorescence spectra of tryptophan in human gamma-crystallin mutants: site-dependent ultrafast quenching. *Journal of the American Chemical Society*, 131(46), pp.16751–7.

Xue, B., Dunker, A.K., and Uversky, V.N., 2012. Orderly order in protein intrinsic disorder distribution: Disorder in 3500 proteomes from viruses and the three domains of life. *Journal of Biomolecular Structure and Dynamics*, 30(2), pp.137–149.

Xue, B., Romero, P.R., Noutsou, M., Maurice, M.M., Rüdiger, S.G.D., William, A.M., Mizianty, M.J., Kurgan, L., Uversky, V.N., and Dunker, A.K., 2013. Stochastic machines as a colocalization mechanism for scaffold protein function.. *FEBS Letters*, 587(11), pp.1587–1591.

Yamamoto, Y., Verma, U.N., Prajapati, S., Kwak, Y.-T., and Gaynor, R.B., 2003. Histone H3 phosphorylation by IKK-α is critical for cytokine-induced gene expression. *Nature*, 423(6940), pp.655–659.

Yamaoka, S, Courtois, G., Bessia, C., Whiteside, S.T., Weil, R., Agou, F., Kirk, H.E., Kay, R.J., and Israel, A., 1998. Complementation cloning of NEMO, a component of the IkB kinase complex essential for NF-kB activation. *Cell*, 93(7), pp.1231–1240.

Yamaoka, Shoji, Courtois, G., Bessia, C., Whiteside, S.T., Weil, R., Agou, F., Kirk, H.E., Kay, R.J., and Israël, A., 1998. Complementation cloning of NEMO, a component of the IκB kinase complex essential for NF-κB activation. *Cell*, 93(7), pp.1231–1240.

Yang, Y., Wu, J., and Wang, J., 2016. A database and functional annotation of NF-κB target genes. 9(5),pp.7986-7995

Yang, Y., Xia, F., Hermance, N., Mabb, A., Simonson, S., Morrissey, S., Gandhi, P., Munson, M., Miyamoto, S., and Kelliher, M.A., 2011. A cytosolic ATM/NEMO/RIP1 complex recruits TAK1 to mediate the NF-kappaB and p38

mitogen-activated protein kinase (MAPK)/MAPK-activated protein 2 responses to DNA damage. *Molecular and cellular biology*, 31(14), pp.2774–86.

Ye, H., Arron, J.R., Lamothe, B., Cirilli, M., Kobayashi, T., Shevde, N.K., Segal, D., Dzivenu, O.K., Vologodskaia, M., Yim, M., Du, K., Singh, S., Pike, J.W., Darnay, B.G., Choi, Y., and Wu, H., 2002. Distinct molecular mechanism for initiating TRAF6 signalling. *Nature*, 418(6896), pp.443–447.

Yoshikawa, A., Sato, Y., Yamashita, M., Mimura, H., Yamagata, A., and Fukai, S., 2009. Crystal structure of the NEMO ubiquitin-binding domain in complex with Lys 63-linked di-ubiquitin. *FEBS Letters*, 583(20), pp.3317–3322.

Yuan, S., Dong, X., Tao, X., Xu, L., Ruan, J., Peng, J., and Xu, A., 2014. Emergence of the A20/ABIN-mediated inhibition of NF- B signaling via modifying the ubiquitinated proteins in a basal chordate .*Proceedings of the National Academy of Sciences*, 111(18), pp.6720–6725.

Zandi, E., Chen, Y., and Karin, M., 1998. Direct Phosphorylation of IB by IKK and IKK: Discrimination Between Free and NF-B-Bound Substrate . *Science*, 281(5381), pp.1360–1363.

Zhang, J., Clark, K., Lawrence, T., Peggie, M.W., and Cohen, P., 2014. An unexpected twist to the activation of IKKβ: TAK1 primes IKKβ for activation by autophosphorylation. *Biochemical Journal*, 461(3), pp.531–537.

Zhang, M., Wang, A., Xia, T., and He, P., 2008. Effects of fluoride on DNA damage, S-phase cell-cycle arrest and the expression of NF-κB in primary cultured rat hippocampal neurons [Online]. *Toxicology Letters*, 179(1), pp.1–5.

Zhao, J., Zhang, L., Mu, X., Doebelin, C., Nguyen, W., Wallace, C., Reay, D.P., McGowan, S.J., Corbo, L., Clemens, P.R., Wilson, G.M., Watkins, S.C., Solt, L.A., Cameron, M.D., Huard, J., Niedernhofer, L.J., Kamenecka, T.M., and Robbins, P.D., 2018. Development of novel NEMO-binding domain mimetics for inhibiting IKK/NF-κB activation. C. Khosla, ed. *PLoS Biology*, 16(6), pp.1–28.

Zhao, Q. and Lee, F.S., 1999. Mitogen-activated protein kinase/ERK kinase kinases 2 and 3 activate nuclear factor-kappaB through IkappaB kinase-alpha and IkappaB kinase-beta. *J Biol Chem. 274(13),pp.8355-8.*

Zhou, J., Ching, Y.Q., and Chng, W.-J., 2015. Aberrant nuclear factor-kappa B activity in acute myeloid leukemia: from molecular pathogenesis to therapeutic target. *Oncotarget*, 6(8), pp.5490–500.

Zhou, L., Yeo, A.T., Ballarano, C., Weber, U., Allen, K.N., Gilmore, T.D., and Whitty, A., 2014. Disulfide-Mediated Stabilization of the IκB Kinase Binding Domain of NF-κB Essential Modulator (NEMO). *Biochemistry*. 53(50),pp.7929-44

Zhu, J., Krishnegowda, G., and Gowda, D.C., 2005. Induction of Proinflammatory Responses in Macrophages by the Glycosylphosphatidylinositols of *Plasmodium falciparum*. *Journal of Biological Chemistry*, 280(9), pp.8617–8627.

Zilberman-Rudenko, J., Shawver, L.M., Wessel, A.W., Luo, Y., Pelletier, M., Tsai, W.L., Lee, Y., Vonortas, S., Cheng, L., Ashwell, J.D., Orange, J.S., Siegel, R.M., and Hanson, E.P., 2016. Recruitment of A20 by the C-terminal domain of NEMO suppresses NF-κB activation and autoinflammatory disease. *Proceedings of the National Academy of Sciences of the United States of America*, 113(6), pp.1612–7.

Zotter, A., Bäuerle, F., Dey, D., Kiss, V., and Schreiber, G., 2017. Quantifying enzyme activity in living cells.. *The Journal of biological chemistry*, 292(38), pp.15838–15848.